

***Mechanisms of Paracetamol
(Acetaminophen) induced
Hypothermia***

Shazma Bashir

**A thesis submitted in partial fulfilment of the requirements of
the University of East London for the degree of Doctor of
Philosophy**

Jan 2018

Abstract

Paracetamol is a potent analgesic and antipyretic with limited side effects compared to the nonsteroidal anti-inflammatory drugs (NSAIDs) and opiates. Worldwide paracetamol is commonly used to treat pain and fever in both children and adults. Although, this drug has been in clinical use for more than a century, the mechanisms of action are not fully understood. Historically some of the actions of paracetamol were attributed to the inhibition of central cyclooxygenase (COX-1 and COX-2) enzymes however given the weak inhibitory effects on COX-1 and COX-2 enzymes, alternative targets have been suggested including a possible novel COX-3.

The inhibition of COX-2 is accepted as the mechanism by which paracetamol reduces core temperature (T_c) in febrile animals. However, in non-febrile animals where COX-2 is not induced, paracetamol has also been shown to cause hypothermia by a mechanism that is not fully understood. Both the reduction of pyresis and induction of hypothermia can only occur when peripheral metabolic rate decreases and/or heat loss increases. In terms of antipyresis and hypothermia, the inhibition of lipolysis, fatty acid oxidation and mitochondria function are obvious alternative targets. Studies were undertaken to identify and characterise the putative COX-3 at protein and mRNA level using western blot analysis and reverse transcription polymerase chain reaction (RT-PCR) in mouse brain endothelial cells (b.End3) and whole brain tissues isolated from male C57BL/6 mice. Additional studies were also undertaken to assess if the hypothermic properties of paracetamol could be attributed to direct inhibition of thermogenic pathways in both 3T3-L1 adipocytes and primary brown adipocytes isolated from male Wistar rats. Adipocytes and isolated mitochondria were exposed to paracetamol and lipolysis, fatty acid oxidation (FAO), mitochondrial electron transport chain (ETC), assessed by measuring oxygen consumption rate (OCR).

In these studies no expression of the COX-3 protein could be detected in brain endothelial cells and homogenates and no evidence of a COX-3 was detected at mRNA level. However, paracetamol caused a significant decrease (upto 70%; $P < 0.01$, from control) in both basal and stimulated lipolysis at 1, 3 and 24 hours without affecting cell viability. Paracetamol (10 mM) and its metabolite N-acetyl-p-benzoquinone imine (NAPQI) at 50 μ M also significantly ($P < 0.01$, from control), reduced endogenous and exogenous FAO by 50% and 70% respectively. NAPQI (50 μ M) had limited effect on mitochondrial uncoupling. Finally, paracetamol and other antipyretic compounds also significantly reduced ETC activity (upto 90%; $P < 0.01$, from control). Both the

maintenance of normal body temperature (T_b) and the induction of pyresis require increased mitochondrial ETC activity normally initiated centrally and driven peripherally by reduction of substrates such as fatty acids and glucose. The failure to identify the COX-3 protein and the direct inhibition of lipolysis, FAO and ETC activity indicate that antipyretic actions of paracetamol could partly be attributed to its actions on peripheral energy generation systems and provide new drug targets for reducing fever and chemically inducing hypothermia.

Keywords: paracetamol, acetaminophen, hypothermia, COX-3, lipolysis, fatty acid oxidation, electron transport chain

Table of contents

Abstract	i
Table of contents	iii
List of tables	vii
List of figures	viii
Abbreviations	xii
Acknowledgements	xvii
Dedication	xviii
1. Introduction.....	1
1.1. Paracetamol.....	1
1.2. Paracetamol: Proposed mechanisms of action.....	2
1.3. Paracetamol absorption and metabolism.....	2
1.4. Paracetamol Toxicity.....	4
1.5. Cyclooxygenases (COX).....	5
1.6. Existence of COX variants.....	6
1.7. Evidence for COX-3.....	7
1.8. Evidence for the involvement of COX-3 in thermoregulation.....	11
1.9. Evidence for COX-3; questions about experimental design.....	12
1.10. Paracetamol induced hypothermia: the role of COX enzymes.....	15
1.11. Paracetamol induced hypothermia: other than COX?.....	16
1.12. Thermoregulation.....	17
1.13. Basic concept of thermogenesis and thermoneutral zone.....	19
1.14. Thermogenic Mechanisms.....	20
1.15. The Adipose Tissue.....	21
1.16. Types of Adipose tissue.....	21
1.17. Adipocytes.....	21
1.18. Adipogenesis and its regulation.....	22
1.19. Lipolysis.....	23
1.20. Brown and beige fat mediated non-shivering thermogenesis.....	25
1.21. Paracetamol and thermogenesis.....	25
1.22. Cellular Respiration.....	27
1.23. Fatty Acid β -Oxidation (FAO).....	27
1.24. Electron Transport Chain (ETC).....	28
1.25. Inhibitors of Oxidative Phosphorylation (OXPHOS).....	29
1.26. Regulated uncoupling and Heat Generation.....	29
1.27. Research Aims and Hypothesis.....	30
1.28. Research Plan.....	31
2. Materials and Methods.....	32
2.1. Suppliers.....	32
2.2. Materials.....	33
2.3. Equipment.....	34
2.4. Methods.....	37
2.4.1. Cell culture.....	38
2.4.2. Sample preparation to determine COX protein expression.....	38
2.4.3. Bradford assay and Western blotting to determine COX protein	

expression.....	39
2.4.4. Dot blots.....	41
2.4.5. Sample preparation for mRNA extraction.....	41
2.4.6. Direct mRNA extraction.....	42
2.4.7. Expression of COX mRNA using RT-PCR.....	43
2.4.8. Differentiation of 3T3-L1 pre-adipocytes	46
2.4.9. Oil Red O staining.....	47
2.4.10. MTT assay on 3T3-L1 differentiated adipocytes	47
2.4.11. Lipolysis assay in 3T3-L1 differentiated adipocytes.....	47
2.4.12. Isolation of rat primary brown adipocytes.....	48
2.4.13. MTT assay on rat primary brown adipocytes.....	49
2.4.14. Lipolysis assay in rat primary brown adipocytes.....	49
2.4.15. Measurement of oxygen consumption rate (OCR) using XFp Seahorse Analyser.....	50
2.4.15.1. Seeding 3T3-L1 cells in Seahorse XFp cell culture miniplates.....	52
2.4.15.2. Hydration of Seahorse XFp sensor cartridge.....	52
2.4.15.3. Loading the Seahorse XFp sensor cartridge with compounds.....	53
2.4.15.4 Washing cells in Seahorse XFp cell culture miniplates.....	54
2.4.16. XFp Experiments.....	54
2.4.16.1. Effect of paracetamol on fatty acid oxidation (FAO).....	54
2.4.16.2. Mitochondrial bioenergetic profile of 3T3-L1 adipocytes using Seahorse XFp cell Mito Stress Test.....	56
2.4.16.3. Effect of paracetamol on basal and norepinephrine and isoproterenol stimulated OCR in 3T3-L1 adipocytes.....	57
2.4.16.4. Effect of paracetamol, aminopyrine and antipyrine on basal and norepinephrine and isoproterenol stimulated OCR in 3T3-L1 adipocytes.....	57
2.4.16.5. Elucidation of mechanistic activity of inhibitors that affect mitochondrial function using electron flow assay.....	58
2.5. Statistical analysis.....	60
3. Identification of COX-3 mRNA and protein in rodents	61
3.1. Introduction.....	61
3.2. Methods.....	62
3.3. Results.....	63
3.3.1. Detection of COX-1 and COX-3 protein expression in b.End3 cells.....	63
3.3.2. Detection of COX-1 and COX-3 protein expression in C57BL/6 mice brain homogenates.....	64
3.3.3. Detection of COX immunoreactivity using Dot blots.....	65
3.3.4. Expression of COX mRNA in naive and LPS stimulated b.End3 cells.....	65
3.3.5. Expression of COX mRNA in C57BL/6 mice brain homogenates.....	67
3.3.6. Expression of COX-1 and COX-3 mRNA in b.End3 cells.....	68
3.3.7. Expression of COX-1 and COX-3 mRNA in C57BL/6 mice brain homogenates.....	69
3.4. Discussion.....	70
4. Effect of paracetamol, aminopyrine and antipyrine on lipolysis in rodent adipocytes.....	72
4.1. Introduction.....	72
4.2. Methods.....	73

4.3. Results.....	74
4.3.1. 3T3-L1 differentiation.....	74
4.3.2. Effect of paracetamol on basal lipolysis in 3T3-L1 adipocytes.....	75
4.3.3. Effect of paracetamol on norepinephrine stimulated lipolysis in 3T3-L1 adipocytes.....	77
4.3.4. Effect of paracetamol on isoproterenol stimulated lipolysis in 3T3-L1 adipocytes (added simultaneously).....	78
4.3.5. Effect of paracetamol pre-treatment on isoproterenol stimulated lipolysis in 3T3-L1 adipocytes.....	80
4.3.6. Chronic effect of paracetamol pre-treatment on isoproterenol stimulated lipolysis in 3T3-L1 adipocytes.....	84
4.3.7. Effect of paracetamol on forskolin stimulated lipolysis in 3T3-L1 adipocytes.....	85
4.3.8. Effect of paracetamol on 8-Br-cAMP stimulated lipolysis in 3T3-L1 adipocytes.....	87
4.3.9. Effect of aminopyrine and antipyrine on basal lipolysis in 3T3-L1 adipocytes.....	88
4.3.10. Effect of paracetamol, aminopyrine and antipyrine on basal lipolysis in rat primary brown adipocytes.....	89
4.3.11. Effect of paracetamol, aminopyrine and antipyrine on basal lipolysis in rat primary brown adipocytes.....	90
4.3.12. Effect of paracetamol, aminopyrine and antipyrine on norepinephrine stimulated lipolysis in rat primary brown adipocytes.....	92
4.4. Discussion.....	94
5. Effect of Paracetamol on Mitochondrial Fatty Acid uptake and Oxidation.....	98
5.1. Introduction.....	98
5.2. Methods.....	100
5.3. Results.....	100
5.3.1. Effect of paracetamol on FAO.....	100
5.3.2. Effect of paracetamol on individual parameters of mitochondrial function using FAO assay.....	103
5.3.3. Effect of paracetamol and N-acetyl-p-benzoquinone imine (NAPQI) on FAO.....	105
5.3.4. Comparison of the effect of paracetamol and NAPQI on FAO.....	107
5.3.5. Effect of paracetamol and NAPQI on individual parameters of mitochondrial function using FAO assay.....	110
5.4. Discussion.....	113
6. Effect of Paracetamol, Aminopyrine and Antipyrine on cellular and mitochondrial oxygen consumption.....	116
6.1. Introduction.....	116
6.2. Methods.....	117
6.3. Results.....	118
6.3.1. Mitochondrial bioenergetic profile of 3T3-L1 adipocytes.....	118
6.3.2. Effect of paracetamol on basal OCR.....	119
6.3.3. Effect of paracetamol on norepinephrine and isoproterenol stimulated OCR.....	120
6.3.4. Effect of paracetamol, aminopyrine and antipyrine on basal OCR.....	121
6.3.5. Effect of paracetamol, aminopyrine and antipyrine on isoproterenol stimulated OCR.....	122
6.3.6. Elucidation of mechanistic activity of inhibitors that affect mitochondrial function.....	124
6.3.7. Elucidation of the mitochondrial target of hypothermic agents.....	126

6.2.8. Elucidation of the mechanistic activity of hypothermic agents.....	127
6.4. Discussion.....	130
7. Final discussion and future work.....	133
8. List of abstracts.....	141
9. References.....	142

List of Tables

Table 1.1: COX-3 experimental data related studies

Table 2.1: COX-1 and COX-3 antibodies

Table 2.2: Published primers

Table 2.3: RT-PCR conditions for published primers

Table 2.4: Custom made primers for COX-1 and COX-3

Table 2.5: RT-PCR conditions for custom made primers for COX-1 and COX-3

Table 2.6: Mitochondrial function parameters

Table 2.7: XF FAO assay parameters

Table 7.1: Key findings of current research

List of Figures

Figure 1.1: Paracetamol metabolism.

Figure 1.2: The arachidonic acid (AA) pathways.

Figure 1.3: Thermoregulatory circuitry.

Figure 1.4: Types of thermogenesis in homeothermic species.

Figure 1.5: Differentiation of preadipocytes into adipocytes.

Figure 1.6: Regulation of lipid metabolism by adipose tissue.

Figure 1.7: Mechanism of fatty acid induced activation of uncoupling protein (UCP) and increased heat generation.

Figure 1.8: The FAO pathway.

Figure 2.1: Primers used for RT-PCR.

Figure 2.2: Schematic of Agilent Seahorse XF Cell Mito Stress Test Profile.

Figure 3.1: Detection of COX-1, COX-3, β -actin protein expression, COX-1 control peptide, secondary antibody control by Western blotting in b.End3 cells.

Figure 3.2: Detection of COX-1, COX-3, COX-1 control peptide, β -actin protein expression by Western blotting in C57BL/6 mice brain homogenates.

Figure 3.3: Detection of immunoreactivity of COX-1 and COX-3 using dot blots.

Figure 3.4: mRNA expression of COX-1 and GAPDH by RT-PCR in naive and LPS stimulated b.End3 cells for 1 and 3 hours.

Figure 3.5: mRNA expression of COX-2 and GAPDH by RT-PCR in naive and LPS stimulated b.End3 cells for 1 and 3 hours.

Figure 3.6: mRNA expression of COX-3 and GAPDH by RT-PCR in naive and LPS stimulated b.End3 cells for 1 and 3 hours.

Figure 3.7: mRNA expression of GAPDH, COX-1 and COX-3 by RT-PCR in mice brain homogenate.

Figure 3.8: mRNA expression of GAPDH, COX-1, COX-2 and COX-3 by RT-PCR in mice brain homogenate.

Figure 3.9: mRNA expression of GAPDH, COX-1 and COX-3 by RT-PCR in b.End3 cells.

Figure 3.10: mRNA expression of GAPDH, COX-1 and COX-3 by RT-PCR in mice brain homogenate.

Figure 4.1: Microscopic images of Oil Red O stained 3T3-L1 cells (passage 8) subjected to adipocyte differentiation for 7 days (Qualitative).

Figure 4.2: Quantitative analysis of 3T3-L1 cells differentiation using Oil Red O staining.

Figure 4.3: Effect of paracetamol on basal lipolysis in 3T3-L1 adipocytes at 1, 3 and 24 hours.

Figure 4.4: Effect of paracetamol on norepinephrine stimulated lipolysis in 3T3-L1 adipocytes at 1 and 3 hours.

Figure 4.5: Effect of paracetamol on isoproterenol stimulated lipolysis in 3T3-L1 adipocytes at 1 hour.

Figure 4.6: Effect of paracetamol on isoproterenol stimulated lipolysis in 3T3-L1 adipocytes at 3 hours.

Figure 4.7: Effect of paracetamol on isoproterenol stimulated lipolysis in 3T3-L1 adipocytes after 24 hours.

Figure 4.8: Effect of paracetamol pre-treatment on isoproterenol stimulated lipolysis in 3T3-L1 adipocytes at 1 hour.

Figure 4.9: Effect of paracetamol pre-treatment on isoproterenol stimulated lipolysis in 3T3-L1 adipocytes at 3 hours.

Figure 4.10: Effect of paracetamol pre-treatment on isoproterenol stimulated lipolysis in 3T3-L1 adipocytes at 24 hours.

Figure 4.11: Chronic effect of paracetamol pre-treatment on isoproterenol stimulated lipolysis in 3T3-L1 adipocytes after 24 and 48 hours.

Figure 4.12: Effect of paracetamol on forskolin stimulated lipolysis in 3T3-L1 adipocytes at 1, 3 and 24 hours.

Figure 4.13: Effect of paracetamol on 8-Br-cAMP stimulated lipolysis in 3T3-L1 adipocytes at 3 and 24 hours.

Figure 4.14: Effect of aminopyrine and antipyrine on basal lipolysis in 3T3-L1 adipocytes at 1, 3 and 24 hours.

Figure 4.15: Effect of paracetamol, aminopyrine and antipyrine on basal lipolysis in rat primary brown adipocytes at 1 hour.

Figure 4.16: Effect of paracetamol on basal lipolysis in rat primary brown adipocytes at 1 and 24 hours.

Figure 4.17: Effect of aminopyrine on basal lipolysis in rat primary brown adipocytes at 1 and 24 hours.

Figure 4.18: Effect of antipyrine on basal lipolysis in rat primary brown adipocytes at 1 and 24 hours.

Figure 4.19: Effect of paracetamol on norepinephrine stimulated lipolysis in rat primary brown adipocytes at 1 and 24 hours.

Figure 4.20: Effect of aminopyrine on norepinephrine stimulated lipolysis in rat primary brown adipocytes at 1 and 24 hours.

Figure 4.21: Effect of antipyrine on norepinephrine stimulated lipolysis in rat primary brown adipocytes at 1 and 24 hours.

Figure 5.1: Effect of paracetamol on FAO during basal and after oligomycin addition in 3T3-L1 adipocytes.

Figure 5.2: Effect of paracetamol on FAO after FCCP and rotenone/ antimycin A addition in 3T3-L1 adipocytes.

Figure 5.3: Effect of paracetamol on individual parameters of mitochondrial function using FAO assay in 3T3-L1 adipocytes.

Figure 5.4: Effect of paracetamol on individual parameters of mitochondrial function using FAO assay in 3T3-L1 adipocytes.

Figure 5.5: Effect of paracetamol and NAPQI on FAO during basal and after oligomycin addition in 3T3-L1 adipocytes.

Figure 5.6: Effect of paracetamol and NAPQI on FAO after FCCP and rotenone/ antimycin A addition in 3T3-L1 adipocytes.

Figure 5.7: Comparison of the effect of paracetamol and NAPQI on FAO during basal and after oligomycin addition in 3T3-L1 adipocytes.

Figure 5.8: Comparison of the effect of paracetamol and NAPQI on FAO after FCCP and rotenone/ antimycin A addition in 3T3-L1 adipocytes.

Figure 5.9: Effect of paracetamol and NAPQI on individual parameters of mitochondrial function using FAO assay in 3T3-L1 adipocytes.

Figure 5.10: Effect of paracetamol and NAPQI on individual parameters of mitochondrial function using FAO assay in 3T3-L1 adipocytes.

Figure 6.1: Bioenergetic profile of 3T3-L1 adipocytes.

Figure 6.2: Effect of paracetamol on basal OCR in 3T3-L1 adipocytes.

Figure 6.3: Effect of paracetamol on norepinephrine and isoproterenol stimulated OCR in 3T3-L1 adipocytes.

Figure 6.4: Effect of paracetamol, aminopyrine and antipyrine on basal OCR in 3T3-L1 adipocytes.

Figure 6.5: Effect of paracetamol on isoproterenol stimulated OCR in 3T3-L1 adipocytes.

Figure 6.6: Effect of aminopyrine and antipyrine on isoproterenol stimulated OCR in 3T3-L1 adipocytes.

Figure 6.7: Elucidation of mechanistic activity of inhibitors that affect mitochondrial function (5 μ g mitochondria).

Figure 6.8: Elucidation of the mitochondrial target of hypothermic agents (5 μ g mitochondria).

Figure 6.9: Elucidation of the mechanistic activity of hypothermic agents (2.5 μ g mitochondria).

Abbreviations

AC	Adenylyl cyclase
ACS	Acyl-CoA synthetases
ADP	Adenosine diphosphate
ATP	Adenosine triphosphate
ATGL	Adipocyte triglyceride lipase
AR	Adrenergic receptor
XFp	Agilent Seahorse Analyzer
ALT	Alanine transaminase
α	Alpha
α_1	Alpha-1 adrenergic receptor
α_2	Alpha-2 adrenergic receptor
Ta	Ambient temperature
AM	Aminopyrine
AT	Antipyrine
A	Ampere
~	Approximately
AA	Arachidonic acid
AST	Aspartate transaminase
N ₃ -	Azide
bp	Base pairs
β	Beta
β_1	Beta-1 adrenergic receptor
β_2	Beta-2 adrenergic receptor
β_3	Beta-3 adrenergic receptor
Tb	Body temperature
BAT	Brown adipose tissue
C57BL/6	C57 black 6
CB ₁	Cannabinoid-1 receptor
CO	Carbon monoxide
CCCP	Carbonyl cyanide m-chlorophenyl hydrazone
FCCP	Carbonyl cyanide-4-(trifluoromethoxy)phenylhydrazone
CPT	Carnitine palmitoyl transferase
CPT1	Carnitine palmitoyltransferase 1

CPT2	Carnitine palmitoyltransferase 2
CAT	Carnitine translocase
CGI-58	Comparative gene identification-58
cm	Centimetre
CNS	Central nervous system
CoA	Coenzyme A
cDNA	Complementary Deoxyribonucleic Acid
T _c	Core temperature
CN-	Cyanide
cAMP	Cyclic adenosine monophosphate; 3',5'-cyclic adenosine monophosphate
COX	Cyclooxygenase
COX-1	Cyclooxygenase-1
COX-1b	Cyclooxygenase-1b
COX-1 ^{+/-}	Cyclooxygenase-1-heterozygous-knockout
COX-1 ^{-/-}	Cyclooxygenase-1-homozygous-knockout
COX-2	Cyclooxygenase-2
COX-2 ^{+/-}	Cyclooxygenase-2-heterozygous-knockout
COX-2 ^{-/-}	Cyclooxygenase-2-homozygous-knockout
COX-3	Cyclooxygenase-3
COX-3 ^{-/-}	Cyclooxygenase-3-homozygous-knockout
CYP450	Cytochrome P450
CYP 1A2	Cytochrome P450 1A2
CYP 2E1	Cytochrome P450 2E1
CYP 3A4	Cytochrome P450 3A4
°C	Degree Celsius
DNA	Deoxyribonucleic acid
DGs	Diglycerides
DILI	Drug induced liver injury
ETC	Electron transport chain
Eto	Etomoxir
XF	Extracellular flux
ERK	Extracellular signal regulated kinases
FAAH	Fatty acid amide hydrolase
FAO	Fatty acid oxidation

FAT/CD36	Fatty acid translocase/ cluster of differentiation 36
FACS	Fatty acyl CoA synthase
Fe ⁴⁺ =OPP* ⁺	Ferryl protoporphyrin IX radical cation
FFA	Free fatty acid
GABA	Gamma-aminobutyric acid
GAPDH	Glyceraldehyde 3-phosphate dehydrogenase
GSH	Glutathione
G _{αs}	Gs alpha subunit
G _{αi}	Gi alpha subunit
g/day	Grams/day
>	Greater than
IC ₅₀	Half maximal inhibitory concentration
h	Hour
HSL	Hormone sensitive lipase
H ⁺	Hydrogen ions
H ₂ O ₂	Hydrogen peroxide
PGG ₂	Hydroperoxy endoperoxide
PGH ₂	Hydroxy endoperoxide
IMM	Inner mitochondrial membrane
IU/L	International Units/Litre
Iso	Isoproterenol
kb	Kilobyte
kDa	Kilodaltons
KO	Knockout
LPS	Lipopolysaccharide
LCFA	Long-chain (C ₁₄ –C ₁₈) fatty acids
M	Molar
MAPK	Mitogen activated protein kinase
MnSOD	Manganese superoxide dismutase
MPTP	Membrane permeability transition pore
FABPpm	Membrane associated fatty acid binding protein
mRNA	Messenger Ribonucleic Acid
μg/mL	Microgram/millilitre
μm	Micrometer
μM	Micromolar

mg/kg	Milligram/kilogram
mM	Millimolar
mV	Millivolts
$\Delta\psi$	Mitochondrial membrane potential
MGs	Monoglycerides
NAC	N-acetylcysteine
APAP	N-acetyl-p-aminophenol
NAPQI	N-acetyl-p-benzoquinone imine
NADPH	Nicotinamide adenine dinucleotide phosphate (reduced form)
NOX4	NADPH oxidase isoform
AM404	N-arachidonoylphenolamine
NADH	Nicotinamide adenine dinucleotide (reduced form)
NOP	Nociceptin/orphanin FQ peptide
NSAIDs	Nonsteroidal anti-inflammatory drugs
NE	Norepinephrine
n	Number of replicates
redox	Oxidation/reduction
OXPPOS	Oxidative phosphorylation
OCR	Oxygen consumption rate
PA	Paracetamol
PCOX-1a	Partial cyclooxygenase-1a
PCOX-1b	Partial cyclooxygenase-1b
%	Percentage
POX	Peroxidase
PGC-1 α	Peroxisome proliferator-activated receptor γ coactivator 1 α
POA	Preoptic area of anterior hypothalamus
PGI ₂	Prostacyclin I ₂
PGD ₂	Prostaglandin D ₂
PGE ₂	Prostaglandin E ₂
PGF _{2α}	Prostaglandin F _{2α}
6-keto PGF _{1α}	6-keto prostaglandin F _{1α}
PGHS	Prostaglandin H synthase
PGHS-1	Prostaglandin-endoperoxide synthase 1
PGHS-2	Prostaglandin-endoperoxide synthase 2
PGs	Prostaglandins

PKA	Protein kinase A
FADH ₂	Reduced flavin adenine dinucleotide
RNA	Ribonucleic acid
RCR	Respiratory control ratio
RT-PCR	Reverse transcription polymerase chain reaction
SD	Standard deviation
SNPs	Single-nucleotide polymorphisms
G _i	Inhibitory regulative G-protein
G _s	Stimulative regulative G-protein
SULT	Sulfotransferase
SNS	Sympathetic nervous system
TXs	Thromboxanes
TXA ₂	Thromboxanes A2
TXB ₂	Thromboxanes B2
TRPA1	Transient receptor potential ankyrin 1
TRPA1 ^{-/-}	Transient receptor potential ankyrin 1 knockout
TRPV1	Transient receptor potential vanilloid 1
TRPV1 ^{-/-}	Transient receptor potential vanilloid 1 knockout
TCA	Tricarboxylic acid cycle
TGs	Triglycerides
UDP	Uridine 5'-diphospho
UGT	UDP-glucuronosyl transferases
UCPs	Uncoupling proteins
UCP1	Uncoupling protein 1
UCP2	Uncoupling protein 2
UCP3	Uncoupling protein 3
U.K.	United Kingdom
U.S.A.	United States of America
V	Volts
WAT	White adipose tissue
WT	Wild type

Acknowledgements

In the name of God, the Most Gracious, the Most Merciful.

I would like to sincerely acknowledge Dr Winston A. Morgan for always being very supportive, encouraging and motivating. My learning experience was exceptional under his kind supervision and guidance. I would also like to express my gratitude to Dr Samir S. Ayoub for his excellent skills, experience and additional support. Also, special thanks go to Dr Mohammed S. Meah and Dr Elizabeth K. Westhead for their unlimited support and encouragement throughout my studies. I greatly appreciate Ms Elizabeth Wood for providing b.End3 cells, Dr Steven Millership for his guidance in culturing and differentiating 3T3-L1 pre-adipocytes and Prof Michael P. Seed for his help with animal tissues. Lastly, big thanks to Mr Nick Howe and Agilent Seahorse for an instrument loan and providing great technical support during the final stages of my PhD.

Dedication

This PhD thesis is dedicated to my beloved family.

Chapter 1: Introduction

1.1. Paracetamol

Paracetamol, (acetaminophen) or N-acetyl-p-aminophenol (APAP) is one of the most widely used antipyretic and analgesic drugs worldwide (Yoon et al., 2016; Józwiak-Bebenista and Nowak, 2014). Paracetamol related compounds first came to notice in the 1880s when acetanilide was dispensed by mistake to a patient in place of naphthalene and caused a significant reduction in fever.

Phenacetin and paracetamol were originally synthesized by Morse in 1878 (Morse, 1878), however clinical trials by Von Mering concluded by error that paracetamol was more toxic therefore phenacetin was introduced into medical practice in 1887 and became the most widely used analgesic until it was discovered to be nephrotoxic (Von Mering, 1893). In 1948, paracetamol was rediscovered (Brodie and Axelrod, 1948) and by 1955, paracetamol was being marketed by McNeil Laboratories in the form of a prescribed medication (Tylenol) for children (Józwiak-Bebenista and Nowak, 2014). One year later, paracetamol was available as an over the counter medication (Panadol) in the United Kingdom (U.K.) produced by Frederick Stearns & Co (Józwiak-Bebenista and Nowak, 2014). Today many prescription and non-prescription formulations contain paracetamol alone or in combination with other drugs (Ghanem et al., 2016). Paracetamol is available as tablets, effervescent tablets, suspension, powder (sachets) and rectal suppositories (Józwiak-Bebenista and Nowak, 2014). When administered orally the clinical actions of paracetamol can be seen by 30 minutes or after 15 minutes using fast-release tablets.

Since the 1980's paracetamol has become the first drug of choice for treating pain and fever in children in situations where use of nonsteroidal anti-inflammatory drugs (NSAIDs) are contraindicated (Cranswick and Coghlan, 2000; Leung, 2012). After of over a century of discovery and use some of the mechanism of actions of paracetamol particularly around the impact on cyclooxygenase (COX) enzymes remains a matter fierce of debate (Gentry et al., 2015; Eberhardt et al., 2017). It is generally accepted that paracetamol has similar analgesic and antipyretic properties as NSAIDs, without anti-inflammatory activity. By contrast paracetamol is associated with fewer side effects than the NSAIDs (Józwiak-Bebenista and Nowak, 2014).

1.2. Paracetamol: Proposed mechanisms of action

In terms of their main actions, traditionally both paracetamol and the NSAIDs were thought to inhibit the conversion of arachidonic acid (AA) into prostaglandin H - PGH₂, catalysed by prostaglandin H synthase (PGHS) or cyclooxygenase (COX). Historically two isoenzymes of PGHS termed COX-1 (PGHS-1) and COX-2 (PGHS-2) (Hinz and Brune, 2002) have been discovered.

Traditional NSAIDs and COX-2 inhibiting drugs exert their actions by inhibiting the COX enzyme by competing with arachidonic acid to bind to the enzyme active site (Anderson, 2008). By contrast paracetamol is thought to act by reducing a ferryl protoporphyrin IX radical cation (Fe⁴⁺=OPP*+) at peroxidase site.

1.3. Paracetamol absorption and metabolism

The absorption of paracetamol occurs rapidly in the duodenum (McGill and Jaeschke, 2013). At safe doses, peak concentrations will be achieved within 1.5 hours and half-life of 1.5 – 3 hours, at overdose peak serum concentrations is observed within 4 hours (McGill and Jaeschke, 2013). Paracetamol goes through the blood brain barrier with ease and is distributed uniformly in the central nervous system (CNS) at all doses (Courad et al., 2001; Kumpulainen et al., 2007; Ara and Ahmad, 1980; Massey et al., 1982; Fischer et al., 1981). In man a plasma concentration of 200-300 µg/mL is considered toxic and the patient is in need of serious treatment. Similarly in rodent studies doses of 100 mg/kg and above are associated with some biomarkers of toxicity, by 300 mg/kg there is gross evidence of toxicity. In addition doses of 100-500 mg/kg have been linked to plasma concentration of 1-10 mM in rodents. *In vitro*, similar concentrations are normally associated with alterations of cellular and mitochondrial function (Fischer et al., 1981; Orbach et al., 2017).

Metabolism primarily occurs within liver and involves three major routes (Figure 1.1). The majority (~90%) of the drug enters phase II metabolic pathways, where paracetamol is conjugated via UDP-glucuronosyl transferases (UGT) or sulfotransferase (SULT), with conversion to glucuronidated and sulfated metabolites eliminated in the urine (McGill and Jaeschke, 2013). About 2% of the drug is excreted in the urine without having undergone any metabolism (McGill and Jaeschke, 2013). Another portion of paracetamol (~10%) undergoes phase I oxidation by hepatic cytochrome

CYP 2E1 (to a lesser extent with CYP 1A2 and 3A4) producing the highly reactive toxic metabolite, N-Acetyl-p-benzoquinone imine (NAPQI), (Jaeschke et al., 2012a; 2012b; Yuan and Kaplowitz, 2013; McGill et al., 2012; Jaeschke et al., 2015). In addition to the urine, paracetamol metabolites are also excreted into the bile (McGill and Jaeschke, 2013). At non-toxic doses, NAPQI undergoes rapid conjugation by hepatic GSH to form non-toxic mercaptate and cysteine compounds (McGill and Jaeschke, 2013). At hepatotoxic doses, the glucuronidation and sulfonation pathways become saturated; as a result majority of paracetamol is metabolized to NAPQI resulting in GSH depletion and then increased toxicity (Jaeschke et al., 2012a; 2012b). Most of the toxicity of paracetamol can be attributed to the covalent binding of NAPQI to sulfhydryl groups on cysteine and lysine molecules in proteins within the mitochondria of hepatocytes and other cells (McGill and Jaeschke, 2013; Yuan and Kaplowitz, 2013). The mitochondrial protein adducts formed, lead to oxidative injury and hepatocellular necrosis.

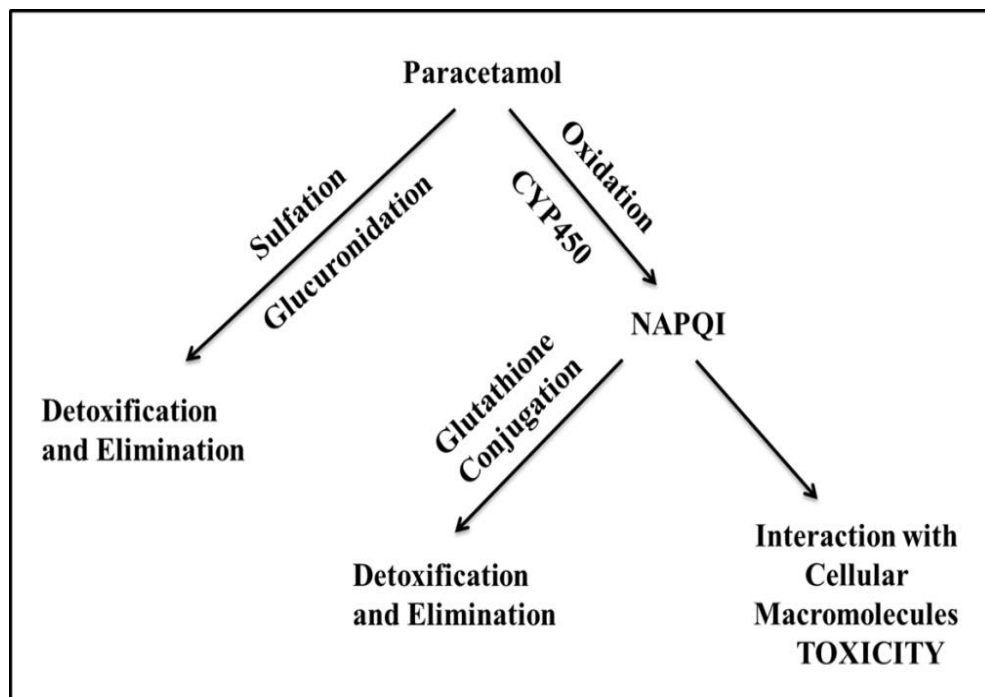


Figure 1.1: Paracetamol metabolism. Paracetamol mainly undergoes metabolism via sulfation and glucuronidation. NAPQI formation results via oxidation by CYPs, leading to toxicity, or detoxification via GSH conjugation (Adapted from Moyer et al., 2011).

In the CNS paracetamol undergoes other important reactions which are beyond the scope of this thesis, for example interaction with fatty acid amide hydrolase (FAAH) and AA and producing fatty acid amide N-(4-hydroxyphenyl) arachidonamide (AM404) in the CNS of rodents (Rivera et al., 2017; Muramatsu et al., 2016).

1.4. Paracetamol Toxicity

Paracetamol induced liver injury is the most common form of drug induced liver injury (DILI) in humans and a leading cause for almost 50% of the cases of acute liver failure around the world (Lee, 2012). This damage can be demonstrated in rodents after acute administration of doses above 100mg/kg (Riveria et al., 2017).

Several studies involving mouse models have been conducted. Paracetamol metabolite protein adducts seem to cause disruption of the electron transport chain (ETC) and results in reactive oxygen and reactive nitrogen species formation in mitochondria (Jaeschke et al., 2012a). In C57BL/6 mice (150 mg/kg) other actions include opening of membrane permeability transition pore (MPTP) and deoxyribonucleic acid (DNA) breakage linked to mitochondrial dysfunction in hepatocytes with no alanine transaminase (ALT) release. However, high dose (300 mg/kg) resulted irreversible mitochondrial dysfunction and necrosis (Jaeschke et al., 2012a; Kon et al., 2004; Gujral et al., 2002; Hu et al., 2016).

In relating the animal studies to humans the Rumack-Matthew nomogram suggest that patients with levels of 200 µg/mL at 4 hours and 25 µg/mL at 16 hours falls under “probable toxicity line”, with 60% incidence of severe hepatotoxicity (defined as aspartate transaminase (AST) > 1000 IU/L) and 5% mortality (Rumack 2002; Heard, 2008; Prescott et al., 1979; Harrison et al., 1991; Smilkstein et al., 1988; Kerr et al., 2005; de Andrade et al., 2015; McGovern et al., 2015). A “high toxicity line” starting with 300 µg/mL at 4 hours shows 90% incidence of severe hepatotoxicity and 24% mortality (Heard, 2008). In the United States of America (U.S.A), Australia and New Zealand, a different “treatment line,” was introduced beginning at a 4-hour paracetamol concentration of 150 µg/mL to avoid errors in intake history and lab results (Rumack 2002; Smilkstein et al., 1988).

1.5. Cyclooxygenases

COXs are important enzymes with a number of key physiological roles including catalysing the formation of prostaglandins and thromboxane (Figure 1.2). Prostaglandins (PGs) are autocooid mediators affecting processes under physiological and pathological conditions. There is extensive evidence linking the activity of COX enzymes to both pyresis and hypothermia. COXs are member of heme-dependent myeloperoxidase superfamily (Daiyasu and Toh, 2000) are the main enzymes catalysing the alteration of AA to prostanoids such as PGs, thromboxanes (TXs) and prostacyclins (PGI₂). These AA metabolites are involved in fever, pain, inflammation, renal function, platelet aggregation and gastrointestinal integrity (Toussaint et al., 2010).

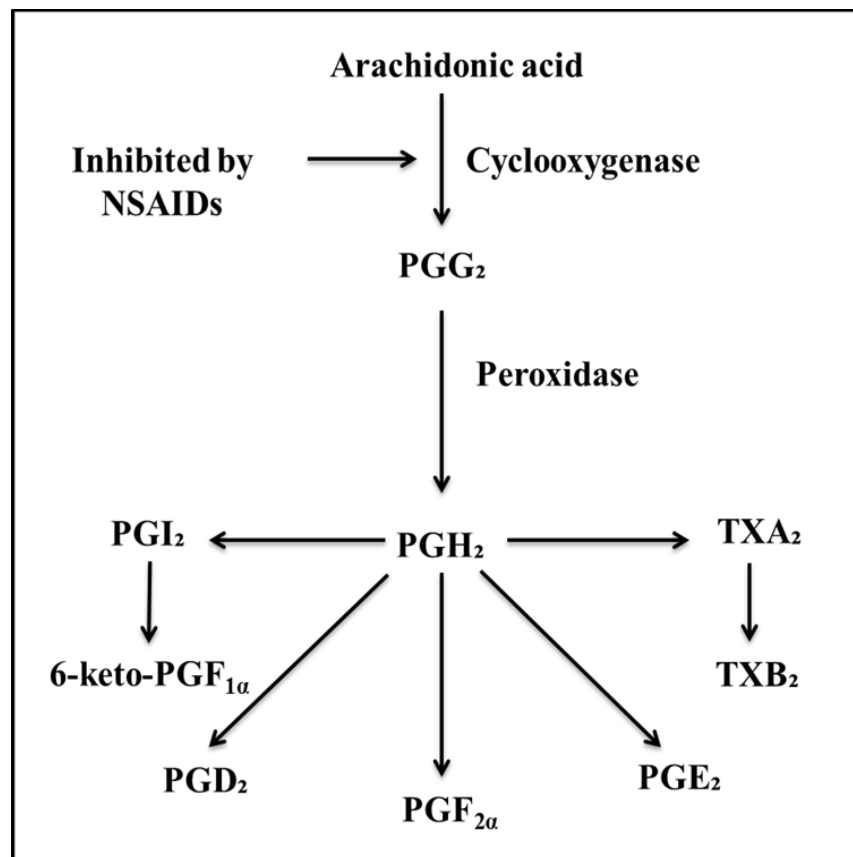


Figure 1.2: The arachidonic acid (AA) pathways. AA is converted by COX-1 or COX-2 to PGG₂ and PGH₂. Later on, PGH₂ is metabolized by cytosolic prostaglandin synthases to different prostanoid products (Adapted from Botting, 2004).

Based on the phylogenetic analysis, both isoforms of COXs appeared to arise from a duplication of an ancestral COX gene which occurred early on or before origin of vertebrate species (Kawamura et al., 2014; Jarving et al., 2004). Both enzymes are almost identical in their structures with 60-65% homology, 85%-90% between species (Kawamura et al., 2014) and contain 600 amino acids (Simmons et al., 1991). Three high mannose oligosaccharides are present in both COX-1 and COX-2, thus helps in folding of protein whereas a fourth is only present in COX-2, responsible for degradation (Rouzer and Marnett, 2009).

Both COX isoforms are located in the lumen of nuclear membrane and endoplasmic reticulum (Simmons et al., 2004); however, COX-1 is also found in lipid bodies in cells (Bozza et al., 1996). The hydrophobic signal peptides are different in size in both isoforms (Simmons et al., 2004). COX-1 contains eight amino acids after the signal peptide unlike COX-2. In 2010, Xu et al. showed that removal of these 7 amino acids in human COX-1 resulted in enzymatically active mutant and sensitive to aspirin to a similar extent. In COX-1, glycosylation of asparagine at 410 is crucial for COX and POX functions and to fold protein properly (Otto et al., 1993).

The gene for human COX-1 and COX-2 is found on chromosome 9q32–q33.3 and 1q25.2–q25.3. A large human COX-1 gene (>28 kb) has 11 exons and 10 introns. In case of COX-2, the gene (~8 kb) is short (Simmons et al., 2004). COX-2 consists of 10 exons and 9 introns. In the COX-1 gene (5' end), signal peptide is encoded by exon 1 and 2, dimerization domain by exon 3 and membrane-binding domain by exon 4. Encoding of catalytic domain occur by exon 6–11 (Roos and Simmons, 2005). Therefore, complete exon skipping intron retention would affect the resulting protein (Roos and Simmons 2005).

1.6. Existence of COX variants

Various types of alternative splicing have been proposed for the COXs isoforms. COX-1 alternative transcripts are thought to be more common than COX-2 (Roos and Simmons, 2005). Diaz et al. (1992) first reported a COX-1 splice variant that lacked exon 9 in human fibroblasts, thus eliminating the *N*-glycosylation site at residue 409, essential for proper folding and enzyme activity. The protein resulting from partially deleted exon 9 was detected in mammalian as well as insect cells; however, no COX

products were observed *in vivo* (Schneider et al., 2005). In addition, a splice variant of COX-1 was identified that lacked exon 1 with partially retained intron 2 in rat and thought to form nonsense enzyme (Kitzler et al., 1995). Another variant of COX-1 was observed in endothelial cells (Hla, 1996).

In an attempt to evaluate the biological relevance of COX splice variants, Roos and Simmons (2005) emphasised that such variants should represent physiologically relevant concentrations and cell-specificity, that COX translation must be identified as a functional protein *in vivo*. In 2018, in almost all cases these requirements have yet to be achieved.

1.7. Evidence for COX-3

The somewhat different properties of paracetamol to classical NSAIDs led to the suggestion of a previously unknown COX isoform more sensitive to paracetamol than COX-1 or COX-2 and named as COX-3 (Vane and Botting, 1996; Botting et al., 2000). Furthermore, it was proposed that the activity of this inducible enzyme could account for the antipyretic and analgesic actions of paracetamol (Simmons et al., 1999).

The evidence for a COX-3 has been supported by the cloning, characterisation and expression of COX-1 splice variant initially named as COX-3 from dog and human brain (Chandrasekharan et al., 2002). It differs from COX-1 only in the retention of intron 1, resulting in a potential in-frame insertion of 30 amino acids to the N-terminal hydrophobic signal peptide of the COX-3 molecule. COX-3 is thought to have similar catalytic and structural features to that of the other two COX isoforms (Chandrasekharan et al., 2002).

COX-1 contains 10 introns, whereas COX-2 has 9 introns with the difference in the placement of intron 1. There is a high degree of conservation of the intron 1 sequence from species such as dog, human and mouse. Further investigations revealed retention of intron 1 results in the insertion of 90 nucleotides with 75% sequence matching to COX-1 of human or mouse intron 1 sequences. However, alignment of the gene sequences from the start codon with no gaps showed little sequence homology and would result in a totally different protein in different species (Kis et al., 2005).

The COX messenger ribonucleic acid (mRNA) transcript corresponded to the 2.6 kb complementary deoxyribonucleic acid (cDNA) clone with unspliced intron 1; termed as

COX-3. COX-3 mRNA is found at about 5% of COX-1 mRNA in canine cerebral cortex (Chandrasekharan et al., 2002). Like COX-1, canine COX-3 was thought to be regulated during development due to its high expression in some cells and tissues (Schwab et al., 2003a). As canine COX-3 matches to COX-1, apart from the N-terminus which does not contribute to the enzymatic activity, it was proposed that canine COX-3 would have similar activity to other COX enzymes (Simmons et al., 2004).

The presence of two previously uncharacterized COX-1-related mRNA transcripts (5.2 and 2.8 kb) was also reported in human tissues with human intron-1-targeting probe with highest levels of 5.2 kb transcript hybridised in the cerebral cortex and then heart (Chandrasekharan et al., 2002). However, these observations were different from previously reported COX-1 mRNA expression patterns (O'Neill and Ford-Hutchinson, 1993).

Retention of intron 1 in COX-1 in humans would result in the addition of 94 nucleotides, thus shifting the downstream COX-3 sequence out of frame, a strong argument against a functional protein (Dinchuk et al., 2003). However, those who proposed the active COX-3 protein argue that processes such as ribosomal frame shifting could result an active COX-3 protein (Chandrasekharan et al., 2002). However, it was argued that no downstream alternative splices would be able to rescue the reading frame and a catalytically active form of this enzyme making it unlikely to present in humans (Schwab et al., 2003b; Dinchuck et al., 2003). Moreover, COX-3 is more likely to simply be a splice error (Shaftel et al., 2003).

Another argument against the reported COX-3 protein is that using antibodies raised in one species targeting another species. This primarily due to the minimal sequence homology between human and canine COX-3 if we consider the actual reading frame following inclusion of intron 1. It would only be 7 out of the 12 amino acids from the target peptide that would match between human and canine COX-3, making unlikely for an antibody targeting N-terminus of human COX-3 to identify canine COX-3 (Kis et al., 2005; Davies et al., 2004). However, using antibodies specific to intron 1 amino acid sequence (MSREXDPXA) predicted in mammals, expression of both COX-3 and PCOX-1a was detected in insect cells (Chandrasekharan et al., 2002). Looking at the actual published data some argue that it is difficult to interpretate the cropped western blots due to lack of molecular weight marker (Kis et al., 2005) whereas the author justified the cropped blots due to space limitations (Simmons et al., 2005). In terms of

activity, the PGE₂ levels produced by COX-3 were found to be 20% of that of COX-1 (about 20% of the activity of COX-2). However, lack of appropriate controls made it difficult to conclude if the low levels of PGE₂ production actually represented canine COX-3 activity (Kis et al., 2005).

The half-life of COX-3 mRNA in humans was similar to COX-1 (Cui et al., 2004) and human COX-3 protein was expected to be only 8.7 kDa. However, using either COX-1 monoclonal or COX-3 polyclonal antibodies, a COX-3 65 kDa protein was detected in human aorta and about 25% of the level of COX-1. Moving from the molecular evidence to enzyme activity, the IC₅₀ value of paracetamol was 64 μM at 5 μM of arachidonic acid as a substrate and the order of selectivity was COX-3 > COX-1 > COX-2. At higher substrate concentrations (30 μM), dipyron was slightly more potent inhibitor of COX-3 with an IC₅₀ of 52 μM different to phenacetin (102 μM) and paracetamol (460 μM) (Chandrasekharan et al., 2002). Interestingly, antipyrine and aminopyrine showed a reduced ability to inhibit this enzyme. However, these analgesic/antipyretic drugs with low anti-inflammatory activity were demonstrated to preferentially inhibit COX-3. The enzyme activity also confirm that although paracetamol inhibits the putative COX-3, it is not unique or the most sensitive drug. Those who advocate the unique activity of paracetamol against COX-3 argue that the altered sub-cellular localisation of COX-3 could change redox environments and substrate concentrations, thus affecting inhibition by paracetamol (Simmons, 2003). Differences in the IC₅₀ of COX-1 and canine COX-3 *in vitro* only suggest the possibility of specific inhibition of canine COX-3 by paracetamol.

Among NSAIDs, diclofenac was the most potent COX-3 inhibitor (IC₅₀ value 0.008) followed by indomethacin, ibuprofen, aspirin. Although these drugs (except aspirin) inhibited COX-3 preferably over COX-1 and COX-2 they were far more potent than paracetamol against COX-3. However, it has been proposed that the polar nature of diclofenac and ibuprofen make them less likely to reach COX-3 expressed in brain effectively (Chandrasekharan et al., 2002; Botting and Ayoub, 2005; Berenbaum, 2004).

One explanation from the frameshifting argument is that alternative polyadenylation is considered to overcome the impact of frameshift in intron-1, resulting in intron-1 antibody-identified proteins (Simmons, 2003). However, others argue that although, two stem-loop structures which are thought to be relevant in splicing intron-1 and transcription of COX-1 or COX-3 cannot also explain the possible -1 frameshifting (Kis et al., 2005). In 2003, Shaftel et al. confirmed the existence of COX-3 mRNA in

multiple C57BL/6 mice tissues such as spleen, astrocyte, brain and cultured glial cells using standard RT-PCR. COX-1 expression was greater than COX-3. The primers designed for this study was COX-1/3 that would anneal within exon 1 and 3 of COX-1, resulting in COX-3 (349 base pairs) and COX-1 (247 base pairs) products whereas COX-3 specific primers would be confined to the first intron of COX-1 and within exon 3 resulting in 164 base pair COX-3 product. Using COX-3 specific primers, abundance of this splice variant was observed in spleen, brain and microglial samples. Retention of intron 1 resulted in addition of 102 nucleotides in-frame in the mouse. It was pointed out that intron 1 in mice and rats is 98 nucleotides and expected to cause a frameshift and resulting in a protein entirely different than COX-1, and with doubtful COX activity. Theoretically, another site of initiation or downstream alternative splicing could cause restoration of the reading frame and a functional COX-3 (Kis et al., 2005).

As COX-3 mRNA matches to COX-1 but retains intron 1, the sense primer targeted intron 1 and antisense primer anneals to exon 5 (497 base pairs). There was highest mRNA expression of COX-3 in cerebral endothelial cells (Kis et al., 2003), and suggesting the target for antipyretic the actions of paracetamol may be due to the key role of cerebral endothelial cells in mediating temperature regulation (Matsumura et al., 1998).

Schwab et al. (2003c) assumed that the analgesic effect of paracetamol is answered in the form of COX-3, however the results demonstrated by Kis group could not support this idea due to lack of COX-3 mRNA expressed in neurons. By contrast paracetamol does not seem to inhibit COX-3 at standard oral doses (0.5–1 g/day) (Schwab et al., 2003c). Also, there is no correlation between the site of COX-3 expression (cerebral cortex) and temperature regulation in the hypothalamus. From the height of the COX-3 research to the present day, an active COX-3 protein has yet to be proven in humans (Berenbaum, 2004).

Evaluation of the appearance of three COXs after lipopolysaccharide (LPS) treatment in endothelial cells, astrocytes, epithelial cells, and pericytes showed an increase in COX-2 mRNA expressed but COX-1 and COX-3 did not alter, confirming constitutive COX-3 expressed in rat brain at mRNA level similar to COX-1 (Kis et al., 2003). The results indicate involvement of COX-3 in membrane-based COX signalling or when basal COX-1 or COX-2 expression levels persist. Using an anti-human COX-3 antibody raised against the N-terminal peptides (first 13 amino acids of COX-3 in humans) (MSRECDPGARWGC), COX-3 protein immunoreactivity was detected in human

hippocampus and stressed neurons without any specific information about the COX-3 band size (Cui et al., 2004).

In 2004, Kis et al. went a step ahead and demonstrated the presence of COX-3 mRNA in male Wistar rat brain in vivo using primers that could differ COX-1 and COX-3. Furthermore, this study showed regional demonstration of COX-3 mRNA in different brain regions with considerable variability. In addition to Kis's findings, COX-3 (497 base pairs) expressed in aorta, brain, cerebellum, heart, and lung of male Wistar rats. However, western blot analysis showed that commercially available anti-canine or anti-human antibodies could not detect COX-3 protein (data not shown in the article), COX-1 protein expression was demonstrated in all tissues whereas only brain and cerebellum were COX-2 immunopositive. It was noted that commercially available anti-COX-3 antibodies are species-selective (Warner et al., 2004).

Another study suggested there was no evidence of paracetamol sensitive COX activity in cerebellum or brain when compared to naproxen, rofecoxib and SC560. They also argue that COX-3 mRNA if expressed would lead to a production of a different protein and may explain the absence of COX-3 activity (Warner et al., 2004).

1.8. Evidence for the involvement of COX-3 in thermoregulation

Considering the hypothesis that COX-3 in rodents would have a totally altered amino acid sequence than COX-1 and COX-2 without being active (Snipes et al., 2005), some found the findings of Ayoub et al. (2004) surprising (Davies et al., 2004). In the same year, a study was published by Ayoub et al. suggested COX-3 inhibition is associated with paracetamol induced hypothermia. Under basal conditions, when paracetamol is administered intraperitoneally (100–300 mg/kg) in C57/BL6 male mice, it resulted in a dose dependent decrease of 0.4°C, 0.8°C, and 2°C in rectal temperature. Although no toxicity was assessed, these doses correlate with reported toxic doses of paracetamol (Jollow et al., 1973; James et al., 2003; Williams et al., 2010; Agarwal et al., 2011; Ramachandran et al., 2011; Bajit et al., 2011; McGill et al., 2012; McGill et al., 2013; Ramachandran et al., 2013; Xie et al., 2015; Noh et al., 2015; Zhang et al., 2015; Du et al., 2017).

A time course study showed a maximum hypothermic effect 1 hour after taking 300 mg/kg paracetamol and returned to normal after 4–5 hours. The hypothermic effects were suggested to correlate with paracetamol plasma concentrations (Fischer et al.,

1981). Other putative COX-3 inhibitors showed the greatest hypothermic response with 50 mg/kg aminopyrine after 30 minutes with the same recovery time as that of paracetamol treatment. Similarly 100 mg/kg antipyrine showed maximum hypothermia after 30 minutes to the same extent as shown by paracetamol treatment; however the recovery was inconsistent after 4-5 hours. Furthermore, there seemed to be a direct relationship between body temperature and PGE₂ levels in brain with maximum effect after 1 hour resulting in 96% reduction in PGE₂ levels in paracetamol treated group and 60% after 30 minutes of antipyrine and aminopyrine treatment (data not shown in the article) (Ayoub et al., 2004).

At doses of 300 mg/kg, COX-1 KO mice showed a decrease in the hypothermic effect of paracetamol, whereas it was unaltered in COX-2^{+/-} and COX-2^{-/-} mice. Interestingly, the greatest drop in body temperature was noticed in COX-2^{-/-} paracetamol treated group. However, paracetamol induced hypothermia was not fully diminished in COX-1^{-/-} group (-2.05°C in COX-1^{-/-} and -3.9°C in WT group) suggesting only partial involvement of COX-independent mechanisms.

Reduction of brain PGE₂ levels after 1 hour of administration of 300 mg/kg paracetamol was completely disappeared in COX-1^{-/-} mice. In COX-1^{-/-} group, the basal PGE₂ levels were 30% of those in WT mice, demonstrating COX-1 as a major source of PGE₂ production in brain. Changes in PGE₂ levels in vehicle treated wild-type, COX-1^{+/-} and COX-1^{-/-} groups was not very clear. Also, if paracetamol exerts its hypothermic actions through COX-1 gene derived protein then one would expect a dramatic decrease in the PGE₂ levels in COX-2^{+/-} or COX-2^{-/-} versus WT mice.

1.9. Evidence for COX-3; questions about experimental design

COX-3 mRNA was detected as 290 base pairs product in whole brain tissues of all genotypes of COX-2 KO and WT mice. This study also suggested that constitutive COX-3 is a target for hypothermic action of paracetamol and this COX-1 gene derived enzyme is located most probably in brain endothelial cells and involved in regulation of body temperature in mice through COX-3 derived PGE₂ (Ayoub et al., 2004). It was speculated that COX-3 is present in hypothalamic region of the CNS and responsible for a constant PGE₂ release for thought to be required for temperature regulation. As a majority of laboratory animals are kept at 22°C and the thermoneutral temperature of

mice is 32–34°C and, a constant biosynthesis of PGE₂ is proposed to be required to maintain body temperature (Botting and Ayoub, 2005).

The techniques used to determine the COX-3 data prompt a few questions. Given that COX-3, a splice variant of COX-1 there has to be a question whether a COX-1^{-/-} mouse is also a COX-3^{-/-} mouse. The disruption of C-terminus of COX-1 by the retention of intron-1 would possibly result in a protein without the C-terminus sequence of 120 amino acids responsible for COX-1 activity, but would still retain the full sequence of COX-3 protein (Kis et al., 2005). mRNA data of COX-1^{+/-} and COX-1^{-/-} mice in Ayoub et al. (2004) and Dou et al. (2004) studies would have been helpful (Davies et al., 2004) to conclude whether paracetamol induced hypothermia is mediated by COX-3 inhibition. In addition, the primer sets used in the COX-3 mRNA studies targeted PCOXa (Ayoub et al., 2004; Dou et al., 2004). More importantly, COX-3 remain unidentified in Western blot analysis and immunohistochemistry data was not considered as conclusive considering the non-specificity of the technique and polyclonal antibodies used (Kis et al., 2005). There seemed to be an issue with anti-mouse COX-3 antibody used specific to sequence of 13-amino acids (MSREFDPEAPRNC); being more than 50% different from the actual sequence for COX-3 in mouse or rat (MSRESDPSGAPTR), thus COX-3 remain unrecognised in mouse or rat (Davies, 2004). Simmons et al. (2005) clarified that the antibody used was a human and mouse peptides mixture (50:50) corresponding to first 12 amino acids encoded by exon 1 and the retained intron 1.

In an attempt to better reflect the role of COX-3, Snipes et al. (2005) preferably called COX-1 variant as COX-1b. Sequence analysis has shown the generation of COX-1b mRNA (573 base pairs) from cerebral endothelial cells (CECs) and cerebral microvessels retaining 98 bp intron 1. This encodes an expected protein of 127 amino acid without homology to existing COX sequence. An anti-rat polyclonal antibody corresponding to 2–17 amino acids (SRESDPSGAPTRPGIR) was generated. The highest expression of COX-1b protein was detected in heart, kidney, and neuronal tissues. This finding was further confirmed by immunostaining of rat primary CECs (Snipes et al., 2005).

However using exogenous arachidonic acid in COS-7 cells, rat COX-1b was found not to be catalytically active and sensitive to paracetamol inhibition. Two COX-1 transcripts retaining intron 1 (>4.5 kb and 2.8 kb) was found in majority of human tissues using an intron 1-specific probe (26 to 63 base pair within intron 1) were

reported. In brain, the expression was highest in the cerebral cortex. Using anti-human COX-1 intron 1 targeted antibody, COX-1b (75 kDa) and PCOX-1a (55 kDa) proteins alongside two smaller uncharacterized proteins (15 kDa) were detected (Qin et al., 2005).

To generate a protein there could be two possibilities as to how the reading frameshift was restored; single-nucleotide polymorphisms (SNPs) or RNA editing resulting in removal of a single nucleotide. DNA sequencing study showed the presence of three splice variants of COX-1b. Major COX-1b₁ retains entire intron 1, leading to a frameshift and addition of a stop codon approximately after 249 bp which would most likely form a COX-inactive protein. COX-1b₂ and COX-1b₃ contain almost the full intron 1 with only exception of guanidine or cytosine, which would lead to a self-rectifying frameshift and thus encoding probably a full length COX-active protein. These variants showed less than 25% identity between human and canine versions (Qin et al., 2005).

When COX-1b₂ was expressed in insect Sf9 cells, COX-1 was found to be more active in conversion of arachidonic acid to PGF_{2α}. Paracetamol, dipyrrone and phenacetin did not show varied potency between human COX-1 and COX-1b₂. It was suggested that retention of intron 1 may change protein topology resulting in a different glycosylation pattern, enzyme activity and selectivity. When human COX-1 and COX-1b₂ were compared, it showed no significant differences, proposing human COX-1b₂ is not the target for paracetamol's actions (Qin et al., 2005). The key publications related to COX-3 is presented in Table 1.1.

Table 1.1: COX-3 experimental data related studies

Canine	Mouse	Rat	Human
Chandrasekharan et al., 2002.	Shaftel et al., 2003; Dou et al., 2004; Ayoub et al., 2004; Cui et al., 2004; Kis et al., 2006; Ayoub et al., 2006.	Kis et al., 2003; Kis et al., 2004; Warner et al., 2004; Kis et al., 2005; Snipes et al., 2005; Abd el-aleem et al., 2009; Oksuz et al., 2016.	Chandrasekharan et al., 2002; Qin et al., 2005; Nurmi et al., 2005; Censarek et al., 2006; Reinauer et al., 2013.

1.10. Paracetamol induced hypothermia: the role of COX enzymes

The antipyretic action of paracetamol during fever has been extensively studied over the last 30 years and there is general consensus about this aspect of the mechanisms involved. The most widely accepted view is that paracetamol inhibits the COX-2 enzyme which is normally expressed following infection or trauma which leads to fever (Engström et al., 2013). It has also been known for some time that in many small mammals paracetamol can cause hypothermia (Walker et al., 1981; Massey et al., 1982; Ayoub et al., 2004; Li et al., 2008; Corley et al., 2009; Ayoub et al., 2011; Briyal and Glutai 2013; Gentry et al., 2015; Ahangar et al., 2016; Fukushima et al., 2017).

Over the last 15 years there has been increased interest in paracetamol induced hypothermia in non-febrile rodents (rats and mice). This phenomenon has been noted at doses >100mg/kg which is the same dose required to reduce LPS induced fever in these animals. However in non-febrile animals there is no involvement of the COX-2 enzyme (Ayoub et al., 2004, 2011; Ayoub and Botting 2005). Another point for consideration is that the equivalent of the therapeutic dose (>100 mg/kg) of paracetamol in mice, at least in terms of antipyresis is very close to the dose where there is clear evidence of biomarkers of toxicity, particularly in mice.

The mechanism by which paracetamol causes hypothermia in pyrogen free rodents has been the subject of fierce debate, primarily around the role of the COX-1 enzyme. In particular the suggestion that the hypothermia was due to the inhibition of the COX-1 variant enzyme (Ayoub et al., 2004). The suggestion was that the expression of this novel variant COX-1 was to regulate core temperature (T_c) in rodents housed at temperatures which require them to produce extra heat to maintain normal body temperature (Ayoub et al., 2004). A more detailed discussion on the regulation of T_c will be undertaken later in this chapter. However, this interpretation of the data has been challenged and there have been numerous studies to determine both the existence and role of the COX-1 variant termed COX-3 in paracetamol induced hypothermia (Kis et al., 2005; Li et al., 2008). Confirmation of the existence and role of COX-3 could transform our understanding of how both paracetamol and the NSAIDs work, with obvious implications.

1.11. Paracetamol induced hypothermia: other than COX?

Walker et al. (1981) demonstrated a central mechanism of action of paracetamol induced hypothermia and proposed that hypothermia and hepatotoxicity are two separate events in mice as administration of paracetamol (125–750 mg/kg) in Swiss white mice resulted in decreased body temperature (T_b) before liver injury and hepatic congestion became evident. However it is possible for the hypothermic of paracetamol to be evident before gross toxicity. When N-acetylcysteine (NAC) coadministered with paracetamol, hepatotoxicity was prevented and to some extent hypothermia was protected confirming the above (Walker et al., 1981).

The same research group indicated that the parent compound is responsible for causing early hypothermia in mice rather than its toxic reactive metabolite as mice pre-treated with phenobarbital that induces oxidative drug metabolism did not have any effect on paracetamol induced hypothermia. However, this hypothermic effect was enhanced when pre-treated with mixed-function oxidase blockers. In the same study, it was also indicated that paracetamol induced hypothermia is mediated centrally as the levels of parent compound in brain was associated with the degree of hypothermia, while it was not the case in liver. Paracetamol administered intracerebroventricularly caused significant hypothermic effect within 20 minutes (Massey et al., 1982).

In 2009, Corley et al. hypothesised that paracetamol induced hypothermia might be dependent on opioid and cannabinoid (CB₁) or activating nociceptin/orphanin FQ peptide (NOP) receptor. Dose dependent hypothermia was observed with paracetamol administered intraperitoneally (100, 250, 375 or 500 mg/kg) in rats. Pre-treatment with an opioid, CB₁ or NOP antagonists could not alter the hypothermic effect of paracetamol (400 mg/kg).

After presenting findings that paracetamol induced hypothermia may be mediated through COX-1 gene derived protein in mice, Ayoub et al. (2011) showed this phenomena does not rely on CB and transient receptor potential vanilloid 1 (TRPV1). BQ123, an endothelin-A receptor antagonist and paracetamol resulted in a significant increase (41%) in hypothermic response as opposed to paracetamol group alone (Briyal and Glutai, 2013).

Other researchers further investigated the hypothermic activity of paracetamol. Subcutaneous, but not intrathecal, administration of this drug has shown to decrease

body temperature in WT mice dose dependently. Pre-treatment with resiniferatoxin that destroy or defunctionalize peripheral TRPV1 expressing terminals, but resistant to COX inhibition abolished the hypothermic effect. As paracetamol evoked hypothermia was identical in wildtype and TRPV1^{-/-} mice, and not reduced by the maximum effective dose of a TRPV1 antagonist, it was concluded that this phenomena is independent of TRPV1. Since Transient receptor potential ankyrin 1 (TRPA1) is co-expressed with TRPV1, it was predicted to cause hypothermia similar to TRPV1 agonists. Interestingly, a TRPA1 antagonist inhibited the hypothermic effect of paracetamol and this drug did not have an effect on body temperature in TRPA1^{-/-} mice (Gentry et al., 2015).

The hypothermic effect of paracetamol has also been linked to Gamma-aminobutyric acid (GABA) and benzodiazepine receptors (Ahangar et al., 2016). An acute therapeutic dose of paracetamol (20 mg/kg lean body mass) was shown to impact on Tc of non-febrile humans in a sub-neutral environment. This observation suggested that paracetamol might cause an inhibition of the mechanisms involved in thermogenesis which are important to maintain Tc in humans (Foster et al., 2016).

1.12. Thermoregulation

There is clear evidence that paracetamol and the NSAIDs have an impact on body temperature either in febrile or non-febrile animals. Thermoregulation is a complex process involving both temperature receptors and receptors located centrally and peripherally. Regulation of Tb depends on the ability of a thermoregulatory circuitry to sense and integrate thermal information from the external environment and deep within the body core (Bicego et al., 2007), thus involving various relatively independent thermoeffector loops along with afferent and efferent pathways (Romanovsky, 2007) (Figure 1.3).

Homeotherms are capable of maintaining their Tc within a fairly constant range (36.0-37.5°C) through the process of thermoregulation. The reference or set-point temperature is established by the firing rate of thermoregulatory neurons in the hypothalamus (Boulant, 2000). However, certain environmental and biological factors such as time of day, site of temperature measurements, level of physical activity, age, sex and race can cause slight variations.

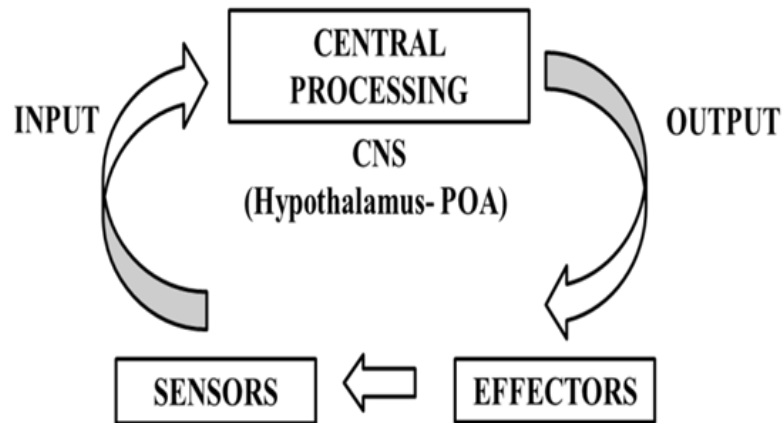


Figure 1.3: Thermoregulatory circuitry. Peripheral thermosensors detect body surface temperature. These are cold sensors (most common, location; epidermis, signals; thin myelinated $A \delta$ fibers) and warm sensors (less common, location; slightly deeper in the dermis, signals; unmyelinated C fibers). Peripheral deep-body sensors respond to the T_c (location; esophagus, stomach, large intra-abdominal veins, and other organs). Brain temperature is detected by central thermosensors (most common; warm-sensitive whereas less common; cold sensitive). The preoptic area of anterior hypothalamus (POA) is a region thought to integrate information about local brain temperature and other body temperatures and to regulate the level of output for a set of thermoregulatory responses that are most suitable for given internal and environmental temperatures. Warm sensitive neurons are inherently sensitive to their own hypothalamic temperature and synaptically receive afferent information from skin and spinal thermoreceptors (Romanovsky, 2007). Preoptic warming elicits a variety of heat loss responses including panting, increased saliva secretion and increased skin blood flow, as well as behavioural responses. Preoptic cooling evokes heat production responses such as shivering and non-shivering thermogenesis, and heat retention responses including cutaneous vasoconstriction and behavioural responses (Adapted from Bicego et al., 2007).

Generally, it is believed that mice share the same thermoeffector mechanisms of other homeotherms with few exceptions. They replace grooming saliva for sweating to increase evaporative heat loss and possess BAT as a source of heat production. Due to their large surface area mass ratio, smaller mammals rely more on changing their metabolic heat production to regulate T_c . Additionally; rodents may also employ

behavioural thermoregulation strategies such as huddling and nest building to respond to changes in ambient temperature (T_a). Mice are nocturnal and exhibit a circadian rhythm, the average daytime T_c of laboratory mice at midday is 36.0°C whereas during the night due to increased activity this increases to 37°C . Laboratory mice tend to regulate their T_c approximately 1°C below that of laboratory rats. They prefer warm T_a during the daytime when the animal is inactive and cooler temperature at night during the time of higher activity and elevated T_c .

1.13. Basic concept of thermogenesis and thermoneutral zone

Heat production or thermogenesis is a key component of thermoregulation and could be either obligatory or facultative (Figure 1.4).

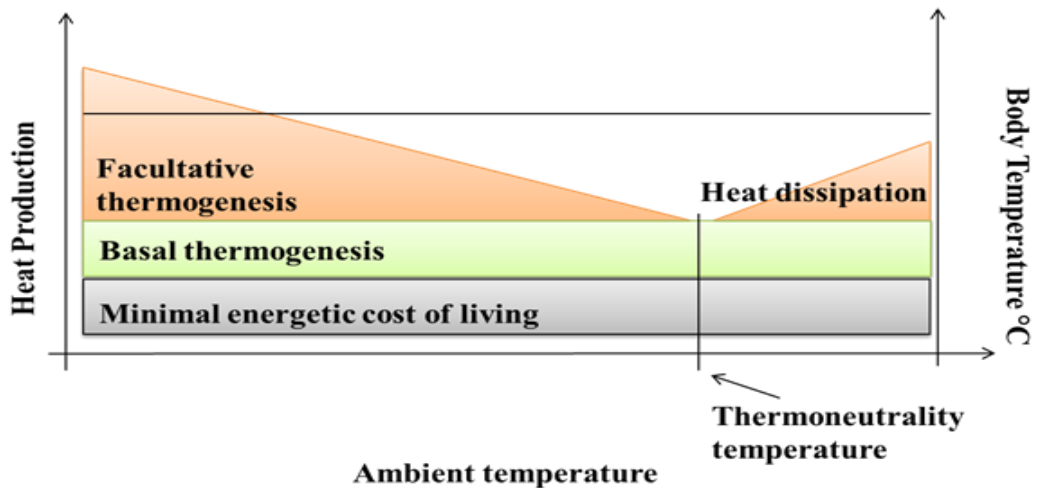


Figure 1.4: Types of thermogenesis in homeothermic species. The horizontal line on the right vertical axis represents constant body temperature independent of the environment. Thermoneutrality temperature is represented on the x-axis. In colder environment, there is an increase in the magnitude of facultative thermogenesis whereas in warmer ambient temperature, thermoneutrality temperature is reached at which obligatory thermogenesis is enough for maintenance of body temperature (Adapted from Silva, 2003).

Heat production is usually derived from sustaining vital functions or obligatory thermogenesis sometimes such as basal metabolic rate or resting energy expenditure. Obligatory thermogenesis comprised of two components; the heat resulting via

minimum energy cost of living that is not enough for maintaining T_b in cold environments. Secondly, the excess heat results from basal metabolic activity called *basal thermogenesis* and it is independent of T_a (Silva, 2003). Basal thermogenesis could be explained by more active metabolism of homeothermic species than poikilotherms, thus sustaining greater energy transactions/time (Silva, 2003; Else and Hulbert, 1981).

A number of strategies are used to augment obligatory thermogenesis; these include vasoconstriction, piloerection, changed posture and reduced mobility. Due to the limitations of these mechanisms, additional facultative or adaptive thermogenesis is needed. In birds, the major site of this form of thermogenesis is likely to be the skeletal muscle and in case of mammals, it is brown adipose tissue (BAT) (Silva, 2006; Duchamp, 1993; Cannon and Nedergaard, 2004). Apart from cold stimuli, facultative thermogenesis can be activated by food, dissipating excess calories (Silva, 2003).

Thermoneutrality or thermoneutral zone is a range of T_a where the obligatory thermogenesis is enough to maintain a stable T_c . The thermoneutral temperature of an animal varies according to body surface area-to-volume ratio resulting in a value of about 23°C in an adult man, 28°C in rats and 30°C in mice (Silva, 2003; Gordon, 1993).

1.14. Thermogenic Mechanisms

Homeotherms generally use two major mechanisms to increase heat generation. Increased production and utilization of adenosine triphosphate (ATP) (same amount of heat per ATP), most notably by accelerating ion movement against gradients. Ironically increased heat generation occur by reducing the efficiency of the mitochondrial ATP production through regulated proton leak in many tissues including brown adipose. Although mechanism is still not clear it involves uncoupling proteins (UCPs) particularly uncoupling protein 1 (UCP1). Hormones such as thyroid hormone may also be a regulator of thermogenesis (Silva, 2006). All the varying forms of thermogenesis require the supply of substrates to the mitochondria; the greater the demand for heat, the more substrate is required. Substrate supply relies on the catabolism/metabolism of glucose and triglycerides (TGs) producing primarily NADH for the ETC. The greater the demand for heat the more susceptible the substrate supply or ETC is to disruption.

1.15. The Adipose Tissue:

Adipose tissue plays a major role in metabolic regulation (Luo and Liu, 2016). Adipose tissue acts as the fuel reservoir, involved in conservation of heat and responsible for regulating lipid utilization (Luo and Liu, 2016). Excess energy is stored as neutral TGs via lipogenesis (Vaughan, 1962). When energy intake is insufficient or increased demands are stimulated, glycerol and fatty acids can be released from TGs into the blood and penetrate into different organs, thus distributing lipids and control energy balance (Luo and Liu, 2016). In addition to a fuel reservoir, adipose tissue is a major endocrine organ secreting various bioactive compounds that affect muscles, liver, pancreas and brain thus acts as a modulator of systemic metabolism (Luo and Liu, 2016).

1.16. Types of Adipose tissue

Adipose tissue is divided into two main categories: white adipose tissue (WAT) and BAT. WAT stores excess energy as TGs whereas BAT which contain abundant UCP1, also called thermogenin, short-circuits the coupling of the respiratory chain to ATP synthetase (Ràfols, 2014). As a result, it dissipates chemical energy as heat (Cannon and Nedergaard, 2004) and prevents hypothermia and obesity via oxidation of lipids (Luo and Liu, 2016).

1.17. Adipocytes

Adipocytes are the main cell type in adipose tissue (Luo and Liu, 2016). They can vary in origin, morphology, mitochondria number and genes expressed in thermogenesis (Luo and Liu, 2016). Primarily based in WAT, white adipocytes vary in size from 25–200 μm , appear as unilocular lipid droplet, and possess a small number of mitochondria with limited rate of oxidation (Luo and Liu, 2016). They possess high capacity of storing energy as TGs (Tan and Vidal-Puig, 2008).

Brown adipocytes appeared as multilocular, abundant mitochondria as well as UCP1, and dissipate stored energy as heat via uncoupling ATP synthesis from the ETC (Luo and Liu, 2016). Increased expression of β -adrenergic receptors mediate cold-induced lipolysis in adipose tissues. Also, during cold stress, movement of large amounts of

lipids occur from WAT into BAT is accompanied by mitochondrial biogenesis (Blüher et al., 2004). As a result of β -adrenergic signalling in BAT, peroxisome proliferator-activated receptor γ coactivator 1 α (PGC-1 α) is expressed, this stimulates UCP1 expression and mitochondrial genes (Fortier et al., 2005).

Unlike WAT, BAT is only found in mammals (Ràfols, 2014). In rodents, BAT is particularly abundant in the perinatal period, but persists throughout their adult life (Ràfols, 2014). In rodents, brown adipocytes mainly present in the interscapular and peri-renal sections whereas in humans and infants, it is located in abdominal sites which have a good blood supply (Luo and Liu, 2016).

1.18. Adipogenesis and its regulation

Differentiation of preadipocytes into mature fat cells is called adipogenesis, an important process for adipose tissue growth and energy balance (Lefterova and Lazar 2009; Ali et al., 2013). Preadipocytes are small cells with fibroblasts morphology which upon stimulation form mature adipocytes. Adipocyte volume reflects the balance between lipogenesis and lipolysis whereas adipocyte number reflects the balance between preadipocyte proliferation, differentiation, and apoptosis, and apoptosis of adipocytes depending on tissue sites (Ràfols, 2014; Tchkonina et al., 2005). Various cell models of white preadipocytes (3T3-L1, 3T3-F442A) and immortal lines of brown preadipocytes have been used to investigate the differentiation process (Rosen, 2000).

The four stages reported includes proliferation arrest induced by contact inhibition indicates confluence (Figure 1.5). Clonal expansion induced by hormone signals and represented by a few mitotic divisions for cell cycle synchronisation. Early differentiation stage arresting cell division, expressing characteristic adipocyte genes and initiating lipid accumulation. Lastly, typical adipocyte morphology is finally reached with the terminal differentiation phase with induction of transcription of genes, typical of mature adipocytes. In addition to the heterogeneity of the preadipocyte population when cultured *in vitro*, differences between mature adipocytes in a same WAT site have also been reported (Ràfols, 2014).

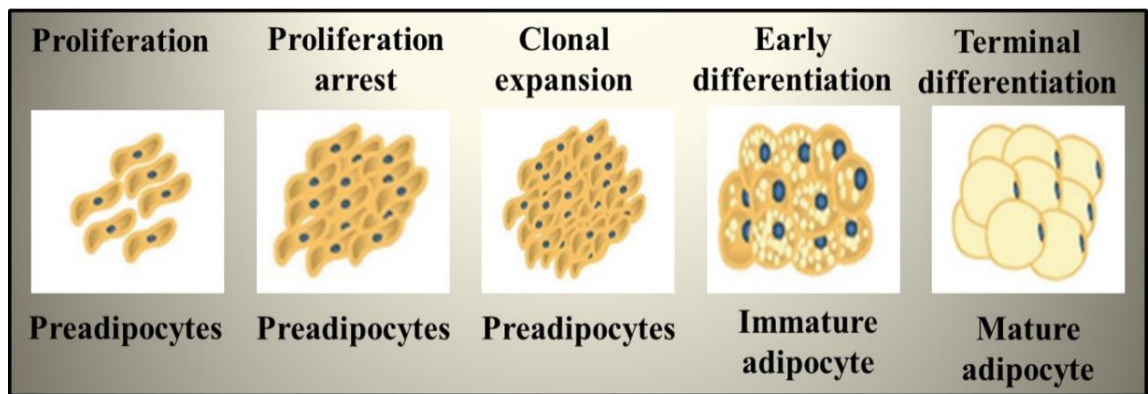


Figure 1.5: Differentiation of preadipocytes into adipocytes. Different stages of adipogenesis (Adapted from Ràfols, 2014).

1.19. Lipolysis

Lipolysis is the catabolic process result in conversion of stored TGs into free fatty acids (FFAs) and glycerol release (Luo and Liu, 2016). The classical physiological lipolytic pathway involves catecholamine release via sympathetic nervous system (SNS). Catecholamines bind to plasma membrane bound β -adrenergic receptors and activate membrane-bound AC leading to activation of cyclic adenosine monophosphate (cAMP) dependent PKA (Taylor et al. 2004; Carmen and Victor, 2006; Thompson et al., 2010) (Figure 1.6).

Adrenergic receptors have seven transmembrane domains and are G-protein coupled receptors. β_1 , β_2 and β_3 adrenergic receptors are couple to $G_{\alpha s}$ which stimulate adenylyl cyclase (AC) activity. α_1 and α_2 adrenergic receptors are coupled to $G_{\alpha i}$ which inhibits AC activity (Lafontan and Berlan, 1993). Due to a lower affinity of β -receptors for catecholamines than the α -receptors, the AC activity will be low under basal conditions as catecholamine levels are low (Thompson et al., 2010). Increased AC activity is favoured at high concentrations of catecholamines due to activation of the β -receptors and increased abundance compared to the α -receptors (Thompson et al., 2010).

The β_3 -adrenergic receptor is highly expressed in rodent BAT and, unlike the β_1 and β_2 adrenergic receptors; it is relatively specific to these tissues (Chaves et al., 2011). In mice the β_3 receptor is the major regulator of lipolysis (Lafontan and Berlan, 1993). In humans, β_1 and β_2 provide the stimulating side while α_2 controls the inhibitory side

(Lafontan and Berlan, 1993). The main mechanism in the regulation of lipolysis in adipocytes is the balance of AC activity (Thompson et al., 2010).

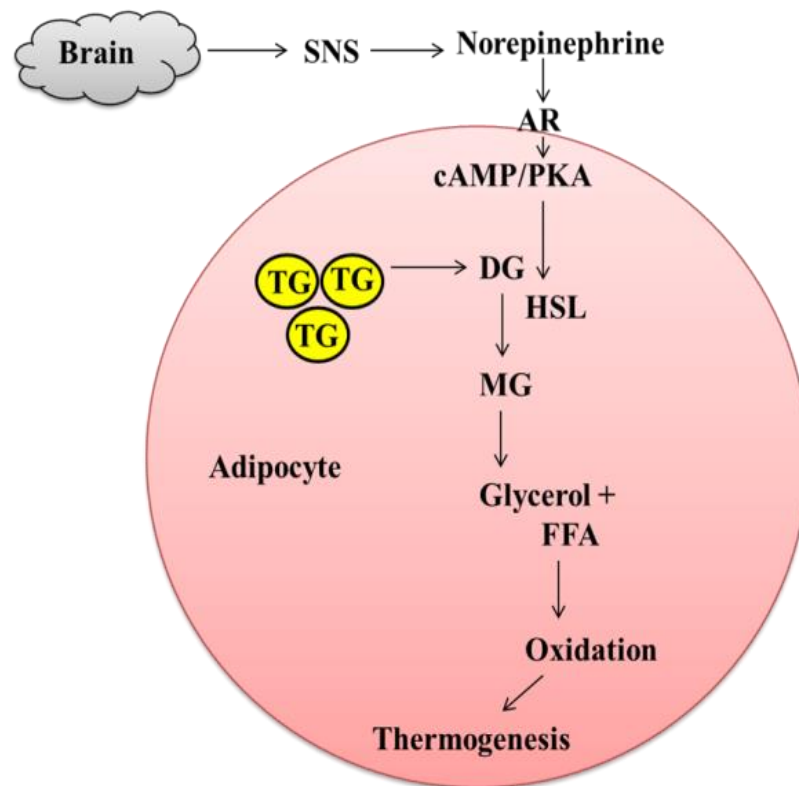


Figure 1.6: Regulation of lipid metabolism by adipose tissue. Lipolysis converts TG to FFA and glycerol that undergoes oxidation. SNS =sympathetic nervous system; AR = adrenergic receptor; cAMP = cyclic adenosine monophosphate; PKA = protein kinase A; TG = Triglyceride; DG = Diglyceride; HSL = Hormone sensitive lipase; MG = Monoglyceride; FFA = Free fatty acid (Adapted from Luo and Liu, 2016).

During basal state, hormone sensitive lipase (HSL) is present in the cytoplasm. Perilipin A (perilipin 1) is a structural protein coating lipid droplets, thus protecting TG molecules from HSL access and thus inhibits basal lipolysis (Zhang et al., 2008). Adipose triglyceride lipase (ATGL) is located in the cytosol as well as on the surface (MacPherson and Peters, 2015). A key coactivator of ATGL is comparative gene identification-58 (CGI-58), (MacPherson and Peters, 2015), its binding to perilipin A restrict CGI-58-ATGL interaction. This results in low lipolytic activity and fatty acids

released due to TG hydrolysis are re-esterified (Lafontan and Langin, 2009), thus TG levels remain relatively constant.

Under stimulated state, PKA causes phosphorylation of Perilipin A, ATGL, CGI-58 and HSL (MacPherson and Peters, 2015). Once phosphorylated, perilipin A causes ATGL activation and allows ATGL and HSL to access lipid droplet (MacPherson and Peters, 2015). Catecholamines can stimulate lipolysis not only by PKA, mitogen-activated protein kinase (MAPK) and extracellular signal-regulated kinase (ERK) (Greenberg et al., 2001). It was suggested that lipolysis has an impact on heat generation and energy utilization by providing a source of fatty acids for increased β -oxidation (MacPherson and Peters, 2015).

1.20. Brown and beige fat mediated non-shivering thermogenesis

Brown and beige fat are responsible for dissipating energy as heat and provide a new option to fight obesity and related conditions (Luo and Liu, 2016; Lowell and Spiegelman, 2000; Cannon and Nedergaard, 2004). As a result of cold, feeding or stress exposure, norepinephrine (NE) release from sympathetic fibres bind to β_3 -adrenergic receptor located on fat cells (Ueta et al., 2012). This leads to activating cAMP dependent PKA, lipolytic process and thermogenesis (Luo and Liu, 2016). Prolonged cold exposure activates BAT in adult humans, increases moving of lipids to BAT and oxidation of lipids via heat generation in mitochondria (Luo and Liu, 2016).

1.21. Paracetamol and thermogenesis

Regardless of the impact of paracetamol on COX activity, the relatively high concentrations of paracetamol required to induce hypothermia in rodents may have other effects on the animals both centrally and peripherally. Mice (and other rodents) rely on increased metabolic activity to maintain their T_c at T_a below their thermoneutral zone (30°C). In particular, increased activity of BAT is key to thermoregulation in many species.

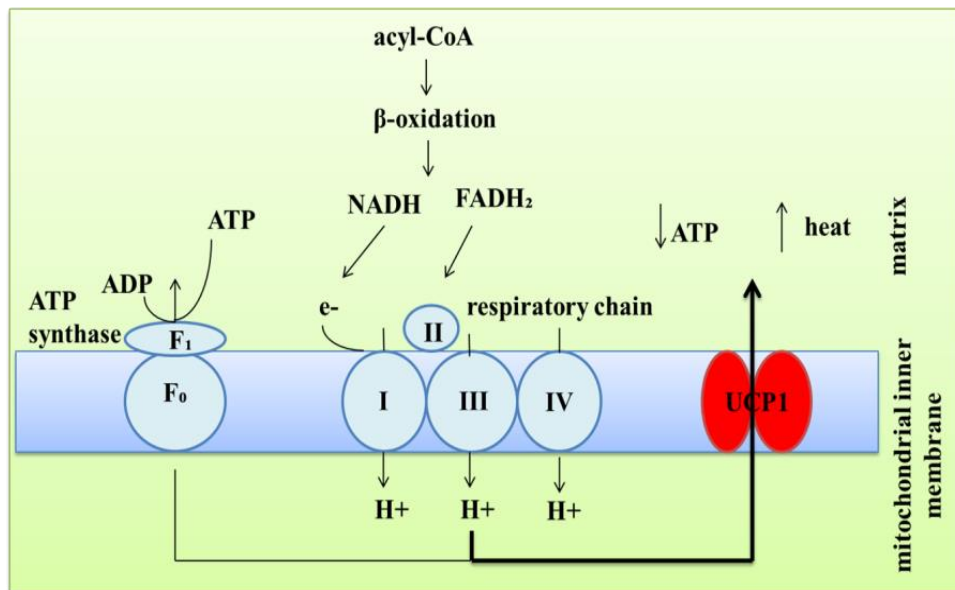


Figure 1.7: Mechanism of fatty acid induced activation of uncoupling protein (UCP) and increased heat generation. FFA are transformed into acyl-CoA and transported into mitochondria as acyl-carnitine. Thus, generates the electron donors, nicotinamide adenine dinucleotide (NADH) and flavin adenine dinucleotide (FADH₂). NADH- and FADH₂-derived electrons move down the respiratory chain, and pumping of protons from mitochondrial matrix into the intermembrane space. This creates across the inner mitochondrial membrane an electrochemical proton gradient which generates the proton motive force being used in most tissues to drive conversion of ADP to ATP by ATP synthase. Hence, fatty acids activate UCP1, which causes the dissipation of proton motive force as heat and results in a reduction of the mitochondrial membrane potential. Secondly, free fatty acids are metabolized by mitochondrial β-oxidation (Adapted from Sell et al., 2004).

Paracetamol may cause hypothermia by disrupting thermogenesis at one or more of the following stages. Signalling from the hypothalamus, the ability of the nerve innervations to release norepinephrine, lipolysis, oxidation of fatty acids or the interaction of fatty acids with the UCP.

One of the most likely potential targets for paracetamol is preventing the binding of fatty acids (AA) to UCP1 thereby preventing uncoupling (Figure 1.7). It is possible that paracetamol may compete with arachidonic acid and other fatty acids in a manner similar to the inhibition of COX enzymes.

1.22. Cellular Respiration

Energy is a pre-requisite for all life processes including biological and molecular events as well as for various cellular functions (Owen et al., 2011) and made available via a process of cellular respiration (Hill, 2014). The chemical energy in food is stored as ATP through slow combustion of carbohydrates, fats, and proteins or released as heat (Shutt and McBride, 2013). The majority of ATP production occurs via aerobic cellular respiration of glucose that represents 80% of carbohydrate metabolism (Owen et al., 2011).

1.23. Fatty Acid β -Oxidation

Fatty acid oxidation involves breaking long chain acyl-CoA to acetyl-CoA in mitochondria. Fatty acids require protein transporters located on the cell surface to enter a cell (Lopaschuk et al., 2010) (Figure 1.8). These transporters are fatty acid translocase (FAT/CD36), and plasma membrane bound fatty acid binding protein (FABP_{pm}) (Lopaschuk et al., 2010).

The next step involves addition of a CoA to the molecule of fatty acid via fatty acyl-CoA synthase (FACS) and leads to long chain acyl-CoA formation and then long chain acylcarnitine via carnitine palmitoyltransferase 1 (CPT1). This would allow the transportation of fatty acid moiety across the inner membrane of the mitochondria via carnitine translocase (CAT), thus exchanging long chain acylcarnitines and carnitine. The former then converts again to long chain acyl-CoA via inner mitochondrial membrane carnitine palmitoyltransferase 2 (CPT2) which then enters the β -oxidation pathway. This would form one acetyl-CoA per β -oxidation cycle.

The final step in fatty acid β -oxidation involves a series of complex enzyme catalysed steps including acyl-CoA dehydrogenase, enoyl-CoA hydratase, hydroxyacyl-CoA dehydrogenase, and ketoacyl-CoA thiolase enzymes ((Fillmore et al., 2017; Schulz, 2008). NADH and FADH₂ formation occur during β -oxidation which then utilized by ETC to generate ATP.

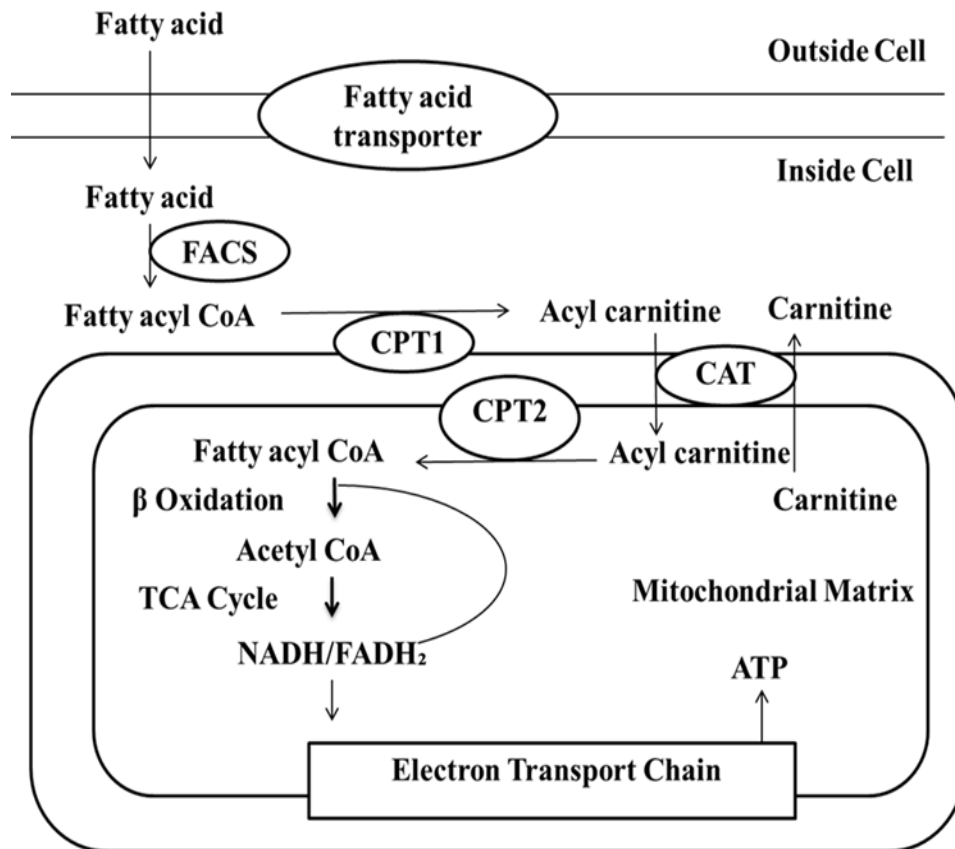


Figure 1.8: The fatty acid β -oxidation (FAO) pathway. Fatty acid protein transporters allow fatty acids entry inside the cell. FACS then adds a CoA group to the fatty acid forming long-chain acyl-CoA. It is then converted to long-chain acylcarnitine via CPT1, transported by CAT across the inner mitochondrial membrane and converted back to long-chain acyl-CoA via CPT2. Long-chain acyl-CoA follows β -oxidation pathway, forming one acetyl-CoA which then enters the tricarboxylic acid (TCA) cycle. NADH and FADH₂ produced utilised to produce ATP via electron transport chain (ETC). (Adapted from Fillmore et al., 2017).

1.24. Electron Transport Chain

The ETC consists of five protein complexes including NADH dehydrogenase-ubiquinone oxidoreductase or complex I with approximately 46 subunits, catalysing NADH electron. Succinate dehydrogenase-ubiquinone oxidoreductase or complex II with 4 subunits, also an enzyme of the Krebs/TCA cycle. Ubiquinone-cytochrome *c* oxidoreductase or complex III with 11 subunits, catalyses electron transfer from reduced ubiquinone or coenzyme Q10 to cytochrome *c*.

Cytochrome *c* oxidase or complex IV with 13 subunits and ATP synthase or complex V, with approximately 16 subunits. The ETC also need two small electron carriers, ubiquinone/coenzyme Q and cytochrome *c* (Perier and Vila, 2012). Coenzyme Q (CoQ), or *ubiquinone*, is unique in that it is a carrier that is not a protein-bound prosthetic group. It only carries hydrogen atoms (protons plus electrons).

Electrons formed via energy substrates (such as NADH and FADH₂) formed in glycolysis, β -oxidation and the TCA cycle pass through different complexes to molecular oxygen and produce water. Also, proton pumping out of the mitochondria via complexes I, III, and IV, generates an electrochemical gradient called mitochondrial membrane potential, $\Delta\psi$ or the proton motive force which promotes the ADP phosphorylation via the ATP synthase (F₀F₁ ATPase — complex V) (Perier and Vila, 2012; Bratic and Trifunovic, 2010). F₀ domain of complex V couples proton translocation across the inner mitochondrial membrane (IMM) with the phosphorylation of ADP to ATP (Bratic and Trifunovic, 2010).

1.25. Inhibitors of Oxidative Phosphorylation

Rotenone and amytal block electron transfer at Complex I, thus preventing NADH utilization. However, oxidation of succinate remains unimpaired as these electrons enter via Complex II. Malonate blocks Complex II. Antimycin A interferes with electron flow from Complex III whereas cyanide (CN⁻) blocks complex IV. Other agents include azide (N₃⁻) or carbon monoxide (CO). As a result of ETC inhibition, ATP synthesis is also inhibited as there is no proton-motive force generated. Oligomycin prevent protons entering through ATP synthase, thus ceasing ETC to operate which clearly illustrates tight coupling between electron transport and ATP synthesis (Berg et al., 2002).

1.26. Regulated Uncoupling and Heat Generation

Proton leaking or mitochondrial uncoupling occurs with the re-entry of protons into mitochondrial matrix and releasing energy of proton electrochemical gradient as heat instead of ATP production (Cannon et al., 2006). Protonophores (such as FCCP) and UCPs can facilitate this process (Voet and Voet, 2004; Mozo et al., 2005). It is an important process to generate heat during hibernation, in newborns and cold adapted mammals. Adipose tissue specializes in non-shivering thermogenesis with high levels

of UCP1 or thermogenin of 33 kDa subunits and resembling ATP-ADP translocase. UCP1 short-circuits the mitochondrial proton battery to produce heat and primarily relies on FFAs for its activation. These fatty acids are released from TGs via signals such as β -agonists (Berg et al., 2002).

UCP2 and UCP3 have also been identified. The former shows 56% sequence similarity to UCP1, present in various tissues. UCP3, exhibits 57% sequence similarity with UCP1 and 73% with UCP2 and found in the skeletal muscle and brown fat. UCP2 and UCP3 may be involved in energy homeostasis. The use of uncoupling proteins is not restricted to animals (Osellame et al., 2012; Berg et al., 2002).

The ability of electrons to leak from the ETC prematurely allows their access to oxygen as opposed to being transferred to oxygen to produce water at complex IV, causing thus superoxide formation and oxidative stress (Osellame et al., 2012).

1.27. Research Aims and Hypothesis

Current understanding and research shows that the administration of paracetamol to mammals leads to the attenuation of increased temperature during fever and to hypothermia in non-febrile animals. The attenuation of increased temperature in humans can be achieved at non-toxic concentrations making paracetamol a safe antipyretic medication. This action is thought to be linked to the inhibition of COX-2. By contrast, the induction of hypothermia observed in non-febrile small mammals is at paracetamol concentrations where markers of toxicity are also detected. One explanation for the hypothermia is the inhibition of a variant of the COX-1 gene called COX-3. However, the evidence for the existence and biological activity of the COX-3 protein is inconclusive and disputed. Given the toxicity associated with hypothermia in non-febrile mammals, other mechanisms may be involved and must be investigated. Elucidation of this pathway could lead to the development of more effective novel antipyretic agents.

The aim of this research is to investigate the mechanisms by which paracetamol induces hypothermia in non-febrile rodents (mice and rats). The working hypothesis: paracetamol induced hypothermia in rodents is due to the inhibition of a novel COX-1 variant protein (COX-3) expressed in brain endothelial cells. The alternative hypothesis is that paracetamol induced hypothermia is linked to inhibition of peripheral thermogenic pathways.

1.28. Research Plan

In order to test the above hypothesis, two approaches are being used:

1. Identification and Characterisation of the putative variant COX-3 enzyme:

- Studies were undertaken to isolate and identify the COX-3 mRNA and protein in endothelial cells and tissues from mice.
- *The successful isolation of the protein would have been followed by characterisation of the putative COX-3 protein in terms of effect of paracetamol and other antipyretic compounds on the catalytic activity of the enzyme. No COX-3 protein was isolated so studies switched to the effect of paracetamol on peripheral thermogenesis.*

2. Investigation of the effect of paracetamol on peripheral thermogenesis:

Studies on the peripheral pathways involved assessing the effect of paracetamol and other putative specific COX-3 inhibitors on thermogenesis pathways including:

- Lipolysis by measuring the release of glycerol from triglycerides.
- Mitochondrial fatty acid uptake and oxidation.
- The impact on the function of the mitochondrial ETC.

Chapter 2: Materials & Methods

2.1. Suppliers

- Ms Elizabeth Wood, Queen Mary University of London, U.K.
- Sigma-Aldrich, Dorset, U.K.
- Envigo, Huntingdon, U.K.
- Melford, Suffolk, U.K.
- Bio-Rad, Watford, U.K.
- Fisher Scientific, Loughborough, U.K.
- Cayman Chemical, Michigan, U.S.A. (U.K. Distributor: Cambridge Bioscience, Cambridge, U.K.).
- Alpha Diagnostics International, San Antonio, U.S.A. (U.K. Distributor: Source Bioscience, Nottingham, U.K.).
- Eurofin Genomics, Wolverhampton, U.K.
- Life Technologies, Thermo Fisher Scientific, Loughborough, U.K.
- Promega, Southampton, U.K.
- Roche Diagnostics, Basel, Switzerland.
- Agilent Technologies, Cheshire, U.K.
- Nuair, Caerphilly, U.K.
- RS Biotech, Irvine, U.K.
- Beckman Coulter, High Wycombe, U.K.
- B.Braun, Sheffield, U.K.
- OPTIKA, Bergamo, Italy.
- AMG, Mill Creek, U.S.A.
- Edmund Bühler, Bodelshausen, Germany.
- BioTek, Winooski, U.S.A.
- Eppendorf, Hamburg, Germany.
- Thermo Scientific, Waltham, U.S.A.
- HANNA instruments, Leighton Buzzard, U.K.
- Hettich, Manchester, U.K.
- Nanodrop Technologies, Wilmington, U.S.A.
- Janke & Kunkel (IKA), Staufen im Breisgau, Germany.
- Scie-Plas, Cambridge, U.K.
- GraphPad Software, San Diego, U.S.A.

2.2. Materials

Items	Manufacturer/Supplier
Mouse brain endothelial cell line (b.End3)	Ms Elizabeth Wood
Mouse pre-adipocyte cell line (3T3-L1)	Sigma-Aldrich
Dulbecco's Modified Eagle's Medium (DMEM) – high glucose for b.End3 cell line	Sigma-Aldrich
Dulbecco's Modified Eagle's Medium (DMEM) – high glucose for 3T3-L1 cell line	Sigma-Aldrich
Fetal Bovine Serum (FBS)	Sigma-Aldrich
MEM Non-essential Amino Acid Solution (100×)	Sigma-Aldrich
L-Glutamine	Sigma-Aldrich
2-Mercaptoethanol	Sigma-Aldrich
Sodium Pyruvate	Sigma-Aldrich
Penicillin/Streptomycin	Sigma-Aldrich
Amphotericin B	Sigma-Aldrich
Phosphate buffered saline (PBS) tablets	Sigma-Aldrich
Trypsin from porcine pancreas	Sigma-Aldrich
Ethylenediaminetetraacetic acid (EDTA) disodium salt	Sigma-Aldrich
Trypan blue solution	Sigma-Aldrich
Dimethyl Sulfoxide (DMSO)	Sigma-Aldrich
C57BL/6J OlaHsd (Male, 8-10 weeks old)	Envigo
Male Wistar Rats 300 g	Envigo
Mammalian Cell Lysis Kit	Sigma-Aldrich
Tris(hydroxymethyl) aminomethane (TRIS)	Melford
Bovine Serum Albumin (BSA)	Sigma-Aldrich
Bradford Reagent	Bio-Rad
4X Laemmli Sample Buffer	Bio-Rad
Dithiothreitol (DTT)	Bio-Rad
Trans-Blot® Turbo™ Mini PVDF Transfer Packs	Bio-Rad
Glycine	Sigma-Aldrich

Sodium dodecyl sulfate (SDS)	Fisher Scientific
Methanol	Fisher Scientific
Sodium Chloride (NaCl)	Fisher Scientific
Triton x-100	Sigma-Aldrich
Clarity Western ECL Substrate	Bio-Rad
COX-1 mouse Polyclonal antibody	Cayman Chemical
COX-1 mouse blocking peptide	Cayman Chemical
Goat anti-rabbit IgG HRP	Cayman Chemical
Goat anti-mouse IgG HRP	Cayman Chemical
Anti-Mouse Cyclooxygenase 3 (COX-3), (Polyclonal)	Alpha Diagnostics International
Mouse Monoclonal Anti- β -Actin antibody	Sigma-Aldrich
Mouse Cyclooxygenase 3 (COX-3) Control/blocking peptide	Alpha Diagnostics International
Precision Plus Protein™ Dual Color Standards	Bio-Rad
Lipopolysaccharides from Escherichia coli 0111:B4	Sigma-Aldrich
GenElute™ Direct mRNA Miniprep Kit	Sigma-Aldrich
Custom-made oligonucleotides	Eurofin Genomics
Agarose	Melford
SYBR® Safe DNA Gel Stain	Life Technologies
Blue/orange 6X loading dye	Promega
DNA Molecular Weight Marker VI	Roche Diagnostics
AccessQuick™ RT-PCR System	Promega
Nuclease-Free Water	Promega
Acetic acid	Fisher Scientific
Insulin solution from bovine pancreas	Sigma-Aldrich
Isobutylmethylxanthine (IBMX)	Sigma-Aldrich
Dexamethasone	Sigma-Aldrich
Rosiglitazone	Cayman Chemical
Formaldehyde, Pure, Solution, 10% (v/v) in 0.9% Sodium Chloride Solution	Fisher Scientific
Isopropanol	Fisher Scientific

Oil Red O solution	Sigma-Aldrich
Thiazolyl Blue Tetrazolium Bromide (MTT)	Sigma-Aldrich
Dulbecco's Modified Eagle's Medium - low glucose	Sigma-Aldrich
Bovine Serum Albumin (fatty acid free)	Sigma-Aldrich
Free glycerol reagent	Sigma-Aldrich
Glycerol standard solution	Sigma-Aldrich
Acetaminophen (Paracetamol)	Sigma-Aldrich
4-Dimethylaminoantipyrine (Aminopyrine)	Sigma-Aldrich
Antipyrine	Sigma-Aldrich
Isoprenaline hydrochloride (Isoproterenol)	Sigma-Aldrich
(±)-Norepinephrine (+)-bitartrate salt	Sigma-Aldrich
Forskolin	Sigma-Aldrich
8-Bromoadenosine 3',5'-cyclic monophosphate (8-Br-cAMP)	Sigma-Aldrich
Potassium Chloride (KCl)	Fisher Scientific
Calcium Chloride (CaCl ₂)	Fisher Scientific
Magnesium Sulfate (MgSO ₄ (7H ₂ O))	Fisher Scientific
Potassium dihydrogen orthophosphate (KH ₂ PO ₄)	Sigma-Aldrich
Sodium phosphate dibasic (Na ₂ HPO ₄)	Sigma-Aldrich
Glucose	Sigma-Aldrich
Fructose	Fisher Scientific
Bovine Serum Albumin (BSA)	Sigma-Aldrich
Collagenase from Clostridium histolyticum	Sigma-Aldrich
Seahorse XFp Cell Culture Miniplates	Agilent Technologies
Seahorse XFp FluxPak	Agilent Technologies
Seahorse XF Calibrant	Agilent Technologies
Seahorse XF Base Medium	Agilent Technologies
Sodium hydroxide (NaOH)	Fisher Scientific
Seahorse XFP Cell Mito Stress Test kit	Agilent Technologies
Sucrose	Sigma-Aldrich
Mannitol	Sigma-Aldrich
4-(2-hydroxyethyl)-1-piperazineethanesulfonic acid) (HEPES)	Sigma-Aldrich
Ethylene glycol-bis(β-aminoethyl ether)-	Sigma-Aldrich

N,N,N',N'-tetraacetic acid) (EGTA)	
Magnesium chloride (MgCl ₂)	Sigma-Aldrich
Sodium succinate dibasic hexahydrate	Sigma-Aldrich
D-(+)-Malic acid	Sigma-Aldrich
Potassium hydroxide (KOH)	Fisher Scientific
Carbonyl cyanide 4-(trifluoromethoxy)phenylhydrazone (FCCP)	Sigma-Aldrich
Rotenone	Sigma-Aldrich
Oligomycin A	Sigma-Aldrich
Antimycin A from Streptomyces sp	Sigma-Aldrich
Ethanol	Fisher Scientific
L-Ascorbic acid	Sigma-Aldrich
N1,N1,N1,N1 tetramethyl-1,4-phenylene diamine (TMPD)	Sigma-Aldrich
Malonate	Sigma-Aldrich
Sodium Azide	Sigma-Aldrich
Dulbecco's Modified Eagle's Medium (DMEM) – no glucose, no glutamine, no phenol red for FAO Assay	Fisher Scientific
L-Carnitine hydrochloride	Sigma-Aldrich
(+)-Etomoxir sodium salt hydrate	Sigma-Aldrich
XF Palmitate-BSA FAO Substrate	Agilent Technologies
XF BSA control FAO	Agilent Technologies
N-Acetyl-p-benzoquinone imine (NAPQI)	Cayman Chemical
4–15% Mini-PROTEAN® TGX™ Precast Protein Gels, 10-well	Bio-Rad

2.3. Equipment

Equipment (model)	Manufacturer
Class II Biological Safety Cabinet (CELLGARD)	Nuaire
CO ₂ Incubator (Galaxy R+)	RS Biotech
Centrifuge (Avanti J-26S XP)	Beckman Coulter
Waterbath (Thermomix® Me)	B.Braun
LED Microscope (B-190)	OPTIKA
Digital Inverted Microscope (EVOS® XI)	AMG
Orbital shaker (KS 10)	Edmund Bühler
Tissue homogeniser (Ultra Turrax TP 18/10)	Janke & Kunkel
Multi-Mode Reader (Synergy HTX)	BioTek
Thermomixer Comfort (Comfort)	Eppendorf
Electrophoresis System (Mini-PROTEAN® Tetra Cell)	Bio-Rad
Power Supply (PowerPac™ Basic)	Bio-Rad
Imaging System for immunoblots (ChemiDoc™ XRS+)	Bio-Rad
Western Blotting Transfer System (Trans-Blot® Turbo™)	Bio-Rad
Imaging System for nucleic acids (Gel Doc™ EZ)	Bio-Rad
Horizontal gel electrophoresis unit (HU6 Mini)	Scie-Plas
Non-CO ₂ 37°C incubator (Heratherm™)	Thermo Scientific
Seahorse Analyzer (XFp)	Agilent Technologies
Multiparameter pH Meter (edge® 2210)	HANNA instruments
Centrifuge (5920R)	Eppendorf
Benchtop Centrifuge (Mikro 120)	Hettich
Thermal Cycler (T100)	Bio-Rad
Nanodrop spectrophotometer (ND-1000)	Nanodrop Technologies

2.4. Methods

2.4.1. Cell culture

The mouse brain endothelial cell line (b.End3) was maintained under standard culture conditions (37°C, 5% CO₂, 95% air) with medium containing DMEM supplemented with 10% fetal bovine serum (FBS), 1% w/v non-essential amino acids, 2 mM glutamine, 1 mM sodium pyruvate, 5 µM 2-mercaptoethanol, 10,000 units penicillin/mL, 10 mg streptomycin/mL (5 mL/500 mL of medium) and 250 µg/mL amphotericin B (5 mL/500 mL of medium) (Public Health England, U.K.). Sub-confluent cultures (70-80%) were seeded at 20-40,000 cells/cm² using 0.25% trypsin and 0.03% EDTA. The confluency of cells was at 60%-70% in experiments. Cell viability was assessed by trypan blue dye assay.

The mouse 3T3-L1 pre-adipocyte cell line was maintained in the same manner as the b.End3 cells with medium containing DMEM supplemented with 10% FBS, 2 mM glutamine, 10,000 units penicillin/mL, 10 mg streptomycin/mL (5 mL/500 mL of medium) and 250 µg/mL amphotericin B (5 mL/500 mL of medium) (Public Health England, U.K.). Sub-confluent cultures (70-80%) were seeded at 10-20,000/ cm² using 0.25% trypsin and 0.03% EDTA. The culture was not allowed to become fully confluent and subcultured every 3 days. Cell viability was assessed by trypan blue dye assay.

2.4.2. Sample preparation to determine COX protein expression

Mouse brain endothelial cells at 60%-70% confluent were removed by gentle scraping, placed in a centrifuge tube and spun at 500 x g for 5 minutes at 4°C to remove the medium. Cells were resuspended in 1 ml of PBS at 4°C, spun at 13000 x g for 2 minutes at 4°C and the cell pellet was kept at -20°C.

Animals (male C57BL/6 mice) were killed by cervical dislocation and whole brain tissues were removed immediately, washed in PBS at 4°C and stored immediately in -80°C.

2.4.3. Bradford protein assay and western blotting to determine COX protein expression

Samples (cells or tissues) were incubated with cell lysis buffer for 15 minutes at 4°C on an orbital shaker according to manufacturer's instructions (Sigma-Aldrich, U.K.). In case of tissues, samples were then homogenized at 4°C (Sigma-Aldrich, U.K.). Protein concentration was determined using Bradford assay. BSA stock (1 mg/mL) was prepared by dissolving BSA in distilled water. BSA standards (0.05 mg/mL, 0.1 mg/mL, 0.2 mg/mL, 0.3 mg/mL, 0.4 mg/mL, and 0.5 mg/mL) were prepared. The samples were diluted in 50 mM Tris buffer (pH 7.5) and 10 µL of this was transferred to a 96-well plate. 200 µL Bradford reagent (1:4 dilution) was added and the plate was read at 595 nm (Bradford, 1976).

For western blotting, samples were reconstituted in 4X Laemmli sample buffer (25 µL of 2 M DTT added) and then heated at 99°C for 5 minutes in a thermomixer. 4-15% Mini-PROTEAN® TGX™ precast gels were placed in the frames of the protean system after taking out the bottom tape. The gel plate frames were filled with 1X running buffer (25 mM Tris base, 250 mM Glycine, 0.1% (w/v) SDS dissolved in distilled water and the pH was 8.3). 10 µL of prestained molecular weight marker was added in the 1st well and the rest of the wells were loaded with samples according to the plan of each experiment. The gel plate frames were placed in the tank and 1X running buffer was added upto the mark according to the total number of the gels in the tank. The lid was placed and tank was attached to the Power Pac set at 100 V and was switched off as samples were 2 cm from the bottom of the gel.

The prepackaged transfer pack was opened and the bottom of the pack containing the membrane was placed on the Bio-Rad transfer cassette. After removing the gels between the glass plates, the stacking gel was removed and placed on the top of the membrane followed by the top portion of the pack. The transfer sandwich was rolled using a roller to avoid air bubbles. The lid of the transfer cassette was placed and inserted in the Trans-Blot® Turbo™ Transfer System and Bio-Rad mini tgx 3 minutes transfer (2.5 A; upto 25 V) was selected. Once transfer was completed, membranes were placed in a container containing small volume of 1X washing buffer (50 mM Tris base, 150 mM Sodium Chloride, 0.1% (v/v) Triton x-100 dissolved in distilled water) to cover the membrane.

Washing of membranes involved using 1X washing buffer 3 times for 5 minutes followed by addition of 10 mL of 1X blocking buffer (0.1% (w/v) BSA, 5% (w/v) Dried Skimmed milk (less than 1% fat) in washing buffer) to each membrane. The membranes were kept on a rotating platform for the duration of an hour at room temperature.

Again, washing of membranes involved using 1X washing buffer 3 times for 5 minutes. COX-1 and COX-3 polyclonal antibodies were diluted in 1X blocking buffer as outlined in Table 2.1 (Ayoub et al., 2006). β -actin (mouse) monoclonal antibody was diluted 1:10,000 in 1X blocking buffer (Sigma-Aldrich, U.K.).

For COX-1 control peptide + COX-1 immunoblot, COX-1 (mouse) polyclonal antibody and COX-1 (mouse) blocking peptide were mixed together in a 1:1 (v/v) ratio i.e. 10 μ L of antibody and 10 μ L of peptide in a microfuge tube. This mixture was incubated at room temperature for an hour with occasional mixing prior to further dilution and application of mixture to the immunoblot. This mixture was further diluted to 1:1000 and added to the respective membrane (Cayman Chemical, U.S.A.).

Table 2.1: COX-1 and COX-3 antibodies

Name	Antigen	Antibody host/type	Reactivity	Dilution
COX-1	274-288 amino acids peptide of Mouse COX-1, internal region of COX-1	Rabbit, polyclonal (affinity- purified IgG)	Mouse, Rat	1:1000
COX-3	1-12 amino acids peptide of Mouse COX-3, N-terminus	Rabbit, polyclonal (affinity- purified IgG)	Mouse	1:250

For COX-1 mouse blocking peptide immunoblot, COX-1 (mouse) polyclonal antibody and COX-1 mouse blocking peptide were mixed together in a 1:1 (v/v) ratio i.e. 10 μ L of antibody and 10 μ L of peptide in a microfuge tube. This mixture was incubated at room temperature for an hour with occasional mixing prior to further dilution and application of mixture to the immunoblot. This mixture was further diluted to 1:1000 and added to the respective membrane (Cayman Chemical, U.S.A.).

After adding respective primary antibodies, membranes were kept on a rotating platform overnight at 4°C. Next day, washing of membranes involved using 1X washing buffer 3 times for 5 minutes. The Goat anti-Rabbit IgG-HRP, a secondary antibody in 1:2000 dilution whereas for β -actin, Goat anti-mouse IgG HRP a secondary antibody in 1:2000 dilution in 1X blocking buffer and the membranes were kept for an hour on rotating platform at room temperature.

Washing of membranes involved using 1X washing buffer 2 times for 5 minutes and then placed on cling film. The membranes were incubated with 2 mL of Clarity western ECL substrate (kit components were mixed in a 1:1 ratio) for 5 minutes and then placed in the ChemiDoc imaging system.

2.4.4. Dot blots

For COX-1 and COX-3 blots, 10 μ L of COX-1 or COX-3 control peptide was added on nitrocellulose membrane, dried and then 5 mL of 1X blocking buffer was added to the membrane and incubated for an hour on rotating platform at room temperature. It was washed twice with 5 mL 1X washing buffer per blot for 5 minutes. 10 μ L of COX-1 or COX-3 antibody was added to 10 mL of 1X blocking buffer (1:1000) and then placed on COX-1 or COX-3 blots with 5 mL/blot.

Blots were incubated overnight at 4°C. The next day, blots were washed twice with 5 mL washing buffer/blot for 5 minutes. 10 μ L of secondary antibody was added in 20 mL of blocking buffer (1:2000) and 5 mL/blot was added and incubated for an hour. After washing twice, blots were visualised with 250 μ L of Clarity western ECL substrate (kit components were mixed in a 1:1 ratio) for 5 minutes and then placed in the ChemiDoc imaging system.

2.4.5. Sample preparation for mRNA extraction

Unstimulated and LPS stimulated b.End3 cells for 3 hours (1 μ g/mL LPS dissolved in complete DMEM) were scraped and placed in a centrifuge tube and spun at 500 x g for 5 minutes at 4°C. Cells were resuspended in PBS at 4°C, they were spun at 13000 x g for 2 minutes at 4°C and the pellet was kept at -80°C.

2.4.6. Direct mRNA extraction

Direct mRNA extraction was performed with the help of manufacturer's kit instructions (Sigma Aldrich, U.K). For b.End3 cells, the cells were lysed using lysis solution, pipetted thoroughly until all clumps disappeared and then transferred into a filtration column and spun at 16,000 x *g* for 2 minutes. The homogenized lysate (flow-through liquid) was then incubated at 65 °C for 10 minutes. Sodium chloride solution was added to the digested cell lysate and then resuspended oligo(dT) beads were added to the lysate-sodium chloride mixture and mixed thoroughly by vortexing until homogenous. The lysate/bead mixture was kept at room temperature for 10 minutes. The oligo(dT) beads:mRNA complex was pelleted by centrifuging for 5 minutes at 16,000 x *g* and the supernatant was carefully removed and discarded by pipetting without disturbing the pellet.

For mRNA enrichment, initially the bound material first set free from beads into fresh lysis solution; mRNA is then rebounded to the same beads by adding lysis solution and sodium chloride solution and vortexed thoroughly. The suspension was kept at 65 °C for 5 minutes followed by at room temperature for 5 minutes. The bead:mRNA complex was pelleted for 2 min and the supernatant was removed and discarded. The pellet was resuspended in wash solution and transferred to spin filter-collection tube assembly by pipetting and spun for 1-2 minutes at 16,000 x *g*. The flow through liquid was discarded but retained the collection tube. Same steps were repeated for second and third wash using low salt wash solution. The spin filter was placed into a fresh collection tube and preheated elution solution (65°C) was added onto the spin filter ensuring that it contacts the bead:mRNA complex and incubated for 2-5 minutes at 65°C, spun for 1-2 minutes and the flow-through liquid contained most of the purified mRNA. Same steps were repeated for second elution. For qualitative and quantitative measurements, samples were analysed using Nanodrop and stored at -80°C.

For frozen whole brain tissues, samples were quickly sliced and weighed upto 40 mg per preparation. The tissues were homogenised using the lysis solution immediately until no visible pieces remained and same steps were performed as above.

2.4.7. Expression of COX mRNA using RT-PCR

Using 0.1 µg of extracted mRNA from each sample, cDNA was synthesized and amplified by a one step RT-PCRs according to manufacturer's kit instructions (Promega, U.K.) using primer sets targeting the COXs mRNA. Glyceraldehyde 3-phosphate dehydrogenase (GAPDH) primers were also included as controls to evaluate the quality of the extracted mRNA samples. Also reverse transcription was omitted in controls.

The published primers (Ayoub et al., 2004) of COX-1, COX-2, COX-3, and GAPDH were used (Figure 2.1; Table; 2.2). A few errors were noted in the nucleotide sequence of published GAPDH primer set (2, 15 and 18 positions in sense primer and 21 position in antisense primer and the corrected sequence includes sense 5'- ATG GTG AAG GTC GGT GTG AA CG-3' and antisense 5'-GCC AAA AGG GTC ATC ATC TCC GCC-3'). However, the published GAPDH primer set was able to amplified product of expected size. The published RT-PCR conditions of all the primers were used, but further optimisation was carried out for COX-1 and COX-3 (Table 2.3).

Primer sets were also specifically designed for COX-1 and COX-3 (Figure 2.1; Table 2.4). The first primer set named as COX-1/3. The sense primer anneals within exon 1 and the antisense primer within exon 3 of COX-1, to amplify a smaller fragment for COX-1 (product size of 227 bp) and a larger sequence for COX-3 (325 bp), thus distinguishes between COX-1 and COX-3. The second set of primers named as COX-1/3P. The sense primer anneals within exon 1, and the antisense primer within exon 4 and 5 of COX-1, to amplify a smaller fragment for COX-1 (product size of 402 bp) and a larger sequence for COX-3 (500 bp). This differ between COX-1 and COX-3 as well as COX-3 and "partial" COXs (PCOX-1a, PCOX-1b) as antisense primer binds to exon 5, which is lacking in PCOXs (Chandrasekharan et al., 2002). The RT-PCR conditions of these primers are outlined in Table 2.5.

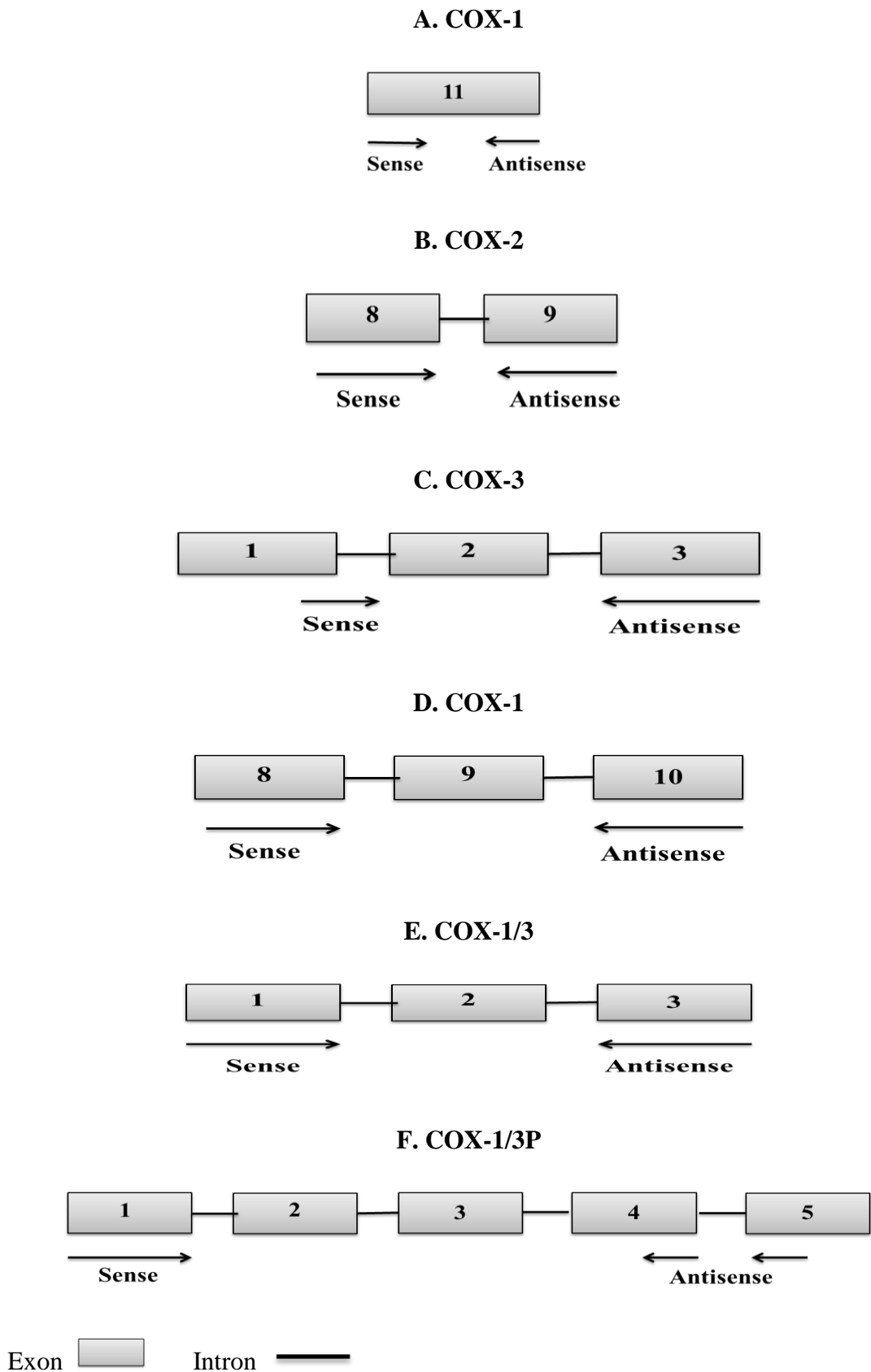


Figure 2.1: Primers used for RT-PCR: A,B,C. Published primers for COX-1, COX-2 and COX-3 (Ayoub et al., 2004). **C,D,E.** Custom made primers for COX-1 and COX-3.

Table 2.2: Published primers

Gene	Primer Sequences	Melting Temperature	Product (bp)
COX-1 Sense Antisense	5'-AGG AGA TGG CTG CTG AGT TGG-3' 5'-AAT CTG ACT TTC TGA GTT GCC-3'	61.8 55.9	602
COX-2 Sense Antisense	5'-ACA CAC TCT ATC ACT GGC ACC-3' 5'-TTC AGG GAG AAG CGT TTG C-3'	59.8 56.7	274
COX-3 Sense Antisense	5'-ATG AGT CGT GAG TCC GAC CCC AGT-3' 5'-TGT CGA GGC CAA AGC GGA-3'	66.1 58.2	290
GAPDH Sense Antisense	5'-AAG GTG AAG GTC GGA GTC AAC G-3' 5'-GGC AGA GAT GAT GAC CCT TTT GGC-3'	62.1 64.4	363

Table 2.3: RT-PCR conditions for published primers

Primers	Reverse Transcription	Denaturation	Annealing	Extension	Final Extension	Cycles
COX-1	94°C for 3 min	94°C for 15 sec	60°C for 15 sec	65°C for 1 min	72°C for 7 min	32
COX-2	94°C for 3 min	94°C for 15 sec	55°C for 15 sec	72°C for 1 min	72°C for 7 min	40
COX-3	95°C for 2 min	95°C for 30 sec	56°C for 1 min	72°C for 1 min	72°C for 7 min	35
GAPDH	94°C for 3 min	94°C for 30 sec	60°C for 30 sec	72°C for 1 min	72°C for 10 min	30
(Ayoub et al., 2004)						
COX-1	94°C for 3 min	94°C for 15 sec	50°C for 30 sec	72°C for 1 min	72°C for 7 min	32
COX-3	95°C for 2 min	95°C for 30 sec	53°C for 1 min	72°C for 1 min	72°C for 7 min	35
(Further optimised)						

Table 2.4: Custom made primers for COX-1 and COX-3:

Gene	Primer Sequences	Melting temperature	Product length (bp)
COX-1 Sense Antisense	5'-GGC TTC GTG AAC ATA ACC GC-3' 5'-ATC CAC AGC CAC ATG CAG AA-3'	59.4 57.3	437
COX-1/3 Sense Antisense	5'-GGC ATT GCA CAT CCA TCC AC-3' 5'-TAG CCC GTG CGA GTA CAA TC-3'	59.4 59.4	COX-1 (227) COX-3 (325)
COX-1/3P Sense Antisense	5'-GGC ATT GCA CAT CCA TCC AC-3' 5'-GTT GGA CCG CAC TGT GAG TA-3'	59.4 59.4	COX-1 (402) COX-3 (500)

(NCBI Reference Sequence: NM_008969.4)

Table 2.5: RT-PCR conditions for custom made primers for COX-1 and COX-3:

Primers	Reverse Transcription	Denaturation	Annealing	Extension	Final Extension	Cycles
COX-1	94°C for 3 min	94°C for 15 sec	52°C for 30 sec	72°C for 1 min	72°C for 7 min	32
COX-1/3 and COX-1/3P	95°C for 2 min	95°C for 30 sec	54°C for 1 min	72°C for 1 min	72°C for 7 min	35

The cDNA products were viewed on 2% (w/v) agarose gel. The gel was directly prepared in SYBR Safe gel stain. The stain was diluted in 1X TAE buffer (40 mM Tris, 20 mM acetic acid, 1 mM EDTA, pH 8.0), added to the powdered agarose and heated in a microwave for 2 minutes to dissolve. The gel was left to set for 30 minutes. The gel was placed in a tank filled with 1X TAE buffer and loaded with 10 µL PCR product mixed with blue/orange 6X loading dye and 5 µL of DNA ladder. The gel was run at 100 V for 30 minutes and the bands were visualised using Gel Doc™ EZ system.

2.4.8. Differentiation of 3T3-L1 pre-adipocytes

For the differentiation of pre-adipocytes, once cells become confluent, they were further allowed to grow for four additional days and this was treated as Day 0. At Day 1, cells were placed in DMEM differentiation medium with 10% fetal bovine serum, 1 µg/mL insulin, 0.5 mM isobutylmethylxanthine (IBMX), 1 µM dexamethasone, 2 µM

rosiglitazone for 48 hours. On day 3, the differentiation medium was switched to DMEM containing 10% FBS and 1 µg/mL insulin and changed after every 48 hours from this stage until fully differentiated 3T3-L1 adipocytes formation (Public Health England, U.K.; Zebisch et al., 2012; Zenbio, U.S.A).

2.4.9. Oil Red O staining

The differentiation process was confirmed by Oil Red O staining. The culture medium was removed and after washing cells twice with sterile PBS and fixed with 10% formalin for 30 minutes at room temperature. Washing step involved using sterile water and incubated with 60% isopropanol solution. After 5 minutes, 60% isopropanol was removed and working solution of Oil Red O was prepared by mixing 3 parts of stock solution to 2 parts of sterile water was filtered and added to the cells. After 15-20 minutes, the cells were again washed twice with sterile water and the staining of lipid droplets and cell morphology was observed under microscope. For quantification, sterile water was removed and the stain was extracted with 100% isopropanol by adding 100 µL of 100% isopropanol in each well and placed on orbital shaker at room temperature for 5 minutes with gentle rocking. The absorbance was read at 510 nm (BioVision, U.S.A.).

2.4.10. MTT assay on 3T3-L1 differentiated adipocytes

The 3T3-L1 adipocytes were exposed to different concentrations of test compounds in 24-well plates. After 24 or 48 hours, 50 µL MTT solution (5 mg/mL in PBS and filter sterilised) was added to cells and kept for an hour. After an hour exposure with MTT, the medium was aspirated and 100% isopropanol was added to each well and mixed until the formazan crystal product get dissolved. The absorbance was measured at 570 nm.

2.4.11. Lipolysis assay in 3T3-L1 differentiated adipocytes

After two hours of serum-free incubation (Schweiger et al., 2014) for all experiments, the differentiated cells were exposed to different concentrations of paracetamol or

aminopyrine or antipyrine (1 mM or 10 mM) with 2% BSA (fatty acid free) and glycerol release was measured after 1, 3 and 24 hours for basal lipolysis.

For norepinephrine stimulated lipolysis, cells were pre-incubated with different concentrations of paracetamol (1 mM or 10 mM) with 2% BSA (fatty acid free) for 30 minutes and then incubated with norepinephrine (1 μ M) with 2% BSA (fatty acid free) and glycerol release was measured after 1, 3 hours.

For isoproterenol stimulated lipolysis, cells were treated with different concentrations of paracetamol (1 mM or 10 mM) and isoproterenol (0.001 - 0.1 μ M) with 2% BSA (fatty acid free) added simultaneously. Alternatively, cells were pre-incubated with different concentrations of paracetamol (1 mM or 10 mM) with 2% BSA (fatty acid free) for 30 minutes and then incubated with different concentrations of isoproterenol (0.001 - 10 μ M) with 2% BSA (fatty acid free) and glycerol release was measured after 1, 3, 24 and 48 hours.

For forskolin and 8-Br-cAMP stimulated lipolysis, cells were pre-incubated with different concentrations of paracetamol (1 mM or 10 mM) with 2% BSA (fatty acid free) for 30 minutes and then incubated with forskolin (100 μ M) or 8-Br-cAMP (1 mM) with 2% BSA (fatty acid free) and glycerol release was measured after 1, 3 and 24 hours.

Glycerol standards (1.95 μ g/mL, 3.9 μ g/mL, 7.8 μ g/mL, 15.6 μ g/mL, 31.25 μ g/mL, 62.5 μ g/mL, 125 μ g/mL) were prepared using glycerol standard solution (260 μ g/mL) in distilled water. 25 μ L of each sample or standard was transferred to a new 96-well plate and 100 μ L of glycerol reagent was added and read at 540 nm (Sigma-Aldrich, U.K.).

2.4.12. Isolation of rat primary brown adipocytes

2 rats were killed by cervical dislocation and brown adipose tissue from the interscapular depots was dissected out and placed on a parafilm in a small volume of Krebs/Ringer phosphate buffer (114.7 mM NaCl, 1.3 mM KCl, 1.5 mM CaCl₂, 1.4 mM MgSO₄ (7H₂O), 5.6 mM KH₂PO₄, 16.7 mM Na₂HPO₄, 10 mM glucose, 10 mM fructose; pH was adjusted with Tris-OH or HCl to 7.4). The tissue was cleaned from white fat and connective tissue, and pooled (Cannon and Nedergaard, 2008). The brown adipose tissue was minced with scissors and placed in a centrifuge tube containing 3 mL

Krebs/Ringer phosphate buffer with 4% crude bovine serum albumin and 0.83 mg/mL collagenase. The first incubation was carried out for 5 minutes in a water bath set at 37°C and the tube was vortexed for 5 seconds after the addition of 7 mL of Krebs/Ringer phosphate buffer.

The tissue fragments were filtered through a cell strainer and the filtrate was discarded. The tissue fragments were transferred to a small volume of Krebs/Ringer phosphate buffer on a square of parafilm and minced with scissors. The second incubation was carried out for in 3 mL fresh, albumin and collagenase containing buffer as above for 25 minutes, with 5 seconds vortexing every fifth minute. The contents of the vial were filtered after adding 7 mL of Krebs/Ringer phosphate buffer and vortexing the vial for 15 seconds.

The filtrate was collected and centrifuged at 65 x g for 5 minutes. The remaining tissue pieces were incubated as above for 15 minutes and the cells were collected in order to increase the yield. The infranatants in all tubes were discarded and the cells were combined and washed with 10 mL of Krebs/Ringer phosphate buffer and centrifuged at 65 x g for 2 minutes and allowed to stand at room temperature. The cells were counted and used immediately for experiments.

2.4.13. MTT assay on rat primary brown adipocytes

Isolated rat primary brown adipocytes were cultured in 96-well plates and then treated with different concentrations of test compounds. After 2 and 24 hours, 10 µL MTT solution (5 mg/mL in PBS and filter sterilised) added to cells and kept for an hour. After an hour exposure with MTT, 100% isopropanol was added to each well and mixed until the formazan crystal product get dissolved. The absorbance was measured at 570 nm.

2.4.14. Lipolysis assay in rat primary brown adipocytes

Brown adipocytes were treated with different concentrations of paracetamol or aminopyrine or antipyrine (250 µM - 10 mM) and glycerol release was measured after 1 and 24 hours as in section 2.4.11.

For norepinephrine stimulated lipolysis, brown adipocytes were pre-incubated with different concentrations of paracetamol or aminopyrine or antipyrine (1 mM or 10 mM)

for an hour followed by addition of norepinephrine (1 μ M) and then glycerol release was assayed after 1 and 24 hours as in section 2.4.11.

2.4.15. Measurement of oxygen consumption rate (OCR) using XFp Seahorse Analyser

When assessing how agents affect fatty acid oxidation and mitochondrial function, the oxygen consumption rate (OCR) of cells and isolated mitochondria can be assessed using the Agilent Seahorse XF Cell Mito Stress Test (Figure 2.2). By measuring OCR, the Seahorse equipment allows the determination of key parameters of cellular and mitochondrial function (Table 2.6.).

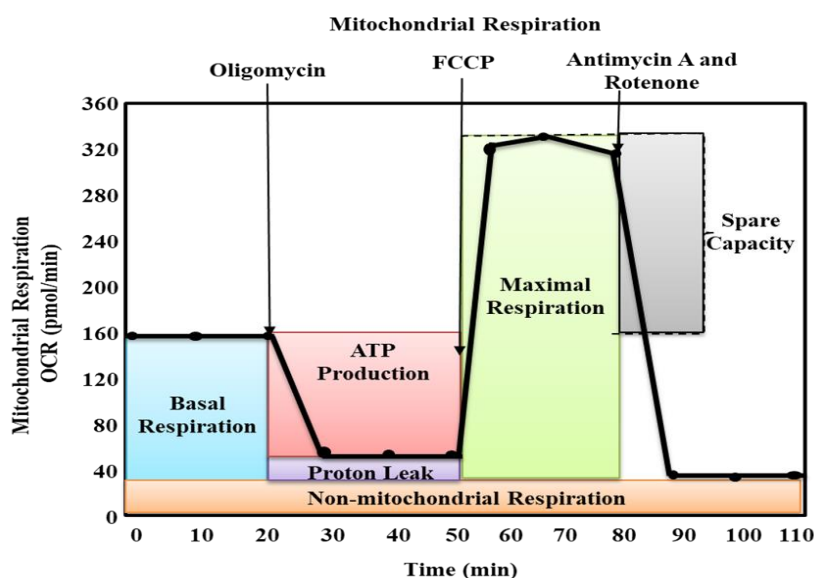


Figure 2.2: Schematic of Agilent Seahorse XF Cell Mito Stress Test Profile (Figure adapted from Agilent Seahorse, U.K.).

The process starts by establishing the OCR required for basal respiration and this reflects the oxygen consumption needed to support the basic energetic requirement of a cell. Basal OCR is made up of the oxygen required for both cellular ATP demand and mitochondrial proton leak. Once basal respiration has been established, oligomycin can be added. Oligomycin blocks ATP synthase and will therefore block all oxygen consumption linked to ATP production, the remaining consumption will be due to proton leak. The ratio of OCR between ATP production and proton leak is a measure of

coupling efficiency with adipocytes having very low (<30%) coupling efficiency. A high rate of proton leak in the absence of an exogenous chemical will normally indicate damaged mitochondria possibly during preparation or storage. Carbonyl cyanide-4 (trifluoromethoxy) phenylhydrazone (FCCP) is then added to determine the OCR at maximal respiration. FCCP is known as an uncoupler as it breaks the link between oxidation from the production of ATP in the mitochondria. Oxygen consumption in the presence of FCCP demonstrates the theoretical maximum capacity of mitochondrial ETC. The addition of rotenone and antimycin A will completely block any substrate driven oxygen consumption. Any oxygen consumption observed following the addition of rotenone and antimycin A will be due to non-mitochondrial respiration. Determination of non-mitochondrial respiration is necessary to accurately assess other cellular enzyme activity which consumes oxygen. The system also allows the measurement of spare respiratory capacity which indicates how closely cells respire to their maximum respiration rate.

Table 2.6: Mitochondrial function parameters

Parameter Value	Equation
Non-mitochondrial Oxygen Consumption	Minimum rate measurement after Rotenone/antimycin A injection
Basal Respiration	(Last rate measurement before first injection) – (Non-Mitochondrial Respiration Rate)
Maximal Respiration	(Maximum rate measurement after FCCP injection) – (Non-Mitochondrial Respiration)
Proton Leak	(Minimum rate measurement after Oligomycin injection) – (Non-Mitochondrial Respiration)
ATP Production	(Last rate measurement before Oligomycin injection) – (Minimum rate measurement after Oligomycin injection)
Spare Respiratory Capacity	(Maximal Respiration) – (Basal Respiration)
Spare Respiratory Capacity (%)	(Maximal Respiration) – (Basal Respiration) x 100
Coupling Efficiency (%)	(ATP Production Rate) / (Basal Respiration Rate) x 100

(Table adapted from Agilent Seahorse, U.K.).

2.4.15.1. General Setup: seeding 3T3-L1 cells in Seahorse XFp cell culture miniplates

Model no. 1:

In an XFp cell culture miniplate, using 8-channel pipettor set to 180 μL , sterile water was added to both sides of the moat (two tips will fit into each chamber) around the cell culture wells. 100 μL of growth medium only (no cells) was added to background correction wells A and H. Cells were harvested and resuspended in growth medium, counted and then diluted to the desired seeding concentration (5000 cells/well). 100 μL of cell suspension was added to wells B-G. Cells were allowed to grow in a cell culture incubator and differentiated. Cells were monitored to ensure that the moat did not dry out during this period. The growth and health of cells were checked using a microscope (Agilent Seahorse, U.K.).

Model no. 2:

3T3-L1 cells were differentiated in 24-well plates. In an XFp cell culture miniplate, using 8-channel pipettor set to 180 μL , sterile water was added to both sides of the moat (two tips will fit into each chamber) around the cell culture wells. 100 μL of growth medium only (no cells) was added to background correction wells A and H. Differentiated cells were then harvested and resuspended in growth medium, counted and then diluted to the desired seeding concentration (5000 cells/well). 100 μL of cell suspension was added to wells B-G. Cells were placed in a cell culture incubator overnight. Cells were monitored to ensure that the moat did not dry out during this period. The growth and health of cells were checked using a microscope.

2.4.15.2. Hydration of Seahorse XFp sensor cartridge

Procedure no.1

The day prior to assay, the utility plate and sensor cartridge were separated and the sensor cartridge was placed upside down on the bench. Each well of the utility plate was filled with 200 μL of Seahorse XF calibrant whereas the moats around the outside of the wells were filled with 400 μL per chamber. The Seahorse XFp sensor cartridge was returned to the utility plate that now contains calibrant. The cartridge assembly was placed in a non- CO_2 37°C incubator overnight. To prevent evaporation of the Seahorse

XF calibrant, the incubator was humidified. Following the overnight incubation and on the day of assay, the cartridge assembly was removed from the incubator. The sensor cartridge was lifted completely out of the calibrant and utility plate and was then immediately returned back onto the utility plate, submerging the sensors in calibrant. This step eliminated any bubbles that might have formed during the overnight hydration (Agilent Seahorse, U.K.).

Procedure no.2

The day prior to assay, 5 mL of Seahorse XF calibrant was aliquoted into a 15 mL conical tube and placed in a non-CO₂ 37°C incubator overnight. The sensor cartridge was placed upside down next to the utility plate. Each well of the utility plate was filled with 200 µL of sterile water and moats around the outside of the wells were filled with 400 µL per chamber. The sensor cartridge placed on the utility plate submerging the sensors in water. The water level was verified as high enough to keep the sensors submerged and was placed in a non-CO₂ 37°C incubator overnight. To prevent evaporation, the incubator was humidified.

On the assay day, the conical tube of calibrant and assembled sensor cartridge with utility plate was removed from incubator. The sensor cartridge was placed upside down next to the utility plate and the water was removed from the utility plate. Each well of the utility plate was filled with 200 µL of pre-warmed Seahorse XF calibrant and the moats around the outside of the wells with 400 µL of calibrant per chamber. The sensor cartridge was placed on the utility plate submerging the sensors in calibrant and was placed in a non-CO₂ 37°C incubator for 45 – 60 minutes prior to loading drug ports of the sensor cartridge (Agilent Seahorse, U.K.).

2.4.15.3. Loading the Seahorse XFp sensor cartridge with compounds

Before starting the compound loading process, the compounds were prepared in the assay medium of choice and a loading plan based on the experimental design. The Seahorse XFp assay cartridge was placed on bench with well labels (A-H) to the left and the triangular notch in the bottom left-hand corner. A constant compound concentration (10X of the final port concentration) and variable loading volume approach was selected. Using p100 or p200 µL pipette, the desired volume of compound to be injected was dispensed into the desired port at an angle (<5°). The

assay template based on the experimental design was selected on the Seahorse XFp. Unless specified, the default Mix-Wait-Measure times of 3 minutes – 0 minute – 3 minutes were selected. Each measurement cycle consisted of a mixing time of 3 minutes and a data acquisition period of 3 minutes (data points). 3 basal measurements were taken prior to the addition of each reagent, and 3 response measurements were taken after the addition of each compound. OCR data points referred to the average rates during the measurement cycles. OCR reported as absolute rates (pmoles/min for OCR). On the Run Screen, 'Start' option was selected. The plate lid of the cartridge/utility plate assembly was removed before inserting the cartridge into the Seahorse XFp Analyzer to start calibration (Agilent Seahorse, U.K.).

2.4.15.4. Washing cells in Seahorse XFp cell culture miniplates

The growth medium was replaced with assay medium for adherent cells grown in Seahorse XFp cell culture miniplates prior to being assayed using a Seahorse XFp Analyzer. The assay medium was warmed up to 37°C and the Seahorse XFp cell culture miniplate was removed from the tissue culture incubator. The time was noted and cells were checked under the microscope. It was made sure that the background wells (A and H) did not contain cells. The culture medium was removed from each well leaving behind 20 µL to keep the cells from drying out. Approximately 200 µL of assay medium was added and then removed but again leaving behind 20 µL. Assay medium to a total volume of 180 µL or the volume recommended by the particular assay protocol was added. The assay wells were observed under the microscope to ensure that cells were attached. The plate was placed in a 37°C incubator without CO₂ for one hour prior to the assay. When prompted by the XFp Seahorse Analyser, the utility plate was replaced with the cell plate and assay was initiated (Agilent Seahorse, U.K.).

2.4.16. XFp Experiments

2.4.16.1. Effect of paracetamol on fatty acid oxidation (FAO):

Reagents preparation:

Substrate-Limited Medium: DMEM containing 0.5 mM glucose, 1 mM glutamine, 0.5 mM carnitine, and 1% FBS. Carnitine was included fresh on the day of media change.

FAO Assay Medium: Krebs Henseleit Buffer (KHB): (111 mM NaCl, 4.7 mM KCl, 1.25 mM CaCl₂, 2 mM MgSO₄, 1.2 mM NaH₂PO₄ dissolved in H₂O and filter sterilized) and 2.5 mM glucose, 0.5 mM carnitine, and 5 mM HEPES was added on assay day; pH 7.4 at 37°C. Respiration Reagent Stocks: 10 mM FCCP, 2 mM rotenone, 5 mg/mL oligomycin and 40 mM antimycin A in 95% ethanol were prepared. 0.5 mM carnitine and 10 mM etomoxir dissolved in H₂O with pH 7.4. XF Palmitate-BSA FAO Substrate and stock respiration reagents were kept at -20°C (Agilent Seahorse, U.K.).

Assay preparation:

In this assay, model no. 2 was used for seeding cells and procedure no.2 for hydrating XFp sensor cartridges. The growth medium was removed and substrate-limited medium added 24 hours prior to the assay. The cells were washed twice with FAO assay medium 45 min before the assay (t = -45 min). 135 µL FAO assay medium was added to the each well of cells and kept in a non-CO₂ incubator for 30-45 min at 37°C. The assay cartridge was loaded with XFp Cell Mito Stress Test reagents using FAO assay medium as port A, 20 µL of 25 µg/mL oligomycin (2.5 µg/mL, final); port B, 22 µL of 40 µM FCCP (4 µM, final); port C, 24 µL of 20 µM rotenone/ 40 µM antimycin A (2 µM/4 µM, final, respectively). The default template of the Seahorse XFp Cell Mito Stress Test was selected on the Seahorse XFp. The plate lid of the cartridge/utility plate assembly was removed before inserting the cartridge into the Seahorse XFp Analyzer to start calibration. 10 mM stock solution of etomoxir was diluted to 400 µM in FAO assay medium 15 minutes before initiating prior the assay (t = -15 minutes). 15 µL etomoxir was added or vehicle to each well (final concentration; 40 µM). For paracetamol group, 100 mM paracetamol (final concentration in the wells was 10 mM) was added. For NAPQI group, 500 µM NAPQI (final concentration in the wells was 50 µM) was added. The XFp cell culture miniplate was incubated for 15 minutes min at 37°C in a non-CO₂ incubator. Before initiating the assay (t = 0 minute), 30 µL XF Palmitate-BSA FAO Substrate (1 mM: 0.17 mM) or BSA control (0.17 mM) was added to the appropriate wells. The XFp cell culture miniplate was immediately inserted into the XFp Analyzer and the assay was initiated (Agilent Seahorse, U.K.). Different XF FAO assay parameters were measured as outlined in Table 2.7.

Table 2.7: XF FAO assay parameters

Parameter Value	Equation
Oxygen Consumption due to uncoupling by FFA	Oligomycin Palm:BSA-Eto rate minus Oligomycin BSA-Eto rate.
Basal Respiration due to utilization of exogenous FAs	Basal Palm:BSA-Eto rate minus Basal BSA-Eto rate minus OCR due to uncoupling by FFA.
Basal Respiration due to utilization of endogenous FAs	Basal BSA-Eto rate minus basal BSA+Eto rate.
Maximal Respiration due to utilization of endogenous FAs	Maximal BSA-ETO rate minus maximal BSA+Eto rate
Maximal Respiration due to utilization of endogenous FAs	Maximal Palm:BSA-Eto rate minus Maximal BSA-Eto rate - OCR due to uncoupling by FFA.

(Table adapted from Agilent Seahorse, U.K.).

2.4.16.2. Mitochondrial bioenergetic profile of 3T3-L1 adipocytes using Seahorse XFp Cell Mito Stress Test

In this assay, model no. 1 was used for seeding cells and procedure no.1 for hydrating XFp sensor cartridges. 10 mM glucose, 2 mM glutamine and 1 mM pyruvate was added in the required volume of XF Seahorse base medium and allowed to dissolve; pH 7.4 using 1 N NaOH and this medium was filter sterilized. The medium was warmed at 37°C until use. The contents of each reagent of Seahorse XFP Cell Mito Stress Test kit was re-suspended with prepared assay medium and loaded as port A, 20 µL of 50 µM oligomycin (5 µM, final); port B, 22 µL of 50 µM FCCP (5 µM, final); port C, 25 µL of 25 µM rotenone/ antimycin A (2.5 µM, final, respectively). The default template of the Seahorse XFp Cell Mito Stress Test was selected on the Seahorse XFp (Agilent Seahorse, U.K.).

2.4.16.3. Effect of paracetamol on basal and norepinephrine and isoproterenol stimulated OCR in 3T3-L1 adipocytes:

In this assay, model no. 1 was used for seeding cells and procedure no.1 for hydrating XFp sensor cartridges. Using assay medium, the port injections were: port A, 20 μ L of 50 mM (5 mM, final) or 100 mM (10 mM, final) paracetamol (Agilent Seahorse, U.K.).

For norepinephrine or isoproterenol stimulated OCR and using assay medium, the port injections were: port A, 20 μ L of 10 μ M (1 μ M, final) norepinephrine or 10 μ M (1 μ M, final) isoproterenol (Agilent Seahorse, U.K.).

In subsequent assays, using assay medium, the port injections were: port A, 20 μ L of 10 μ M (1 μ M, final) norepinephrine or 10 μ M (1 μ M, final) isoproterenol, port B, 22 μ L of 10 mM (1 mM, final); port C, 25 μ L of 40 mM (4 mM, final); port D, 27 μ L of 50 mM (5 mM, final) paracetamol (Agilent Seahorse, U.K.).

2.4.16.4. Effect of paracetamol, aminopyrine and antipyrine on basal and norepinephrine and isoproterenol stimulated OCR in 3T3-L1 adipocytes:

In this assay, model no. 2 was used for seeding cells and procedure no.2 for hydrating XFp sensor cartridges. Using assay medium, the port injections were: port A, 20 μ L of 10 mM (1 mM, final); port B, 22 μ L of 40 mM (4 mM, final); port C, 25 μ L of 50 mM (5 mM, final); 27 μ L of 10 mM (10 mM, final) paracetamol. In subsequent assays, port A, 20 μ L of 10 mM (1 mM, final); port B, 22 μ L of 40 mM (4 mM, final); port C, 25 μ L of 50 mM (5 mM, final) aminopyrine or antipyrine (Agilent Seahorse, U.K.).

For isoproterenol stimulated OCR and using assay medium, the port injections were: port A, 20 μ L of 0.1 μ M (0.01 μ M, final); port B, 22 μ L of 1 μ M (0.1 μ M, final); port C, 25 μ L of 10 μ M (1 μ M, final); 27 μ L of 100 μ M (10 μ M, final) isoproterenol (Agilent Seahorse, U.K.).

In subsequent assays, port A, 20 μ L of 50 mM (5 mM, final) or 100 mM (10 mM, final) paracetamol or aminopyrine or antipyrine, port B, 22 μ L of 1 μ M (0.1 μ M, final); port C, 25 μ L of 10 μ M (1 μ M, final); 27 μ L of 100 μ M (10 μ M, final) isoproterenol (Agilent Seahorse, U.K.).

2.4.16.5. Elucidation of mechanistic activity of inhibitors that affect mitochondrial function using electron flow assay:

Reagents preparation:

Mitochondrial Isolation Buffer consists of 70 mM sucrose, 210 mM mannitol, 5 mM HEPES, 1 mM EGTA and 0.5% (w/v) fatty acid-free BSA, pH 7.2. Mitochondrial Assay Solution (MAS, 1X) consists of 70 mM sucrose, 220 mM mannitol, 10 mM KH_2PO_4 , 5 mM MgCl_2 , 2 mM HEPES, 1 mM EGTA and 0.2% (w/v) fatty acid-free BSA, pH 7.2 and kept at 37°C. 3X stock MAS was used to dilute substrates and respiratory reagents. Substrate stocks: 0.5 M succinate, 0.5 M malate, 0.5 M glutamic acid, 0.5 M pyruvic acid made in water; pH 7.2 with potassium hydroxide. Pyruvate stock was made fresh on assay day. Respiration Reagent Stocks: 10 mM FCCP, 2 mM rotenone, 5 mg/mL oligomycin and 40 mM antimycin A in 95% ethanol. 1.0 M ascorbate in H_2O , pH 7.2 was mixed with 10 mM N1,N1,N1,N1tetramethyl-1,4-phenylene diamine (TMPD) in H_2O , pH 7.2. All reagents were kept at -20°C (Agilent Seahorse, U.K.).

Isolation of Rat Liver Mitochondria:

The liver was extracted from male Wistar rat and placed in a chilled beaker, weighed and washed with PBS 2-3 times. It was finely chopped with scissors, washed with small volume of isolation buffer twice, minced with 7X volume of isolation buffer at 4°C. All steps were carried out on ice. The tissue was then homogenised using a glass tissue homogenizer using 2-3 strokes. The homogenate was spun at 800 x g for 5 minutes at 4°C. Supernatant was placed in another tube and spun at 8000 x g for 10 minutes at 4°C. This time, the supernatant was removed whereas the pellet was dissolved in small volume of isolation buffer. Total protein (mg/mL) was assessed by Bradford reagent (Agilent Seahorse, U.K.).

Assay Preparation:

After diluting mitochondria 10X in 1X MAS containing substrate at 4°C, further dilution was made based on the concentration needed to plate them. The substrate was added during the initial dilution steps and centrifugation. 25 μL of mitochondrial

preparation was added to each well (excluding background correction wells) of plate kept on ice. It was then spun in a centrifuge containing a microplate swinging bucket, at 2000 x g for 20 minutes at 4°C (Agilent Seahorse, U.K.). Using the procedure no.2 for hydrating XFp sensor cartridges, the port injections were loaded as follows:

With 2.5 and 5 µg isolated rat liver mitochondria

For control group, with isolated rat liver mitochondria per well, initial substrate mix of 10 mM and 2 mM of pyruvate and malate + 4 µM FCCP. For known ETC inhibitors controls, 2 µM rotenone, 10 mM malonate, 4 µM antimycin A, 20 mM sodium azide, 2.5 µg/ml oligomycin were also added in the initial substrate mix. Port injections were made as: port A, 20 µL of 20 µM rotenone (2 µM, final); port B, 22 µL of 100 mM succinate (10 mM, final); port C, 24 µL of 40 µM antimycin A (4 µM, final); port D, 26 µL of 100 mM ascorbate and 1 mM TMPD (10 mM and 100 µM final) (Agilent Seahorse, U.K.).

For paracetamol groups, 1-10 mM paracetamol was also added in the initial substrate mix. Port injections were made as: port A, 20 µL of 40 mM paracetamol (4 mM, final) or 20 µL of 50 mM paracetamol (5 mM, final) or 20 µL of 100 mM paracetamol (10 mM, final); port B, 22 µL of 100 mM succinate (10 mM, final); port C, 24 µL of 50 mM paracetamol (5 mM, final) or 24 µL of 100 mM paracetamol (10 mM, final); port D, 26 µL of 100 mM ascorbate and 1 mM TMPD (10 mM and 100 µM final) (Agilent Seahorse, U.K.).

For aminopyrine group, 10 mM aminopyrine was also added in the initial substrate mix. Port injections were made as: port A, 20 µL of 100 mM aminopyrine (10 mM, final); port B, 22 µL of 100 mM succinate (10 mM, final); port C, 24 µL of 100 mM aminopyrine (10 mM, final); port D, 26 µL of 100 mM ascorbate and 1 mM TMPD (10 mM and 100 µM final) (Agilent Seahorse, U.K.).

For antipyrine group, 10 mM antipyrine was also added in the initial substrate mix. Port injections were made as: port A, 20 µL of 100 mM antipyrine (10 mM, final); port B, 22 µL of 100 mM succinate (10 mM, final); port C, 24 µL of 100 mM antipyrine (10 mM, final); port D, 26 µL of 100 mM ascorbate and 1 mM TMPD (10 mM and 100 µM final) (Agilent Seahorse, U.K.).

With isolated rat liver mitochondria per well, compounds that affect mitochondrial function were added as initial conditions. The initial substrate mix of 10 mM and 2 mM pyruvate and malate + 4 μ M FCCP allows for the evaluation of maximal respiration driven by Complex I, while the injection of rotenone (2 μ M) followed by succinate (10 mM) allows for the assessment of maximal respiration driven by Complex II. The injection of Antimycin A (4 μ M), an inhibitor of Complex III, followed by the injection of ascorbate and TMPD (10 mM and 100 μ M) allow for the evaluation of respiration driven by Complex IV since the Ascorbate and TMPD is an electron donor to Complex IV (Rogers et al., 2011).

The Mix-Wait-Measure times of 1 minute – 0 minute – 2.5 minutes were selected. 3 basal measurements were taken prior to the addition of each reagent, and 2 response measurements were taken after the addition of each compound. On the Run Screen, ‘Start’ option was selected. The plate lid of the cartridge/utility plate assembly was removed before inserting the cartridge into the Seahorse XFp Analyzer to start calibration. Once centrifuged, 155 μ L pre-warmed (37°C) 1X MAS + substrate + initial conditions were transferred to each well. Also, plates were checked using microscope at 20X to confirm that mitochondria were still attached and then plates were placed in the Seahorse XFp Analyzer and the experiment begun (Agilent Seahorse, U.K.).

2.5. Statistical analysis

The results were analysed using GraphPad Prism 4.02 and presented as mean \pm standard deviation (SD). The results were analysed with analysis of variance (ANOVA), followed by Dunnett's Multiple Comparison Test or Bonferroni's Multiple Comparison Test. A *P < 0.05, ** P<0.01, *** P<0.001 from control was considered statistically significant.

Chapter 3: Identification of COX-3 mRNA and protein in rodents

3.1. Introduction

Historically pharmacologists have struggled to explain the varying degrees to which paracetamol inhibits the synthesis of PGs in different tissues. It is generally accepted that paracetamol has a greater impact on COX activity in CNS particularly the brain when compared to peripheral tissues (Flower and Vane, 1972). One possible explanation was that there may be subtle variations in the COX enzymes expressed in the different tissues. In 2002, Chandrasekharan et al. characterised and cloned a COX enzyme from canine brain which they argued was more sensitive to paracetamol inhibition than COX-1 or COX-2. They argued that this enzyme was a variant of COX-1 gene and designated it COX-3. They further argued that the activity of this variant enzyme could explain the pharmacological actions of antipyretic analgesic drugs such as paracetamol which were weak inhibitors of COX-1 and COX-2. The *in vivo* actions of paracetamol on this putative COX-1 variant enzyme were suggested to be due to the ability of this group compounds to easily penetrate the CNS where this variant enzyme was thought to be primarily expressed. By contrast NSAIDs including diclofenac or ibuprofen which also potently inhibited the variant enzyme do not accumulate in the CNS in sufficient concentrations to have a physiological effect (Chandrasekharan et al., 2002; Botting and Ayoub 2005).

The variant enzyme is thought to result from a splice variant which results in the translation of the COX-1 gene with an N-terminus extended due to retained intron-1 and the signal peptide (Chandrasekharan et al., 2002). If intron 1 is retained, it would result in a protein with extra 30-34 amino acids in mammals. The group also claimed COX-3 mRNA appeared to be selectively expressed in tissues and greatest in the heart and brain in humans (Chandrasekharan et al., 2002). The story then moved on when it was suggested that in rodents particularly mice, paracetamol induces hypothermia (in the absence of fever) by a mechanism that did not involve COX-2 inhibition (Ayoub et al., 2004). The potential discovery of a COX-3 mRNA in whole brain tissues of mice was used to suggest that paracetamol induced hypothermia was due to the inhibition of COX-3 in the CNS. It was proposed that in order for mice to maintain their normal T_b at T_a (22°C) which is significantly below their thermoneutral zone (32-34°C), COX-3 was constitutively expressed, most likely in brain endothelial cells, involved in the

PGE₂ synthesis. However, the hypothermic action of paracetamol was only partially decreased in COX-1 knockout animals and the brain levels of PGE₂ were only approximately 30% of those of controls and these were not reduced further by paracetamol treatment. This finding suggested that the hypothermic actions of paracetamol could involve another mechanism not related to COX inhibition (Ayoub et al., 2004).

Despite a series of publications led by the Simmon's group supporting the existence and possible function of the COX-3 enzyme. Other groups argued that at the molecular level even if the COX-3 mRNA existed, it would be unlikely to be expressed in many species including mouse, rat and humans (Schwab et al., 2003b; Kis et al., 2005). In addition to the molecular biology arguments, there were issues with experimental design and the quality of the data presentation (Schwab et al., 2003b; Kis et al., 2005). One of the key issues was around primer design and the fact that there were very few studies which showed COX-3 at protein level. In an attempt to determine the role of the COX-1 variant protein (COX-3) in paracetamol induced hypothermia, studies were undertaken to determine the level of COX-3 protein and mRNA level in mouse b.End3 cells and brain tissues.

3.2 Methods

3.2.1. Studies were undertaken to detect the level of COX-1 and COX-3 protein in mouse b.End3 cells and brain homogenates as described in sections 2.42 -2.44.

3.2.2. Studies were undertaken to detect the level of COX-1 and COX-3 mRNA in mouse b.End3 cells and brain homogenates as described in sections 2.45 -2.47.

3.3. Results

3.3.1. Detection of COX-1 and COX-3 protein expression in b.End3 cells

COX-1 protein expression was observed in b.End3 cells in Figure 3.1(A) whereas no COX-3 protein expression was detected in Figure 3.1(B).

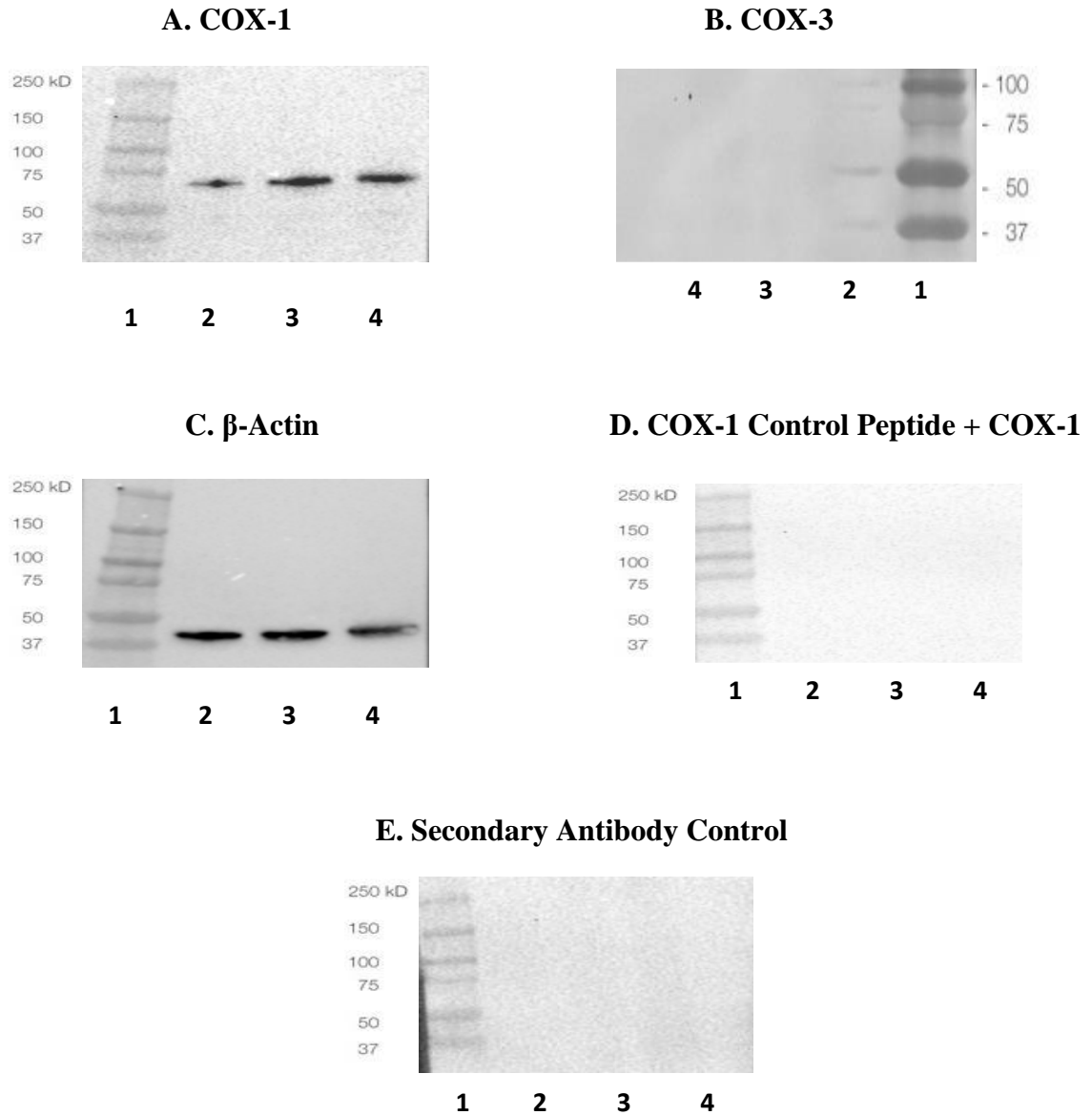


Figure 3.1 (A-E): Detection of COX-1, COX-3, β -actin protein expression, COX-1 control peptide, secondary antibody control by Western blotting in b.End3 cells. Lane 1= Molecular weight marker, Lane 2-4= 30 μ g, 50 μ g and 100 μ g of protein. COX-1 molecular weight = 70 kDa, COX-3 molecular weight = 65kDa, β -actin molecular weight = 42 kDa. Data are representative of 4 replicates.

β -actin protein expression has been detected in the protein loaded in Figure 3.1(C). Absence of bands in Figure 3.1(D) confirmed that the bands observed in Figure 3.1(A) were specific to COX-1 primary antibody immunoreactivity. Absence of bands in Figure 3.1(E) further confirmed that the secondary antibody is specific to the COX-1 primary antibody.

3.3.2. Detection of COX-1 and COX-3 protein expression in C57BL/6 mice brain homogenates

Two distinct bands of approx. 100 kDa and 45 kDa were detected with COX-1 immunoreactivity in Figure 3.2(A), whereas no COX-3 protein expression was detected in Figure 3.2(B). Absence of bands in the presence of COX-1 control peptide in Figure 3.2(C) further confirmed that the bands observed in Figure 3.2(A) were specific to COX-1 primary antibody immunoreactivity. Increased β -actin protein expression has been detected with an increase for protein loaded in Figure 3.2(D).

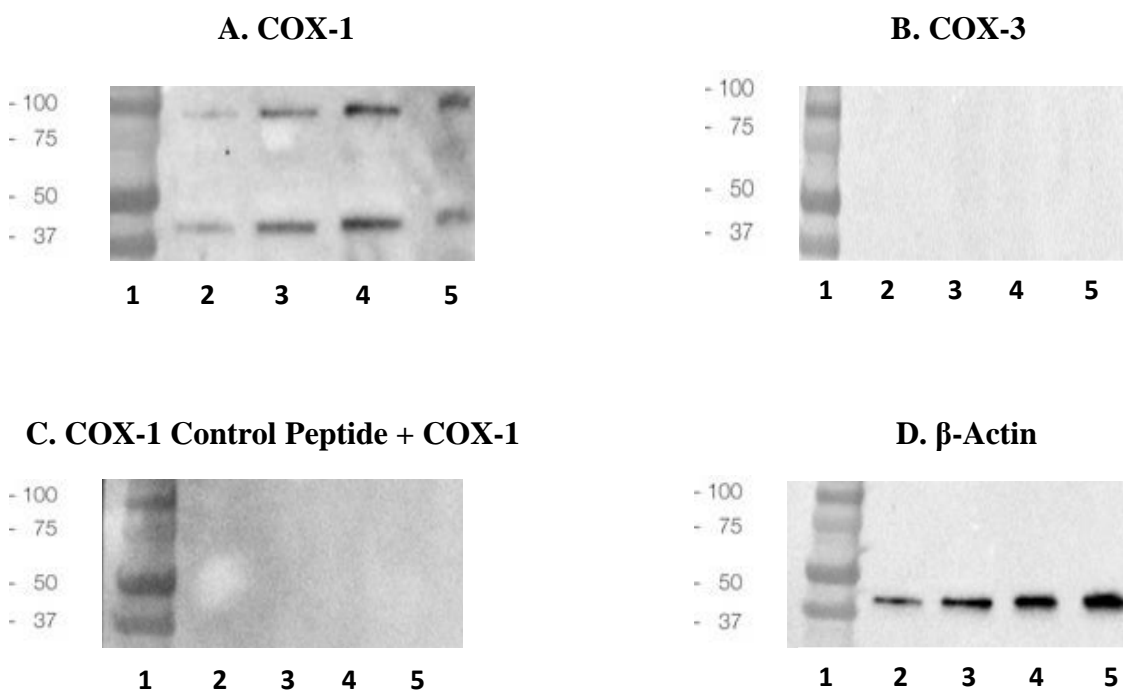
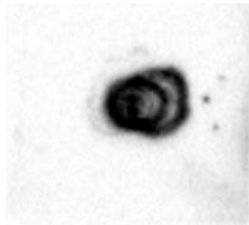


Figure 3.2 (A-D): Detection of COX-1, COX-3, COX-1 control peptide, β -actin protein expression by Western blotting in C57BL/6 mice brain homogenates. Lane 1= Molecular weight Marker, Lane 2-5= 15 μ g, 30 μ g, 50 μ g and 100 μ g of protein. COX-1 molecular weight = 70 kDa, β -actin molecular weight = 42 kDa, COX-3 molecular weight = 65kDa. Data are representative of 4 replicates.

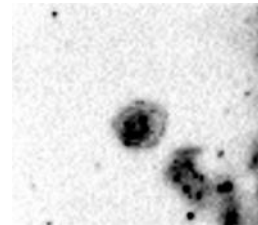
3.3.3. Detection of COX immunoreactivity using Dot blots

In an attempt to confirm antibody specificity, dot blots were performed using antibodies and control peptides (Hawkes et al., 1982). COX-1 antibody showed immunoreactivity with COX-1 control peptide sequence in Figure 3.3(A). COX-3 antibody showed immunoreactivity with COX-3 control peptide confirming that the antibody has the potential to bind to the cognate sequence in Figure 3.3(B). Interestingly, COX-1 antibody also showed immunoreactivity to the COX-3 peptide sequence in Figure 3.3(D) whereas COX-3 antibody could not detect the COX-1 control peptide in Figure 3.3(C). These findings further confirmed the functionality of the commercially available antibodies and their specific immunoreactivities.

A. COX-1 Control Peptide + COX-1



B. COX-3 Control Peptide + COX-3



C. COX-1 Control Peptide + COX-3



D. COX-3 Control Peptide + COX-1



Figure 3.3 (A-D): Detection of immunoreactivity of COX-1 and COX-3 using dot blots. Data are representative of 3 replicates.

3.3.4. Expression of COX mRNA in naive and LPS stimulated b.End3 cells

Expression of COX-1, COX-2, and COX-3 mRNA was investigated in naive and LPS stimulated b.End3 cells using RT-PCR. Faint COX-1 bands were detected in both naive and LPS stimulated b.End3 cells after 1 and 3 hours in Figure 3.4 whereas distinct COX-2 mRNA expressed in naive b.End3 cells and an increase in the expression of COX-2 in LPS stimulated b.End3 cells at 3 hours was observed in Figure 3.5. The

COX-3 mRNA expression could not be detected in the same set of samples in Figure 3.6. GAPDH mRNA expressed in both the samples.

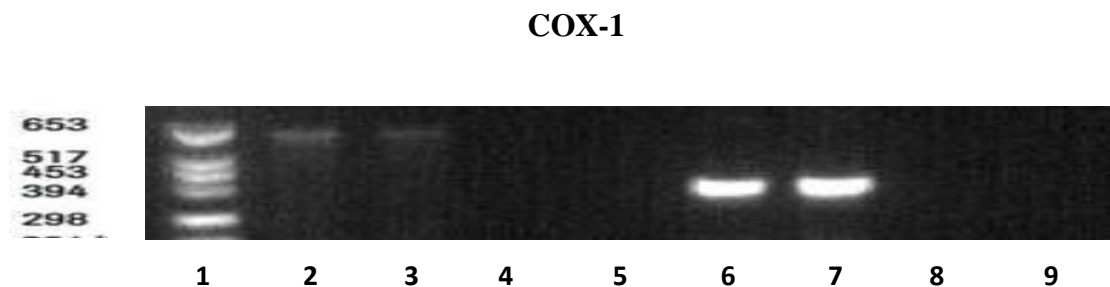


Figure 3.4: mRNA expression of COX-1 and GAPDH by RT-PCR in naive and LPS stimulated *b.End3* cells for 1 and 3 hours: Lane 1= Molecular weight marker, Lane 2-3= COX-1 expression in control (naive *b.End3* cells) at 1 hour and in *b.End3* cells stimulated with LPS 1 µg/ml at 3 hours, Lane 4-5= Negative control for RT-PCR, Lane 6-7 = GAPDH expression in control (naive *b.End3* cells) at 1 hour and in *b.End3* cells stimulated with LPS 1 µg/ml at 3 hours, Lane 8-9 = Negative control for RT-PCR. Molecular weights for amplified products for COX-1 and GAPDH are 602 bp and 363 bp (RT-PCR conditions for GAPDH were based on Ayoub et al., 2004 whereas RT-PCR conditions for COX-1 were optimised).

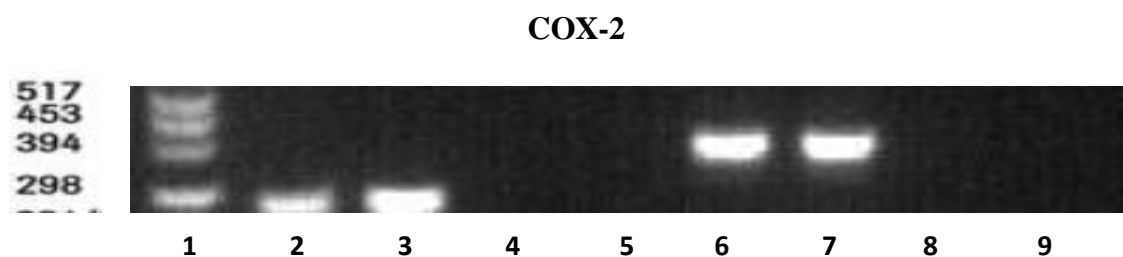


Figure 3.5: mRNA expression of COX-2 and GAPDH by RT-PCR in naive and LPS stimulated *b.End3* cells for 1 and 3 hours: Lane 1= Molecular weight marker, Lane 2-3= COX-2 expression in control (naive *b.End3* cells) at 1 hour and in *b.End3* cells stimulated with LPS 1 µg/ml at 3 hours, Lane 4-5= Negative control for RT-PCR, Lane 6-7 = GAPDH expression in control (naive *b.End3* cells) at 1 hour and in *b.End3* cells stimulated with LPS 1 µg/ml at 3 hours, Lane 8-9= Negative control for RT-PCR. Molecular weights for amplified products for COX-2 and GAPDH are 274 bp and 363 bp (RT-PCR conditions for GAPDH and COX-2 were based on Ayoub et al., 2004).

COX-3



Figure 3.6: mRNA expression of COX-3 and GAPDH by RT-PCR in naive and LPS stimulated *b.End3* cells for 1 and 3 hours: Lane 1= Molecular weight marker, Lane 2-3= COX-3 expression in control (naive *b.End3* cells) at 1 hour and in *b.End3* cells stimulated with LPS 1 $\mu\text{g/ml}$ at 3 hours, Lane 4-5= Negative control for RT-PCR, Lane 6-7= GAPDH expression in control (naive *b.End3* cells) at 1 hour and in *b.End3* cells stimulated with LPS 1 $\mu\text{g/ml}$ at 3 hours, Lane 8-9 = Negative control for RT-PCR. Molecular weights for amplified products for COX-3 and GAPDH are 290 bp and 363 bp (RT-PCR conditions for GAPDH and COX-3 were based on Ayoub et al., 2004).

3.3.5. Expression of COX mRNA in C57BL/6 mice brain homogenates

Expression of COX-1, COX-2, and COX-3 mRNA was investigated in C57BL/6 mice brain homogenate using RT-PCR. Distinct GAPDH (lane 2), however the published set of COX-1 and COX-3 primers could not detect COX-1 (lane 3) and COX-3 (lane 4) in mice brain homogenate in Figure 3.7.

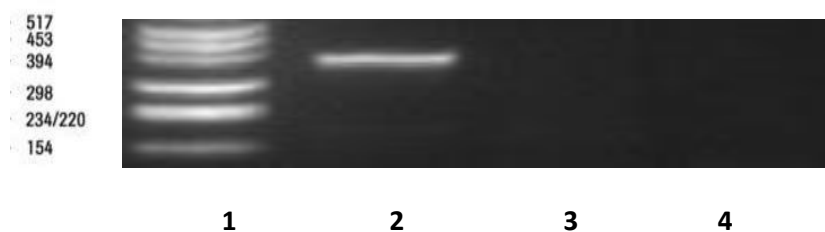


Figure 3.7: mRNA expression of GAPDH, COX-1 and COX-3 by RT-PCR in mice brain homogenate. Lane 1= Molecular weight marker, Lane 2 = GAPDH, Lane 3 = COX-1 and Lane 4 = COX-3 expression. Molecular weights for amplified products for GAPDH, COX-1 and COX-3 are 363 bp, 602 bp and 290 bp (RT-PCR conditions for GAPDH, COX-1 and COX-3 were based on Ayoub et al., 2004).

When RT-PCR conditions were further optimised, there was a distinct GAPDH (lane 2), no COX-1 (lane 3), only faint COX-2 band (lane 4) and no COX-3 was detected in Figure 3.8.

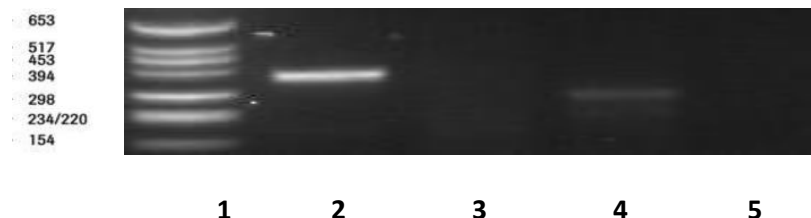


Figure 3.8: mRNA expression of GAPDH, COX-1, COX-2 and COX-3 by RT-PCR in mice brain homogenate. Lane 1= Molecular weight marker, Lane 2 = GAPDH, Lane 3 = COX-1, Lane 4 = COX-2 and Lane 5 = COX-3 expression. Molecular weights for amplified products for GAPDH, COX-1, COX-2 and COX-3 are 363 bp, 602 bp, 274 bp and 290 bp (RT-PCR conditions for GAPDH and COX-2 were based on Ayoub et al., 2004 whereas RT-PCR conditions for COX-1 and COX-3 were optimised).

3.3.6. Expression of COX-1 and COX-3 mRNA in b.End3 cells

Expression of COX-1 and COX-3 mRNA was investigated in b.End3 cells using new set of specifically designed RT-PCR primers in Figure 3.9.

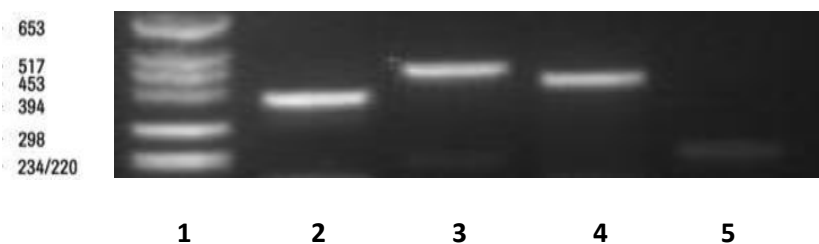


Figure 3.9: mRNA expression of GAPDH, COX-1 and COX-3 by RT-PCR in b.End3 cells: Lane 1= Molecular weight marker, Lane 2 = GAPDH, Lane 3 = COX-1, Lane 4 = a smaller fragment for COX-1 using COX-1/3P primer set and Lane 5 = a smaller fragment for COX-1 using COX-1/3 primer set. Molecular weights for amplified products for GAPDH, COX-1, COX-1(COX-1/3P primer set) and COX-1(COX-1/3 primer set) are 363 bp, 437 bp, 402 bp and 227 bp (RT-PCR conditions for GAPDH were based on Ayoub et al., 2004 whereas RT-PCR conditions for COX-1, COX-1/3P and COX-1/3 were optimised).

Distinct GAPDH (lane 2) and COX-1 (lane 3) were detected in Figure 3.9. Using COX-1/3P and COX-1/3 primers that could amplify both COX-1 and COX-3, only a smaller fragment for COX-1 (lane 4 and lane 5) was detected. However, these primer sets did not amplify any COX-3 product of expected sizes (500 bp and 325 bp) in lane 4 and 5 in Figure 3.9.

3.3.7. Expression of COX-1 and COX-3 mRNA in C57BL/6 mice brain homogenates

Expression of COX-1 and COX-3 mRNA was investigated in C57BL/6 mice brain homogenates using new set of specifically designed RT-PCR primers. Distinct GAPDH (lane 2) and COX-1 (lane 3) were detected in Figure 3.10. However, both COX-1/3P and COX-1/3 primers did not amplify both COX-1 and COX-3 products of expected size in lane 4 and 5 in Figure 3.9.

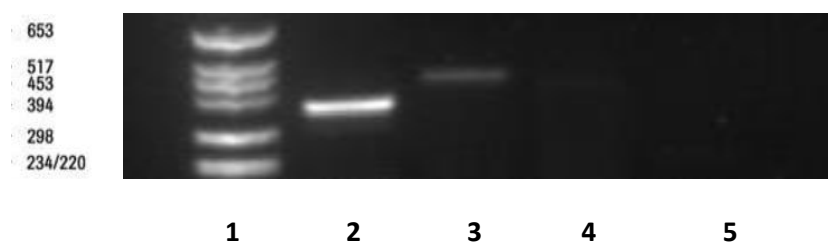


Figure 3.10: mRNA expression of GAPDH, COX-1 and COX-3 by RT-PCR in mice brain homogenate: Lane 1= molecular weight marker, Lane 2 = GAPDH, Lane 3 = COX-1, Lane 4 = COX-1/3P primer set and Lane 5 = COX-1/3 primer set. Molecular weights for amplified products for GAPDH and COX-1 are 363 bp and 437 bp (RT-PCR conditions for GAPDH were based on Ayoub et al., 2004 whereas RT-PCR conditions for COX-1, COX-1/3P and COX-1/3 were optimised).

3.4. Discussion:

The possibility of a viable COX-3 protein poses two major questions; what species and tissues is the protein expressed in and what is the role of the protein? The strongest evidence for the COX-3 has primarily been at the mRNA level in canine brain, rat, human and mouse. In terms of a protein (functional) the evidence is less clear. In terms of the hypothermia induced by paracetamol most studies were undertaken in rats and mice. In the present study, western blot using the previously reported anti-COX-3 antibody, could not detect the COX-3 protein in mouse brain endothelial cells or mouse brain homogenates (Figure 3.1-3.2). By contrast in terms of immunoreactivity, there was clear COX-1 protein detected in cells and tissues. These studies were controlled for both primary and secondary antibodies for COX-1 and COX-3. Furthermore, the immunoreactivity of the COX-1 and COX-3 antibody was confirmed with blotting assays using the COX-1 and COX-3 peptides (Figure 3.3).

The failure to detect the COX-3 protein in mouse brain endothelial cells is not surprising and in line with what is known about the COX-1 gene where a viable protein is unlikely (Schwab et al., 2003b; Warner et al., 2004; Snipes et al., 2005). Retention of intron-1 in the mouse will result in an out of frame sequence and no protein should be produced. The detection of the COX-3 protein from mouse brain previously may be due to the use of polyclonal antibody which is more likely to produce cross reactivity (Ayoub et al., 2006). In the present study, it was demonstrated that the COX-1 antibody binds to COX-3 peptide. This would also confirm that had the COX-3 protein existed in mouse brain tissue there was a double chance of seeing it. A similar argument can be used for the COX-3 in rat.

These studies also failed to confirm the presence of a COX-3 mRNA in the endothelial cells and in mouse brain (Figure 3.6-3.10). No definitive conclusions can be drawn from the failure to isolate COX-3 mRNA in these samples in terms of the existence of COX-3 generally. However, given the varying levels of COX-1 observed under the varying experimental conditions in this study it may be possible that the cells and tissues analysed in these studies simply did not express COX-3. However, given the proposed conditions required for COX-3 expression by those who propose a role for COX-3 in thermoregulation it would have been expected that COX-3 would have been seen in the brain tissue homogenates at the very least (Ayoub et al., 2004). One possible explanation for the previously reported COX-3 mRNA could be the amplification of incompletely processed mRNA before intron-1 is spliced. The COX-3 primer is targeted at intron-1

so at any given time in a cell expressing COX-1 a small proportion of the mRNA will be unprocessed and could be amplified. This would explain the widespread expression of the COX-3 mRNA alongside the COX-1 mRNA but always at a significantly lower level; around 10% of the COX-1. However, only the final COX-1 mRNA would be translated into active COX-1 protein.

The initial aim of these studies was to identify and characterise the COX-3 protein at the molecular level. Studies would then have moved onto enzyme activity and inhibition by paracetamol, NSAIDs and other antipyretic drugs. However, in the absence of the protein in cells and tissues, studies were then undertaken to assess how paracetamol would impact on other aspects of the thermogenesis pathway in particular, lipolysis, FAO and the ETC.

Chapter 4: Effect of paracetamol, aminopyrine and antipyrine on lipolysis in rodent adipocytes

4.1. Introduction

Fever in mammals is mainly associated with increased COX-2/PGE₂ activity. Historically it has generally been assumed that paracetamol and NSAID exerts their antipyretic actions by inhibiting the COX-2 enzyme. Over the last 20 years, many studies have revealed that the administration of paracetamol (>100 mg/kg) to non-febrile rodents, for which there is no induction of COX-2 results in hypothermia, suggesting other mechanisms may be involved. The initial suggestion was that paracetamol was inhibiting a novel COX-1 variant (COX-3). The COX-3 hypothesis was supported by the observation that other drugs such as aminopyrine and antipyrine, which are putative COX-3 inhibitors, also produce hypothermia in mice. However, in the absence of clear evidence of a COX-3 enzyme in the previous chapter combined with the prevailing evidence in the literature suggest that the existence of COX-3 cannot solely explain the hypothermic properties of paracetamol, alternative explanations were sought.

In terms of thermoregulation, rodents (homeotherms) are capable of maintaining their T_c within a fairly constant range (36.0-37.5°C). Small mammals at temperatures below their thermoneutral zone due to their large surface area mass ratio must rely more on changing their metabolic heat production to regulate T_c (Gordon, 2012). To maintain T_c, rodents rely on metabolism in BAT to generate fuel for heat production (Gordon, 2012). The process usually starts with the stimulation of lipolysis, a catabolic process converting TGs stored in adipocytes and causing fatty acids and glycerol release (Luo and Liu, 2016). Upon cold stress, NE is released from sympathetic fibres. It binds to β₃-receptor located on adipocytes (Ueta et al., 2012). As a result, a sequence of events is initiated starting with the release of AC, cAMP/PKA pathway leading to lipolysis (Luo and Liu, 2016). BAT is also activated following prolonged cold treatment in adult humans and leads to increase in mobilizing lipids from other fat stores to BAT. In turn, promoting FAO via heat generation inside mitochondria (Luo and Liu, 2016).

In most laboratory situations, mice are housed at 20–24°C (Gordon, 1993, 2004) but their thermoneutral zone range is 26–34°C whereas the range for rats is 26–30°C (Gordon, 1993). However, most researchers agree that the lower critical temperature of

a single mouse is around 30°C (Gordon, 2004). When animals are kept at or just below the standard housing temperatures, such mild cold stressors are enough to increase basal metabolic rates (Gordon, 1985, 1990, 1993). It is reasonable to hypothesize that animals housed under conditions where there is increased metabolic stress may be more sensitive to compounds which could even mildly decrease metabolic activity and lead to hypothermia.

In an attempt to better understand the possible mechanisms by which paracetamol and other putative COX-3 inhibitors could induce hypothermia as reported by Ayoub et al. (2004). Studies were undertaken to assess the impact of paracetamol, aminopyrine and antipyrine on lipolysis in a mouse pre-adipocyte cell line (3T3-L1) and in rat primary adipocyte cultures. Lipolysis was assessed in basal and catecholamine stimulated cells by measuring the level of glycerol release.

4.2. Methods

4.2.1. Studies were initially undertaken to differentiate 3T3-L1 pre-adipocytes and assess viability as described in sections 2.4.8-2.4.10.

4.2.2. Studies were then undertaken to assess the level of lipolysis in basal and catecholamine stimulated 3T3-L1 adipocytes. In addition, studies were conducted to assess the impact of various compounds including paracetamol on lipolysis in these cells as described in section 2.4.11.

4.2.3. Studies were also undertaken to assess viability and the level of lipolysis in basal and catecholamine stimulated primary brown adipocytes. In addition, studies were conducted to assess the impact of various compounds including paracetamol on lipolysis in these cells as described in sections 2.4.12-2.4.14.

The results were analysed with analysis of variance (ANOVA), followed by Dunnett's Multiple Comparison Test. A *P < 0.05, ** P<0.01, from control was considered statistically significant.

4.3. Results:

4.3.1. 3T3-L1 differentiation

Modification of the currently available protocols resulted in the complete differentiation of 3T3-L1 pre-adipocytes into adipocytes (Public Health England; Zebisch et al., 2012). Within a week from the start of differentiation, lipid droplets increased both in number and size (Figure 4.1). The extent of adipose conversion was quantitated by staining the accumulated lipid using Oil Red O (Figure 4.2). The differentiated 3T3-L1 adipocytes were then used for the lipolysis studies.

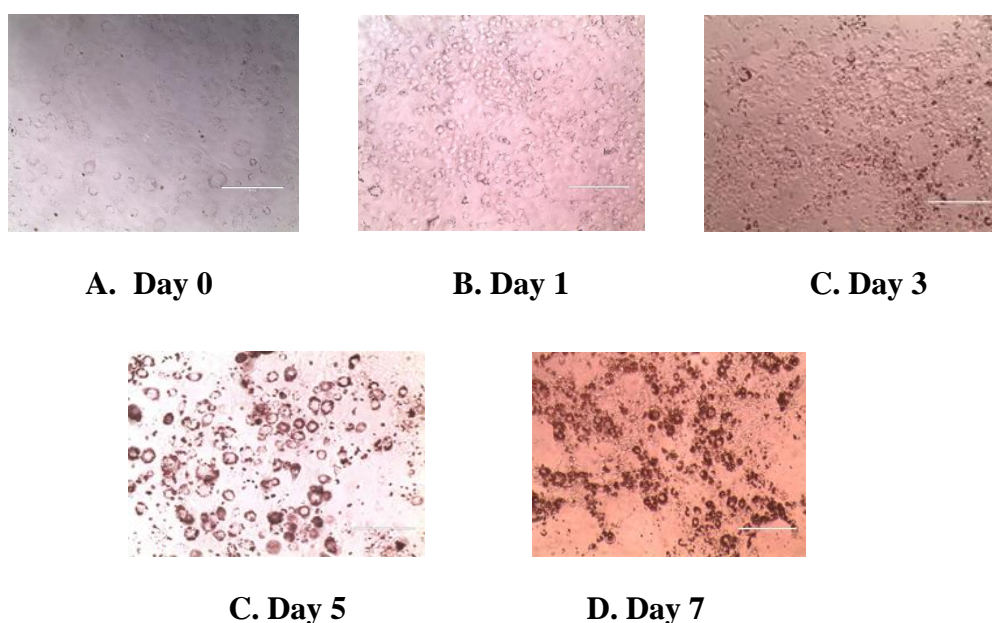


Figure 4.1: Microscopic images of Oil Red O stained 3T3-L1 cells (passage 8) subjected to adipocyte differentiation for 7 days (Qualitative). Lipid accumulation in the adipocytes was measured by oil red o-staining. Lipid droplets increased in both number, size over the following days, and took a week to become fully differentiated. Data are representative of 4 replicates.

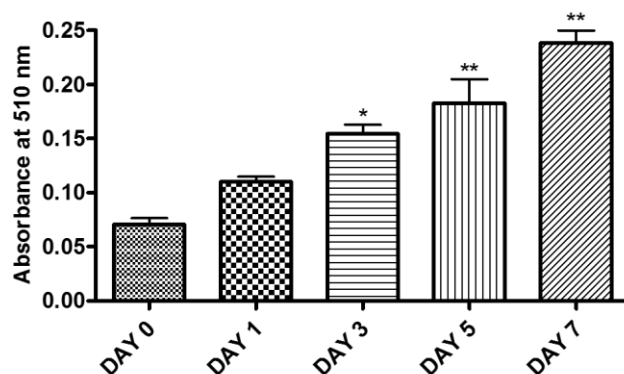


Figure 4.2: Quantitative analysis of 3T3-L1 cells differentiation using Oil Red O staining: Lipid droplets increased in both number, size over the following days, and took a week to become fully differentiated. Data are representative of $n=3$ replicates expressed as means \pm Standard deviations (* $P < 0.05$, ** $P < 0.01$ from control).

4.3.2. Effect of paracetamol on basal lipolysis in 3T3-L1 adipocytes

Prior to the lipolysis studies, the cells were assessed for the impact of paracetamol, aminopyrine and antipyrine on cell viability and proliferation over 48 hours. These compounds had no effect on the viability and proliferation of 3T3-L1 and primary adipocytes up to 48 hours (data not shown).

TGs hydrolysis results in glycerol and FFA release from adipocytes, glycerol release was assayed as an indicator of lipolytic pathway (Schweiger et al., 2014). In 3T3-L1 adipocytes incubated with paracetamol at 10 mM there was a significant decrease in glycerol release indicating a reduction in basal lipolysis. This inhibitory effect began as early as 1 hour with a 47% decrease in glycerol levels, followed by 57% and 52% at 3 and 24 hours in Figure 4.3.

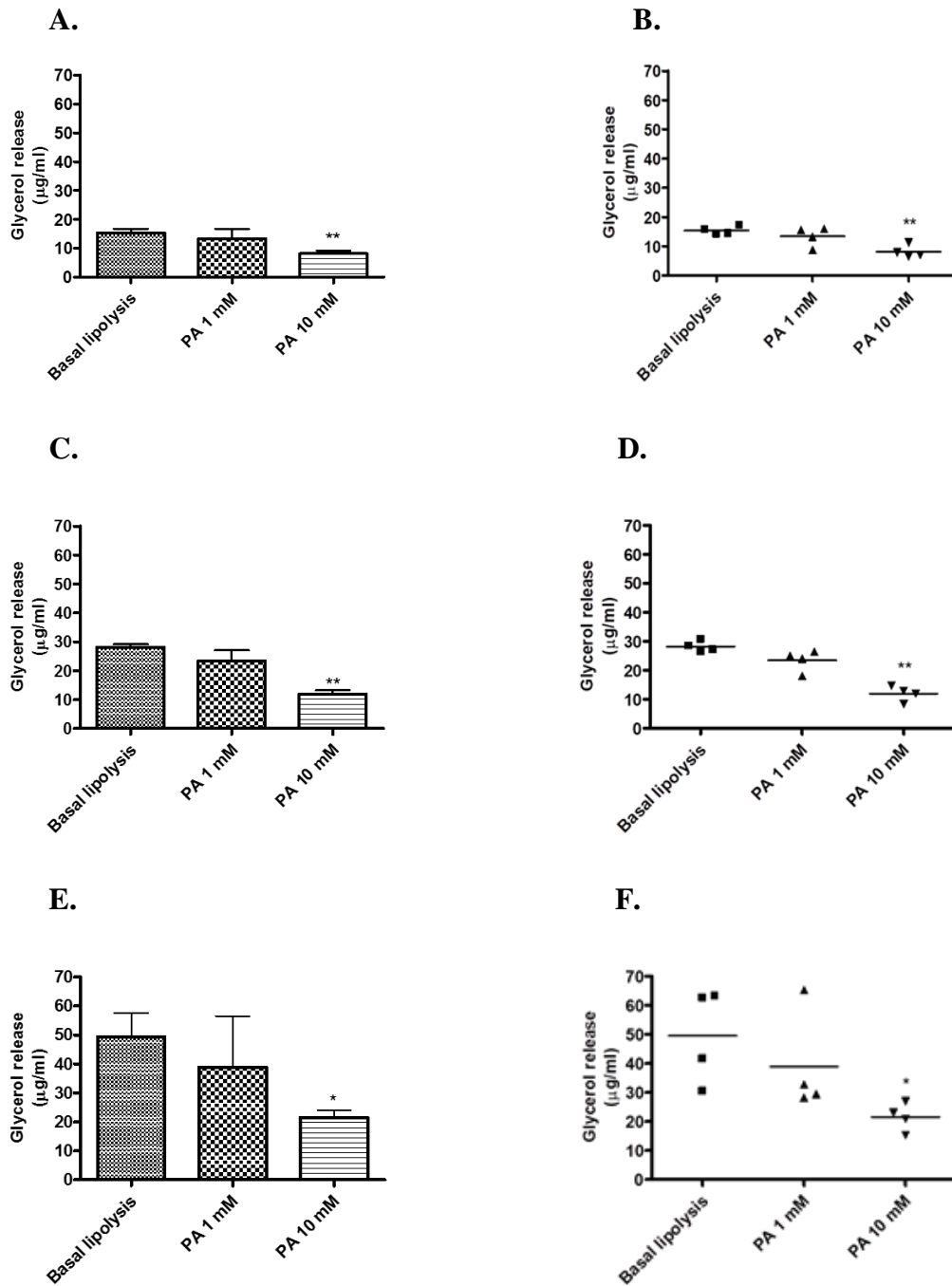


Figure 4.3: Effect of paracetamol on basal lipolysis in 3T3-L1 adipocytes at 1, 3 and 24 hours: Differentiated 3T3-L1 adipocytes were treated with serum free DMEM for 2 hours and were then treated with different concentrations of paracetamol (PA). For basal lipolysis, cells were treated at the same time with an appropriate volume of vehicle. Lipolysis was determined by measuring glycerol released into the culture media at 1(A), 3(C) and 24(E) hours. Data are representative of $n=4$ replicates expressed as means \pm Standard deviations (* $P < 0.05$, ** $P < 0.01$ from control). Same data was plotted as scatter graphs (B, D, F) for each time point to show individual data points.

4.3.3. Effect of paracetamol on norepinephrine stimulated lipolysis in 3T3-L1 adipocytes

To determine whether paracetamol has an impact on adrenergic stimulated lipolysis, the effect of paracetamol was examined using a well-known catecholamine norepinephrine (combined α/β agonist). Norepinephrine stimulated lipolysis in control cells in Figure 4.4 (A,B). In paracetamol (10 mM) pre-treated cells, the response to norepinephrine-stimulated lipolysis was significantly attenuated (43% and 24%) at 1 and 3 hours in Figure 4.4 (C,D).

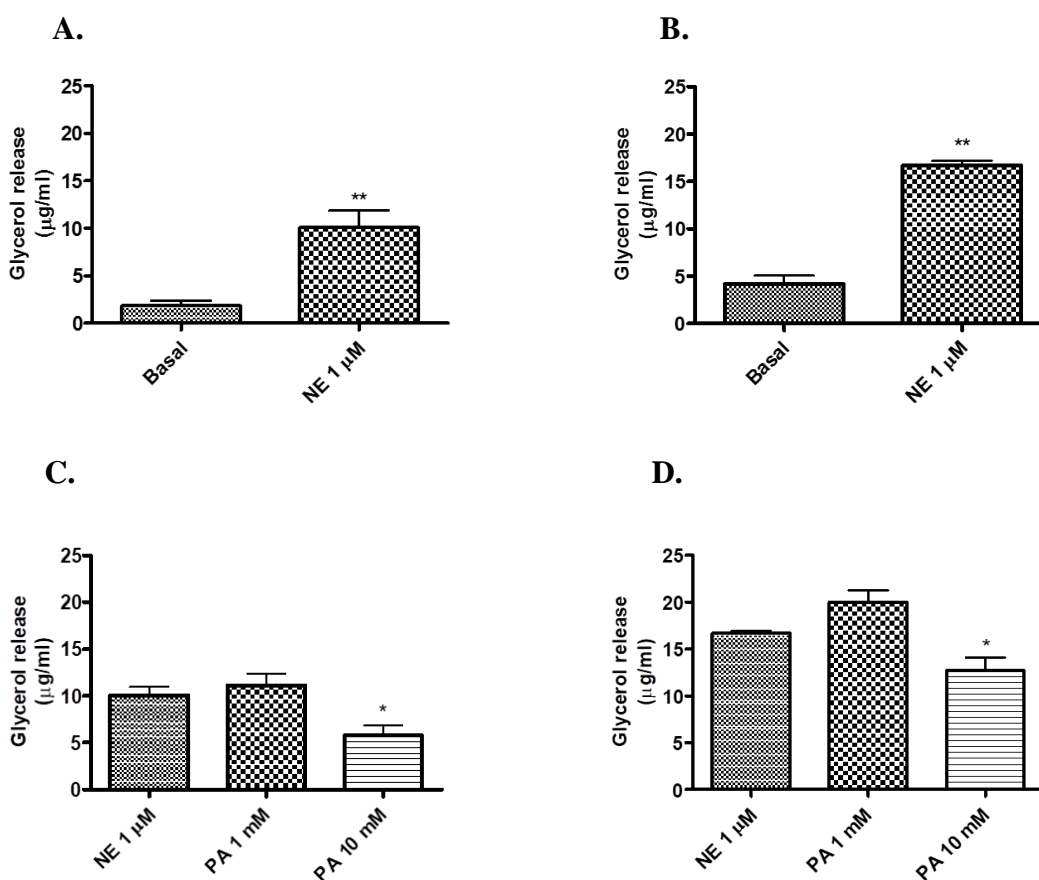


Figure 4.4: Effect of paracetamol on norepinephrine stimulated lipolysis in 3T3-L1 adipocytes at 1 and 3 hours: Differentiated 3T3-L1 adipocytes were treated with serum free DMEM for 2 hours. Cells were either treated with norepinephrine (NE) alone (A) or pre-incubated with different concentrations of paracetamol for 30 minutes and then norepinephrine was added (C). Lipolysis was determined by measuring glycerol released into the culture media at 1 hour (A,C) and 3 hours (B,D). Data are representative of $n=4$ replicates expressed as means \pm Standard deviations (* $P < 0.05$, ** $P < 0.01$ from control).

4.3.4. Effect of paracetamol on isoproterenol stimulated lipolysis in 3T3-L1 adipocytes (added simultaneously)

The effect of paracetamol on lipolytic stimulation by isoproterenol (an activator of β -adrenoceptor) was then examined. 3T3-L1 adipocytes were incubated with various concentrations of isoproterenol alone or paracetamol and isoproterenol added simultaneously. Addition of isoproterenol elevated glycerol release from adipocytes as compared with that under basal conditions in Figure 4.5-4.7 (A).

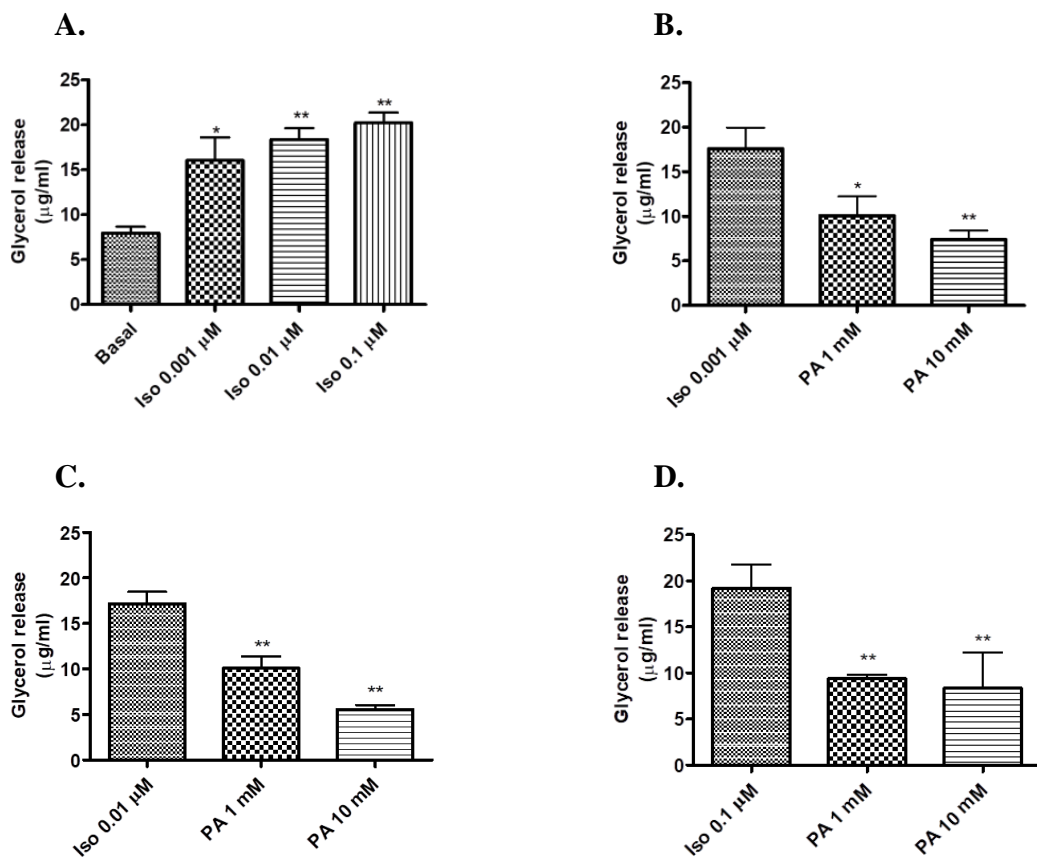


Figure 4.5: Effect of paracetamol on isoproterenol stimulated lipolysis in 3T3-L1 adipocytes at 1 hour: Differentiated 3T3-L1 adipocytes were treated with serum free DMEM for 2 hours. Cells were either treated with different concentrations of isoproterenol (Iso) alone (A) or treated with different concentrations of paracetamol and isoproterenol added simultaneously (B-D). Lipolysis was determined by measuring glycerol released into the culture media at 1 hour. Data are representative of $n=4$ replicates expressed as means \pm Standard deviations (* $P < 0.05$, ** $P < 0.01$ from control).

Paracetamol at both 1 and 10 mM concentration suppressed isoproterenol-stimulated release of glycerol (41% and 54%; Iso 0.001 μ M), (39% and 66%; Iso 0.01 μ M) and (51% and 56%; Iso 0.1 μ M) at 1 hour in Figure 4.5 (B-D), (36% and 49%; Iso 0.001 μ M), (32% and 61%; Iso 0.01 μ M), (50% and 66% Iso 0.1 μ M) at 3 hours in Figure 4.6 (B-D) and (29% and 48%; Iso 0.001 μ M), (36% and 65%; Iso 0.01 μ M), (50% and 66%; Iso 0.1 μ M) at 24 hours in Figure 4.7 (B-D).

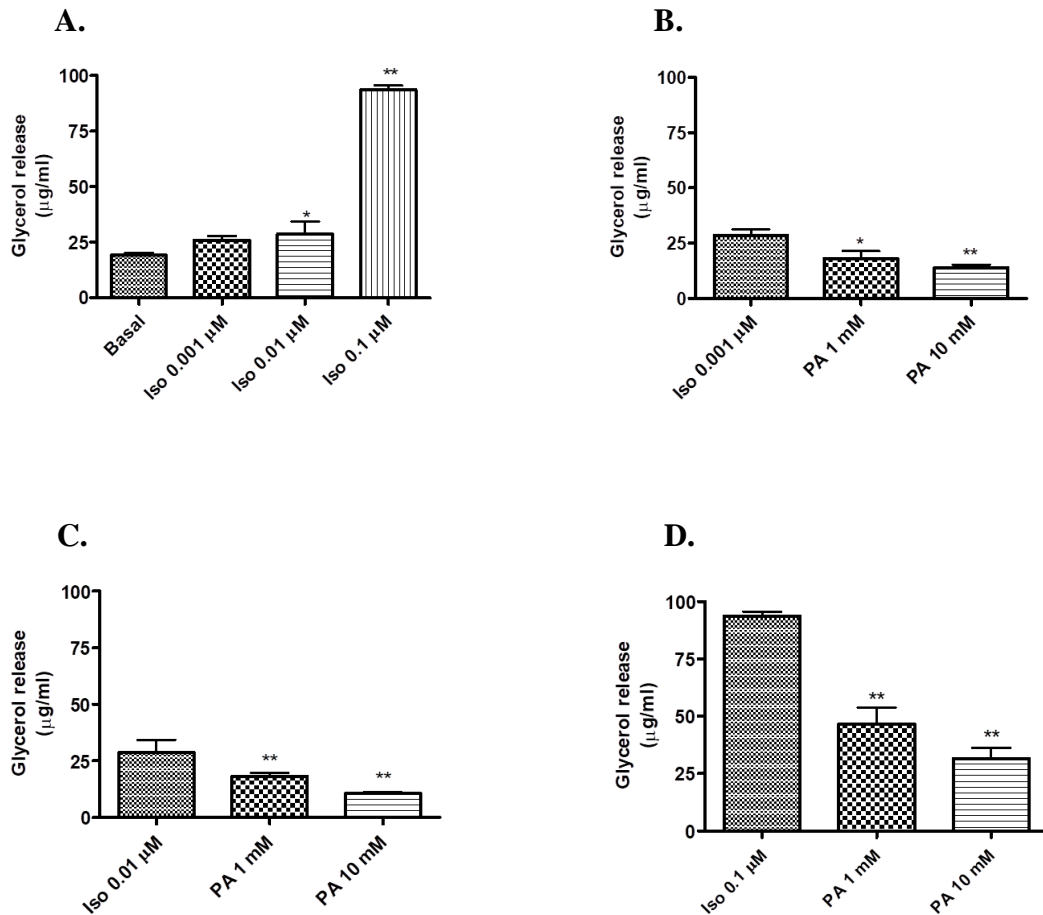


Figure 4.6: Effect of paracetamol on isoproterenol stimulated lipolysis in 3T3-L1 adipocytes at 3 hours: Differentiated 3T3-L1 adipocytes were treated with serum free DMEM for 2 hours. Cells were either treated with different concentrations of isoproterenol alone (A) or treated with different concentrations of paracetamol and isoproterenol added simultaneously (B-D). Lipolysis was determined by measuring glycerol released into the culture media at 3 hours. Data are representative of $n=4$ replicates expressed as means \pm Standard deviations (* $P < 0.05$, ** $P < 0.01$ from control).

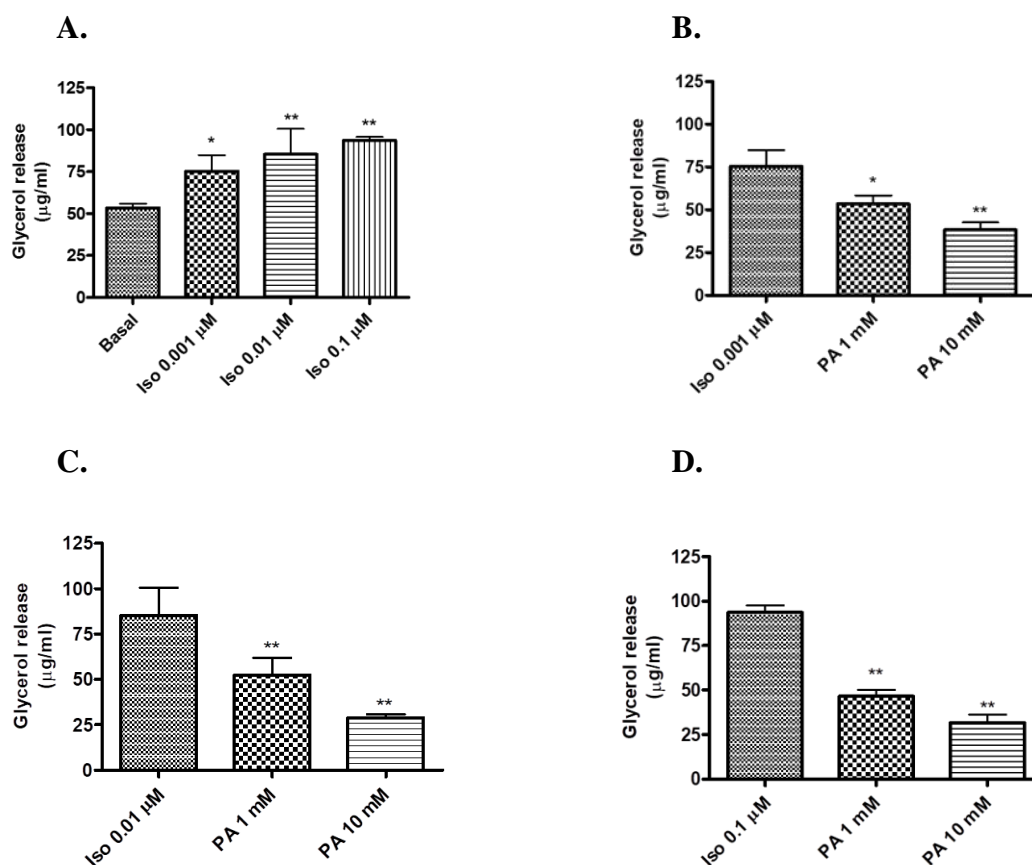


Figure 4.7: Effect of paracetamol on isoproterenol stimulated lipolysis in 3T3-L1 adipocytes after 24 hours: Differentiated 3T3-L1 adipocytes were treated with serum free DMEM for 2 hours. Cells were either treated with different concentrations of isoproterenol alone (A) or treated with different concentrations of paracetamol and isoproterenol added simultaneously (B-D). Lipolysis was determined by measuring glycerol released into the culture media at 24 hours. Data are representative of n=4 replicates expressed as means \pm Standard deviations (* $P < 0.05$, ** $P < 0.01$ from control).

4.3.5. Effect of paracetamol pre-treatment on isoproterenol stimulated lipolysis in 3T3-L1 adipocytes

Prior exposure of 3T3-L1 adipocytes with paracetamol for 30 minutes followed by isoproterenol (0.001 µM - 0.1 µM) treatment resulted in attenuated lipolysis at 1, 3 and 24 hours. Isoproterenol stimulated lipolysis in control cells in Figure 4.8-4.10 (A). Paracetamol significantly inhibited the glycerol release (24% and 72%; Iso 0.001 µM), (21% and 52%; Iso 0.01 µM), (35% and 63%; Iso 0.1 µM) at 1 hour in Figure 4.8 (B-D), (18% and 80%; Iso 0.001 µM), (41%; Iso 0.01 µM), (42%; Iso 0.1 µM) at 3 hours

in Figure 4.9 (B-D), and (6% and 44%; Iso 0.001 μM), (10% and 47% Iso 0.01 μM), (38% and 33% Iso 0.1 μM) at 24 hours in Figure 4.10 (B-D).

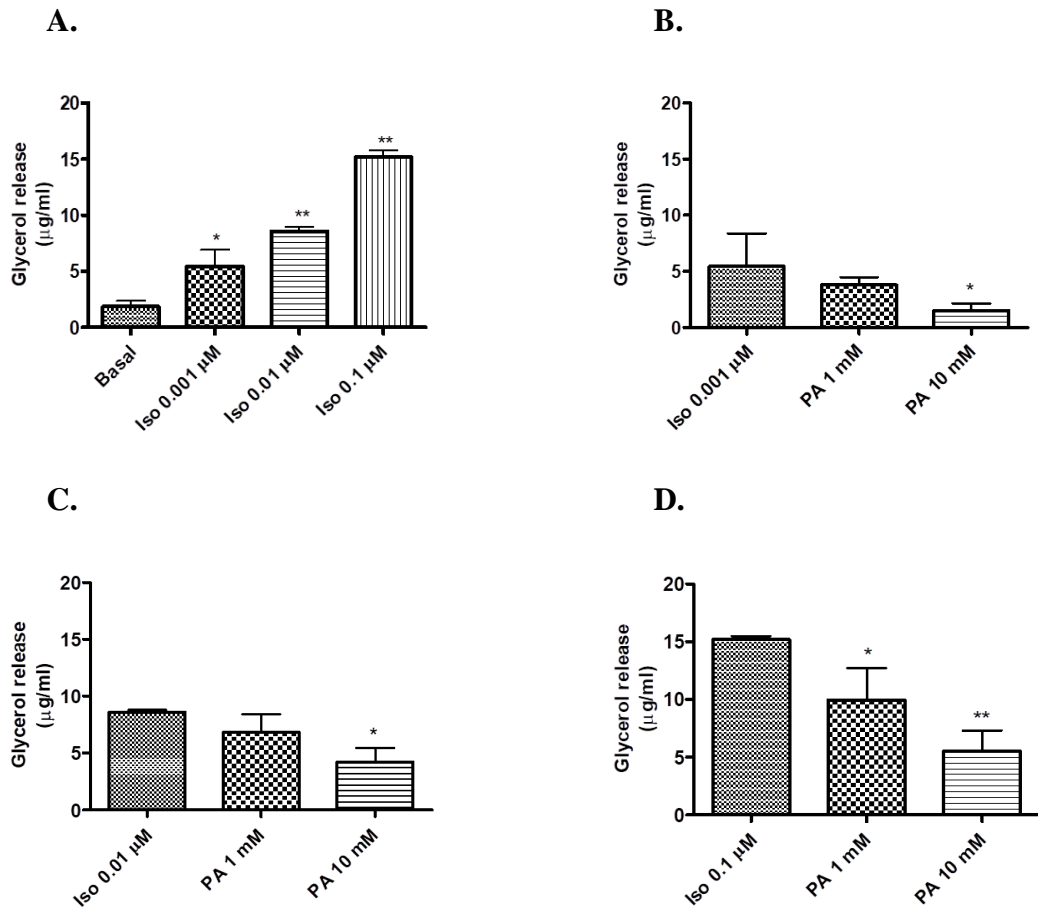


Figure 4.8: Effect of paracetamol pre-treatment on isoproterenol stimulated lipolysis in 3T3-L1 adipocytes at 1 hour: Differentiated 3T3-L1 adipocytes were treated with serum free DMEM for 2 hours. Cells were either treated with different concentrations of isoproterenol alone (A) or preincubated with different concentrations of paracetamol for 30 minutes and then isoproterenol added (B-D). Lipolysis was determined by measuring glycerol released into the culture media at 1 hour. Data are representative of $n=4$ replicates expressed as means \pm Standard deviations (* $P < 0.05$, ** $P < 0.01$ from control).

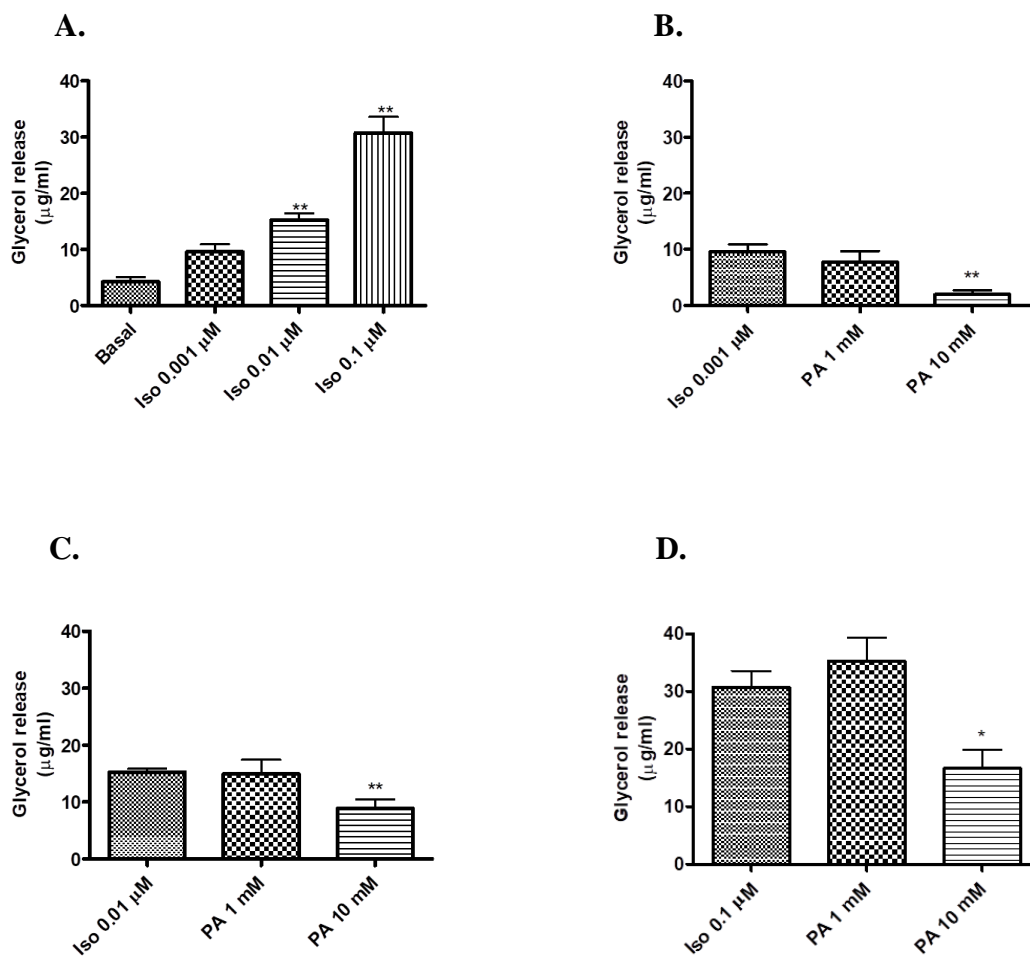


Figure 4.9: Effect of paracetamol pre-treatment on isoproterenol stimulated lipolysis in 3T3-L1 adipocytes at 3 hours: Differentiated 3T3-L1 adipocytes were treated with serum free DMEM for 2 hours. Cells were either treated with different concentrations of isoproterenol alone (A) or preincubated with different concentrations of paracetamol for 30 minutes and then isoproterenol added (B-D). Lipolysis was determined by measuring glycerol released into the culture media at 3 hours. Data are representative of $n=4$ replicates expressed as means \pm Standard deviations (* $P < 0.05$, ** $P < 0.01$ from control).

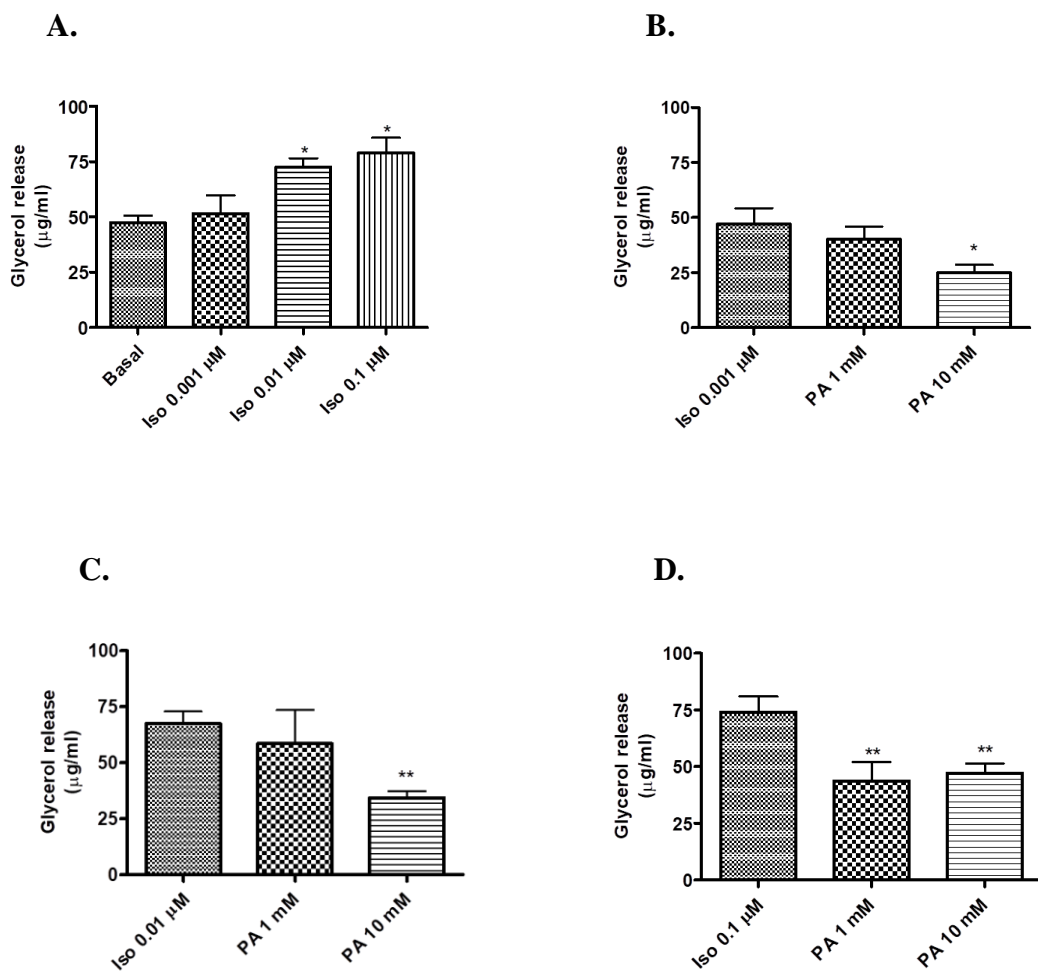


Figure 4.10: Effect of paracetamol pre-treatment on isoproterenol stimulated lipolysis in 3T3-L1 adipocytes at 24 hours: Differentiated 3T3-L1 adipocytes were treated with serum free DMEM for 2 hours. Cells were either treated with different concentrations of isoproterenol alone (A) or preincubated with different concentrations of paracetamol for 30 minutes and then isoproterenol added (B-D). Lipolysis was determined by measuring glycerol released into the culture media at 24 hours. Data are representative of $n=4$ replicates expressed as means \pm Standard deviations (* $P < 0.05$, ** $P < 0.01$ from control).

4.3.6. Chronic effect of paracetamol pre-treatment on isoproterenol stimulated lipolysis in 3T3-L1 adipocytes

3T3-L1 adipocytes were pre-treated with paracetamol for 30 minutes followed by stimulation with isoproterenol (1 μ M - 10 μ M) and glycerol release was measured after 24 and 48 hours.

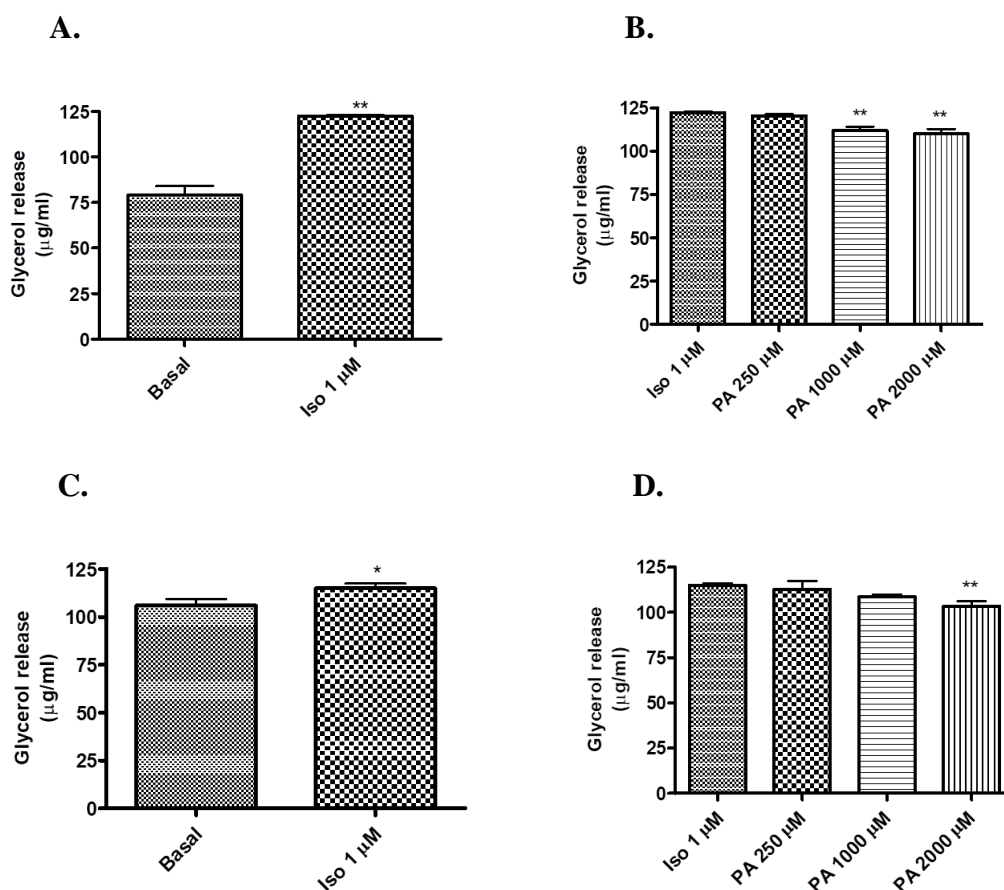


Figure 4.11(A-D): Chronic effect of paracetamol pre-treatment on isoproterenol stimulated lipolysis in 3T3-L1 adipocytes after 24 and 48 hours: Differentiated 3T3-L1 adipocytes were treated with serum free DMEM for 2 hours. Cells were either treated with isoproterenol alone (A) or preincubated with different concentrations of paracetamol for 30 minutes and then isoproterenol added (B). Lipolysis was determined by measuring glycerol released into the culture media at 24 (A,B) and 48 (C,D) hours. Data are representative of $n=4$ replicates expressed as means \pm Standard deviations (* $P < 0.05$, ** $P < 0.01$ from control).

Isoproterenol stimulated lipolysis in control cells in Figure 4.11 (A,C,E). In the case of 1 μM isoproterenol stimulation, paracetamol (1000 μM and 2000 μM) significantly inhibited the glycerol release (9% and 10%) at 24 hours in Figure 4.11 (B) whereas the inhibitory effect of paracetamol (2000 μM) on lipolysis in response to isoproterenol was not abrogated at 48 hours and decreased glycerol release (10%) in Figure 4.11(D).

Interestingly, paracetamol (250 μM and 1000 μM) seemed to be less effective to produce the same extent of inhibition at higher isoproterenol stimulation (10 μM). However, paracetamol (2000 μM) still decrease glycerol release (21%) significantly at 24 hours in Figure 4.11(F).

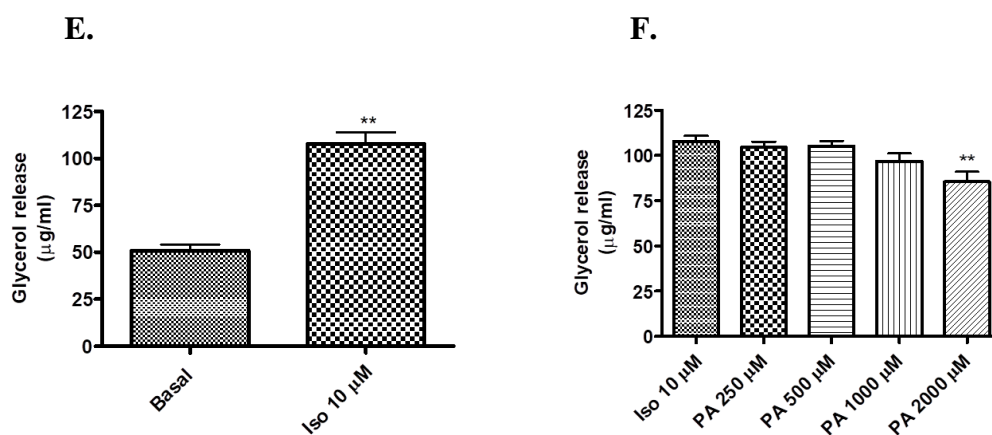


Figure 4.11(E-F): Chronic effect of paracetamol pre-treatment on isoproterenol stimulated lipolysis in 3T3-L1 adipocytes after 24 hours: Differentiated 3T3-L1 adipocytes were treated with serum free DMEM for 2 hours. Cells were either treated with isoproterenol alone (E) or preincubated with different concentrations of paracetamol for 30 minutes and then isoproterenol added (F). Lipolysis was determined by measuring glycerol released into the culture media at 24 (E,F) hours. Data are representative of $n=4$ replicates expressed as means \pm Standard deviations (* $P < 0.05$, ** $P < 0.01$ from control).

4.3.7. Effect of paracetamol on forskolin stimulated lipolysis in 3T3-L1 adipocytes

In order to assess the post receptor impact of paracetamol, forskolin (an activator of AC) was used. Forskolin stimulated lipolysis in control cells in Figure 4.12 (A,C,E). Prior exposure of 3T3-L1 adipocytes to paracetamol (10 mM) decreased the lipolysis induced by forskolin by 32%, 35% and 46% at 1, 3 and 24 hours in Figure 4.12 (B,D,F) similar to norepinephrine.

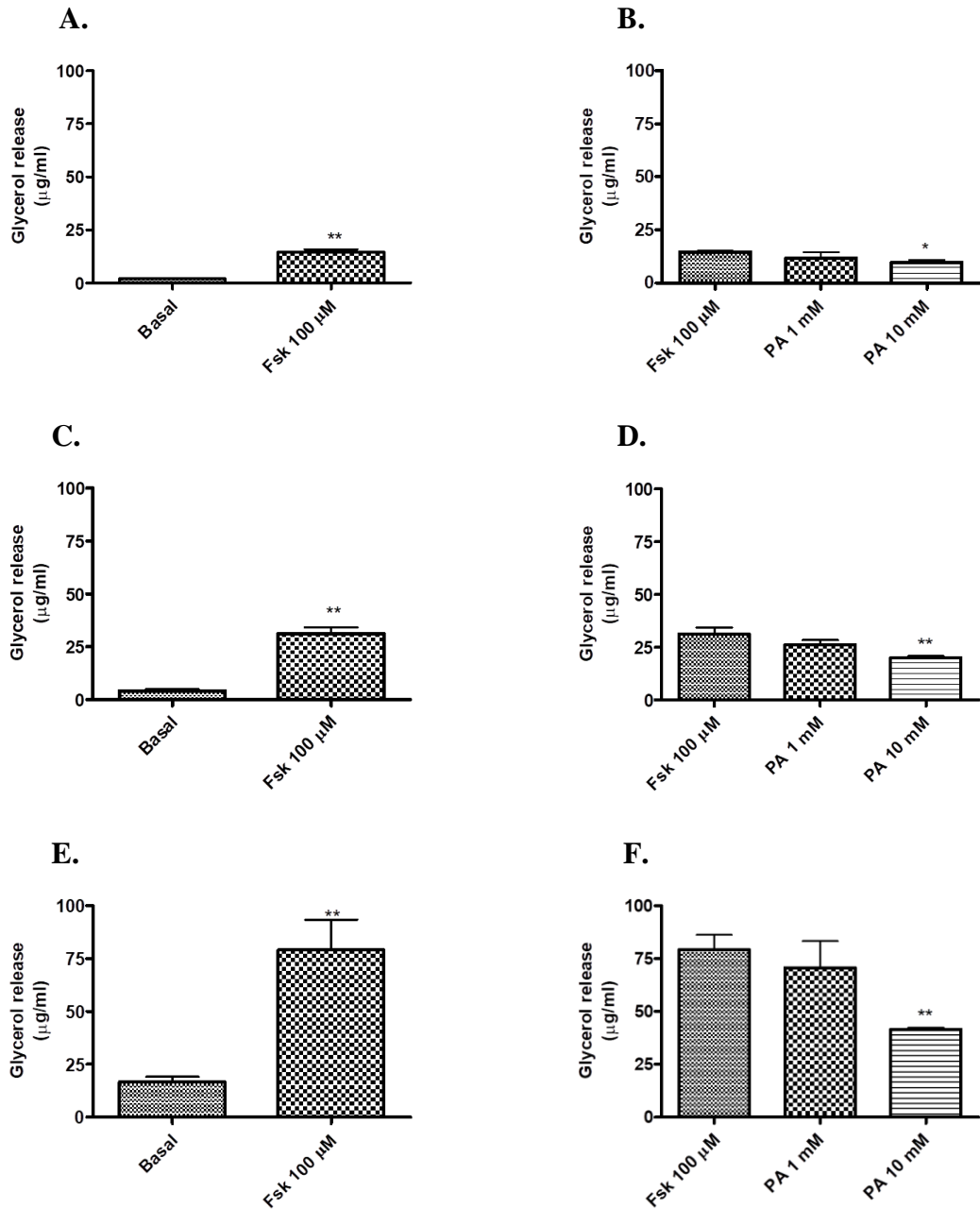


Figure 4.12: Effect of paracetamol on forskolin stimulated lipolysis in 3T3-L1 adipocytes at 1(A), 3(B) and 24(C) hours: Differentiated 3T3-L1 adipocytes were treated with serum free DMEM for 2 hours. Cells were either treated with forskolin (Fsk) alone (A) or preincubated with different concentrations of paracetamol for 30 minutes and then forskolin added (B). Lipolysis was determined by measuring glycerol released into the culture media at 1(A,B), 3(C,D) and 24(E,F) hours. Data are representative of $n=4$ replicates expressed as means \pm Standard deviations (* $P < 0.05$, ** $P < 0.01$ from control).

4.3.8. Effect of paracetamol on 8-Br-cAMP stimulated lipolysis in 3T3-L1 adipocytes

To assess the impact of paracetamol at the level of cAMP, a cAMP analog 8-Br-cAMP which has greater resistance to phosphodiesterases than cAMP was used.

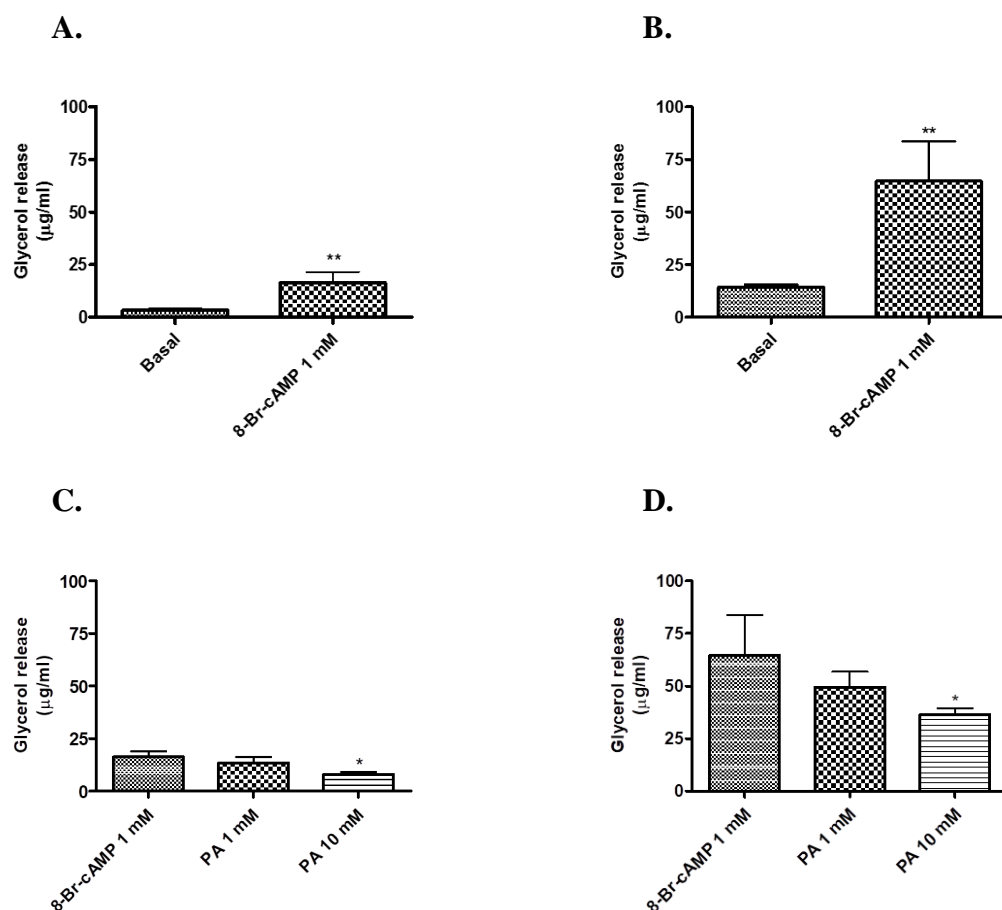


Figure 4.13: Effect of paracetamol on 8-Br-cAMP stimulated lipolysis in 3T3-L1 adipocytes at 3 and 24 hours: Differentiated 3T3-L1 adipocytes were treated with serum free DMEM for 2 hours. Cells were either treated with 8-Br-cAMP alone (A) or preincubated with different concentrations of paracetamol for 30 minutes and then 8-Br-cAMP added (C). Lipolysis was determined by measuring glycerol released into the culture media at 3(A,C) and 24(B,D) hours. Data are representative of $n=4$ replicates expressed as means \pm Standard deviations (* $P < 0.05$, ** $P < 0.01$ from control).

8-Br-cAMP stimulated lipolysis in control cells in Figure 4.13 (A,B). Paracetamol (10 mM) still showed marked decrease in glycerol release (45%) at 3 hours and still

persisted (40%) at 24 hours in Figure 4.13 (C,D) confirming that the paracetamol effect was not located at the cAMP level.

4.3.9. Effect of aminopyrine and antipyrene on basal lipolysis in 3T3-L1 adipocytes

In addition to paracetamol, the effect of aminopyrine and antipyrene on lipolysis under basal conditions was also investigated considering their previously reported involvement in induced hypothermia (Ayoub et al., 2004).

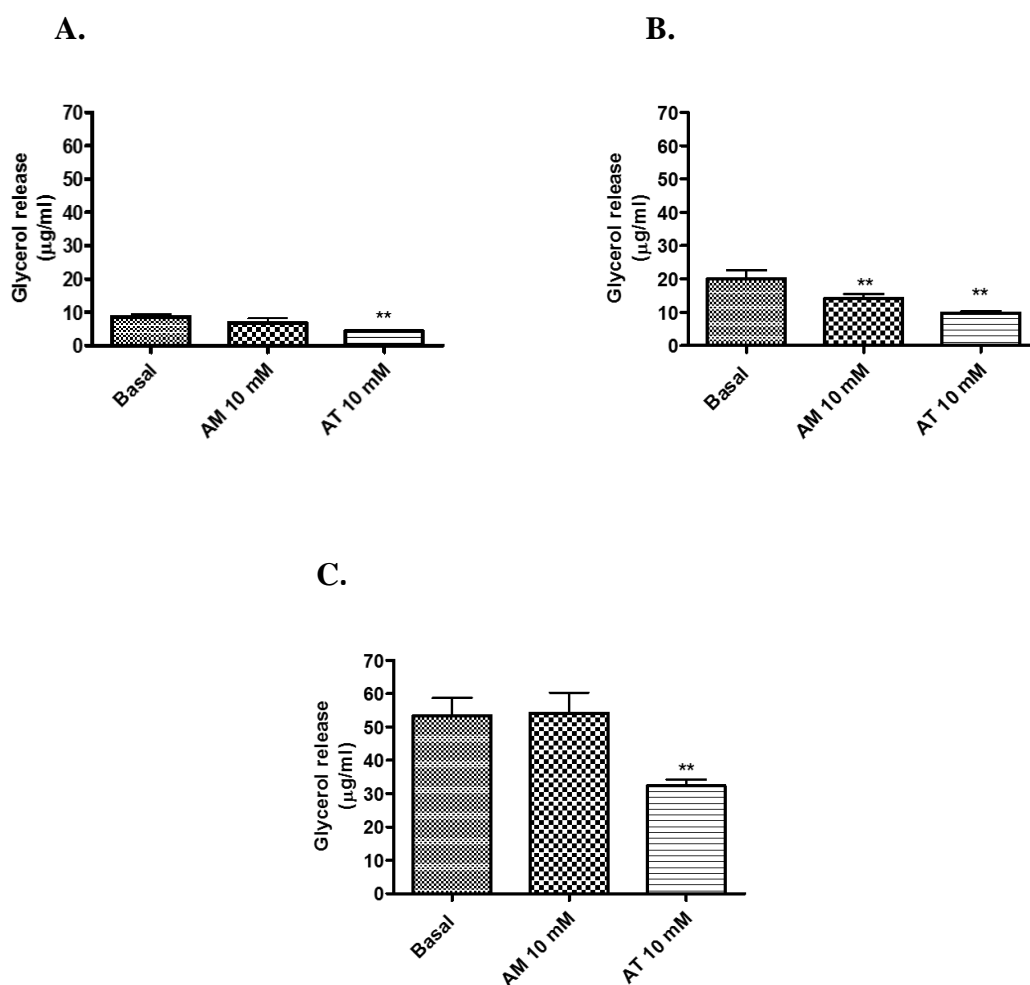


Figure 4.14: Effect of aminopyrine and antipyrene on basal lipolysis in 3T3-L1 adipocytes at 1, 3 and 24 hours: Differentiated 3T3-L1 adipocytes were treated with serum free DMEM for 2 hours and were then treated with aminopyrine (AM) or antipyrene (AT). Lipolysis was determined by measuring glycerol released into the culture media at 1(A), 3(B) and 24(C) hours. For basal lipolysis, cells were treated at the same time with an appropriate volume of vehicle. Data are representative of $n=4$ replicates expressed as means \pm Standard deviations (** $P < 0.01$ from control).

4.3.10. Effect of paracetamol, aminopyrine and antipyrine on basal lipolysis in rat primary brown adipocytes

In addition to cultured adipocytes lipolysis was assessed in rat primary brown fat adipocytes. High level of basal lipolysis was noticed in primary brown adipocytes. When cells were preincubated with various concentrations of paracetamol for an hour and glycerol release was measured, there was a significant decrease in basal lipolysis by 17%, 15% and 16% with increasing concentrations of paracetamol in Figure 4.15 (A). Aminopyrine (250 μ M – 1000 μ M) also attenuated glycerol release (25%, 29% and 23%) at 1 hour whereas antipyrine treated cells showed a decrease in glycerol levels (18%, 15% and 21%) in Figure 4.15 (B,C). The observed inhibition was not as extensive as with the 3T3 cells.

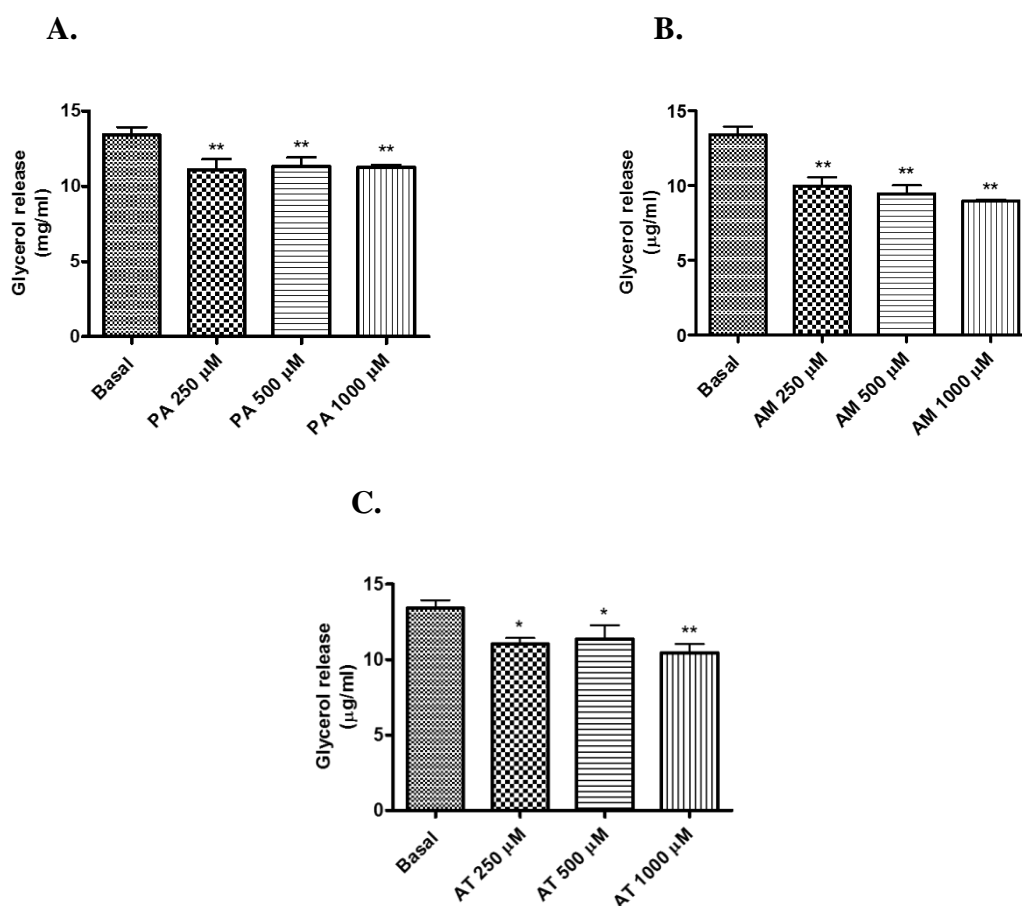


Figure 4.15: Effect of paracetamol, aminopyrine and antipyrine on basal lipolysis in rat primary brown adipocytes at 1 hour: Brown adipocytes were treated with different concentrations of paracetamol, aminopyrine and antipyrine and glycerol release was measured at 1 hour. Data are representative of $n=4$ replicates expressed as means \pm Standard deviations (* $P < 0.05$, ** $P < 0.01$ from control).

4.3.11. Effect of paracetamol, aminopyrine and antipyrine on basal lipolysis in rat primary brown adipocytes

Pre-treatment of primary brown adipocytes with higher concentrations of paracetamol (PA 1 mM – 10 mM) for an hour reduced basal lipolysis with a significant decrease in glycerol levels (10% and 19%) at 1 hour and (19% and 26%) at 24 hours (Figure 4.16). Similarly, aminopyrine (AM 1 mM – 10 mM) attenuated glycerol release (22% and 17%) at 1 hour and (34% and 26%) at 24 hours (Figure 4.17). In case of antipyrine treated cells, there was a marked decrease in glycerol release (10% and 11%) at 1 hour and (21% and 19%) at 24 hours (Figure 4.18) at all concentrations used.

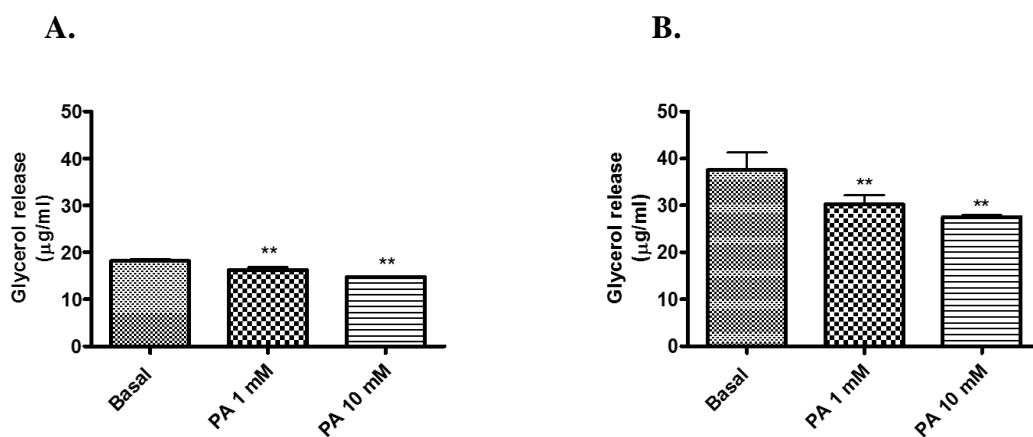


Figure 4.16: Effect of paracetamol on basal lipolysis in rat primary brown adipocytes at 1 and 24 hours: Brown adipocytes were treated with different concentrations of paracetamol and glycerol release was measured at 1(A) and 24(B) hours. Data are representative of $n=4$ replicates expressed as means \pm Standard deviations (** $P < 0.01$ from control).

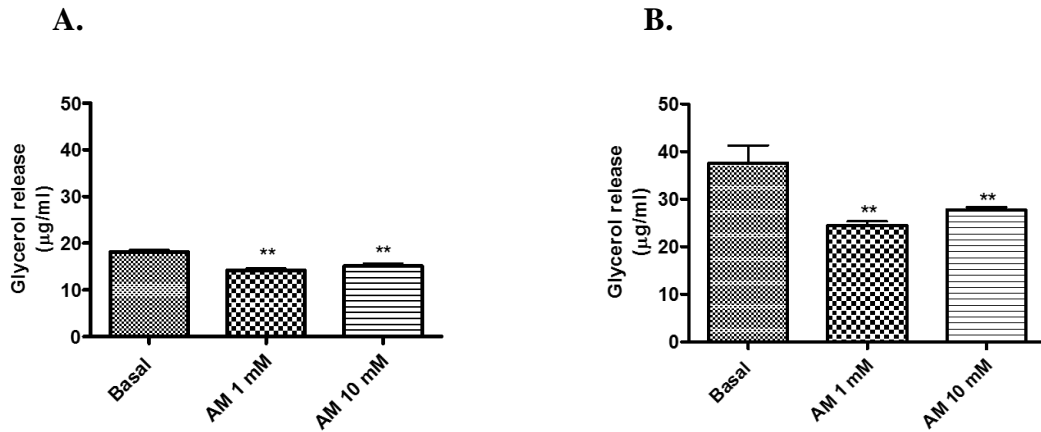


Figure 4.17: Effect of aminopyrine on basal lipolysis in rat primary brown adipocytes at 1 and 24 hours: Brown adipocytes were treated with different concentrations of aminopyrine and glycerol release was measured at 1(A) and 24(B) hours. Data are representative of $n=4$ replicates expressed as means \pm Standard deviations (** $P < 0.01$ from control).

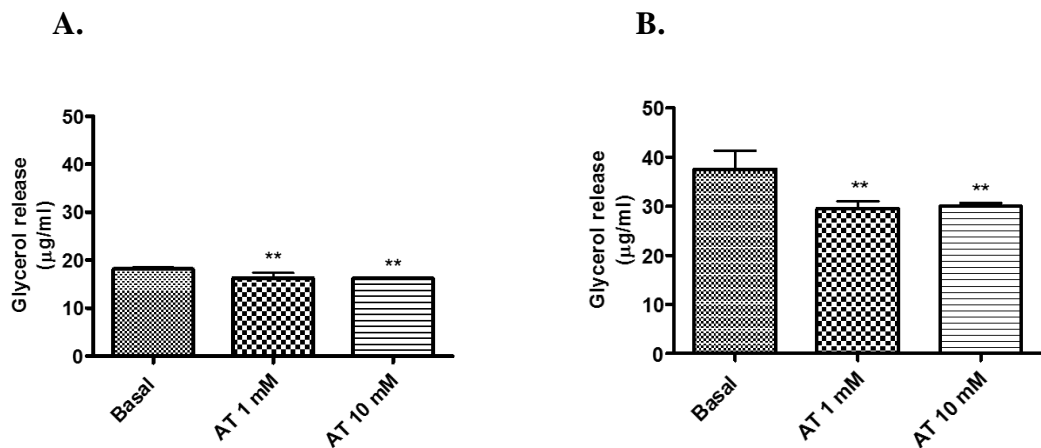


Figure 4.18: Effect of antipyrine on basal lipolysis in rat primary brown adipocytes at 1 and 24 hours: Brown adipocytes were treated with different concentrations of antipyrine and glycerol release was measured at 1(A) and 24(B) hours. Data are representative of $n=4$ replicates expressed as means \pm Standard deviations (** $P < 0.01$ from control).

4.3.12. Effect of paracetamol, aminopyrine and antipyrine on norepinephrine stimulated lipolysis in rat primary brown adipocytes

Primary brown adipocytes were preincubated with higher concentrations of paracetamol, aminopyrine and antipyrine for 1 hour followed by addition of norepinephrine and then glycerol release was assayed after 1 and 24 hours. Paracetamol (PA 1 mM – 10 mM) caused a significant inhibition of lipolysis in the presence of norepinephrine (15% and 16%) at 1 hour and (14% and 21%) at 24 hours (Figure 4.19). Similarly, aminopyrine (AM 1 mM – 10 mM) attenuated glycerol release (21% and 19%) at 1 hour and (26% and 17%) markedly at 24 hours (Figure 4.20). In case of antipyrine treated cells, there was a decrease in glycerol release (12% and 12%) at 1 hour and (15% and 21%) at 24 hours (Figure 4.21) at all concentrations used.

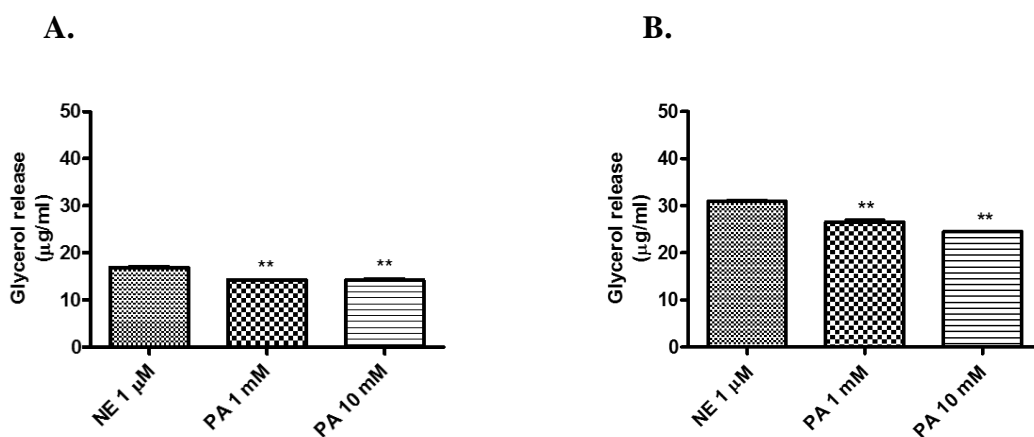


Figure 4.19: Effect of paracetamol on norepinephrine stimulated lipolysis in rat primary brown adipocytes at 1 and 24 hours: Brown adipocytes were preincubated with different concentrations of paracetamol for an hour and then treated with norepinephrine. Lipolysis was determined by measuring glycerol released into the culture media at 1(A) and 24(B) hours. Data are representative of n=4 replicates expressed as means \pm Standard deviations (** $P < 0.01$ from control).

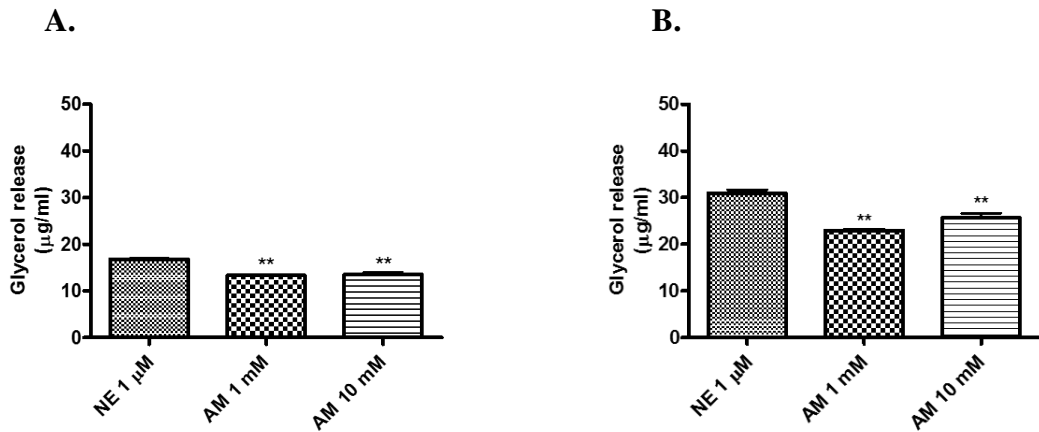


Figure 4.20: Effect of aminopyrine on norepinephrine stimulated lipolysis in rat primary brown adipocytes at 1 and 24 hours: Brown adipocytes were preincubated with different concentrations of aminopyrine for an hour and then treated with norepinephrine. Lipolysis was determined by measuring glycerol released into the culture media at 1(A) and 24(B) hours. Data are representative of $n=4$ replicates expressed as means \pm Standard deviations (** $P < 0.01$ from control).

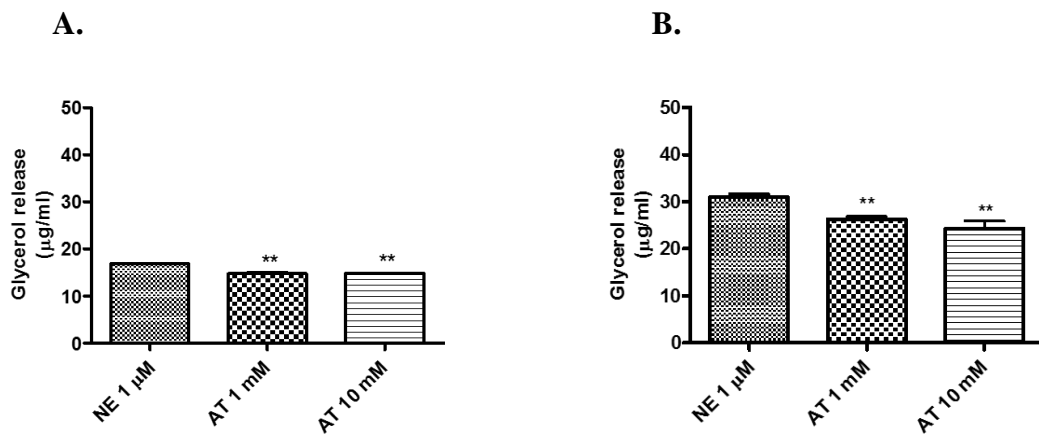


Figure 4.21: Effect of antipyrine on norepinephrine stimulated lipolysis in rat primary brown adipocytes at 1 and 24 hours: Brown adipocytes were preincubated with different concentrations of antipyrine for an hour and then treated with norepinephrine. Lipolysis was determined by measuring glycerol released into the culture media at 1(A) and 24(B) hours. Data are representative of $n=4$ replicates expressed as means \pm Standard deviations (** $P < 0.01$ from control).

4.4. Discussion:

For homeotherms housed at temperature below their thermoneutral zone, heat generation starts with signals coming from the preoptic area of anterior hypothalamus (POA) to stimulate peripheral effectors leading to the increased lipolysis, mitochondrial metabolism and heat generation. Given the lack of agreement about the actions of paracetamol centrally, it is reasonable to examine its impact at other points along the heat generation pathway.

Lipolysis is a critical metabolic function of adipocytes and is a key process that provides fatty acids for combustion and to induce UCP1 activation, thus directly leading to thermogenesis (Ohlson et al., 2004). Conversion of stored TGs into FFAs through a process of lipolysis is stimulated by β -adrenergic signalling to activate the cAMP mediated PKA pathway (Chrysovergis et al., 2014; McKnight et al., 1998). This mediates phosphorylation and activation of lipolytic enzymes including HSL, ATGL, and perilipin (MacPherson and Peters, 2015; Schweiger et al., 2006; Heeren and Münzberg 2013; Marcelin and Chua 2010).

Prior to the lipolysis studies, the 3T3-L1 cells were assessed for the impact of paracetamol on viability at the concentrations used. The concentrations (up to 10 mM) were similar to or lower than concentrations known to induce hypothermia in animals *in vivo*. At these concentrations over 48 hours, there was no loss of viability indicating that the effects observed could not be attributed to loss of cell numbers or viability. Prior to the lipolysis assays, the 3T3-L1 pre-adipocytes were shown to successfully differentiate into adipocytes.

Although lipolysis can be directly assessed by measuring glycerol release (Schweiger et al., 2014), the addition of BSA (fatty acid-free) to the culture medium is required to prevent fatty acid reesterification (Paar et al., 2012). In this study, to examine whether paracetamol could have an impact on lipolysis, glycerol release was measured in mouse 3T3-L1 adipocytes, the most frequently used an *in vitro* model of lipolysis. In the model used, adipocytes were incubated in a low glucose medium to ensure lipolysis. Under basal conditions, paracetamol at 10 mM was found to significantly reduce glycerol release as early as 1 hour (Figure 4.3). This initial observation suggests that paracetamol is impacting on the lipolysis pathway in the absence of any form of external stimulation, possible indication that the actions of paracetamol may be post receptor. Another possibility is that paracetamol could act on the α_1 or α_2 receptors which are thought to

inhibit lipolysis. Stimulation of α_2 -receptors is thought to decrease AC activity and thus cAMP production (Fain et al., 1984) whereas stimulation of α_1 -receptors activates a calcium-dependent phosphodiesterase and possibly decrease cAMP (Bronnikov et al., 1984) and thermogenesis.

To investigate whether stimulation of inhibitory α_1 or α_2 pathways was necessary to observe the inhibitory effect of paracetamol, the effect of paracetamol could have been compared with α -receptor agonist. When cells were stimulated with NE, a combined α -/ β -agonist for different subtypes of α / β -adrenergic receptors lipolysis was increased. Again, paracetamol was able to lower NE stimulated lipolysis (43% and 24%) at 1 and 3 hours (Figure 4.4).

To further investigate the impact of paracetamol on the catecholamine receptor, the β -agonist such as isoproterenol was selected to stimulate lipolysis. Paracetamol also inhibited isoproterenol induced lipolysis when added simultaneously with the agonist (Figure 4.5-4.7). This effect was concentration dependent, moreover, paracetamol pre-treatment of 3T3-L1 adipocytes attenuated isoproterenol stimulated lipolysis, however the effect was better observed at the higher concentrations and after a short (1,3 hours) incubation, suggesting an impact of drug metabolism (Figure 4.8-4.10).

The inhibitory effect of paracetamol could be located downstream of the coupling process between the β -receptor and AC. To investigate whether the paracetamol effect is located at the level of AC, forskolin a direct activator of AC was used. Forskolin stimulated lipolysis in the control cells. In the paracetamol preincubated cells, there was a time dependent decrease in lipolysis and the response to forskolin (Figure 4.12). This observation confirmed that the paracetamol inhibition was not located at the receptor/cyclase coupling process and must therefore be distally located.

The next step was to investigate the effect on paracetamol on cAMP levels which would partly impact on phosphodiesterases activity. To determine the role of increased cAMP breakdown in paracetamol inhibition, a cAMP analog 8-Br-cAMP with a greater resistance to phosphodiesterases than cAMP itself was used. 8-Br-cAMP induced an increase in lipolysis in control cells. The glycerol release was, however, still much attenuated by paracetamol, about 45% lower than in control cells at 3 hours (Figure 4.13), confirming that the paracetamol effect was not located to phosphodiesterase function.

If time allowed, the effect of paracetamol on the link between a given amount of cAMP and the resulting lipolysis could have been measured simultaneously in cells stimulated with the AC activator forskolin. Moreover, to confirm whether paracetamol had a direct effect on AC, its activity could have been directly measured in membrane preparations from 3T3-L1 adipocytes. More importantly the effect of paracetamol on other key enzymes in the lipolysis process such as HSL, ATGL and perilipin activities needs to be investigated.

In addition to paracetamol, the effect of aminopyrine and antipyrine was also studied primarily as they were reported to be putative COX-3 inhibitors. These agents are classified as pyrazolones and considered as oldest synthetic pharmaceuticals. Antipyrine (phenazone) exhibits analgesic, antipyretic and antirheumatic activity. Aminopyrine (aminophenazone) is thought to possess greater antipyretic and analgesic activity, marked anti-inflammatory property but more toxic than antipyrine (Volz and Kellner, 1980). However like paracetamol, little is understood about the impact of these compounds on lipolysis. In the present studies, both aminopyrine and antipyrine were effective in significantly reducing glycerol release at 1 and 3 hours in 3T3-L1 cells in a manner similar to paracetamol (Figure 4.14). In addition, like paracetamol the effect was most pronounced at the earlier time points suggesting the parent compounds may be involved rather than metabolites. The results parallel the hypothermic and COX-3 inhibitors action of all three compounds.

Although the differentiated 3T3-L1 cells are a widely used model for lipolysis and fat metabolism studies, investigations were also undertaken using rat primary brown adipocytes which are known for their involvement in thermoregulation in small mammals. In addition, these cells may give a more realistic picture of the effect of the test compound on lipolysis. The cells showed high levels of basal lipolysis which may reflect the fact that they have just been removed from an animal below their thermoneutral zone and simply it may be a reflection of the level of both cold and other stress in freshly isolated cells. The compounds (paracetamol, aminopyrine and antipyrine) inhibited lipolysis in the primary cells in a manner similar to the 3T3-L1 cells under basal conditions and to a greater limit when NE was present (4.15-4.21)

Paracetamol, aminopyrine and antipyrine are not the only antipyretic compounds to inhibit lipolysis. Indomethacin has shown to inhibit enzymes involved in basal and stimulated lipolysis in the kidney, thus inhibiting PG synthesis via lowering the AA and through directly interacting (Erman et al., 1980). NSAIDs (aspirin, naproxen,

nimesulide, and piroxicam) are known to activate NADPH oxidase (NOX) isoform (NOX4) in adipocytes to produce hydrogen peroxide (H₂O₂), which impairs cAMP-dependent PKA-II activation, thus inhibiting isoproterenol activated lipolysis. H₂O₂ signalling is a novel COX independent effect of NSAIDs in adipocytes and may play a role in antipyresis (Vázquez-Meza et al., 2013).

These studies confirm that hypothermic agents such as paracetamol, aminopyrine and antipyrene are capable of inhibiting lipolysis. Even at the level of inhibition reported in this study could negatively impact on a small mammal's ability to thermoregulate at temperatures below their thermoneutral zone.

Although lipolysis is a key step in the thermogenesis process, paracetamol and other hypothermic compounds could also work at sites downstream to the generation of fatty acids, for example by inhibiting FAO.

Chapter 5: Effect of Paracetamol on Mitochondrial Fatty Acid uptake and Oxidation

5.1. Introduction

Hypothermia occurs only when the metabolic rate (heat production) decreases and/or heat loss increases (Moriyama et al., 2006). The ultimate determinant of T_c in small mammals at T_a below their thermoneutral zone is their ability to switch on and maintain thermogenesis process in peripheral tissues, regardless of the existence and role of COX-3. The observation of hypothermia in rodents following administration of paracetamol may indicate that paracetamol might have an impact on peripheral thermoregulatory effector mechanisms. In the previous chapter, paracetamol was shown to attenuate lipolysis. However, it may be possible that this compound may also have additional effects further down on the thermogenesis effector pathways.

Following lipolysis, a main step in the process of heat production is the conversion of reduced cofactors such as NADH and fatty acids in the mitochondria directly to heat (uncoupling), or indirectly through the production of ATP. Fatty acids released via lipolysis can only undergo β -oxidation (Pauw et al., 2009) once they cross the mitochondrial membranes (Begrache et al., 2011). Entry of fatty acids into the mitochondria depends on their lengths; with short to medium fatty acids penetrate easily whereas long chain (C₁₄–C₁₈) fatty acids, also called LCFA rely on a shuttle system (Begrache et al., 2011). They are first changed to LCFA-coenzyme A (acyl-CoA) thioesters through the action of acyl-CoA synthetases (ACS) and then to acyl-carnitine derivative by CPT 1 (Begrache et al., 2011) and translocated into the matrix via CAT (Begrache et al., 2011). The acyl group in carnitine moves back to coenzyme A via CPT 2 (Begrache et al., 2011). LCFA-CoA thioesters undergoes β -oxidation and form acetyl-CoA moieties.

Oxidation of fatty acids in mitochondria forms NADH and FADH₂ and electrons are transferred to the respiratory complexes (Begrache et al., 2011). In the mitochondrial ETC, electrons are sequentially transferred from the reduced co-factors to various complexes to oxygen (Begrache et al., 2011). ATP produced from fatty acid oxidation is a key requirement for lipolysis. For some time it has been known that decreased ATP levels resulting from the actions of uncouplers or inhibitors of the mitochondrial ETC can inhibit catecholamine induced lipolysis (Fassina et al., 1974). This indicates a

direct link between lipolysis and the functionality of mitochondrial oxidative phosphorylation (OXPHOS) system (Pauw et al., 2009).

Drug-induced inhibition of mitochondrial FAO involves various mechanisms and may require interactions with different mitochondrial enzymes (Fromenty and Pessayre, 1995; Labbe et al., 2008). Drugs including ibuprofen can cause direct inhibition of one or more mitochondrial FAO enzymes (Fromenty and Pessayre, 1995). Many of the toxic properties of paracetamol are mediated by the metabolism by cytochrome P450 system to the highly reactive metabolite NAPQI including the inhibition of FAO enzymes (Chen et al., 2009). CPT1 could be a key target for these drugs (Begrache et al., 2011). Drug induced blockade of mitochondrial FAO can also occur via formation of coenzyme A and l-carnitine esters, decreasing important cofactors involved in FAO as in case of salicylic acid, and ibuprofen (Fromenty and Pessayre, 1995; Deschamps et al., 1991; Fréneaux et al., 1990). Severe inhibition of the ETC can directly inhibit mitochondrial FAO by reducing the level of co-factors and ATP (Fromenty and Pessayre, 1995; Labbe et al., 2008). Other process that could be considered includes ETC damage and lactic acidosis via inhibition of the TCA cycle (Labbe et al., 2008; Cornejo-Juarez et al., 2003; Walker et al., 2004).

In an attempt to establish if the hypothermia caused by paracetamol and related compounds is due to the inhibition of endogenous or exogenous FAO, oxygen consumption rate (OCR) was assessed in 3T3-L1 cells in the absence and presence of palmitate and results compared to etomoxir (Eto), a known inhibitor of fatty acid uptake into the mitochondria. The Agilent Seahorse XF FAO assay allows the sources of fatty acid (endogenous or exogenous) to be identified and how specific test compounds affect mitochondrial function. The rate of oxidation of exogenously added fatty acids to cells will depend on the availability of other substrates and the demand for ATP. In addition, fatty acids from exogenous source can also uncouple mitochondria reducing coupling efficiency. Both can be assessed by measuring OCR in the presence of palmitate-BSA, an extensively used substrate and the classic inhibitor Eto which inhibits CPT1 (Agilent Seahorse, U.K.).

5.2. Methods

5.2.1. Effect of paracetamol, etomoxir and NAPQI on both endogenous and exogenous (in the presence of palmitate:BSA) FAO was determined using the Agilent Seahorse XF FAO Assay as described in section 2.4.15-2.4.16.1.

The results were analysed with analysis of variance (ANOVA), followed by Dunnett's Multiple Comparison Test or Bonferroni's Multiple Comparison Test. A * $P < 0.05$, ** $P < 0.01$, *** $P < 0.001$ from control was considered statistically significant.

5.3. Results:

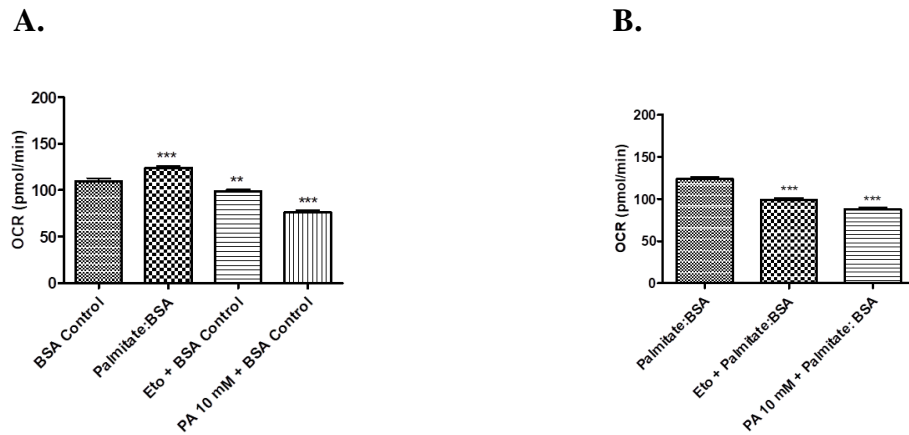
5.3.1. Effect of paracetamol on FAO:

Under conditions of limited substrate concentration, the XF Palmitate-BSA FAO substrate was used along with Eto, and the XF Cell Mito Stress Test, the XF FAO assay measures FAO in cells during basal and stressed energy needs (Agilent Seahorse, U.K.). The effect of paracetamol (10 mM) was investigated under basal conditions and after oligomycin addition (2.5 $\mu\text{g/ml}$), FCCP (4 μM) and rotenone/antimycin A (2 $\mu\text{M}/4 \mu\text{M}$) versus BSA control and Palmitate: BSA control.

During basal respiration, there was a significant decrease in OCR by 10% and 31% in BSA+Eto and BSA+PA group. The Palm: BSA+Eto and Palm:BSA+PA group resulted in a reduction in OCR by 20% and 29% indicating that a small segment of the basal respiration was as a result of oxidation of endogenous fatty acids in Figure 5.1(A,B). After the addition of oligomycin, the BSA+Eto and BSA+PA treatment group resulted in a further decrease by 12% and 15%, whereas reduced OCR was noticed in Palm:BSA+PA by 17% in Figure 5.1(C,D).

Introduction of FCCP resulted in a significant rise in maximum respiration in the Palm:BSA treatment group that was supported by oxidizing exogenous fatty acids as Palm:BSA+Eto and Palm:BSA+PA group has shown a reduction in OCR by 42% and 25% in Figure 5.2(A,B). The BSA+Eto and BSA+PA treatment group attenuated OCR by 8% and 18%. Finally, rotenone/antimycin A caused a further reduction in OCR by 17% and 16% (BSA+Eto and BSA+PA) and 23% and 14% (Palm:BSA+Eto and Palm:BSA+PA in Figure 5.2(C,D) respectively.

Basal



Oligomycin addition

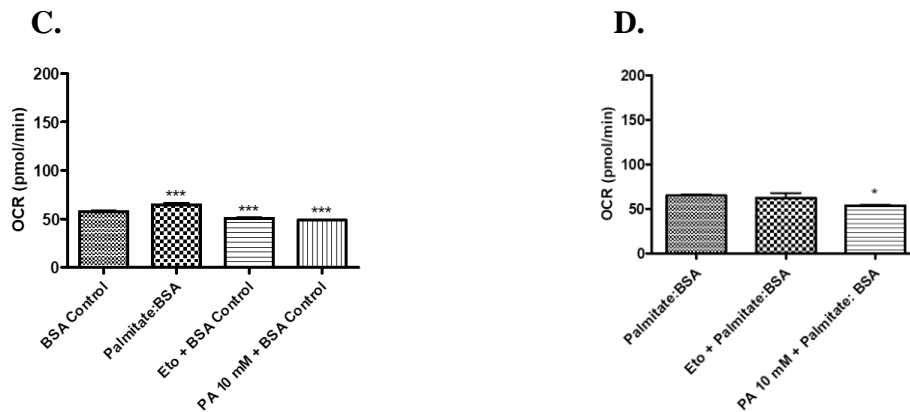
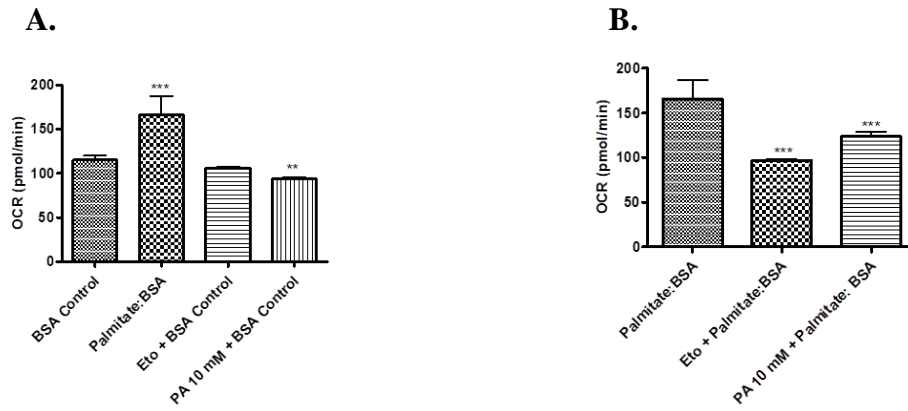


Figure 5.1: Effect of paracetamol on FAO during basal and after oligomycin addition in 3T3-L1 adipocytes. Differentiated 3T3-L1 adipocytes grown in substrate-limited medium overnight and combination of XF Palmitate-BSA FAO Substrate and the XF Cell Mito Stress Test was used. Data are representative of $n=3$ replicates expressed as means \pm Standard deviations (* $P < 0.05$, ** $P < 0.01$, *** $P < 0.001$ from control).

FCCP addition



Rotenone/Antimycin A addition

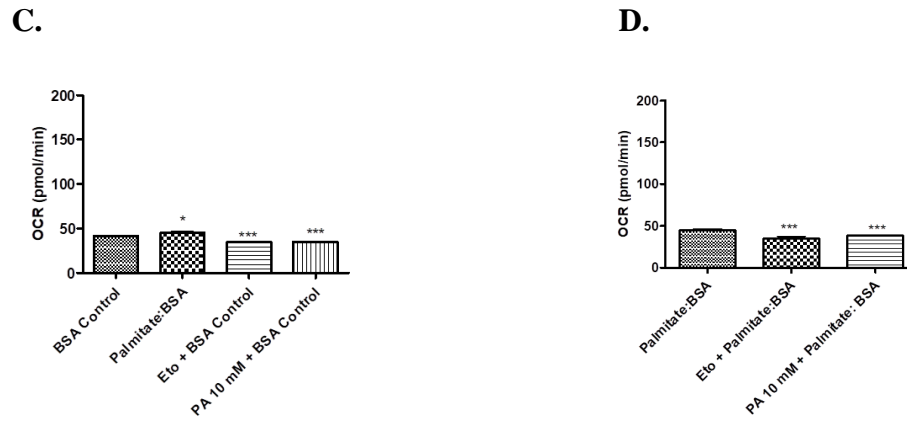


Figure 5.2: Effect of paracetamol on FAO after FCCP and rotenone/ antimycin A addition in 3T3-L1 adipocytes. Differentiated 3T3-L1 adipocytes grown in substrate-limited medium overnight and combination of XF Palmitate-BSA FAO Substrate and the XF Cell Mito Stress Test was used. Data are representative of n=3 replicates expressed as means \pm Standard deviations (* $P < 0.05$, ** $P < 0.01$, *** $P < 0.001$ from control).

5.3.2. Effect of paracetamol on individual parameters of mitochondrial function using FAO assay

In an attempt to investigate further the effect of paracetamol (10mM) on FAO, individual parameters of mitochondrial function were assessed and compared to Eto (Figure 5.3-5.4). 3T3-L1 adipocytes with Palm:BSA respired at basal rate of 12 pmol O₂/min higher than the BSA group in Figure 5.3(A). Difference in proton leak between these groups confirmed that uncoupling contributed 5 pmol O₂/min to the increased basal respiratory rate, exogenous fatty acids contributed 7 pmol O₂/min. Paracetamol significantly decreased the basal respiration of both endogenous (PA+BSA) and exogenous (PA+Palmitate:BSA) fatty acid respiration by 44% and 29% in Figure 5.3(A) respectively.

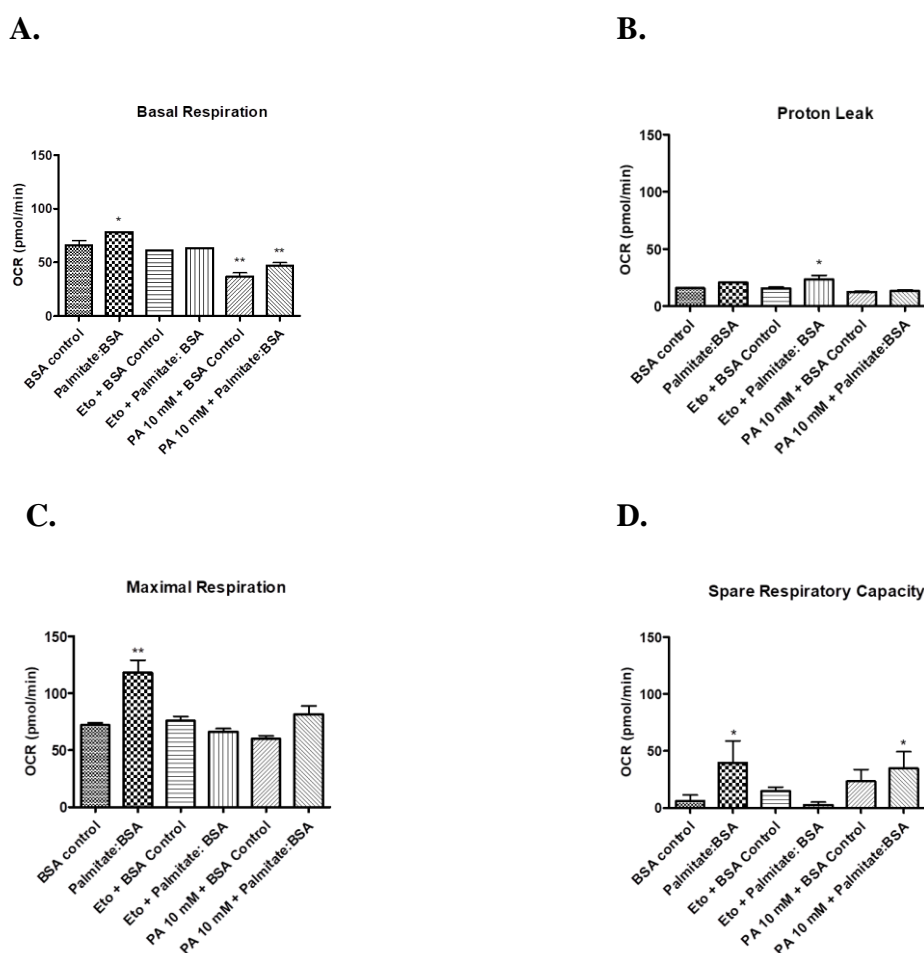


Figure 5.3: Effect of paracetamol on individual parameters of mitochondrial function using FAO assay in 3T3-L1 adipocytes. Basal respiration, proton leak, maximal respiration, spare respiratory capacity following the addition of oligomycin, FCCP, and rotenone/antimycin A respectively. Data are representative of n=3 replicates expressed as means ± Standard deviations (*P < 0.05, **P < 0.01 from control).

However paracetamol had no effect on proton leak, spare respiratory capacity or maximal respiration. Paracetamol attenuated non-mitochondrial respiration by 15% in Figure 5.4(A). Paracetamol hindered ATP production in both endogenous (PA+BSA) and exogenous (PA+Palmitate:BSA) fatty acid respiration by 51% and 33% in Figure 5.4 (B). Endogenous (PA+BSA) spare respiratory capacity was significantly increased (59%) by paracetamol in Figure 5.4(D). In the presence of paracetamol there was no change in maximal respiration in Figure 5.3(C).

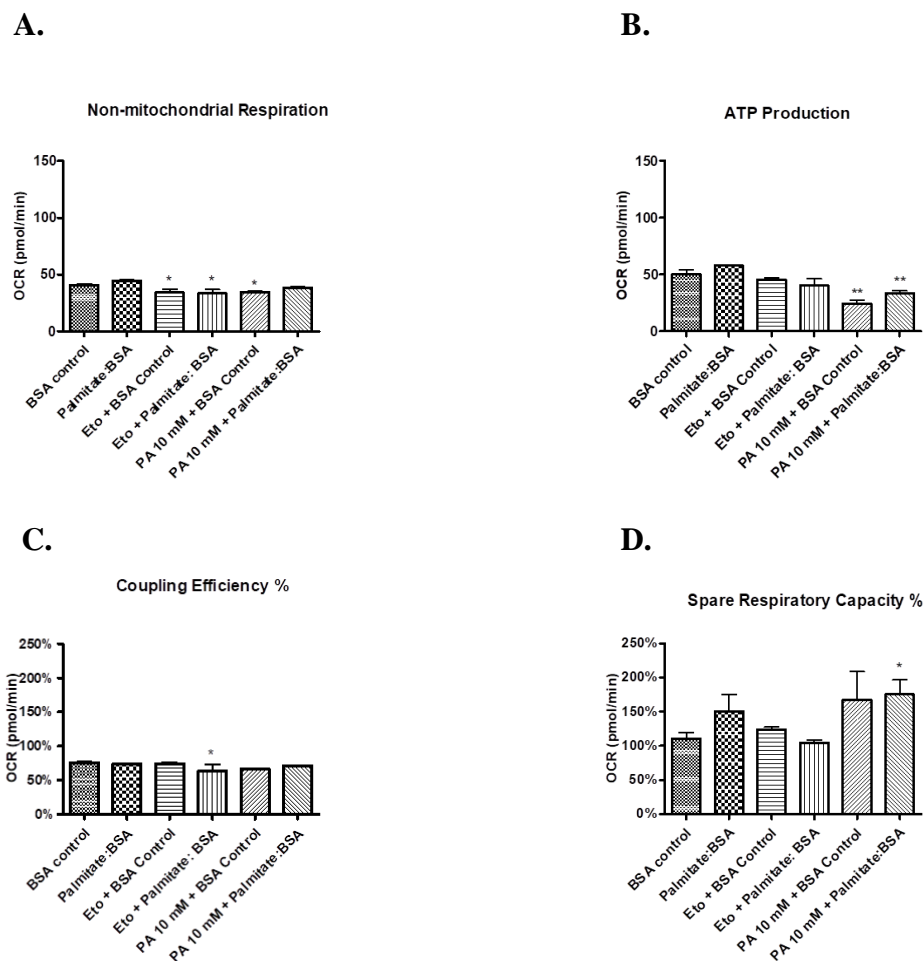


Figure 5.4: Effect of paracetamol on individual parameters of mitochondrial function using FAO assay in 3T3-L1 adipocytes. Non-mitochondrial respiration and ATP production following the addition of oligomycin, FCCP, and rotenone/antimycin A respectively. Coupling efficiency and spare respiratory capacity represented as %. Data are representative of $n=3$ replicates expressed as means \pm Standard deviations (* $P < 0.05$, ** $P < 0.01$ from control).

5.3.3. Effect of paracetamol and NAPQI on FAO:

In an attempt to determine whether paracetamol exerted some of its actions through the toxic metabolite, NAPQI, the effect of paracetamol (10 mM) and NAPQI (50 μ M; Copple et al., 2008; Jan et al., 2014) on both endogenous and exogenous FAO was investigated under basal conditions and after oligomycin addition (2.5 μ g/ml), FCCP (4 μ M) and rotenone/antimycin A (2 μ M/4 μ M) versus BSA control and Palmitate: BSA control. During basal respiration, there was a significant decrease in OCR by 63% in BSA+NAPQI group, a similar decrease was observed for the Palm:BSA+NAPQI group also showing a reduction in OCR by 63% Figure 5.5(A,B).

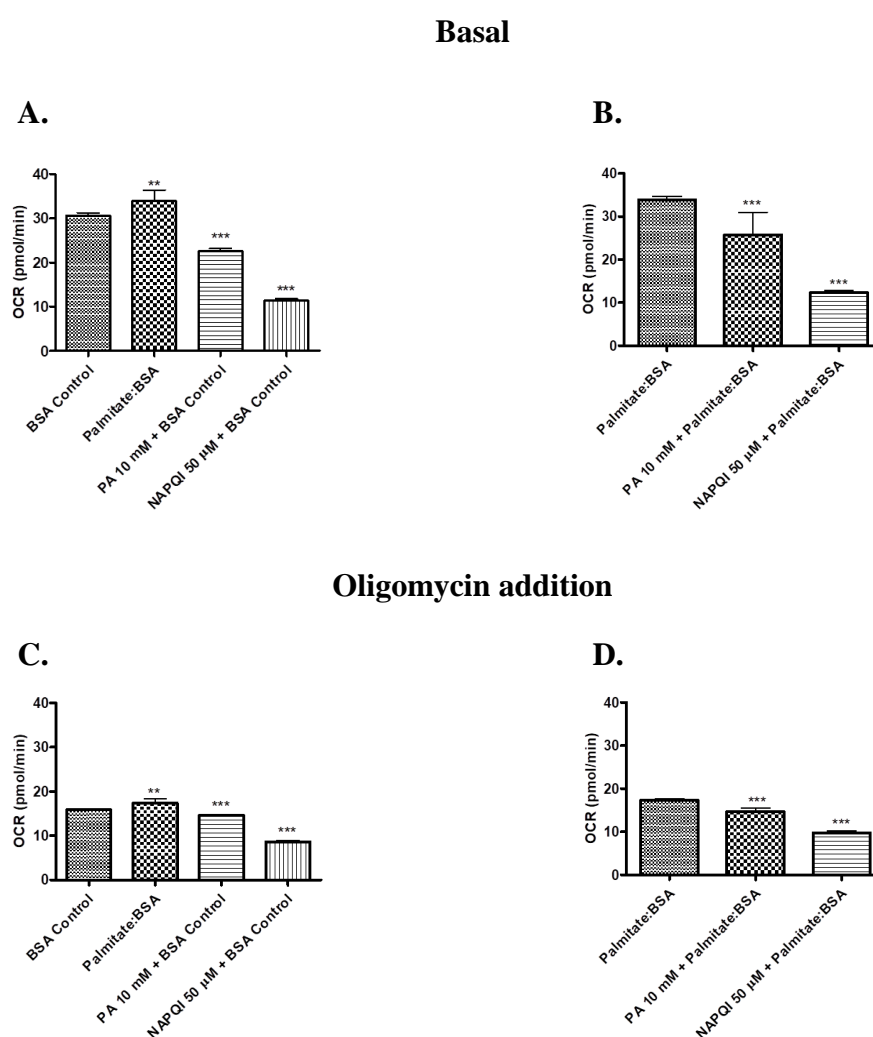
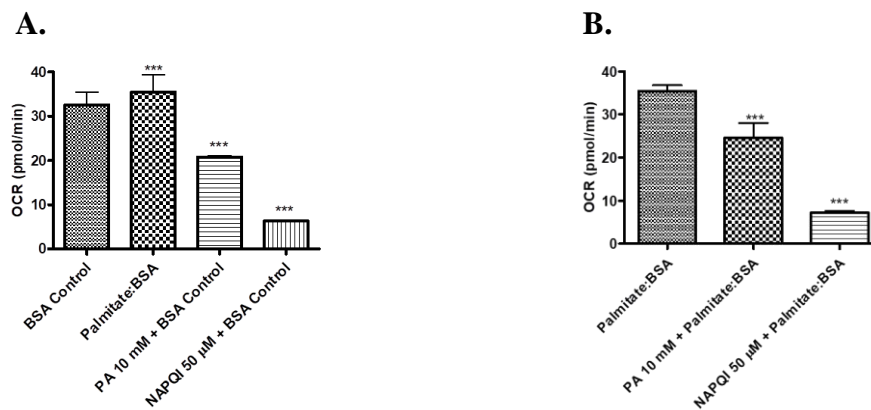


Figure 5.5: Effect of paracetamol and NAPQI on fatty acid oxidation during basal and after oligomycin addition in 3T3-L1 adipocytes. Differentiated 3T3-L1 adipocytes grown in substrate-limited medium overnight and combination of XF Palmitate-BSA FAO Substrate and the XF Cell Mito Stress Test was used. Data are representative of $n=3$ replicates expressed as means \pm Standard deviations (** $P < 0.01$, *** $P < 0.001$ from control).

After oligomycin addition, the decrease in respiration caused by paracetamol and NAPQI for endogenous (BSA+PA) and (BSA+NAPQI) was 8% and 46% respectively. A similar decrease was observed in the exogenous substrate (Palm:BSA+PA) and (Palm:BSA+NAPQI) respiration with OCR decreasing by 16% and 44% respectively Figure 5.5(C,D). Paracetamol and NAPQI did not affect cell viability at concentrations used.

FCCP addition



Rotenone/Antimycin A addition

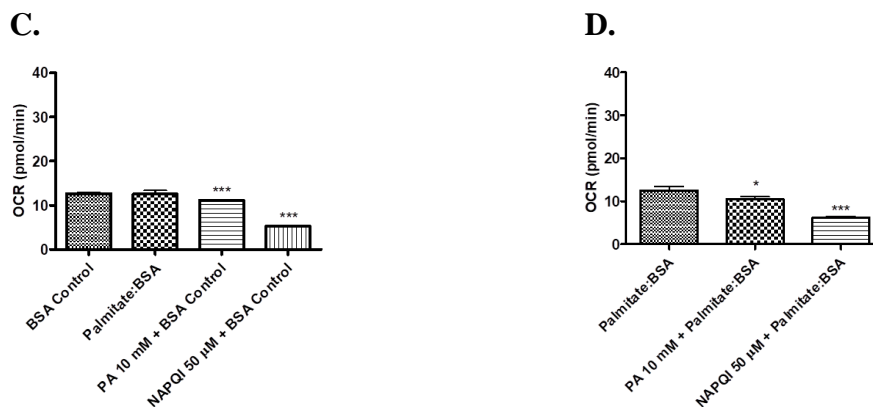


Figure 5.6: Effect of paracetamol and NAPQI on fatty acid oxidation after FCCP and rotenone/ antimycin A addition in 3T3-L1 adipocytes. Differentiated 3T3-L1 adipocytes grown in substrate-limited medium overnight and combination of XF Palmitate-BSA FAO Substrate and the XF Cell Mito Stress Test was used. Data are representative of $n=3$ replicates expressed as means \pm Standard deviations ($*P < 0.05$, $*** P < 0.001$ from control).

Introduction of FCCP resulted in a significantly increased maximal respiration in the Palm:BSA that was supported due to oxidizing exogenous fatty acids. As Palm:BSA+PA and Palm:BSA+NAPQI has shown a reduction in OCR by 31% and 80% in Figure 5.6(A,B). BSA+PA and BSA+NAPQI group attenuated OCR by 30% and 79%.

Finally, rotenone/antimycin A caused a further reduction in OCR by 12% and 58% (BSA+PA and BSA+NAPQI) and 16% and 51% (Palm:BSA+PA and Palm:BSA+NAPQI) in Figure 5.6(C,D) respectively.

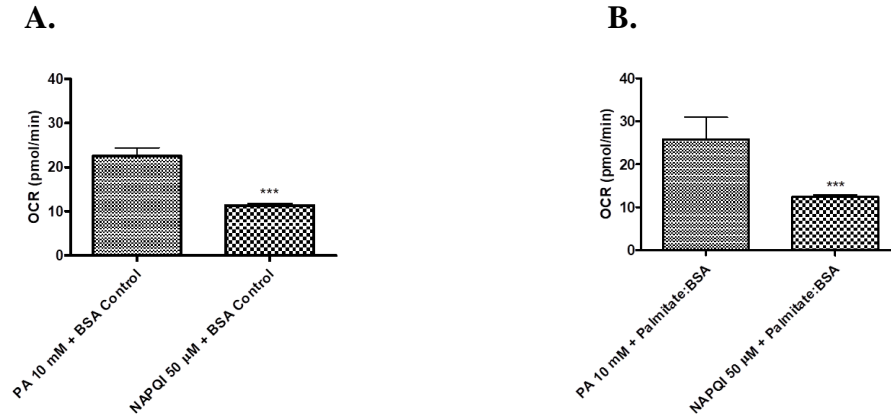
5.3.4. Comparison of the effect of paracetamol and NAPQI on FAO:

The effect of paracetamol and NAPQI on both endogenous and exogenous fatty acid oxidation was examined. At basal respiration, treatment with BSA+NAPQI reduced OCR by 50% compared to BSA+PA and by 52% in the case of Palm:BSA+NAPQI versus Palm: BSA+PA in Figure 5.7(A,B).

After oligomycin addition, the extent of inhibition of OCR was again significantly greater in BSA+NAPQI (41%) as compared to BSA+PA as well as in Palm:BSA+NAPQI (33%) versus Palm: BSA+PA in Figure 5.7(C,D). After FCCP addition, the extent of inhibition of OCR was again significantly greater in BSA+NAPQI (70%) as compared to BSA+PA and in Palm:BSA+NAPQI (71%) versus Palm: BSA+PA in Figure 5.8(A,B).

Finally, after rotenone/antimycin A addition, BSA+NAPQI declined OCR by 53% versus BSA+PA and by 41% in case of Palm:BSA+NAPQI up versus Palm: BSA+PA in Figure 5.8(C,D).

Basal



Oligomycin addition

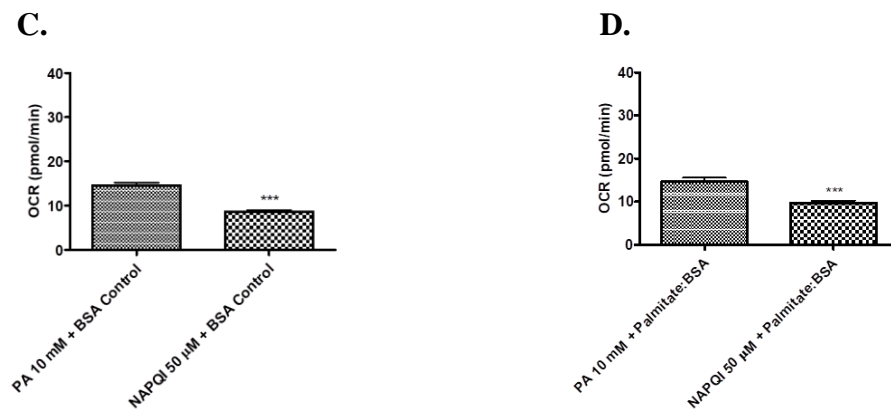
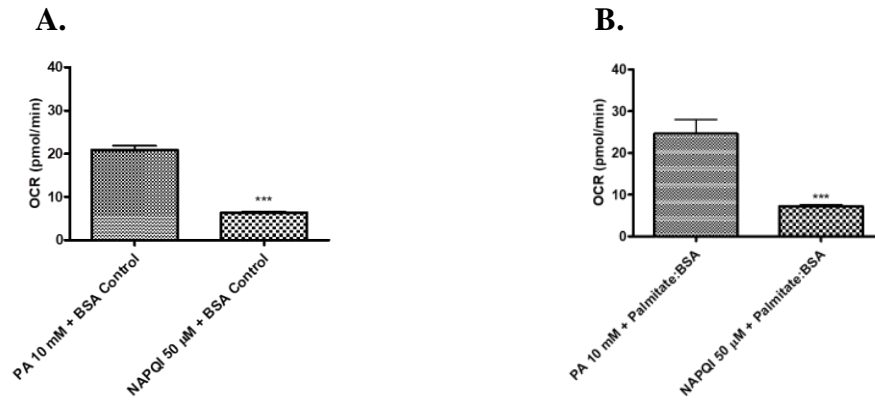


Figure 5.7: Comparison of the effect of paracetamol and NAPQI on fatty acid oxidation during basal and after oligomycin addition in 3T3-L1 adipocytes. Differentiated 3T3-L1 adipocytes grown in substrate-limited medium overnight and combination of XF Palmitate-BSA FAO Substrate and the XF Cell Mito Stress Test was used. Data are representative of $n=3$ replicates expressed as means \pm Standard deviations (***) $P < 0.001$ from control).

FCCP addition



Rotenone/Antimycin A addition

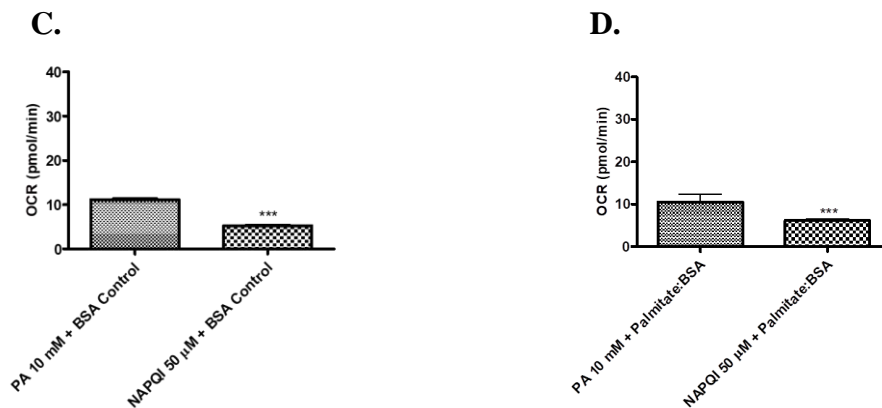


Figure 5.8: Comparison of the effect of paracetamol and NAPQI on fatty acid oxidation after FCCP and rotenone/ antimycin A addition in 3T3-L1 adipocytes. Differentiated 3T3-L1 adipocytes grown in substrate-limited medium overnight and combination of XF Palmitate-BSA FAO Substrate and the XF Cell Mito Stress Test was used. Data are representative of $n=3$ replicates expressed as means \pm Standard deviations (***) $P < 0.001$ from control).

5.3.5. Effect of paracetamol and NAPQI on individual parameters of mitochondrial function using FAO assay:

In an attempt to investigate further the effect of paracetamol and NAPQI on fatty acid oxidation, individual parameters of mitochondrial function were assessed as seen in Figure 5.9 and 5.10. NAPQI at much lower concentrations is a more potent inhibitor of basal respiration than paracetamol. NAPQI+BSA and NAPQI+Palmitate:BSA seemed to have a huge impact on basal respiration declined by 64% and 65% whereas PA+BSA also decreased basal OCR by 14% Figure 5.9(A). There was no effect on proton leak by PA and NAPQI in Figure 5.9(B). Maximum respiratory rates were greatly attenuated by NAPQI+BSA and NAPQI+Palmitate:BSA (93% and 94%) while PA+BSA caused a 43% decrease in Figure 5.9(C). NAPQI completely inhibited spare respiratory capacity in Figure 5.9(D) and reduced non-mitochondrial respiration by 60% (NAPQI+BSA) and 48% (NAPQI+Palmitate:BSA) in Figure 5.10(A). PA+BSA, PA+Palmitate:BSA, NAPQI+BSA and NAPQI+Palmitate:BSA abolished ATP production by 52%, 26%, 78% and 77% in Figure 5.10(B). PA+BSA decreased coupling efficiency by 19% whereas NAPQI+BSA and NAPQI+Palmitate:BSA by 39% and 34% in Figure 5.10(C). Finally, spare respiratory capacity represented in Figure 5.10(D) was significantly reduced by NAPQI+BSA and NAPQI+Palmitate:BSA by 81% and 84%.

Basal respiration of 3T3-L1 adipocytes with BSA is 6 pmol O₂/min more versus BSA+PA group and 10 pmol O₂/min more versus BSA+NAPQI indicating that a small segment of the basal respiratory rate was a result to fatty acids oxidized from endogenous source and/or remaining fatty acids in the BSA preparation. The Palm:BSA+PA and Palm:BSA+NAPQI groups confirmed the significant increase in maximum respiration in the Palm:BSA as a result of oxidation of exogenous fatty acids. Maximum respiration of these cells with BSA is 7 pmol O₂/min more versus BSA+PA group and 15 pmol O₂/min more versus BSA+NAPQI group demonstrating that a segment of maximum respiration was supported due to endogenous oxidation of fatty acids and/or presence of remaining fatty acids in the BSA preparation.

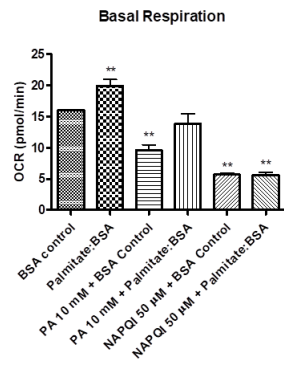
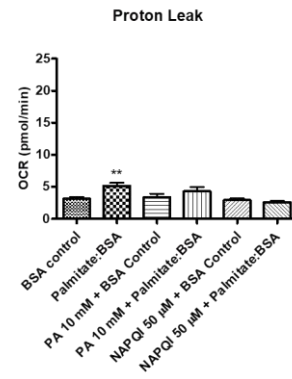
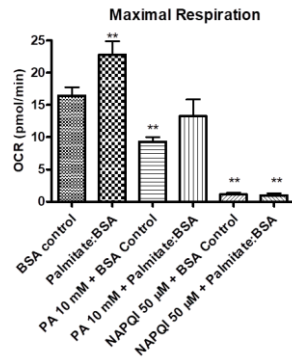
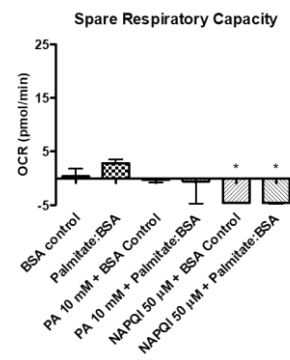
A.**B.****C.****D.**

Figure 5.9: Effect of paracetamol and NAPQI on individual parameters of mitochondrial function using FAO assay in 3T3-L1 adipocytes. Basal respiration, proton leak, maximal respiration and spare respiratory capacity following the addition of oligomycin, FCCP, and rotenone/antimycin A respectively. Data are representative of $n=3$ replicates expressed as means \pm Standard deviations (* $P < 0.05$, ** $P < 0.01$ from control).

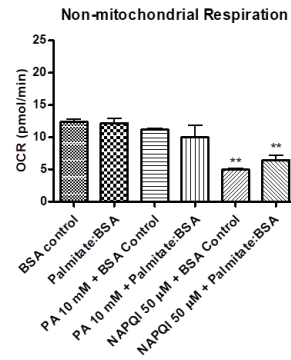
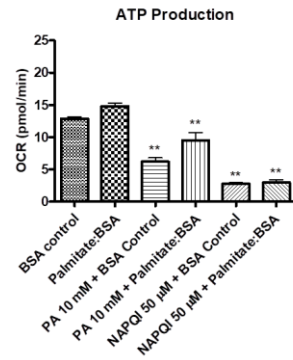
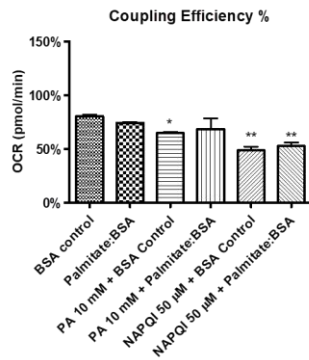
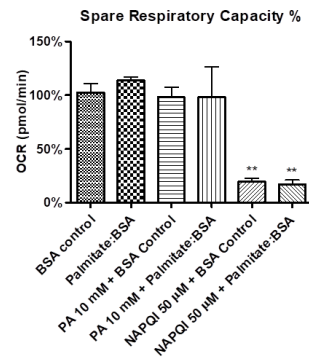
A.**B.****C.****D.**

Figure 5.10: Effect of paracetamol and NAPQI on individual parameters of mitochondrial function using FAO assay in 3T3-L1 adipocytes. Non-mitochondrial respiration and ATP production following the addition of oligomycin, FCCP, and rotenone/antimycin A respectively. Coupling efficiency and spare respiratory capacity represented as %. Data are representative of $n=3$ replicates expressed as means \pm Standard deviations (* $P < 0.05$, ** $P < 0.01$ from control).

5.4. Discussion

Increased lipolysis and the utilization of the released fatty acids is the main source of substrates for thermogenesis in small mammals at temperatures below their thermoneutral zone. The movement of long chain fatty acids inside mitochondria through CPT1 on the outer membrane is the main controlling step for FAO. Blocking the transport of fatty acids into the mitochondria should result in a decrease in the OCR provided there is no compensatory increase in non-fatty acid substrates. The classical fatty acid transport inhibitor is Eto, which binds irreversibly to the CPT1 transporter preventing fatty acid uptake in the mitochondria and ultimately hinders the oxidation process (Pike et al., 2011).

In terms of the potential impact of paracetamol on the capacity of cells to utilize fatty acids liberated following lipolysis to support thermogenesis, OCR was assessed under different conditions and with paracetamol and different mitochondrial stress compounds (Figure 5.1-5.2). The results confirm that paracetamol was effective at inhibiting OCR in the presence and absence of palmitate suggesting the compound is capable of attenuating of both exogenous FAO and OCR driven by other substrates, including endogenous fatty acids. This conclusion was confirmed by the lack of inhibition of FAO in cells treated with Eto in the absence of palmitate. The greater inhibition of OCR in the presence of paracetamol compared to Eto suggest paracetamol may also be directly inhibiting FAO not just uptake. The observation also confirm that paracetamol is affecting other mitochondrial processes such as delivering substrates to complex I/II or the ETC directly. The decrease in OCR in the presence of paracetamol may also indicate the compound does not uncouple the mitochondria.

To further probe the impact of paracetamol on exogenous FAO and the impact on other key mitochondrial parameters, other stress molecules were employed (Figure 5.3-5.4). The use of oligomycin allowed the determination of proton leak. The results confirmed that paracetamol had little effect on proton leak; further confirmed the lack of uncoupling by paracetamol. The use of oligomycin confirms paracetamol had a far greater inhibitory effect on ATP production compared to Eto. The reduction of basal ATP production by 50% confirming a significant direct impact on the mitochondrial ETC. Although paracetamol was able to attenuate exogenous FAO, it was less effective than Eto as measured by the inhibition of maximal capacity. Paradoxically in the presence of the uncoupling agent FCCP, paracetamol appears to not as effective at inhibiting OCR

possibly due to the fact that uncoupling by FCCP may reduce the impact of paracetamol on other aspects of the ETC.

Paracetamol induced toxicity is mediated by initial step of metabolising via cytochrome P450 system to highly reactive metabolite NAPQI. At low doses of paracetamol, any NAPQI produced is efficiently detoxified by GSH but at high paracetamol concentrations the NAPQI produced depletes the GSH (Mitchell et al., 1973a, 1973b) and this results in covalent binding to cellular proteins to form 3-(cystein-S-yl)-paracetamol adducts (Cohen et al., 1997) and oxygen/nitrogen stress occurs (Reid et al., 2005; Burke et al., 2010). NAPQI may also covalently bind to mitochondrial proteins (Jeaschke and Bajt, 2006). In addition to the reduced or loss of mitochondrial function, cellular toxicity is considered to result from mitochondrial dysfunction (Burke et al., 2010). In cellular models, NAPQI (400 μ M) caused both GSH reduction and GSH conjugation of the quinone imine, leading to depletion of the mitochondrial ATP content (> 80% depletion after 1 minute exposure). NAPQI is much more potent than the parent drug, inhibiting ADP-stimulated respiration of liver mitochondria (Ramsay et al., 1989).

Given the high levels of paracetamol in studies where hypothermia is observed, it is likely that some NAPQI would be generated in the mitochondria of animals given paracetamol specially at doses above 100 mg/kg. In this study the concentration of NAPQI selected appeared to have no impact on cell viability. However at micromolar concentrations, NAPQI had a significant impact on OCR and FAO a clear indication that once generated NAPQI could attenuate heat generation (Figure 5.5-5.6). NAPQI proved to be a far more potent inhibitor of OCR than paracetamol at significantly lower concentrations suggesting a broad spectrum of targets on the membrane and within the mitochondria (Figure 5.7-5.8). If replicated *in vivo* this would suggest that once cellular protective mechanisms were overwhelmed which is likely at concentrations reported to cause hypothermia only a small amount of NAPQI would be needed to inhibit cellular respiration leading to hypothermia.

These results also confirm that even at non toxicity concentrations NAPQI will cause mitochondrial dysfunction including inhibition of FAO. Unlike the parent compound NAPQI appeared to partly uncouple mitochondria; however this was complicated by the fact that NAPQI was such a potent inhibitor of the mitochondrial processes. Interestingly there was no evidence of increased proton leak suggesting no uncoupling making data interpretation difficult. As with paracetamol the impact of NAPQI on other

key mitochondrial parameters was also investigated using stress molecules (Figure 5.9-5.10). Because NAPQI had such a devastating effect on all the OCR it is difficult to evaluate the impact on any of the parameters except to say even small amounts of NAPQI could be devastating for mitochondrial energy generation. The impact of NAPQI far exceeded that of paracetamol. The inhibition of fatty acid uptake and oxidation by either paracetamol or NAPQI may explain the accumulation of long chain acylcarnitines and FFAs in the serum of paracetamol treated WT mice (Chen et al., 2009).

The direct inhibition of both exogenous and endogenous fatty acid uptake and oxidation by paracetamol and the metabolite NAPQI has never been reported in adipocytes. These novel observations add to the possible target of paracetamol and related compound which cause hypothermia and antipyresis. The observation also provides an alternative explanation as to why despite their weak inhibition of COX enzymes these compounds are such potent antipyretic.

Having established that paracetamol and NAPQI both reduce the ability of cells to take up and utilise fatty acids as substrates for energy production the final step is to assess the direct impact of these compound on mitochondrial ETC.

Chapter 6: Effect of Paracetamol, Aminopyrine and Antipyrine on cellular and mitochondrial oxygen consumption

6.1. Introduction

The release of catecholamines (norepinephrine) is a key peripheral response of small mammals to cold stress. The release of norepinephrine is known to stimulate not only lipolysis in adipocytes but also leads to the release and oxidation of fatty acids and other reducing cofactors which drive mitochondrial metabolism and heat generation. Mitochondria are essential in the process of heat production where reduced cofactors such as NADH, succinate, and fatty acids are converted in the mitochondria directly to heat (uncoupling), or indirectly through the production of ATP. Regardless of the mechanism, heat generation is always closely linked to the OCR and can be measured as an index of the efficiency of mitochondrial and cellular respiration. Compounds which can be shown to disrupt or inhibit mitochondrial function are therefore potential hypothermic agents.

The disruption of mitochondrial function can occur at different stages, from attenuating substrate supply to the mitochondria to direct inhibition of any of the five complexes in the ETC. Several mechanisms could be involved in drug-induced OXPHOS impairment (Begrache et al., 2011). Alternatively uncoupling agents may compromise mitochondrial membrane integrity. Where substrate oxidation is maintained, ATP synthesis can be hindered leading to direct heat production from the uncoupled mitochondria, provided there is a constant supply of reduced substrates and ATP. It has been shown that some NASIDs can affect mitochondrial function. Drugs such as nimesulide (Berson et al., 2006, 1996), salicylic acid and ibuprofen possess a mild uncoupling effect (Fromenty et al., 1995; Tokumitsu et al., 1977). Compounds such as diclofenac cause OXPHOS uncoupling which is associated with more harmful impact on MPTP opening leading to cell injury (Lim et al., 2006). OXPHOS uncoupling can also occur through blocking of the ETC activity leading to the loss of substrate oxidation such as observed with salicylic acid (Deschamps et al., 1994; Doi and Horie, 2010). There is also a long list of classical inhibitors of the different complexes of the ETC without any prior OXPHOS uncoupling (Begrache et al., 2011). The classical inhibitors can be used to investigate where disruption is taking place (Begrache et al., 2011). Using specific complex inhibitors such as rotenone and amytal which block transfer of electrons at Complex I,

Malonate which blocks Complex II, Antimycin A interferes with electron flow from Complex III and cyanide (CN⁻) which blocks complex IV. There are also specific inhibitors such as atractyloside for the ATP-ADP translocase (complex V).

When assessing how potential hypothermic agents affect mitochondrial function, the OCR of cells and isolated mitochondria can be assessed using the Agilent Seahorse XF Cell Mito Stress Test.

In an attempt to establish if the hypothermia caused by compounds such as paracetamol, antipyrine and aminopyrine in rodents could be linked to impairment of mitochondria function in cells associated with heat generation, studies were undertaken with adipocytes and isolated mitochondria. Adipocytes play a key role in rodent thermoregulation, both in direct thermogenesis and the supply of free fatty acids for mitochondrial oxidation. Differentiated 3T3-L1 adipocytes stimulated with catecholamines are an ideal model to study the impact of paracetamol and other compounds on OCR and ultimately hypothermia. Similarly isolated mitochondria are an ideal model to directly determinate the potential mitochondrial site of action of compound which impact on mitochondrial bioenergetics and heat production (Rogers et al., 2011). Electron flow assays allow the sequential electron flow through different ETC complexes to be examined in an attempt to identify the specific site of action of the test compounds on mitochondrial function.

6.2. Methods

6.2.1. Mitochondrial bioenergetic profile of 3T3-L1 adipocytes was determined using Agilent Seahorse XF Mito Stress Test as described in sections 2.4.15 and 2.4.16.2.

6.2.2. The effect of paracetamol and other antipyretic agents on basal and catecholamine stimulated OCR was determined as described in section 2.4.15 and 2.4.16.3-2.4.16.4.

6.2.3. The effect of classical mitochondrial ETC inhibitors, paracetamol and other antipyretic agents on isolated rat liver mitochondrial OCR was determined using the Agilent Seahorse Electron Flow Assay as described in section 2.4.16.5. The results were analysed with analysis of variance (ANOVA), followed by Dunnett's Multiple Comparison Test. A *P < 0.05, ** P<0.01, from control was considered statistically significant.

6.3. Results:

6.3.1. Mitochondrial bioenergetic profile of 3T3-L1 adipocytes:

To determine how classical inhibitors affect mitochondrial function, 3T3-L1 pre-adipocytes were differentiated in Agilent Seahorse XFp plates and OCR was measured under basal conditions. Following the addition of oligomycin, FCCP, and rotenone/antimycin A, significant changes in OCR were observed.

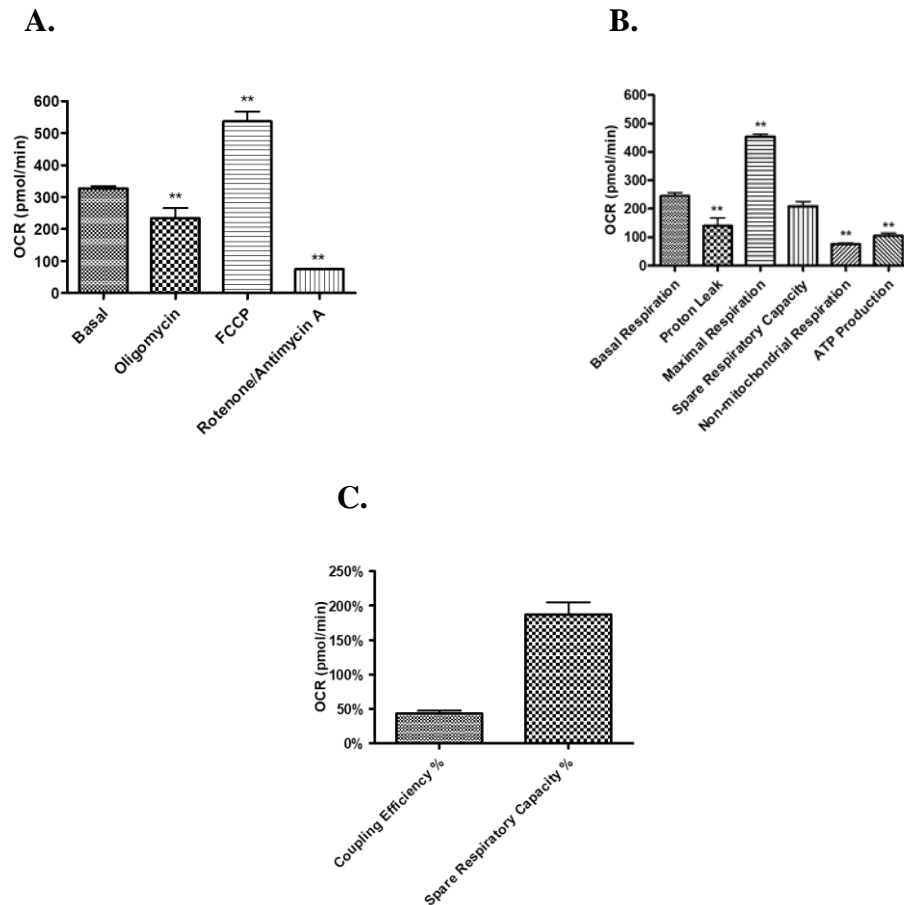


Figure 6.1: Bioenergetic profile of 3T3-L1 adipocytes. *A. Measurement of OCR following the addition of oligomycin (5 μ M), FCCP (5 μ M), and rotenone/antimycin A (2.5 μ M) respectively. B. Measurement of individual parameters of mitochondrial function C. Coupling efficiency and spare respiratory capacity represented as %. Data are representative of $n=3$ replicates expressed as means \pm Standard deviations (** $P<0.01$ from control).*

Oligomycin lowered OCR by 29% whereas FCCP resulted in a marked increase (64%) followed by a 77% reduction in OCR upon rotenone/antimycin A addition in Figure 6.1(A).

When the individual parameters of mitochondrial function were measured as a function of basal respiration rate, the result revealed that OCR was decreased by 43% in proton (H⁺) leak, by 69% in non-mitochondrial respiration and by 57% in ATP production, maximum respiration (86%) in Figure 6.1(B). Coupling efficiency (43%) and spare respiratory capacity (187%) represented in Figure 6.1(C).

6.3.2. Effect of paracetamol on basal OCR:

In an attempt to examine whether paracetamol affect basal respiration, 3T3-L1 pre-adipocytes were differentiated in Agilent Seahorse XFp plates and basal OCR was measured. Paracetamol at both 5 and 10 mM attenuated OCR by 32% and 35% when cells were at basal respiration (Figure 6.2).

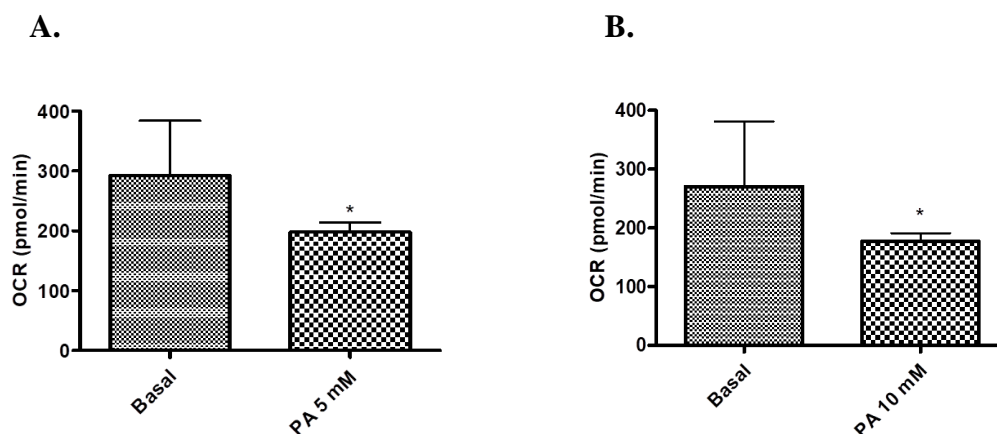
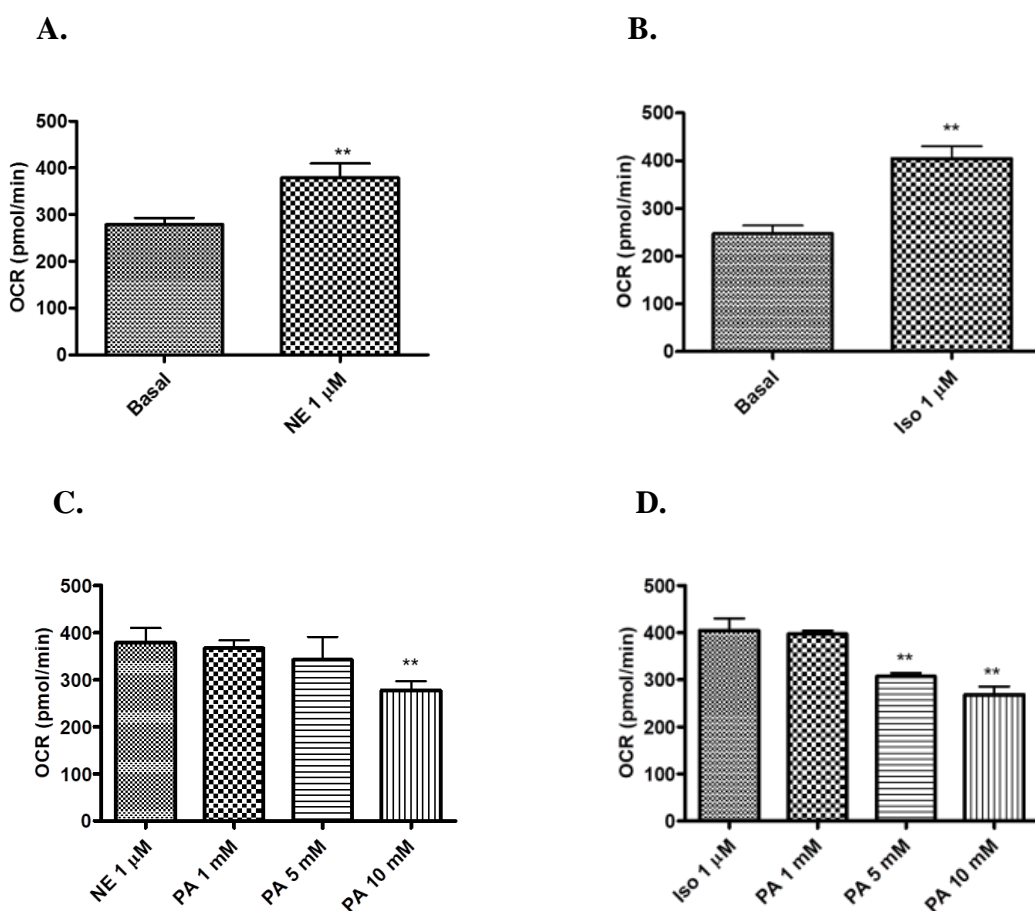


Figure 6.2: Effect of paracetamol on basal OCR in 3T3-L1 adipocytes. Measurement of basal OCR followed by addition of different concentrations of paracetamol. Data are representative of $n=3$ replicates expressed as means \pm Standard deviations (* $P < 0.05$ from control).

6.3.3. Effect of paracetamol on norepinephrine and isoproterenol stimulated OCR:

3T3-L1 adipocytes were assessed for their ability to respond to an acute exposure of the catecholamine. OCR was significantly increased in response to norepinephrine (53%) or isoproterenol (64%) exposure when compared with untreated cells in Figure 6.3(A,B). Paracetamol (10 mM) significantly attenuated catecholamine induced increase in OCR by 27% in case of norepinephrine and 34% for isoproterenol at higher concentrations of the drug in Figure 6.3(C,D).



*Figure 6.3: Effect of paracetamol on norepinephrine and isoproterenol stimulated OCR in 3T3-L1 adipocytes. A, B. Measurement of basal OCR followed by addition of norepinephrine or isoproterenol. C, D. Measurement of stimulated OCR (norepinephrine or isoproterenol) followed by addition of cumulative addition of paracetamol. Data are representative of n=3 replicates expressed as means \pm Standard deviations (** P<0.01 from control).*

6.3.4. Effect of paracetamol, aminopyrine and antipyrene on basal OCR:

In an alternative model, 3T3-L1 cells were differentiated in 24-well plates and then seeded in Agilent Seahorse XFp plates. After basal OCR measurements, all three compounds; paracetamol, aminopyrine and antipyrene were tested. In case of paracetamol at 1 mM, 5 mM, 10 mM and 20 mM, OCR was significantly lowered by 12%, 42%, 61% and 73% respectively in Figure 6.4(A). Similarly, aminopyrine both at 5 mM and 10 mM attenuated OCR by 13% and 27% respectively Figure 6.4(B). Finally, antipyrene treated cells at 1 mM, 5 mM and 10 mM showed a marked decrease in OCR of 9%, 24% and 36% respectively Figure 6.4(C).

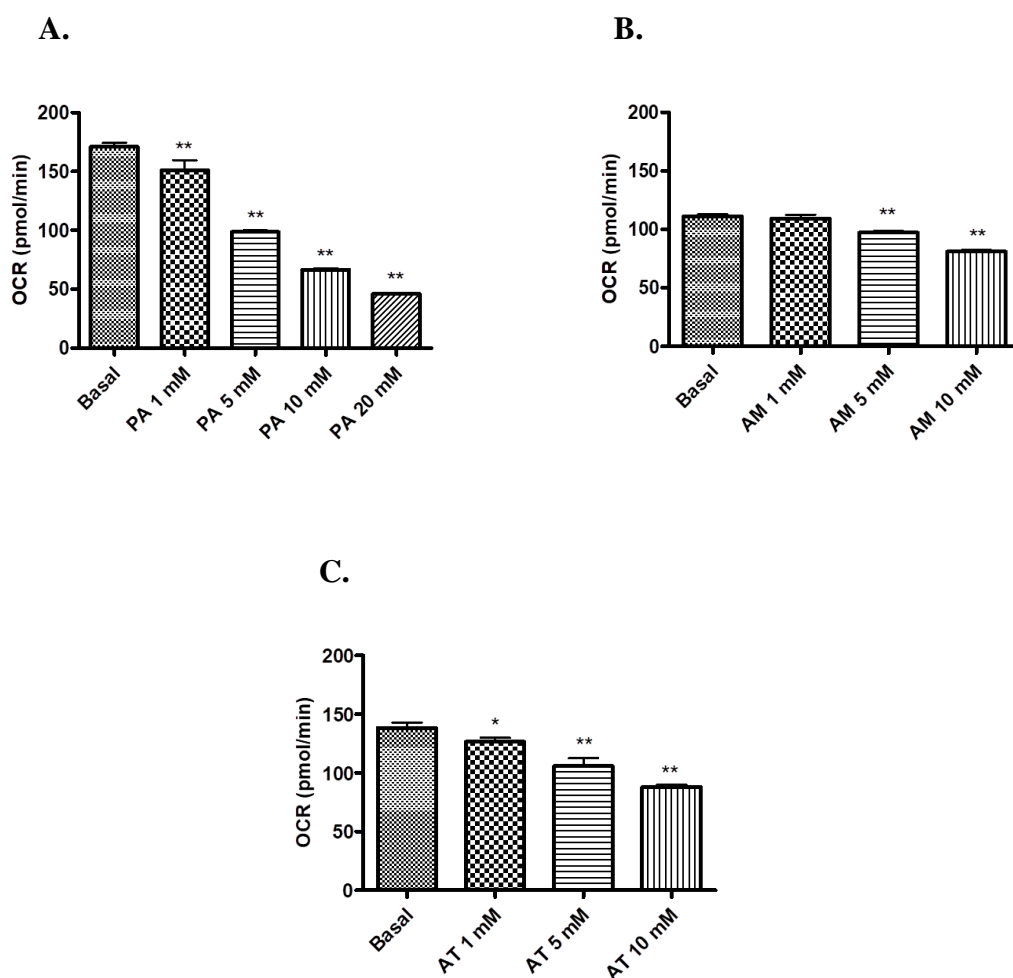


Figure 6.4: Effect of paracetamol, aminopyrine and antipyrene on basal OCR in 3T3-L1 adipocytes. Measurement of basal OCR followed by cumulative addition of paracetamol (A) or aminopyrine (B) or antipyrene (C). Data are representative of $n=3$ replicates expressed as means \pm Standard deviations (* $P < 0.05$, ** $P < 0.01$ from control).

6.3.5. Effect of paracetamol, aminopyrine and antipyrine on isoproterenol stimulated OCR:

When cells were treated with isoproterenol (0.01-10 μ M), there was no increase in OCR most probably due to trypsin treatment of these cells in Figure 6.5(A). Paracetamol reduced the OCR of 3T3-L1 cells by 39% and 54% at 5 mM and 10 mM respectively, addition of isoproterenol failed to reverse the OCR level to basal levels in Figure 6.5 (B,C).

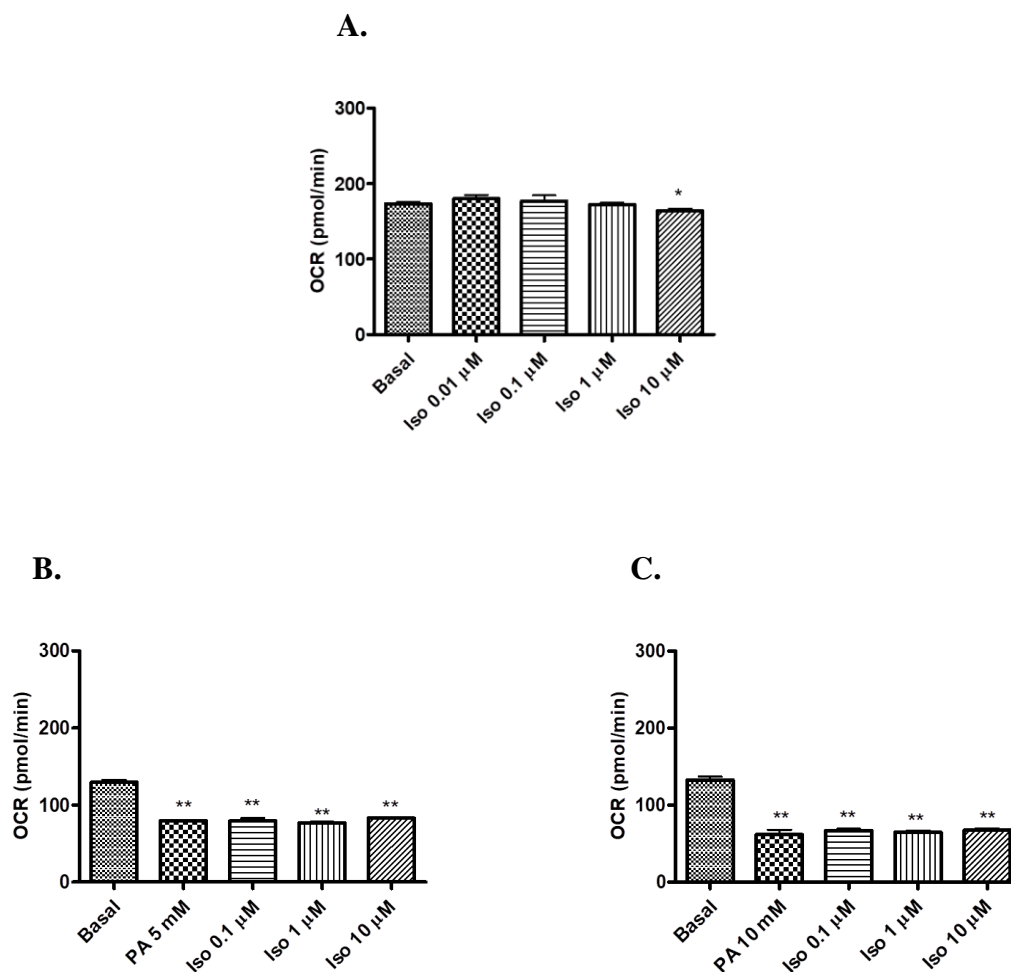


Figure 6.5: Effect of paracetamol on isoproterenol stimulated OCR in 3T3-L1 adipocytes. Measurement of basal OCR followed by addition of different concentrations of isoproterenol (A). Measurement of basal OCR, followed by cumulative addition of paracetamol and then isoproterenol added (B,C). Data are representative of $n=3$ replicates expressed as means \pm Standard deviations (* $P < 0.05$, ** $P < 0.01$ from control).

Aminopyrine at 5 mM and 10 mM also reduced basal OCR levels by 28% and 51% respectively Figure 6.6(A,B). After isoproterenol addition, the OCR decreased to 25%, 28% and 30% at 5 mM and 40%, 41% and 41% at 10 mM Figure 6.6(A,B). In case of antipyrene at 5 mM and 10 mM, basal OCR was reduced by 18% and 42% respectively. Upon isoproterenol (0.1, 1 and 10 μ M) addition OCR further decreased to 27%, 34% and 38% at 5 mM and 36%, 38% and 40% at 10 mM of antipyrene respectively Figure 6.6(C,D).

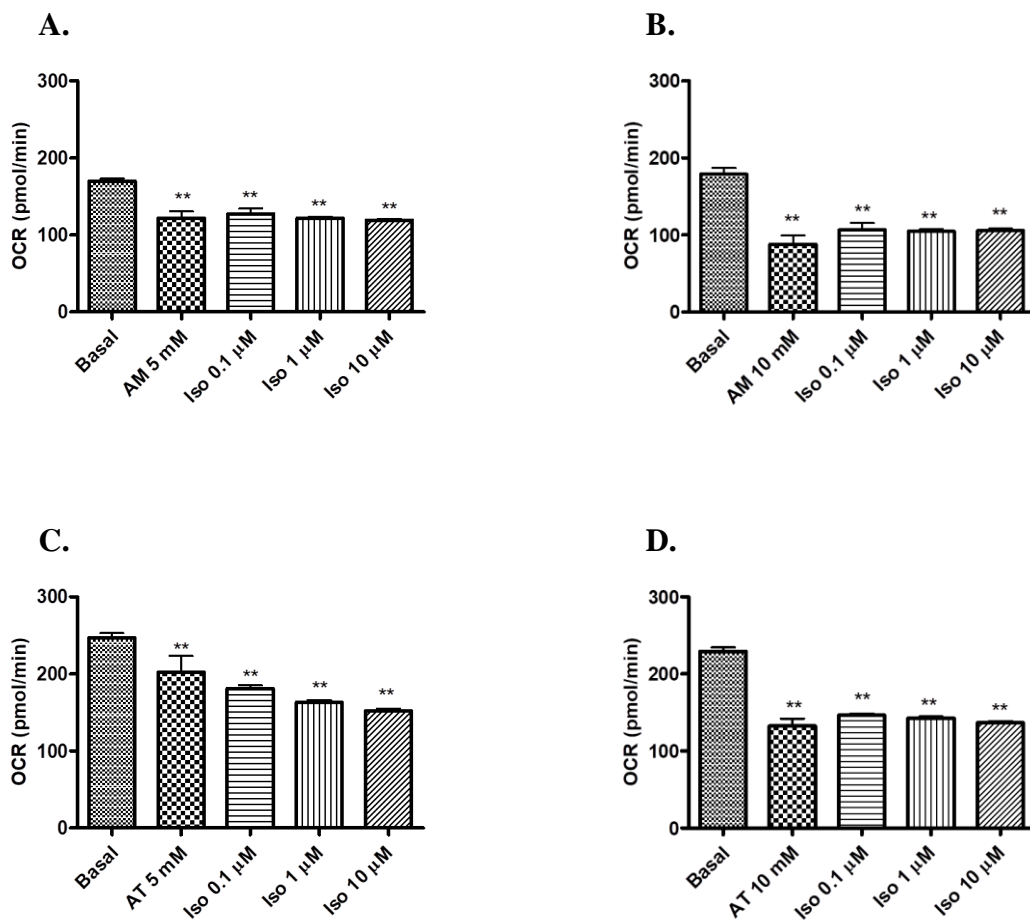


Figure 6.6: Effect of aminopyrine and antipyrene on isoproterenol stimulated OCR in 3T3-L1 adipocytes. Measurement of basal OCR, followed by cumulative addition of aminopyrine (A, B) or antipyrene (C,D) and then isoproterenol added. Data are representative of $n=3$ replicates expressed as means \pm Standard deviations (** $P<0.01$ from control).

6.3.6. Elucidation of mechanistic activity of inhibitors that affect mitochondrial function:

In an attempt to obtain a more direct estimation of the potential target of inhibitors, OCR was assessed with isolated mitochondria (Rogers et al., 2011). Studies were conducted with 5 μg isolated rat liver mitochondria/well. There was a 98% reduction in pyruvate and malate-dependent respiration by rotenone (2 μM), a complex I inhibitor. Addition of succinate as a complex II substrate resulted an increase (136%) in OCR whereas antimycin A that inhibits complex III, prevented complex I- and III-mediated respiration by 89% as complex III was inhibited, causing loss of function throughout until ascorbate and TMPD was added that caused a marked increase in OCR (96%), confirming that complex IV remained active in Figure 6.7(A).

When mitochondria were initially pre-incubated with rotenone (2 μM), pyruvate and malate-dependent respiration reduced by 58% in Figure 6.7(B) as compared to control in which robust respiration was present in Figure 6.7(A). Addition of rotenone resulted in a further 24% decrease followed by an increase in complex II-driven respiration (253%). However the increase was significantly (50%) less than the complex II-driven in the absence of rotenone. Antimycin A caused a 58% decrease in both complex I-and II mediated OCR whereas ascorbate and TMPD-driven IV respiration increased (110%) in Figure 6.7(B). Further injections resulted in normal responses confirming that the rest of the ETC is functioning properly.

When mitochondria were preincubated with malonate (10 mM) which competitively inhibit succinate dehydrogenase, the respiratory rates of complex II and III is inhibited by 85% and 68% without affecting complex I- and IV-driven respiration in Figure 6.7(C).

However, antimycin A (4 μM) that inhibits complex III, prevented complex I- and II-supported respiration due to its inhibitory impact on complex III (-58%), resulting in loss of function throughout the assay (decreased complex I; 42% and complex II; 31%) until ascorbate and TMPD was added, as complex IV still active (254%) in Figure 6.7(D).

Inhibition of complex IV by sodium azide (20 mM) resulted in reduced respiration throughout the assay and ascorbate and TMPD could not increase flow of electrons at complex IV (data not shown). Finally, oligomycin (2.5 $\mu\text{g/ml}$), inhibits complex V

prevented only ATP formation; however it had no effect on the ADP-stimulated rate, only 53% decrease in complex-IV mediated OCR in Figure 6.7(E).

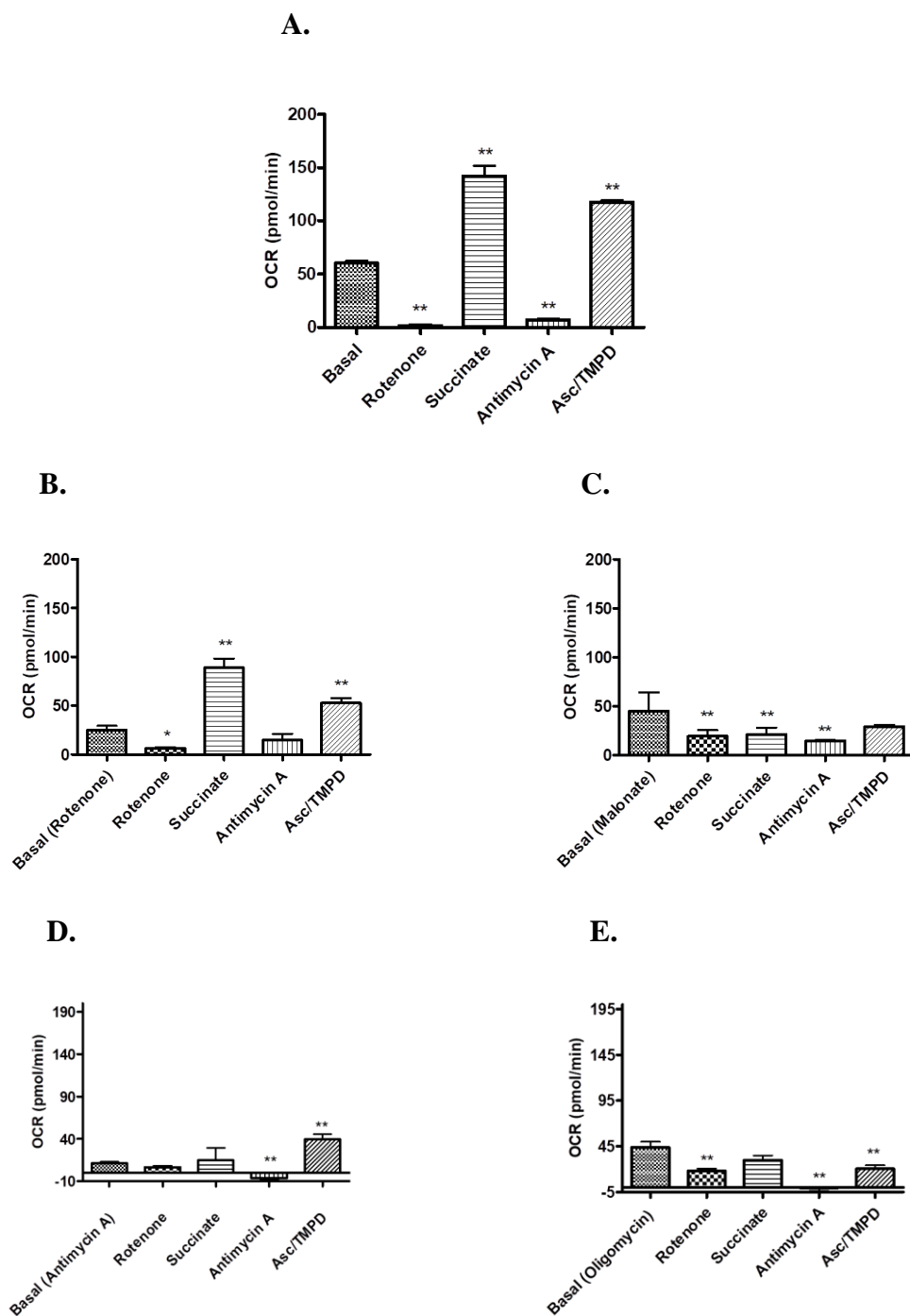


Figure 6.7: Elucidation of mechanistic activity of inhibitors that affect mitochondrial function (5 μ g mitochondria). Electron flow experiments were performed as described in Methods. Initial conditions are as follows: **A.** Control (no additives), **B.** 2 μ M rotenone, **C.** 10 mM malonate, **D.** 4 μ M antimycin-A and **E.** 2.5 μ g/mL oligomycin. Data are representative of $n=3$ replicates expressed as means \pm Standard deviations. (* $P < 0.05$, ** $P < 0.01$ from control).

6.3.7. Elucidation of the mitochondrial target of hypothermic agents

Preincubating mitochondria with paracetamol (1-10 mM) had little effect on basal OCR. A further addition of 5-20 mM resulted in a concentration dependent decrease in basal respiration with OCR falling by 66% at 20 mM Figure 6.8(A-C). The addition of the complex II substrate succinate only cause a significant (30%) increase in OCR at 5 mM compared to a more than 100% in the absence of paracetamol Figure 6.8(A-C). At 10 and 20 mM, there was no increase in OCR in the presence of succinate Figure 6.8(A-C). At very high concentrations (30 mM) of paracetamol there was an inhibition (30%) of complex IV driven OCR Figure 6.8(C).

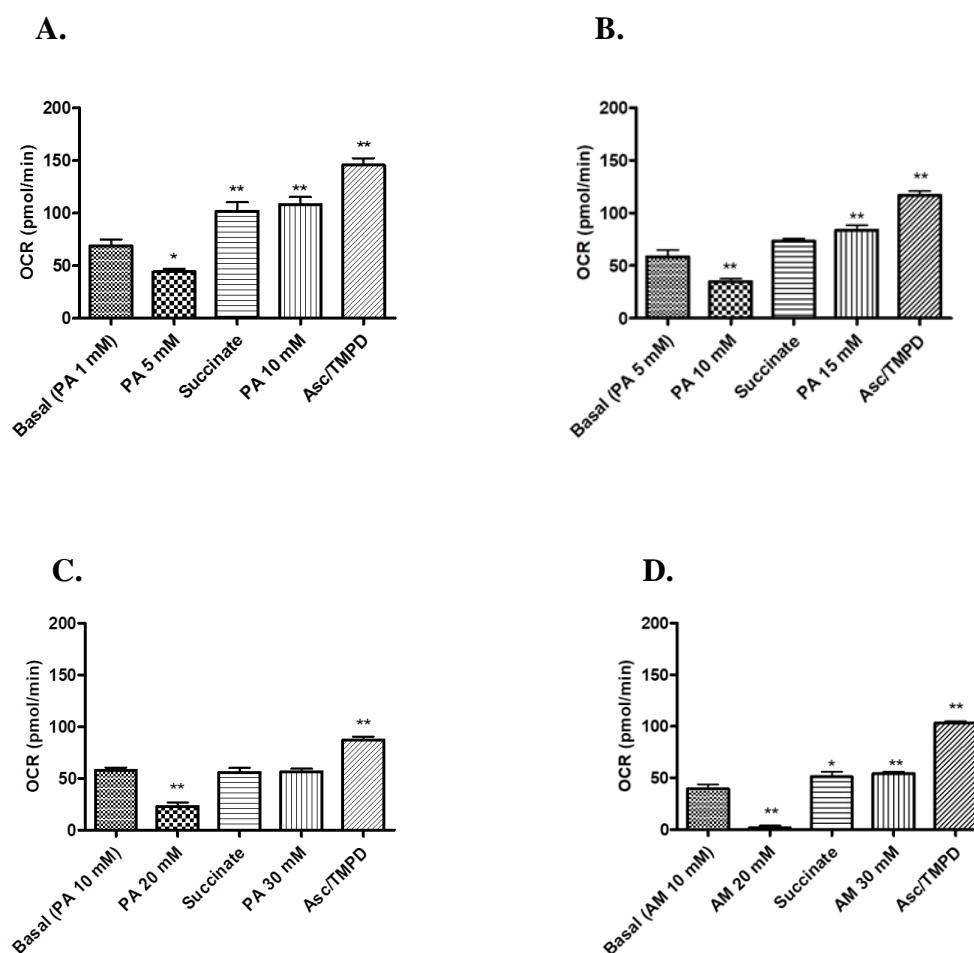


Figure 6.8: Elucidation of the mitochondrial target of hypothermic agents (5 μ g mitochondria). Electron flow experiments were performed as described in Methods. Initial conditions are as follows: **A.** 1 mM paracetamol, **B.** 5 mM paracetamol, **C.** 10 mM paracetamol and **D.** 10 mM aminopyrine. Data are representative of $n=3$ replicates expressed as means \pm Standard deviations (* $P < 0.05$, ** $P < 0.01$ from control).

Paracetamol (5 mM) caused a significant reduction in complex I activity by 36% and induced a significantly reduced (29%) response to complex II stimulation by succinate (48%) in Figure 6.8(A). Respiratory rates for complex III and complex IV were 58% and 113% after cumulative addition of paracetamol (10 mM) in Figure 6.8(A).

Addition of paracetamol (10 mM) resulted in 40% and 49% decrease in complex-I and II mediated respiration (125%) whereas further addition of paracetamol (15 mM) followed by complex III (43%) and complex IV (100%) in Figure 6.8(B).

Moreover, this compound appeared to have a greater impact as the concentration of paracetamol (20 mM) increased, markedly reducing complex I and II-driven respiration by 60% and 61% with compromised complex II (96%) and III (98%) and IV (151%) OCR at 30 mM of this drug in Figure 6.8(C).

Furthermore, aminopyrine (20 mM) attenuated complex I and II-mediated respiration by 96% and 64%. Respiratory rates of succinate were completely inhibited and ascorbate/TMPD OCR was unaffected with OCR increasing to 62% of basal level Figure 6.8(D).

6.3.8. Elucidation of the mechanistic activity of hypothermic agents

In an attempt to further elucidate the inhibitory effects of test compounds and the impact of the concentration of mitochondria, studies were carried out in the presence of 2.5 μ g isolated rat liver mitochondria. In control group in Figure 6.9(A), there was a 93% reduction in pyruvate and malate-dependent respiration by rotenone (2 μ M), followed by an increase in OCR (69%) when succinate was added. Antimycin A prevented complex I- and III-mediated respiration by 91% as it inhibited complex III, causing loss of function throughout until ascorbate and TMPD was added that caused a marked increase in OCR (84%), indicating that complex IV remained active. For malonate (10 mM), the respiratory rates of complex II and III is inhibited by 73% and 58%. No effect on complex I- and IV-driven respiration (98%) mediated by complex IV in Figure 6.9(B).

Paracetamol (10 mM) caused a significant reduction in complex I activity by 55% at the start of the assay versus control and induced a further reduced complex I activity by 57% (20 mM). Paracetamol significantly reduced (62%) response to complex II stimulation by succinate (41%). Respiratory rates for complex III and complex IV were

decreased to 27% and 47% after cumulative addition of paracetamol (30 mM) in Figure 6.9(C).

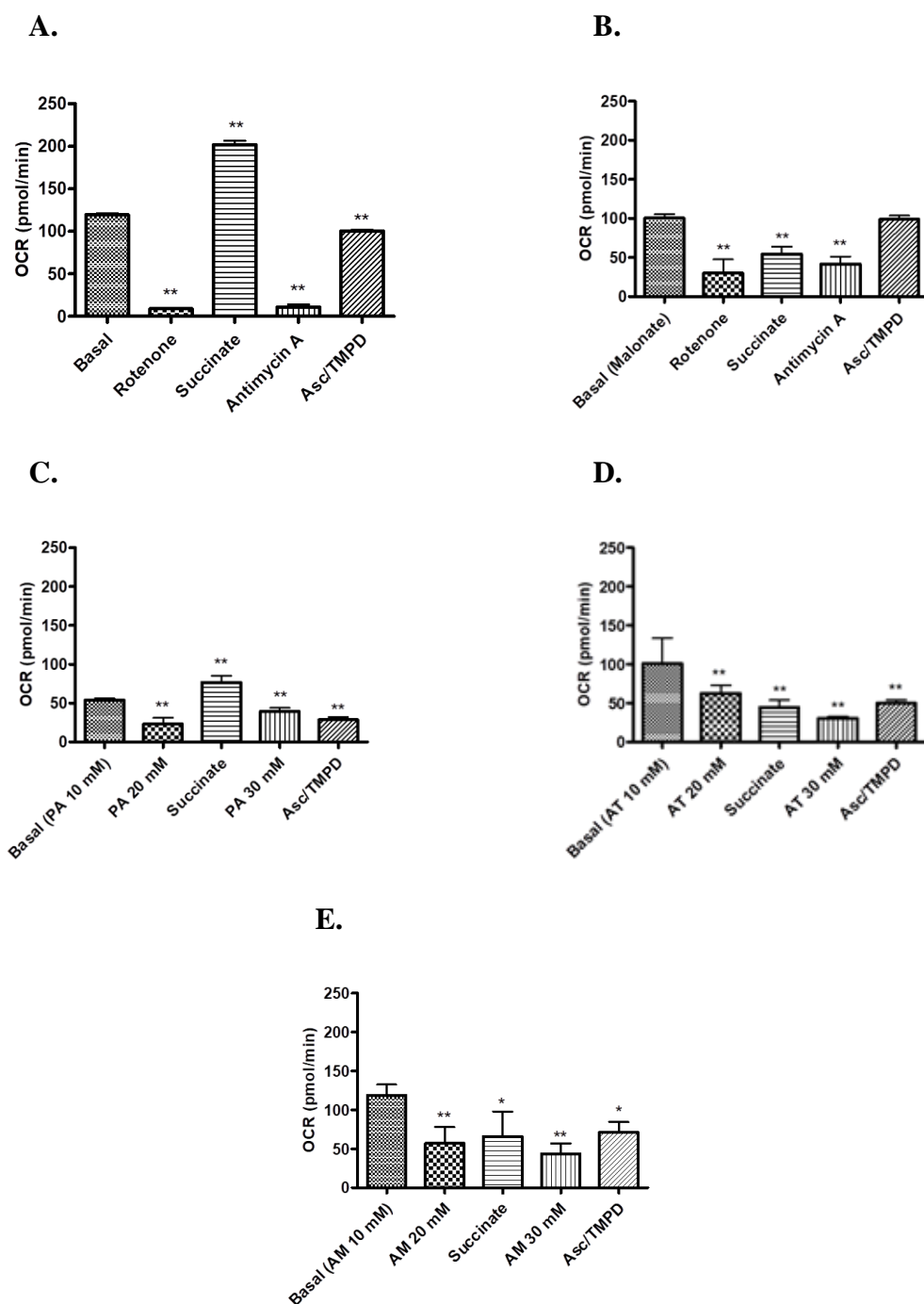


Figure 6.9: Elucidation of the mechanistic activity of hypothermic agents (2.5 μ g mitochondria). Electron flow experiments were performed as described in Methods. Initial conditions are as follows: **A.** Control (no additives), **B.** 10 mM malonate, **C.** 10 mM paracetamol and **D.** 10 mM antipyrene and 10 mM aminopyrene. Data are representative of $n=3$ replicates expressed as means \pm Standard deviations (* $P < 0.05$, ** $P < 0.01$ from control).

In antipyrine treated mitochondria there was a 15% and 38% decrease in complex-I respiration at 10 mM and 20 mM whereas 78% reduction in case of II mediated respiration (45%). whereas further addition of antipyrine (30 mM) abolished respiratory rates of complex III and complex IV by 70% and 51% in Figure 6.9(D).

Furthermore, aminopyrine (10 mM) attenuated complex I activity by 12% whereas further addition of this drug resulted in 46% decrease at 20 mM. Complex II-mediated respiration was inhibited by 73% with compromised activity (48%). Respiratory rates of complex III and ascorbate and TMPD were lowered by 59% and 32% in Figure 6.9(E).

6.4. Discussion

In energy metabolism, the mitochondrial ETC plays a central role. Under normal conditions electrons flow through the complexes I–IV with the pumping out of protons and reducing oxygen to form water, the proton energy from the gradient drives ATP production (Bratic and Trifunovic, 2010). Under some conditions, the re-entering of protons into mitochondrial matrix without associated ATP synthesis can occur resulting in heat generation (Bratic and Trifunovic, 2010). Thus, uncoupling leads to a low ATP production with higher electron transfer and cellular respiration requiring a constant supply of substrates, cofactors and oxygen which is not sustainable (Cannon et al., 2006). Mammals have evolved mechanisms to deal with cold stress including adrenergic stimulation of lipolysis. Fatty acids derived from lipolysis increase the UCP1 H^+ permeability, and the energy derived from the gradient, normally used for ATP synthesis, is converted into heat, although this requires substrates to be generated and supplied to the mitochondria. Drug induced mitochondrial dysfunction can affect OXPHOS (Chan et al., 2005). Loss of mitochondria function following toxic doses of paracetamol has been observed in rodent studies dating back to 1970s (Mitchell et al., 1973a, 1973b).

By using the electron flow assay and the specific complex inhibitors, electron flow through different ETC complexes was examined in an attempt of a more direct estimation of the possible target of agents that affect mitochondrial bioenergetics. Paracetamol (5-30 mM) caused a significant reduction in complex I-IV activities and depressed the ETC components (Figure 6.8-6.9). Furthermore, aminopyrine (20 mM) attenuated complex I and II-mediated respiration. The observation confirms that compounds which caused *in vivo* hypothermia are potent inhibitors of mitochondrial function as expressed by OCR. Complex I was most sensitive to paracetamol; however the compound appeared to be effective against all four complexes. This implies that paracetamol may be disrupting electron transport generally in the mitochondria. Antipyrene also affected all complexes but with greatest inhibition of this drug was at complex-II mediated respiration. A similar pattern was observed for aminopyrine (Figure 6.8-6.9). This is the first study where the effects of paracetamol, aminopyrine and antipyrene have demonstrated inhibition of specific mitochondrial function in both 3T3-L1 adipocytes and isolated mitochondria. Additionally these studies have never been carried out using the Agilent Seahorse XF technology.

In vitro and *in vivo* studies have confirmed the effect of high concentrations of this drug leading to mitochondrial inhibition affecting membrane potential (Nazareth et al., 1991), ATP concentration (Martin and McLean, 1995), and slowed the rate of electron moving from complex I to complex III in isolated kidney mitochondria (Porter and Dawson, 1979). Paracetamol (up to 10 mM) resulted in inhibition of glucose synthesis from glutamine or lactate and decreased ATP level, coupled and uncoupled respiration but not succinate mediated respiration (Porter and Dawson, 1979). Furthermore, inhibition of state 3 respiration by paracetamol reflects some interference with the ETC in mitochondria but did not uncouple oxidative phosphorylation in rat kidney and liver (Mingatto et al., 1996; Somasundaram et al., 1997). *In vitro*, paracetamol inhibited both state 3 and 4 respiration and respiratory control ratio (RCR), in a concentration-dependent manner with glutamate but not succinate as substrate, differing with results obtained following *in vivo* exposure to mice and may result from a direct insult of the parent compound (Meyers et al., 1988).

The impact on mitochondria is not limited to paracetamol but to other drugs with antipyretic properties. NSAIDs including aspirin, diclofenac sodium, mefenamic acid, and piroxicam both uncoupled and inhibited OXPHOS in mitochondria with glutamate/malate or with succinate substrate, while dipyron only uncoupled and paracetamol only inhibited it (Somasundaram et al., 1997). The pattern of inhibition of these compounds was different to paracetamol, but similar to that expressed by the respiratory chain inhibitors in that the drugs inhibited respiration stimulated by both ADP (state 3) and the protonophoric uncoupler CCCP. In the former case, drug-imposed inhibition of state 3 was not released by the CCCP. Paracetamol showed a pattern similar to that expressed by the FoF1-ATPase (oligomycin) and ADP/ATP carrier (atractyloside) inhibitors; that of drug-imposed inhibition of state 3 respiration was released by the uncoupler. Dipyron only stimulated the state 4 respiration (Mingatto et al., 1996). Indomethacin, aspirin, naproxen, and piroxicam stimulate mitochondrial respiration (uncouple OXPHOS) of isolated rat liver mitochondria in micromolar concentrations whereas paracetamol did not. However, both paracetamol and NSAIDs at higher concentrations inhibited respiration in coupled mitochondria. Indomethacin, naproxen, aspirin, and paracetamol inhibit both glutamate/malate and succinate (with rotenone) stimulated respiration in uncoupled mitochondria. All the drugs inhibited electron transfer in complex I, and complexes II plus III, in a concentration dependent manner (data not shown in the article) (Somasundaram et al., 1997). *In vitro* respiratory data showed that NSAIDs are inhibitory uncouplers, i.e. they

uncouple at low and inhibit respiration at higher concentrations (Somasundaram et al., 2000).

The concentration of paracetamol and other compounds used in these *in vitro* studies relate to the concentrations of paracetamol that have been shown to cause hypothermia and toxicity *in vivo* (Orbach et al., 2017; Rivera et al., 2017; Ahmed et al., 2011; Allen et al., 2005; Khetani and Bhatia 2008; Kikkawa et al., 2006; Messner et al., 2013; Nastevska et al., 1999; Shen et al., 2007; Toh et al., 2009).

300 mg/kg is a dose that has been shown to cause significant hypothermia in mice and is a highly toxic dose for mice (Evdokimov et al., 2015). Paracetamol has shown to decrease MnSOD activity at 100, 200, and 300 mg/kg in mice suggesting this enzyme's inactivation as an early effect of paracetamol induced damage again confirming that doses which cause hypothermia is linked to mitochondria toxicity (Agarwal et al., 2010).

Despite the widespread observation of the negative impact of paracetamol and related compounds on various aspects of mitochondrial function this is the first time that these observations have been linked to hypothermia or antipyresis. Regardless of the extent of inhibition *in vivo*, under cold stress conditions only a minor attenuation of energy production is required to cause hypothermia in small mammals in temperatures below their thermoneutral zone.

Chapter 7: Final discussion and future work

The antipyretic properties of paracetamol have always been one of the main reasons for its widespread use, particularly to treat children with fever. The general consensus is that during fever paracetamol inhibits central COX-2 activity which has been upregulated. However, it has always been accepted that once activated centrally, increased temperature associated with fever is generated peripherally. This mode of antipyresis linked to paracetamol is thought to be similar to other COX-2 inhibitors used as antipyretics. However, researchers have always struggled to reconcile the potent antipyretic properties of paracetamol with the relatively weak inhibition of COX activity when compared to NSAIDs (Chandrasekharan et al., 2002).

The situation is complicated by the fact that for some time it has been observed that in non-febrile small mammals the administration of relatively high levels of paracetamol (>100 mg/kg) results in a concentration dependent fall of several degrees in T_c within 30 minutes of exposure. After a few hours, the animals usually recover to normal T_b confirming that the impact on T_b is transient. A fundamental flaw in most of these studies is the failure to assess the extent and long term toxicity impact during the hypothermic event or after. However, in other *in vivo* studies where hypothermia is not the focus but where similar paracetamol concentrations are used, it is widely documented that there are varying but clear signs of toxicity in mice and rats exposed to paracetamol at concentrations greater than 100 mg/kg from 1-24 hours after administration. Given the generally accepted view that the antipyresis of paracetamol is due to inhibiting COX-2 and the fact that COX-2 is not normally expressed in non-febrile animals, an alternative explanation is necessary to explain the hypothermic properties of paracetamol in non-febrile animals.

Over the last 20 years one of the most strongly asserted although very contentious explanations proposed in animals where this phenomenon is observed, is that paracetamol inhibits a novel variant (COX-3) of the COX-1 enzyme. Activation of the enzyme is thought to be necessary for animals to maintain normal T_b under cold stress. It was proposed that COX-3 would act like COX-2 during fever where the enzyme is a key mediator of increased thermogenesis during cold stress, so specific inhibition of COX-3 (by paracetamol) would result in hypothermia. However, there remained questions not only about the existence but also the functionality of such protein in a range of species for which paracetamol was known to cause hypothermia.

To address the working hypothesis that paracetamol induced hypothermia in rodents is due to the inhibition of a novel COX-1 variant protein (COX-3) expressed in brain endothelial cells, a number of questions had to be addressed. Most fundamental was about the existence and functionality of the COX-3 protein. If the protein did not exist or could not be linked to paracetamol induced hypothermia, the alternative question would then be what effect does paracetamol have on the peripheral thermogenic pathways downstream of PGE₂ in small mammals housed at temperatures several degrees below their thermoneutral zone. Given the known effects of paracetamol on mitochondrial function, studies were focused on the impact on lipolysis and mitochondrial energy generation pathways which are essential for heat generation (Table 7.1).

Table 7.1: Key findings of current research

Chapters	Research answers
Is there a COX-3? (chapter 3)	COX-3 mRNA and protein was not identified in mice b.End3 cells and brain homogenates.
Impact on lipolysis? (chapter 4)	Paracetamol, aminopyrine and antipyrine inhibits lipolysis in mice 3T3-L1 adipocytes and rat primary brown adipocytes.
Impact on FAO? (chapter 5)	Paracetamol and NAPQI inhibit FAO in mice 3T3-L1 adipocytes.
Impact on mitochondrial respiration? (chapter 6)	Paracetamol, aminopyrine and antipyrine inhibits mitochondrial respiration in mice 3T3-L1 adipocytes. These compounds also inhibit ETC activity in isolated rat liver mitochondria.

The search for COX-3

The first physical evidence of a COX-3 protein was provided by Chandrasekharan et al. in 2002. They expressed and isolated a canine COX-3 protein in insect cells which was then compared to the activity of murine COX-1 and COX-2. What they failed to address was that paracetamol was far from the most potent drug in the study with the IC₅₀ for COX-3 for paracetamol significantly greater than the NSAIDs. It would then follow that if COX-3 was responsible for temperature regulation in rodents then NSAIDs would

also cause hypothermia in non-febrile animals even if the NSAIDs did not accumulate in the brain at concentrations comparable to paracetamol. The concern was underpinned at a theoretical level by the molecular biology which ruled out the transcription of a viable mRNA. At the practical level, there was paucity of COX-3 protein reported in the literature.

In the present study the main challenge was to confirm the existence of protein with a view of further characterisation. Mouse endothelial cell line was selected as the brain endothelial cells were proposed having the highest levels of expression. Similarly, tissue homogenates particularly brain from animals housed at around 22°C should also reveal any expressed COX-3 protein if COX-3 was acting as a regulator of Tc in these animals as proposed. The failure in this study to find any evidence for the expression of the protein in the endothelial cell line and tissue homogenate could be seen as surprising given the previous *in vivo* and *in vitro* reports. However, a closer look at the literature on studies related to the COX-3 protein in mammalian cells or tissue reveals that only very few studies reported actual COX-3 protein. By contrast, most studies reported COX-3 at mRNA level and this was not established in this study. In this context, the explanation of results of this and previous studies makes a search to find and characterise the COX-3 protein less relevant as almost all reported versions of the COX-3 protein where it has been tested suggest it is non- functional.

The failure to find any COX-3 protein curtailed any experiments to biochemically characterise the protein. However, an examination of the key Chandrasekaran et al., 2002 study will reveal that although the COX-3 was more sensitive to paracetamol and other putative COX-3 inhibitors than COX-1 or COX-2 the protein produced was even more sensitive to several NSAIDs and a different order of magnitude suggesting these NSAIDs should also cause hypothermia. However, no such experimentation has been published to counter or support this idea.

The search for possible paracetamol targets: inhibition of lipolysis

In the absence of a COX-3 protein and a credible explanation for the previously widely reported COX-3 mRNA observed in several animals. Studies were then undertaken to provide possible explanations as to how paracetamol could cause hypothermia in non-febrile mice and other small mammals. It is known that the peripheral pathways for thermogenesis start with the release of NE from neurons which innervate brown

adipocytes or from epinephrine released into the general circulation in response to cold stress. These act on receptors on the brown adipocytes to trigger lipolysis, this is thought to play two key roles in thermogenesis. Brown fat mitochondria are uniquely designed for non-shivering thermogenesis with a high expression of UCP1 which reduces mitochondrial coupling efficiency causing more energy to be diverted directly to heat production. The second role is in the liberation of increased levels of FFAs into the general circulation which is then used to increase general metabolic rate again driving increased oxygen consumption and heat generation.

Numerous hormones and drugs can lead to lipolysis through different pathways (Lafontan and Langin, 2009). The major lipolysis signalling pathway starts with the binding of endogenous or synthetic catecholamines to β -adrenergic receptors on adipocytes. This leads to activation of AC, catalysing the conversion of ATP to cAMP. This secondary messenger activates HSL, which hydrolyzes triglycerides to produce FFAs and glycerol. All the components highlighted above in lipolysis signalling pathway are potential targets for paracetamol or similar drugs. Elevation of the concentration of NE in the plasma of animals under cold stress confirms the importance of this pathway. It can be assumed that in animals functioning at temperatures several degrees below their thermoneutral zone, even a small reduction in the supply of substrates (FFAs) as seen in this study could have an adverse effect on thermoregulation. In this study, paracetamol was shown to reduce both direct catecholamine stimulated and non-stimulated lipolysis in brown adipocytes and 3T3-L1 cells. This novel observation if repeated *in vivo* would impact on the ability of small mammals to maintain sufficient substrate supply and consequently to maintain T_c at 37°C when housed at temperatures several degrees below their thermoneutral zone.

Given the complex signalling pathways involved in lipolysis, from binding to the adrenergic receptor to the release of FFAs, an important objective was to gain an insight into where in the pathway paracetamol and related drugs may be acting. The use of AC activator Forskolin or the cAMP analogs, 8-Br-cAMP confirm the paracetamol inhibition is further downstream of the receptor and secondary messengers and more likely to affect the lipolysis from HSL. The exact target for HSL inhibition is a matter for further investigation.

The search for possible paracetamol targets: inhibition of fatty acid uptake and β -oxidation

The novel observation that paracetamol and other hypothermic agents may inhibit lipolysis *in vitro* points to one possible explanation of paracetamol induced hypothermia. However, there are other potential targets in the thermogenesis pathway that must be explored. In particular the β -oxidation of fatty acids liberated from lipolysis is an essential substrate to drive non-shivering thermogenesis. Before β -oxidation, fatty acids must enter the mitochondria which involved a complex inner mitochondrial membrane shuttle. Paracetamol could either affect the activity of the shuttle, the β -oxidation process or both.

Many compounds inhibit fatty acids β -oxidation with toxic consequences for example the hepatotoxicity induced by aspirin and hypoglycin has been linked to fatty acids β -oxidation. Recently the inhibition of β -oxidation has been implicated in paracetamol-induced hepatotoxicity with the associated disruption of lipid metabolism. In particular the increase in microvesicular steatosis and increase of TGs and FFAs has been linked to disruption of mitochondrial function (Cohen et al., 1998; Buttar et al., 1976). Other studies have shown that paracetamol or its metabolites can negatively affect fatty acid β -oxidation in the liver with increased levels of long-chain acylcarnitines the principal precursors of β -oxidation in the serum following exposure (Sandor et al., 1990).

The present study shows that paracetamol inhibits both exogenously added fatty acids and endogenous oxidation. It is likely that during cold stress or even during fever adipocytes will release fatty acids into the general circulation to increase metabolic rate. However, cells can only metabolise fatty acids if the substrate can freely enter the mitochondria. Unlike the classical inhibitor of fatty acid oxidation Eto which blocks fatty acid entry into the mitochondria and therefore indirectly blocks oxidation, paracetamol appears to have a wider effect. The data shows paracetamol inhibits oxidation even when the source of the substrate is endogenous. Although many compounds have been shown to inhibit oxidation of fatty acids this is the first time that this has been so clearly demonstrated by paracetamol. Further this is the first time the inhibition of FAO was proposed to be a contributory factor in the hypothermia induced by paracetamol and related compounds in small mammals.

The search for possible paracetamol targets: inhibition of mitochondrial electron transport chain

In chapters 4 and 5 the focus was on highlighting newly discovered knowledge around the impact of paracetamol on lipolysis in adipocytes and on FAO in the mitochondria. In chapter 6, the starting point is that paracetamol has been widely shown to alter or inhibit mitochondrial function both *in vitro* and *in vivo*. In C57BL/6 mice paracetamol (150 mg/kg) produces reversible MPTP linked mitochondrial dysfunction without causing ALT release whereas at 300 mg/kg it causes irreversible mitochondrial dysfunction, ALT release and necrosis (Hu et al., 2016). Mitochondrial dysfunction was also observed in paracetamol overdose patients where the release of biomarkers for mitochondrial damage such as mitochondrial DNA (mtDNA), glutamate dehydrogenase (GDH) and the indirect mitochondrial damage biomarker nuclear DNA fragments (nDNA) could be measured in plasma (McGill et al., 2012). *In vitro*, paracetamol (up to 10 mM) has been shown to cause a reversible and concentration based inhibition of mitochondrial respiration in isolated rat kidney. Experiments with submitochondrial particles revealed that the drug did not influence the activity of NADH dehydrogenase but slowed the rate at which electrons were transferred from reduced NADH dehydrogenase.

The main findings in chapter 6 is that paracetamol has been shown to affect numerous mitochondrial functions including disrupting the delivery of substrates or electrons to complex I, II and IV, therefore oxygen consumption is disrupted. There was less evidence of uncoupling by paracetamol which can be associated with permanent damage to the mitochondrial membrane. Similarly the relatively low level of reversible toxicity observed as demonstrated by the attenuation of ETC activity, may explain why paracetamol is such an effective therapeutic compound. At therapeutic doses, the mild and reversible “toxic” effects may in fact be part of its mechanism of action at least in terms of reducing temperature.

In vivo studies of hypothermia all involve animals housed at temperatures which are several degrees below the animal’s thermoneutral zone. These are undertaken on the false basis that small mammals used in laboratory experiments have the same thermoneutral zone as humans. The reality however for most experiments is that such animals are under continued cold stress and their thermogenic systems are required to work at elevated levels. Under such circumstances even a small attenuation of mitochondrial function is likely to have an exaggerated effect on Tb as have been

reported in this study. A similar hypothermia phenomenon has recently been observed in human volunteers exposed to cold stress when given paracetamol (Foster et al., 2016). The study revealed a slight but significant decrease in body temperature at relatively low doses of paracetamol (20 mg/kg) when the volunteers were subject to cold stress for a relatively short period of time. By contrast, most laboratory animals housed around 22°C are continually under cold stress, making them susceptible to relatively minor attenuations of thermogenesis process. By contrast, dramatic temperature changes have been reported in animals exposed to high probably toxic concentrations of paracetamol. Given the subtle temperature changes brought about by the low non-toxic doses of paracetamol in human studies, there is a need to assess temperature changes in non-febrile animals at lower concentrations of paracetamol. These changes are likely to be subtle requiring more sophisticated monitoring to detect.

These mitochondrial changes may also partly explain the antipyretic effects of paracetamol where animals and humans are under other forms of temperature stress. During fever there is a greater demand for metabolic energy to increase T_b ; this involves activating the same mechanisms which are activated during cold stress in laboratory animals, so it is reasonable to assume that paracetamol would have a similar attenuating effect on T_c during fever. If correct, this novel interpretation of well-established observations could lead not only to a better understanding of how paracetamol and many other antipyretic drugs work, but could provide the impetus for designing new drugs to treat pyresis regardless of the cause. Other potential uses could be for inducing hypothermia for medical reasons such as during surgery.

Another novel finding from the data in Chapter 6 is the sheer potency of the paracetamol metabolite NAPQI. Although it is widely accepted that the metabolite is only generated in minute quantities the impact could be far greater than the parent compound on mitochondrial function. Mitochondrial dysfunction and toxicity is observed at significantly much lower concentrations when compared with paracetamol and other compounds. Further the metabolite is far less discriminating, both in the extent of damage to mitochondria but to the targets. There is clear evidence of extensive damage to the ETC function. In addition there is clear evidence of uncoupling which was not seen with the parent compound suggesting the damage is more severe and likely to be permanent. What can be assumed that at therapeutic doses very little NAPQI is generated although this has to be fully investigated particularly in adipocytes where little is understood about the metabolism of paracetamol and NSAIDs.

Conclusion and future direction

This study was initiated to answer key questions about the mechanisms underlying paracetamol induced hypothermia in non-febrile animals. With a working hypothesis that “*paracetamol induced hypothermia in rodents is due to the inhibition of a novel COX-1 variant protein expressed in brain endothelial cells*”. When the putative COX-3 protein could not be found, the focus then changed to possible targets of paracetamol downstream of the central generation of PGs. The data revealed numerous potential targets for paracetamol and similar drugs including lipolysis, fatty acid uptake, FAO and most of the complexes of the ETC. The study revealed both new knowledge and new understanding about how paracetamol could work. The linking of the energy demands for pyresis (fever) to the maintenance of Tc when animals are housed several degrees below their thermoneutral zone provides new opportunities for research.

List of Abstracts:

Oral Communications:

1. British Pharmacology Society Annual Meeting Dec 2017. S.Bashir and W.Morgan. Inhibition of thermogenic pathways: a new target for paracetamol? Queen Elizabeth II Conference Centre, London, England, U.K.
2. Postgraduate Annual Meeting Mar 2017. University of East London, Stratford, London, England, U.K.
3. Postgraduate Annual Meeting Feb 2016. University of East London, Stratford, London, England, U.K.
4. Postgraduate Annual Meeting Oct 2014. University of East London, Stratford, London, England, U.K.

Poster Communications:

1. Abstract accepted for poster presentation at Mitochondria: form and function. British Pharmacology Society Meeting Sept 2017. S.Bashir, S.Ayoub and W.Morgan. Mitochondrial oxygen consumption: a new target for paracetamol? Mary Ward House, Conference and Exhibition Centre, London, England, U.K.
2. Abstract accepted for poster presentation at British Toxicology Annual Congress Apr 2017. S.Bashir, S.Ayoub and W.Morgan. The effect of paracetamol on lipolysis in adipocytes. Hilton Liverpool City Centre, Liverpool, England, U.K.
3. Abstract accepted for poster presentation at Drug Metabolism Group Meeting, Feb 2017. S.Bashir, S.Ayoub and W.Morgan. The effect of paracetamol on lipolysis in adipocytes. Imperial College London, South Kensington Campus, London, England, U.K.
4. Abstract accepted for poster presentation at British Pharmacology Society Annual Meeting Dec 2016. S.Bashir, B. Elegunde and W.Morgan. Antipyresis and the inhibition of mitochondrial function. Queen Elizabeth II Conference Centre, London, England, U.K.

References

Abdel-aleem S.A., Abdel-hamid M. Simmons D.L., Donaldson L.F. (2009). Distribution of Cyclooxygenase-3 (Cox-3) in Rat Nervous System. *Med. J.* 77(3), 245-250.

Agarwal R., MacMillan-Crow L.A., Rafferty T.M., Saba H., Roberts D.W., Fifer E.K., James L.P., Hinson J.A. (2011). Acetaminophen-induced hepatotoxicity in mice occurs with inhibition of activity and nitration of mitochondrial manganese superoxide dismutase. *J Pharmacol Exp Ther.* 337, 110–6.

Agilent Technologies (2017). Agilent Seahorse XF Cell Mito Stress Test Kit Available at: https://www.agilent.com/cs/library/usermanuals/public/XF_Cell_Mito_Stress_Test_Kit_User_Guide.pdf [Accessed 2 August 2017].

Agilent Technologies (2017). Agilent Seahorse XF Palmitate-BSA FAO Substrate Quickstart Guide Available at: https://www.agilent.com/cs/library/usermanuals/public/XF_Palmitate_BSA_Substrate_Quickstart_Guide.pdf [Accessed 2 August 2017].

Agilent Technologies (2017). Analyzing Microgram Quantities of Isolated Mitochondria in the Agilent Seahorse XFe/XF96 Analyzer <https://www.agilent.com/cs/library/applications/5991-7144EN.pdf> [Accessed 2 August 2017].

Agilent Technologies (2017). How to Hydrate an Agilent Seahorse XFp Sensor Cartridge Available at: <https://www.agilent.com/cs/library/usermanuals/public/Hydrating%20an%20XFp%20Sensor%20Cartridge.pdf> [Accessed 2 August 2017].

Agilent Technologies (2017). Loading the Agilent Seahorse XFp Sensor Cartridge Injection Ports Available at: <https://www.agilent.com/cs/library/usermanuals/public>Loading%20Cartridge%20XFp.pdf> [Accessed 2 August 2017].

Agilent Technologies (2017). Preparation of XF assay media Available at: <https://www.agilent.com/cs/library/usermanuals/public/Media%20Prep%20XFp.pdf> [Accessed 2 August 2017].

Agilent Technologies (2017). Report Generator User Guide XF Cell Mito Stress Test Kit Available at: https://www.agilent.com/cs/library/usermanuals/public/Report_Generator_User_Guide_Seahorse_XF_Cell_Mito_Stress_Test_Single_File.pdf [Accessed 2 August 2017].

Agilent Technologies (2017). Seeding Adherent Cells in Agilent Seahorse XFp Cell Culture Miniplates Available at: <https://www.agilent.com/cs/library/>

[usermanuals/public/Seeding%20Adherent%20Cells%20in%20XFp%20Cell%20Culture%20Miniplates.pdf](#) [Accessed 2 August 2017].

Agilent Technologies (2017). Simultaneously Measuring Oxidation of Exogenous and Endogenous Fatty Acids using the XF Palmitate-BSA FAO Substrate with the XF Cell Mito Stress Test Available at: [https://www.agilent.com/cs/pubimages/misc/XF FAO Assay Technical Brief.pdf](https://www.agilent.com/cs/pubimages/misc/XF_FAO_Assay_Technical_Brief.pdf) [Accessed 2 August 2017].

Agilent Technologies (2017). Washing Adherent Cells in Agilent Seahorse XFp Cell Culture Miniplates Available at: <https://www.agilent.com/cs/library/usermanuals/public/Washing%20Cells%20XFp.pdf> [Accessed 2 August 2017].

Ahangar N., Esam Z., Bekhradnia A., Ebrahimzadeh M.A. (2016). Hypothermic activity of acetaminophen; involvement of GABAA receptor, theoretical and experimental studies. *Iran J Basic Med Sci.* 19(5), 470–475.

Ahmed M.M., Wang T., Luo Y., Ye S., Wu Q., Guo Z., Roebuck B.D., Sutter T.R., Yang J.Y. (2011). Aldo-keto reductase-7A protects liver cells and tissues from acetaminophen-induced oxidative stress and hepatotoxicity. *Hepatology.* 54,1322-1332.

Ali A.T., Hochfeld W.E., Myburgh R., Pepper M.S. (2013). Adipocyte and adipogenesis. *European Journal of Cell Biology.* 92, 229–236.

Allen J.W., Khetani S.R., Bhatia S.N. (2005). In vitro zonation and toxicity in a hepatocyte bioreactor. *Toxicol. Sci.* 84, 110-119.

Anderson B.J. Paracetamol (Acetaminophen): mechanisms of action. (2008). *Paediatr Anaesth.* 18(10), 915-21.

Ara K., Ahmad K. (1980). Uptake of paracetamol into brain and liver of rats. *Bangladesh Med Res Counc Bull.* 6, 39–44.

Ayoub S. S., Pryce G., Seed M. P., Bolton C., Flower R. J., Baker D. (2011). Paracetamol-induced hypothermia is independent of cannabinoids and transient receptor potential vanilloid-1 and is not mediated by AM404. *Drug Metab. Dispos.* 39, 1689–1695.

Ayoub S.S., Botting R.M., Goorha S., Colville-Nash P.R., Willoughby D.A., Ballou L.R. (2004). Acetaminophen-induced hypothermia in mice is mediated by a prostaglandin endoperoxide synthase 1 gene-derived protein. *Proc Natl Acad Sci U S A.* 101(30), 11165-9.

Ayoub S.S., Colville-Nash P.R., Willoughby D.A., Botting R.M. (2006). The involvement of a cyclooxygenase 1 gene-derived protein in the antinociceptive action of paracetamol in mice. *Eur J Pharmacol.* 538(1-3), 57-65.

Bajt M.L., Ramachandran A., Yan H.M., Lebofsky M., Farhood A., Lemasters J.J., Jaeschke H. (2011). Apoptosis-inducing factor modulates mitochondrial oxidant stress in acetaminophen hepatotoxicity. *Toxicol Sci.*122(2), 598-605.

Begrache K., Massart J., Robin M.A., Borgne-Sanchez A., Fromenty B. (2011). Drug-induced toxicity on mitochondria and lipid metabolism: mechanistic diversity and deleterious consequences for the liver. *J Hepatol.* 54(4), 773-94.

Berenbaum F. (2004). COX-3: fact or fancy? *Joint Bone Spine.* 71(6), 451-3.

Berg J.M., Tymoczko J.L., Stryer L. (2002). Section 18.6 The Regulation of Cellular Respiration Is Governed Primarily by the Need for ATP. *Biochemistry.* 5th edition. New York: W H Freeman.

Berson A., Cazanave S., Descatoire V., Tinel M., Grodet A., Wolf C., Feldmann G., Pessayre D. (2006). The anti-inflammatory drug, nimesulide (4-nitro-2-phenoxy methane-sulfoanilide), uncouples mitochondria and induces mitochondrial permeability transition in human hepatoma cells: protection by albumin. *J Pharmacol Exp Ther.* 318, 444-454.

Berson A., Renault S., Lettéron P., Robin M.A., Fromenty B., Fau D., Le Bot M.A., Riché C., Durand-Schneider A.M., Feldmann G., Pessayre D. (1996). Uncoupling of rat and human mitochondria: a possible explanation for tacrine-induced liver dysfunction. *Gastroenterology*, 110, 1878-1890.

Bicego K.C., Barros R.C., Branco L.G. (2007). Physiology of temperature regulation: comparative aspects. *Comp Biochem Physiol A Mol Integr Physiol.* 147(3), 616-639.

Biovision. (2017). Available at: https://www.biovision.com/documentation/data_sheets/K580.pdf [Accessed 2 Aug. 2017].

Blüher M., Patti M.E., Gesta S., Kahn B.B., Kahn C.R. (2004). Intrinsic heterogeneity in adipose tissue of fat-specific insulin receptor knock-out mice is associated with differences in patterns of gene expression. *J Biol Chem.* 279, 31891-901.

Botting R., Ayoub S.S. (2005). COX-3 and the mechanism of action of paracetamol/acetaminophen. *Prostaglandins Leukot Essent Fatty Acids.* 72(2):85-7.

Botting R.M. (2000). Mechanism of action of acetaminophen: is there a cyclooxygenase 3? *Clin Infect Dis.* 5, S202-10.

Botting R.M. (2004). Antipyretic therapy. *Front Biosci.* 9, 956-66.

Boulant J.A. (2000). Role of the preoptic-anterior hypothalamus in thermoregulation and fever. *Clin Infect Dis.* 31 Suppl 5, S157-161.

Bozza P.T., Payne J.L., Morham S.G., Langenbach R., Smithies O., Weller P.F. (1996). Leukocyte lipid body formation and eicosanoid generation: cyclooxygenase independent inhibition by aspirin. *Proc Natl Acad Sci USA.* 93, 11091-11096.

Bradford M.M. (1976). A rapid and sensitive method for the quantitation of microgram quantities of protein utilizing the principle of protein-dye binding. *Anal Biochem.* 72:248-54.

Bratic I., Trifunovic A. (2010). Mitochondrial energy metabolism and ageing. *Biochim Biophys Acta.* 1797(6-7), 961-7.

Briyal S., Gulati A. (2010). Endothelin-A receptor antagonist BQ123 potentiates acetaminophen induced hypothermia and reduces infarction following focal cerebral ischemia in rats. *Eur J Pharmacol.* 644(1-3), 73-9.

Brodie B.B., Axelrod J. (1948). The fate of acetanilide in man. *J Pharmacol Exp Ther.* 94, 29–38.

Bronnikov G.E., Zhang S-J., Cannon B., Nedergaard J. (1999). A dual component analysis explains the distinctive kinetics of cAMP accumulation in brown adipocytes. *J Biol Chem.* 274, 37770–80.

Burke A.S., MacMillan-Crow L.A., Hinson J.A. (2010). Reactive nitrogen species in acetaminophen-induced mitochondrial damage and toxicity in mouse hepatocytes. *Chem Res Toxicol.* 23, 1286–1292.

Buttar H.S., Nera E.A., Downie R.H. (1976). Serum enzyme activities and hepatic triglyceride levels in acute and subacute acetaminophen-treated rats. *Toxicology.* 6, 9–20.

Cannon B, Nedergaard J. (2008). Studies of thermogenesis and mitochondrial function in adipose tissues. *Methods Mol Biol.* 456:109-21.

Cannon B., Nedergaard J. (2004). Brown adipose tissue: function and physiological significance. *Physiol Rev* 84, 277–359.

Cannon B., Shabalina I.G., Kramarova T.V., Petrovic N., Nedergaard J. (2006). Uncoupling proteins: a role in protection against reactive oxygen species—or not? *Biochim. Biophys. Acta.* 1757, 449-458.

Carmen G.Y., Victor S.M. (2006). Signalling mechanisms regulating lipolysis. *Cellular Signalling.* 18, 401–408.

Cayman Chemical (2017). COX-1 (mouse) Blocking Peptide Product information Available at: <https://www.caymanchem.com/pdfs/360109.pdf> [Accessed 2 August 2017].

Censarek P., Freidel K., Hohlfeld T., Schrör K., Weber A.A. (2006). Human cyclooxygenase-1b is not the elusive target of acetaminophen. *Eur J Pharmacol.* 551(1-3), 50-3.

Chan K., Truong D., Shangari N., O'Brien P.J. (2005). Drug-induced mitochondrial toxicity. *Expert Opin Drug Metab Toxicol.* 1(4), 655-69.

Chandrasekharan N.V., Dai H., Roos K.L., Evanson N.K., Tomsik J., Elton T.S., Simmons D.L. (2002). COX-3, a cyclooxygenase-1 variant inhibited by acetaminophen and other analgesic/antipyretic drugs: cloning, structure, and expression. *Proc Natl Acad Sci USA.* 99, 13926-13931.

Chaves V.E., Frasson D., Kawashita N.H. (2011). Several agents and pathways regulate lipolysis in adipocytes. *Biochimie.* 93(10), 1631-40.

Chen C., Krausz K.W., Shah Y.M., Idle J.R., Gonzalez F.J. (2009). Serum metabolomics reveals irreversible inhibition of fatty acid β -oxidation through the suppression of PPAR α activation as a contributing mechanism of acetaminophen-induced hepatotoxicity. *Chem Res Toxicol.* 22, 699–707.

Chrysovergis K., Wang X., Kosak J., Lee S-H., Kim J.S., Foley J.F., Travlos G., Singh S., Baek S.J., Eling T.E. (2014). NAG-1/GDF15 prevents obesity by increasing thermogenesis, lipolysis and oxidative metabolism. *Int J Obes (Lond).* 38(12), 1555–1564.

Cohen S.D., Hoivik D.J., Khairallah E.A. (1998). Acetaminophen-Induced Hepatotoxicity. In: Plaa GL, Hewitt WR, editors. *Toxicology of the Liver.* Taylor & Francis. 159–186.

Cohen S.D., Pumford N.R., Khairallah E.A., Boekelheide K., Pohl L.R., Amouzadeh H.R., Hinson J.A. (1997). Selective protein covalent binding and target organ toxicity. *Toxicol Appl Pharmacol.* 143, 1–12.

Copple I.M., Goldring C.E., Jenkins R.E., Chia A.J., Randle L.E., Hayes J.D., Kitteringham N.R., Park B.K. (2008). The hepatotoxic metabolite of

acetaminophen directly activates the Keap1-Nrf2 cell defense system. *Hepatology*. 48(4), 1292-301.

Corley G., Rawls S.M. (2009). Opioid, Cannabinoid CB1 and NOP Receptors Do Not Mediate APAP-induced Hypothermia in Rats. *Pharmacol Biochem Behav*. 92 (3), 503-507.

Cornejo-Juarez P, Sierra-Madero J, Volkow-Fernandez P. Metabolic acidosis and hepatic steatosis in two HIV-infected patients on stavudine (d4T) treatment. *Arch Med Res* 2003;34:64–69.

Courad J.P., Besse D., Delchambre C., Hanoun N., Hamon M., Eschalier A., Caussade F., Cloarec A. (2001). Acetaminophen distribution in the rat central nervous system. *Life Sci*. 69, 1455–1464.

Cranswick N., Coghlan D. (2000). Paracetamol efficacy and safety in children: the first 40 years. *Am J Ther*. 7, 135–141.

Cui J.G., Kuroda H., Chandrasekharan N.V., Pelaez R.P., Simmons D.L., Bazan N.G., Lukiw W.J. (2004). Cyclooxygenase-3 gene expression in Alzheimer hippocampus and in stressed human neural cells. *Neurochem Res*. 29(9), 1731-7.

Daiyasu H., Toh H. (2000). Molecular evolution of the myeloperoxidase family. *J Mol Evol*. 51, 433–445.

Davies N.M., Good R.L., Roupe K.A., Yáñez J.A. (2004). Cyclooxygenase-3: axiom, dogma, anomaly, enigma or splice error?--Not as easy as 1, 2, 3. *J Pharm Pharm Sci*. 7(2), 217-26.

de Andrade K.Q., Moura F.A., dos Santos J.M., de Araújo O.R., de Farias Santos J.C., Goulart M.O. (2015). Oxidative stress and inflammation in hepatic diseases: therapeutic possibilities of N-acetylcysteine. *Int J Mol Sci*. 16, 30269–30308.

Deschamps D., DeBeco V., Fisch C., Fromenty B., Guillouzo A., Pessayre D. (1994). Inhibition by perhexiline of oxidative phosphorylation and the β -oxidation of fatty acids: possible role in pseudoalcoholic liver lesions. *Hepatology*. 19, 948–961.

Deschamps D., Fisch C., Fromenty B., Berson A., Degott C., Pessayre D. (1991). Inhibition by salicylic acid of the activation and thus oxidation of long chain fatty acids. Possible role in the development of Reye's syndrome. *J Pharmacol Exp Ther*. 259, 894–904.

Diaz A., Reginato A.M., Jimenez S.A. (1992). Alternative splicing of human prostaglandin G/H synthase in mRNA and evidence of differential regulation of the resulting transcripts by transforming growth factor beta 1, interleukin 1 beta, and tumor necrosis factor alpha. *J Biol Chem.* 267, 10816-10822.

Dinchuk J.E., Liu R.Q., Trzaskos J.M. (2003). COX-3: in the wrong frame in mind. *Immunol Lett.* 86, 121.

Doi H., Horie T. (2010). Salicylic acid-induced hepatotoxicity triggered by oxidative stress. *Chem Biol Interact.* 183, 363–368.

Dou W., Jiao Y., Goorha S., Raghow R., Ballou L.R. (2004). Nociception and the differential expression of cyclooxygenase-1 (COX-1), the COX-1 variant retaining intron-1 (COX-1v), and COX-2 in mouse dorsal root ganglia (DRG). *Prostaglandins Other Lipid Mediat.* 74(1-4), 29-43.

Du K., Ramachandran A., McGill M.R., Mansouri A., Asselah T., Farhood A., Woolbright B.L., Ding W.X., Jaeschke H. (2017). Induction of mitochondrial biogenesis protects against acetaminophen hepatotoxicity. *Food Chem Toxicol.* 108(Pt A), 339-350.

Duchamp C., Barré H. (1993). Skeletal muscle as the major site of nonshivering thermogenesis in cold-adapted ducklings. *Am J Physiol Regul Integr Comp Physiol.* 265, R1076–R1083.

Eberhardt M.J., Schillers F., Eberhardt E.M., Risser L., de la Roche J., Herzog C., Echtermeyer F., Leffler A. (2017). Reactive metabolites of acetaminophen activate and sensitize the capsaicin receptor TRPV1. *Sci Rep.* 7(1), 12775.

Else P.L., Hulbert A.J. (1981). Comparison of the “mammal machine” and the “reptile machine”: energy production. *Am J Physiol.* 240, R3-9.

Engstrom R.L., Wilhelms D.B., Eskilsson A., Vasilache A.M., Elander L., Engblom D., Blomqvist A. (2013). Acetaminophen reduces lipopolysaccharide-induced fever by inhibiting cyclooxygenase-2. *Neuropharmacology.* 71, 124-9.

Erman A., Schwartzman M., Raz A. (1980). Indomethacin but not aspirin inhibits basal and stimulated lipolysis in rabbit kidney. *Prostaglandins.* 20(4), 689-702.

Evdokimov N.M., Clark P.M., Flores G., Chai T., Faull K.F., Phelps M.E., Witte O.N., Jung M.E. (2015). Development of 2-deoxy-2-[18F]fluororibose for positron emission tomography imaging liver function in vivo. *J Med Chem.* 58, 5538–47.

Fain J.N., Mohell N., Wallace M.A., Mills I. (1984). Metabolic effects of b-, a1-

, and α_2 -adrenoceptor activation on brown adipocytes isolated from the perirenal adipose tissue of fetal lambs. *Metabolism*. 33, 289–94.

Fassina G., Dorigo P., Gaion R.M. (1974). Equilibrium between metabolic pathways producing energy: a key factor in regulating lipolysis. *Pharmacol Res Commun*. 6, 1–21.

Fillmore N., Alrob O.A., Lopaschuk G.D. (2017). Fatty Acid beta-Oxidation Available at <http://lipidlibrary.aocs.org/Biochemistry/content.cfm?ItemNumber=39187> [Accessed 2 August 2017].

Fischer L.J., Green M.D., Harman A.W. (1981). Levels of acetaminophen and its metabolites in mouse tissues after a toxic dose. *J Pharmacol Exp Ther*. 219, 281–286.

Flower R.J., Vane J.R. (1972). Inhibition of prostaglandin synthetase in brain explains the antipyretic activity of paracetamol (4-acetamidophenol). *Nature*. 240, 410–1.

Fortier M., Soni K., Laurin N., Wang S.P., Maurege P., Jirik F.R., Mitchell G.A. (2005). Human hormone-sensitive lipase (HSL): expression in white fat corrects the white adipose phenotype of HSL-deficient mice. *JLipid Res*. 46, 1860-7.42.

Foster J., Mauger A., Thomasson K., White S., Taylor L. (2016). Effect of Acetaminophen Ingestion on Thermoregulation of Normothermic, Non-febrile Humans. *Front Pharmacol*. 7, 54.

Fréneaux E., Fromenty B., Berson A., Labbe G., Degott C., Lettéron P., Larrey D., Pessayre D. (1990). Stereoselective and nonstereoselective effects of ibuprofen enantiomers on mitochondrial beta-oxidation of fatty acids. *J Pharmacol Exp Ther*. 255, 529–535.

Fromenty B., Pessayre D. (1995). Inhibition of mitochondrial beta-oxidation as a mechanism of hepatotoxicity. *Pharmacol Ther*. 67, 101-154.

Fukushima A., Sekiguchi W., Mamada K., Tohma Y., Ono H. (2017). Serotonergic system does not contribute to the hypothermic action of acetaminophen. *Biol Pharm Bull*. 40(2), 227-233.

Gentry C., Andersson D.A., Bevan S. (2015). TRPA1 mediates the hypothermic action of acetaminophen. *Sci Rep*. 5, 12771.

Ghanem I.C., María J.P., Manautou J.E., and Mottino A.D. (2016). Acetaminophen; from liver to brain: new insights into drug pharmacological action and toxicity. *Pharmacol Res*. 109, 119–131.

Gordon C. J. (2012). Thermal physiology of laboratory mice: Defining

thermoneutrality. *Journal of Thermal Biology* 37(8), 654-685.

Gordon C.J. (1985). Relationship between autonomic and behavioral thermoregulation in the mouse. *Physiol. Behav.* 34, 687-690.

Gordon C.J. (1990). Thermal biology of the laboratory rat. *Physiol. Behav.* 47, 963-991.

Gordon C.J. (1993). Temperature regulation in laboratory rodents. New York: Cambridge University Press. Xii, 276.

Gordon C.J. (2004). Effect of cage bedding on temperature regulation and metabolism of group-housed female mice. *Comp. Med.* 54, 51-56.

Greenberg A.S., Shen W.J., Muliro K., Patel S., Souza S.C., Roth R.A, Kraemer F.B. (2001). Stimulation of lipolysis and hormone-sensitive lipase via the extracellular signal-regulated kinase pathway. *J. Biol. Chem.* 276, 45456-45461.

Gujral J.S., Knight T.R., Farhood A., Bajt M.L., Jaeschke H. (2002). Mode of cell death after acetaminophen overdose in mice: apoptosis or oncotic necrosis? *Toxicol Sci.* 67, 322–328.

Harrison P.M., Wendon J.A., Gimson A.E., Alexander G.J., Williams R. (1991). Improvement by acetylcysteine of hemodynamics and oxygen transport in fulminant hepatic failure. *N Engl J Med.* 324, 1852–1857.

Hawkes R., Niday E., Gordon J. (1982). A dot-immunobinding assay for monoclonal and other antibodies. *Anal Biochem.* 119(1), 142-7.

Heard K.J. Acetylcysteine for acetaminophen poisoning. (2008). *N Engl J Med.* 359, 285–292.

Heeren J., Münzberg H. (2013). Novel aspects of brown adipose tissue biology. *Endocrinol Metab Clin.* 42, 89–107.

Hill G.E. (2014). Cellular respiration: the nexus of stress, condition, and ornamentation. *Integr Comp Biol.* 54(4), 645-57.

Hinz B., Brune K. (2002). Cyclooxygenase-2-10 years later. *J Pharmacol Exp Ther.* 300(2), 367-75.

Hla T. (1996). Molecular characterization of the 5.2 KB isoform of the human cyclooxygenase-1 transcript. *Prostaglandins.* 51, 81–85.

Hu J., Ramshesh V.K., McGill M. R., Jaeschke H., Lemasters J.J. (2016). Low dose acetaminophen induces reversible mitochondrial dysfunction associated

with transient c-Jun N-terminal kinase activation in mouse liver. *Toxicol Sci.* 150(1), 204–215.

Jaeschke H., Bajt M.L. (2006). Intracellular signaling mechanisms of acetaminophen-induced liver cell death. *Toxicol Sci.* 89, 31–41.

Jaeschke H., McGill M.R. (2015). Cytochrome P450-derived versus mitochondrial oxidant stress in acetaminophen hepatotoxicity. *Toxicol Lett.* 235, 216–217.

Jaeschke H., McGill M.R., Ramachandran A. (2012a). Oxidant stress, mitochondria, and cell death mechanisms in drug-induced liver injury: lessons learned from acetaminophen hepatotoxicity. *Drug Metab Rev.* 44, 88–106.

Jaeschke H., Williams C.D., Ramachandran A., Bajt M.L. (2012b). Acetaminophen hepatotoxicity and repair: the role of sterile inflammation and innate immunity. *Liver Int.* 32, 8–20.

James L.P., McCullough S.S., Lamps L.W., Hinson J.A. (2003). Effect of N-acetylcysteine on acetaminophen toxicity in mice: relationship to reactive nitrogen and cytokine formation. *Toxicol Sci.* 75(2), 458-67.

Jan Y.H., Heck D.E., Dragomir A.C., Gardner C.R., Laskin D.L., Laskin J.D. (2014). Acetaminophen reactive intermediates target hepatic thioredoxin reductase. *Chem Res Toxicol.* 27(5), 882-94.

Jarving R., Jarving I., Kurg R., Brash A.R., Samel N. (2004). On the evolutionary origin of cyclooxygenase (COX) isozymes: characterization of marine invertebrate COX genes points to independent duplication events in vertebrate and invertebrate lineages. *J Biol Chem.* 279, 13624–13633.

Jollow DJ, Mitchell JR, Potter WZ, Davis DC, Gillette JR, Brodie BB. (1973). Acetaminophen-induced hepatic necrosis. II. Role of covalent binding in vivo. *J Pharmacol Exp Ther.* 187(1):195-202.

Józwiak-Bebenista M., Nowak J. Z. (2014). Paracetamol: mechanism of action, applications and safety concern. *Acta Pol. Pharm.* 71, 11–23.

Kawamura M., Inaoka H., Obata S., Harada Y. (2014). Why do a wide variety of animals retain multiple isoforms of cyclooxygenase? *Prostaglandins Other Lipid Mediat.* 109–111, 14–22.

Kerr F., Dawson A., Whyte I.M., Buckley N., Murray L., Graudins A., et al. (2005). The Australasian Clinical Toxicology Investigators Collaboration randomized trial of different loading infusion rates of N-acetylcysteine. *Ann Emerg Med.* 45, 402–408.

Khetani S.R., Bhatia S.N. (2008). Microscale culture of human liver cells for drug development. *Nat. Biotechnol.* 26, 120-126.

Kikkawa R., Fujikawa M., Yamamoto T., Hamada Y., Yamada H., Horii I. (2006). In vivo hepatotoxicity study of rats in comparison with in vitro hepatotoxicity screening system. *J. Toxicol. Sci.* 31, 23-34.

Kis B., Snipes A., Bari F., Busija D.W. (2004). Regional distribution of cyclooxygenase-3 mRNA in the rat central nervous system. *Brain Res Mol Brain Res.* 126(1), 78-80.

Kis B., Snipes J.A., Busija D.W. (2005). Acetaminophen and the cyclooxygenase-3 puzzle: sorting out facts, fictions, and uncertainties. *J Pharmacol Exp Ther.* 315(1), 1-7.

Kis B., Snipes J.A., Isse T., Nagy K., Busija D.W. (2003). Putative Cyclooxygenase-3 Expression in Rat Brain Cells. *J Cereb Blood Flow Metab.* 23(11), 1287-92.

Kitzler J., Hill E., Hardman R., Reddy N., Philpot R., Eling T.E. (1995) Analysis and quantitation of splicing variants of the TPA-inducible PGHS-1 mRNA in rat tracheal epithelial cells. *Arch Biochem Biophys.* 316, 856-863.

Kon K., Kim J.S., Jaeschke H., Lemasters J.J. (2004). Mitochondrial permeability transition in acetaminophen-induced necrosis and apoptosis of cultured mouse hepatocytes. *Hepatology.* 40, 1170–1179.

Kumpulainen E., Kokki H., Halonen T., Heikkinen M., Savolainen J., Laisalmi M. (2007). Paracetamol (acetaminophen) penetrates readily into the cerebrospinal fluid of children after intravenous administration. *Pediatrics.* 119, 766–771.

Labbe G., Pessayre D., Fromenty B. (2008). Drug-induced liver injury through mitochondrial dysfunction: mechanisms and detection during preclinical safety studies. *Fundam Clin Pharmacol.* 22, 335–353.

Lafontan M., Berlan M. (1993). Fat cell adrenergic receptors and the control of white and brown fat cell function. *J Lipid Res.* 34, 1057–91.

Lafontan M., Langin D. (2009). Lipolysis and lipid mobilization in human adipose tissue. *Progress in Lipid Research.* 48, 275–297.

Lee W.M. (2012). Acute liver failure. *Semin Respir Crit Care Med.* 33, 36–45.

- Lefterova M.I., Lazar M.A. (2009). New developments in adipogenesis. *Trends in Endocrinology and Metabolism*. 20, 107–114.
- Leung L. (2012). From ladder to platform: a new concept for pain management. *J Prim Health Care*. 4(3), 254-8.
- Li S., Dou W., Tang Y., Goorha S., Ballou L.R., Blatteis C.M. (2008). Acetaminophen: antipyretic or hypothermic in mice? In either case, PGHS-1b (COX-3) is irrelevant. *Prostaglandins Other Lipid Mediat*. 85(3-4):89-99.
- Lim M.S., Lim P.L., Gupta R., Boelsterli U.A. (2006). Critical role of free cytosolic calcium, but not uncoupling, in mitochondrial permeability transition and cell death induced by diclofenac oxidative metabolites in immortalized human hepatocytes. *Toxicol Appl Pharmacol*. 217, 322–331.
- Lopaschuk G.D., Ussher, J.R., Folmes C.D., Jaswal J.S. and Stanley W.C. (2010). Myocardial fatty acid metabolism in health and disease. *Physiol Rev*. 90, 207-258.
- Lowell B.B., Spiegelman B.M. (2000). Towards a molecular understanding of adaptive thermogenesis. *Nature*. 404, 652–660.
- Luo L., Liu M. (2016). Adipose tissue in control of metabolism. *J Endocrinol*. 231(3), R77-R99.
- MacPherson R.E., Peters S.J. (2015). Piecing together the puzzle of perilipin proteins and skeletal muscle lipolysis. *Appl Physiol Nutr Metab*. 40(7):641-51.
- Marcelin G., Chua S. (2010). Contributions of adipocyte lipid metabolism to body fat content and implications for the treatment of obesity. *Curr Opin Pharmacol*. 10, 588–593.
- Martin F.L., McLean A.E. (1995). Adenosine triphosphate (ATP) levels in paracetamol-induced cell injury in the rat in vivo and in vitro. *Toxicology*. 104, 91–7.
- Massey T.E., Walker R.M., McElligott T.F., Racz W.J. (1982). Acetaminophen-induced hypothermia in mice: evidence for a central action of the parent compound. *Toxicology*. 25, 187–200.
- Matsumura K., Cao C., Ozaki M., Morii H., Nakadate K., Watanabe Y. (1998). Brain endothelial cells express cyclooxygenase-2 during lipopolysaccharide-induced fever: light and electron microscopic immunocytochemical studies. *J Neurosci*. 18, 6279–6289.

Muramatsu S., Shiraishi S., Miyano K., Sudo Y., Toda A., Mogi M., Hara M., Yokoyama A., Kawasaki Y., Taniguchi M., Uezono Y. (2016). Metabolism of AM404 From Acetaminophen at Human Therapeutic Dosages in the Rat Brain. *Anesth Pain Med.* 6(1), e32873.

McGill M.R., Jaeschke H. (2013). Metabolism and disposition of acetaminophen: recent advances in relation to hepatotoxicity and diagnosis. *Pharm Res.* 30, 2174–2187.

McGill M.R., Lebofsky M., Norris H.R., Slawson M.H., Bajt M.L., Xie Y., Williams C.D., Wilkins D.G., Rollins D.E., Jaeschke H. (2013). Plasma and liver acetaminophen-protein adduct levels in mice after acetaminophen treatment: dose-response, mechanisms, and clinical implications. *Toxicol Appl Pharmacol.* 269, 240–249.

McGill M.R., Sharpe M.R., Williams C.D., Taha M., Curry S.C., Jaeschke H. (2012). The mechanism underlying acetaminophen-induced hepatotoxicity in humans and mice involves mitochondrial damage and nuclear DNA fragmentation. *J Clin Invest.* 122, 1574–1583.

McGovern A.J., Vitkovitsky I.V., Jones D.L., Mullins M.E. (2015). Can AST/ALT ratio indicate recovery after acute paracetamol poisoning? *Clin Toxicol (Phila)* 53, 164–167.

McKnight G.S., Cummings D.E., Amieux P.S., Sikorski M.A., Brandon E.P., Planas J.V., Motamed K., Idzerda R.L. (1998). Cyclic AMP, PKA, and the physiological regulation of adiposity. *Recent Prog Horm Res.* 53, 139–59.

Messner S., Agarkova I., Moritz W., Kelm J.M. (2013). Multi-cell type human liver microtissues for hepatotoxicity testing. *Arch. Toxicol.* 87, 209–213.

Meyers L.L., Beierschmitt W.P., Khairallah E.A., Cohen S.D. (1988). Acetaminophen-induced inhibition of hepatic mitochondrial respiration in mice. *Toxicol Appl Pharmacol.* 93, 378–87.

Mingatto F.E., Santos A.C., Uyemura S.A., Jordani M.C., Curti C. (1996). In vitro interaction of nonsteroidal anti-inflammatory drugs on oxidative phosphorylation of rat kidney mitochondria: respiration and ATP synthesis. *Arch Biochem Biophys.* 334(2), 303–8.

Mitchell J.R., Jollow D.J., Potter W.Z., Davis D.C., Gillette J.R., Brodie B.B. (1973a). Acetaminophen-induced hepatic necrosis. I. Role of drug metabolism. *J Pharmacol Exp Ther.* 187, 185–94.

Mitchell J.R., Jollow D.J., Potter W.Z., Gillette J.R., Brodie B.B. (1973b). Acetaminophen-induced hepatic necrosis. IV. Protective role of glutathione. *J Pharmacol Exp Ther.* 187, 211–217.

Moriyama N., Miyoshi M., Imoto T., Maruyama M., Shido O., Watanabe T. (2006). Systemic administration of polymyxin B induces hypothermia in rats via an inhibitory effect on metabolic rate. *Eur J Pharmacol.* 541(1-2), 38-43.

Morse H.N. (1878). Ueber eine neue Darstellungsmethode der Acetylamidophenole. *Ber Deutscher Chem Ges.* 11, 232–233.

Moyer AM, Fridley BL, Jenkins GD, Batzler AJ, Pellemounter LL, Kalari KR, Ji Y, Chai Y, Nordgren K, Weinshilboum RM. (2011). Acetaminophen-NAPQI Hepatotoxicity: A Cell Line Model System Genome-Wide Association Study. *Toxicol Sci.* 120(1), 33–41.

Mozo J., Emre Y., Bouillaud F., Ricquier D., Criscuolo F. (2005). Thermoregulation: what role for UCPs in mammals and birds? *Biosci. Rep.* 25, 227-249.

Nastevska C., Gerber E., Horbach M., Röhrdanz E., Kahl R. (1999). Impairment of TNF- α expression and secretion in primary rat liver cell cultures by acetaminophen treatment. *Toxicology.* 133, 85-92.

Nazareth W.M., Sethi J.K., McLean A.E. (1991). Effect of paracetamol on mitochondrial membrane function in rat liver slices. *Biochem Pharmacol.* 42, 931–36.

Noh J.R., Kim Y.H., Hwang J.H., Choi D.H., Kim K.S., Oh W.K., et al. (2015). Sulforaphane protects against acetaminophen-induced hepatotoxicity. *Food Chem Toxicol.* 80, 193–200.

Nurmi J.T., Puolakkainen P.A., Rautonen N.E. (2005). Intron 1 retaining cyclooxygenase 1 splice variant is induced by osmotic stress in human intestinal epithelial cells. *Prostaglandins Leukot Essent Fatty Acids.* 73(5), 343-50.

Ohlson K.B., Shabalina I.G., Lennström K., Backlund E.C., Mohell N., Bronnikov G.E., Lindahl S.G., Cannon B., Nedergaard J. (2004). Inhibitory effects of halothane on the thermogenic pathway in brown adipocytes: localization to adenylyl cyclase and mitochondrial fatty acid oxidation. *Biochemical Pharmacology.* 68(3), 463-477.

Oksuz E., Atalar F., Tanırverdi G., Bilir A., Shahzadi A., Yazici Z. (2016). Therapeutic potential of cyclooxygenase-3 inhibitors in the management of glioblastoma. *J Neurooncol.* 126(2), 271-8.

O'Neill G.P., Ford-Hutchinson A.W. (1993). Expression of mRNA for cyclooxygenase-1 and cyclooxygenase-2 in human tissues. *FEBS*. 33, 156–160.

Orbach S.M., Cassin M.E., Ehrich M.F., Rajagopalan P. (2017). Investigating acetaminophen hepatotoxicity in multi-cellular organotypic liver models. *Toxicol In Vitro*. 42, 10-20.

Osellame L.D., Blacker T.S., Duchen M.R. (2012). Cellular and molecular mechanisms of mitochondrial function. *Best Pract Res Clin Endocrinol Metab*. 26(6), 711–723.

Otto J.C., DeWitt D.L., Smith W.L. (1993). N-glycosylation of prostaglandin endoperoxide synthase-1 and -2 and their orientations in the endoplasmic reticulum. *J Biol Chem*. 268, 18234-18242.

Owen L., Sunram-Lea S.I. (2011). Metabolic Agents that Enhance ATP can Improve Cognitive Functioning: A Review of the Evidence for Glucose, Oxygen, Pyruvate, Creatine, and L-Carnitine. *Nutrients*. 3(8), 735–755.

Paar M., Jüngst C., Steiner N., Magnes C., Sinner F., Kolb D., Lass A., Zimmermann R., Zumbusch A., Kohlwein S.D., Wolinski H. (2012). Remodeling of lipid droplets during lipolysis and growth in adipocytes. *The Journal of Biological Chemistry*. 28, 11164–11173.

Pauw A.D., Tejerina S., Raes M., Keijer J., Arnould T. (2009). Mitochondrial (Dys)function in Adipocyte (De)differentiation and Systemic Metabolic Alterations. *Am J Pathol*. 175(3), 927–939.

Perier C., Vila M. (2012). Mitochondrial biology and Parkinson's disease. *Cold Spring Harb Perspect Med*. 2(2), a009332.

Pike L.S., Smift A.L., Croteau N.J., Ferrick D.A., Wu M. (2011). Inhibition of fatty acid oxidation by etomoxir impairs NADPH production and increases reactive oxygen species resulting in ATP depletion and cell death in human glioblastoma cells. *Biochim Biophys Acta*. 1807(6), 726-34.

Porter K.E., Dawson A.G. (1979). Inhibition of respiration and gluconeogenesis by paracetamol in rat kidney preparations. *Biochem Pharmacol*. 28, 3057–62.

Prescott L.F., Illingworth R.N., Critchley J.A., Stewart M.J., Adam R.D., Proudfoot A.T. (1979). Intravenous N-acetylcysteine: the treatment of choice for paracetamol poisoning. *Br Med J*. 2, 1097–1100.

Promega (2017). AccessQuick™ RT-PCR System Protocol Available at: <file:///C:/Users/User/Downloads/accessquick-rt-pcr-system-protocol.pdf> [Accessed 2 August 2017].

Public Health England Culture Collections (2017). ECACC General Cell Collection: 96091929 b.End3 Available at: https://www.phe-culturecollections.org.uk/products/celllines/generalcell/detail.jsp?refId=96091929&collection=ecacc_gc [Accessed 2 August 2017].

Public Health England Culture Collections (2017). ECACC General Cell Collection: 86052701 3T3 L1 Available at: https://www.phe-culturecollections.org.uk/products/celllines/generalcell/detail.jsp?refId=86052701&collection=ecacc_gc [Accessed 2 August 2017].

Qin N., Zhang S.P., Reitz T.L., Mei J.M., Flores C.M. (2005). Cloning, expression, and functional characterization of human cyclooxygenase-1 splicing variants: evidence for intron 1 retention. *J Pharmacol Exp Ther.* 315(3), 1298-305.

Ràfols M.E. (2014). Adipose tissue: Cell heterogeneity and functional diversity *Endocrinol Nutr.* 61(2), 100-112.

Ramachandran A., Lebofsky M., Weinman S.A., Jaeschke H. (2011). The impact of partial manganese superoxide dismutase (SOD2)-deficiency on mitochondrial oxidant stress, DNA fragmentation and liver injury during acetaminophen hepatotoxicity. *Toxicol Appl Pharmacol.* 251(3), 226-33.

Ramachandran A., McGill M.R., Xie Y., Ni H.M., Ding W.X., Jaeschke H. (2013). Receptor interacting protein kinase 3 is a critical early mediator of acetaminophen-induced hepatocyte necrosis in mice. *Hepatology.* 58, 2099–2108.

Ramsay R. R., Rashed M. S., Nelson S. D. (1989). In vitro effects of acetaminophen metabolites and analogs on the respiration of mouse liver mitochondria. *Arch. Biochem. Biophys.* 273, 449–457.

Reid A.B., Kurten R.C., McCullough S.S., Brock R.W., Hinson J.A. (2005). Mechanisms of acetaminophen-induced hepatotoxicity: role of oxidative stress and mitochondrial permeability transition in freshly isolated mouse hepatocytes. *J Pharmacol Exp Ther.* 312, 509–516.

Reinauer C., Censarek P., Kaber G., Weber A.A., Steger G., Klamp T., Schrör K. (2013). Expression and translation of the COX-1b gene in human cells--no evidence of generation of COX-1b protein. *Biol Chem.* 394(6), 753-60.

Rivera P., Pastor A., Arrabal S., Decara J., Vargas A., Sánchez-Marín L., Pavón F.J., Serrano A., Bautista D., Boronat A., Torre R., Baixeras E., Lucena M.I., Fonseca F.R., Suárez J. (2017). Acetaminophen-Induced Liver Injury Alters the

Acyl Ethanolamine-Based Anti-Inflammatory Signaling System in Liver. *Front Pharmacol.* 8, 705.

Rogers G.W., Brand M.D., Petrosyan S., Ashok D., Elorza A.A., Ferrick D.A. (2011). High throughput microplate respiratory measurements using minimal quantities of isolated mitochondria. *PLoS One.* 6, e21746.

Romanovsky A.A. (2007). Thermoregulation: some concepts have changed. Functional architecture of the thermoregulatory system. *Am J Physiol Regul Integr Comp Physiol.* 292(1), R37-46.

Roos K.L., Simmons D.L. (2005). Cyclooxygenase variants: The role of alternative splicing. *Biochemical and Biophysical Research Communications.* 338 (1), 62–69.

Rosen E.D., Walkey C.J., Puigserver P., Spiegelman B.M. (2000). Transcriptional regulation of adipogenesis. *Genes and Development.* 14, 1293–1307.

Rouzer C.A., Marnett L.J. (2009). Cyclooxygenases: structural and functional insights. *J Lipid Res.* 50, S29–S34.

Rumack B.H. (2002). Acetaminophen hepatotoxicity: the first 35 years. *J Toxicol Clin Toxicol.* 40, 3–20.

Sandor A., Cseko J., Kispal G., Alkonyi I. (1990). Surplus acylcarnitines in the plasma of starved rats derive from the liver. *J Biol Chem.* 265, 22313–22316.

Schneider C., Boeglin W.E., Brash A.R. (2005). Human cyclooxygenase-1 and an alternative splice variant: contrasts in expression of mRNA, protein, and catalytic activities. *Biochem. J.* 385, 57–64.

Schulz H. (2008). Oxidation of fatty acids in eukaryotes. In: *Biochemistry of Lipids, Lipoproteins and Membranes (5th Edition)*. 131-154 (D.E. Vance and J. Vance (eds.), Elsevier, Amsterdam).

Schwab J.M., Schluesener H.J., Meyermann R., Serhan C.N. (2003a). COX-3 the enzyme and the concept: steps towards highly specialized pathways and precision therapeutics? *Prostaglandins Leukot Essent Fatty Acids.* 69(5), 339-43.

Schwab J.M., Beiter T., Linder J.U., Laufer S., Schulz J.E., Meyermann R., Schluesener H.J. (2003b). COX-3--a virtual pain target in humans? *FASEB J.* 17(15), 2174-5.

Schwab J.M., Schluesener H.J., Laufer S. (2003c) COX-3: just another COX or the solitary elusive target of paracetamol? *Lancet* 361, 981–982.

Schweiger M., Eichmann T.O., Taschler U., Zimmermann R., Zechner R., Lass A. (2014). Measurement of Lipolysis. *Methods Enzymol.* 538, 171–193.

Schweiger M., Schreiber R., Haemmerle G., Lass A., Fledelius C., Jacobsen P., Tornqvist H., Zechner R., Zimmermann R. (2006). Adipose triglyceride lipase and hormone-sensitive lipase are the major enzymes in adipose tissue triacylglycerol catabolism. *J Biol Chem.* 281, 40236–41.

Sell H., Deshaies Y., Richard D. (2004). The brown adipocyte: update on its metabolic role. *Int J Biochem Cell Biol.* 36(11), 2098-2104.

Shaftel S.S., Olschowka J.A., Hurley S.D., Moore A.H., O'Banion M.K. (2003). COX-3: a splice variant of cyclooxygenase-1 in mouse neural tissue and cells. *Brain Res Mol Brain Res.* 119(2), 213-5.

Shen C., Zhang G., Meng Q. (2007). An in vitro model for long-term hepatotoxicity testing utilizing rat hepatocytes entrapped in micro-hollow fiber reactor. *Biochem. Eng. J.* 34, 267-272.

Shutt T.E., McBride H.M. (2013). Staying cool in difficult times: Mitochondrial dynamics, quality control and the stress response. *BBA-Mol Cell Res.* 1833, 417-24.

Sigma-Aldrich (2017). Free Glycerol Reagent Bulletin Available at: <https://www.sigmaaldrich.com/content/dam/sigma-aldrich/docs/Sigma/Bulletin/f6428bul.pdf> [Accessed 2 August 2017].

Sigma-Aldrich (2017). Monoclonal Anti- β -Actin antibody Datasheet Available at: <https://www.sigmaaldrich.com/content/dam/sigma-aldrich/docs/Sigma/Datasheet/6/a5441dat.pdf> [Accessed 2 August 2017].

Sigma-Aldrich (2017). GenElute™ Direct mRNA Miniprep Kit Bulletin Available at: <https://www.sigmaaldrich.com/content/dam/sigma-aldrich/docs/Sigma/Bulletin/dmn10bul.pdf> [Accessed 2 August 2017].

Sigma-Aldrich (2017). Mammalian Cell Lysis Kit Bulletin Available at: <https://www.sigmaaldrich.com/content/dam/sigma-aldrich/docs/Sigma/Bulletin/mcl1bul.pdf> [Accessed 2 August 2017].

Silva J.E. (2003). The thermogenic effect of thyroid hormone and its clinical implications. *Ann Intern Med.* 139(3), 205-213.

Silva J.E. (2006). Thermogenic mechanisms and their hormonal regulation.

Physiol Rev. 86(2), 435-64.

Simmons D.L. (2003). Variants of cyclooxygenase-1 and their roles in medicine. *Thromb Res.* 2003. 110(5-6), 265-8.

Simmons D.L., Botting R.M., Hla T. (2004). Cyclooxygenase Isozymes: The Biology of Prostaglandin Synthesis and Inhibition. *Pharmacological Reviews.* 56 (3), 387-437.

Simmons D.L., Botting R.M., Robertson P.M., Madsen M.L., Vane J.R. (1999). Induction of an acetaminophen-sensitive cyclooxygenase with reduced sensitivity to nonsteroid anti-inflammatory drugs. *Proc Natl Acad Sci U S A.* 96, 3275–80.

Simmons D.L., Chandrasekharan N.V., Hu D., Roos K.L., Tomsik J. (2005). Comments on “acetaminophen and the cyclooxygenase-3 puzzle: sorting out facts, fictions, and uncertainties”. *J Pharmacol Exp Ther.* 315, 1412–1414; author reply 1415–1416.

Simmons D.L., Xie W., Chipman J., Evett G. (1991). Multiple cyclooxygenases: cloning of a mitogen-inducible form. M. Bailey (Ed.), *Prostaglandin, Leukotrienes, Lipoxins and PAF*, Plenum Press, London. 67–78.

Smilkstein M.J., Knapp G.L., Kulig K.W., Rumack B.H. (1988). Efficiency of oral N-acetylcysteine in the treatment of acetaminophen overdose. Analysis of the national multicenter study (1976 to 1985) *N Engl J Med.* 319, 1557–1562.

Snipes J.A., Kis B., Shelness G.S., Hewett J.A., Busija D.W. (2005). Cloning and characterization of cyclooxygenase-1b (putative cyclooxygenase-3) in rat. *J Pharmacol Exp Ther.* 313(2), 668-76.

Somasundaram S., Rafi S., Hayllar J., Sigthorsson G., Jacob M., Price A., Macpherson A., Mahmud T., Scott D., Wrigglesworth J., Bjarnason I. (1997). Mitochondrial damage: a possible mechanism of the "topical" phase of NSAID induced injury to the rat intestine. *Gut.* 41(3), 344–353.

Somasundaram S., Sigthorsson G., Simpson R.J., Watts J., Jacob M., Tavares I.A., Rafi S., Roseth A., Foster R., Price A.B., Wrigglesworth J.M., Bjarnason I. (2000). Uncoupling of intestinal mitochondrial oxidative phosphorylation and inhibition of cyclooxygenase are required for the development of NSAID-enteropathy in the rat. *Aliment Pharmacol Ther.* 14(5), 639-50.

Tan C.Y., Vidal-Puig A. (2008). Adipose tissue expandability: the metabolic problems of obesity may arise from the inability to become more obese. *Biochemical Society Transactions.* 36, 935–940.

Taylor S.S., Yang J., Wu J., Haste N.M., Radzio-Andzelm E., Anand G. (2004). PKA: a portrait of protein kinase dynamics. *Biochim. Biophys. Acta.* 1697, 259–269.

Tchkonina T., Tchoukalova Y.D., Giorgadze N., Pirtskhalava T., Karagiannides I., Forse R.A., Koo A., Stevenson M., Chinnappan D., Cartwright A., Jensen M.D., Kirkland J.L. (2005). Abundance of two humanpreadipocyte subtypes with distinct capacities for replication, adipogenesis, and apoptosis varies among fat depots. *Am J Physiol Endocrinol Metab.* 288:E267-77.

Thompson B.R., Lobo S., Bernlohr D.A. (2010). Fatty acid flux in adipocytes; the in's and out's of fat cell lipid trafficking. *Mol Cell Endocrinol.* 318(1-2), 24–33.

Toh Y.C., Lim T.C., Tai D., Xiao G., van Noort D., Yu H. (2009). A microfluidic 3D hepatocyte chip for drug toxicity testing. *Lab Chip.* 9, 2026–2035.

Tokumitsu Y., Lee S., Ui M. (1977). In vitro effects of nonsteroidal anti-inflammatory drugs on oxidative phosphorylation in rats liver mitochondria. *Biochem Pharmacol.* 26, 2101-2106.

Toussaint K., Yang X.C., Zielinski M.A., Reigle K.L., Sacavage S.D., Nagar S., Raffa R.B. (2010). What do we (not) know about how paracetamol (acetaminophen) works? *J Clin Pharm Ther.* 35(6), 617-38.

Ueta C.B., Fernandes G.W., Capelo L.P., Fonseca T.L., Maculan F.D., Gouveia C.H., Brum P.C., Christoffolete M.A., Aoki M.S., Lancellotti C.L., Kim B., Bianco A.C., Ribeiro M.O. (2012). beta(1) Adrenergic receptor is key to cold- and diet-induced thermogenesis in mice. *Journal of Endocrinology.* 214, 359–365.

Vane J.R., Botting R.M. (1996). The history of anti-inflammatory drugs and their mechanism of action. In: Bazan N, Botting J, Vane J, eds. *New targets in inflammation: inhibitors of COX-2 or adhesion molecules.* Dordrecht: Kluwer Academic. 1–12.

Vaughan M. (1962). The production and release of glycerol by adipose. Tissue incubated in vitro. *J Biol Chem.* 237, 3354-3358.

Vázquez-Meza H., de Piña M.Z., Pardo J.P., Riveros-Rosas H., Villalobos-Molina R., Piña E. (2013). Non-steroidal anti-inflammatory drugs activate NADPH oxidase in adipocytes and raise the H₂O₂ pool to prevent cAMP-stimulated protein kinase a activation and inhibit lipolysis. *BMC Biochem.* 14, 13.

Voet D., Voet J. (2004). *Biochemistry* (3rd Edition).

Volz M., Kellner H.M. (1980). Kinetics and metabolism of pyrazolones (propyphenazone, aminopyrine and dipyrone). *Br J Clin Pharmacol.* 10 Suppl 2, 299S-308S.

Von Mering J. (1893). Beitrage zur Kenntniss der Antipyretica. *Ther Monatsch.* 7, 577–587.

Walker R.M., Massey T.E., McElligott T.F., Racz W.J. (1981). Acetaminophen-induced hypothermia, hepatic congestion, and modification by N-acetylcysteine in mice. *Toxicol Appl Pharmacol.* 59(3), 500-7.

Walker U.A., Bäuerle J., Laguno M., Murillas J., Mauss S., Schmutz G., Setzer B., Miquel R., Gatell J.M., Mallolas J. (2004). Depletion of mitochondrial DNA in liver under antiretroviral therapy with didanosine, stavudine, or zalcitabine. *Hepatology.* 39, 311–317.

Warner T.D., Vojnovic I., Giuliano F., Jiménez R., Bishop-Bailey D., Mitchell J.A. (2004). Cyclooxygenases 1, 2, and 3 and the production of prostaglandin I₂: investigating the activities of acetaminophen and cyclooxygenase-2-selective inhibitors in rat tissues. *J Pharmacol Exp Ther.* 310(2), 642-7.

Williams C.D., Farhood A., Jaeschke H. (2010). Role of caspase-1 and interleukin-1beta in acetaminophen-induced hepatic inflammation and liver injury. *Toxicol Appl Pharmacol.* 247(3), 169-78.

Xie Y., Ramachandran A., Breckenridge D.G., Liles J.T., Lebofsky M., Farhood A., Jaeschke H. (2015). Inhibitor of apoptosis signal-regulating kinase 1 protects against acetaminophen-induced liver injury. *Toxicol Appl Pharmacol.* 286(1),1-9.

Xu Y., Phipps S., Turner M.J., Simmons D.L. (2010). The N-terminus of COX-1 and its effect on cyclooxygenase-1 catalytic activity. *J Genet Genomics.* 37(2), 117-23.

Yoon E., Babar A., Choudhary M., Kutner M., and Pysopoulos N. (2016). Acetaminophen-Induced Hepatotoxicity: a Comprehensive Update. *J Clin Transl Hepatol.* 4(2), 131–142.

Yuan L., Kaplowitz N. (2013). Mechanisms of drug-induced liver injury. *Clin Liver Dis.* 17, 507–518.

Zebisch K., Voigt V., Wabitsch M., Brandsch M. (2012). Protocol for effective differentiation of 3T3-L1 cells to adipocytes. *Anal Biochem.* 425(1):88-90.

Zen-bio (2017). 3T3-L1 Cell Care Manual Available at: <http://www.zen-bio.com/pdf/ZBM0009.013T3L1CareprotocolRV08.08.pdf> [Accessed 2 August 2017].

Zhang J., Song S., Pang Q., Zhang R., Zhou L., Liu S., et al. (2015). Serotonin deficiency exacerbates acetaminophen-induced liver toxicity in mice. *Sci Rep.* 5, 8098.

Zhang T., He J., Xu C., Zu L., Jiang H., Pu S., Guo X., Xu G. (2008). Mechanisms of metformin inhibiting lipolytic response to isoproterenol in primary rat adipocytes. *J Mol Endocrinol.* 42(1), 57-66.